

INVESTIGATIONS ON CERIA BASED DIELECTRIC CERAMIC MATERIALS FOR WIRELESS COMMUNICATION

THESIS SUBMITTED TO COCHIN UNIVERISTY OF SCIENCE
AND TECHNOLOGY IN PARTIAL FULFILMENT OF
REQUIREMENT FOR THE DEGREE OF
DOCTOR OF PHILOSOPHY IN PHYSICS

P. S. ANJANA

Under the guidance and supervision of
Dr. M. T. SEBASTIAN



**NATIONAL INSTITUTE FOR INTERDISCIPLINARY SCIENCE
AND TECHNOLOGY (CSIR), THIRUVANANTHAPURAM**

NOVEMBER 2008

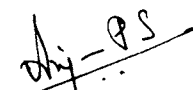
Dedicated to my family

DECLARATION

I hereby declare that the matter presented in the thesis entitled “INVESTIGATIONS ON CERIA BASED DIELECTRIC CERAMIC MATERIALS FOR WIRELESS COMMUNICATION” is the outcome of investigations carried out by me under the supervision of Dr. M. T. Sebastian, Scientist ‘G’, Materials and Minerals Division, National Institute for Interdisciplinary Science and Technology (Formerly Regional Research Laboratory) (CSIR), Thiruvananthapuram, India and the results embodied here has not been submitted elsewhere for the award of any other degree.

Thiruvananthapuram

11.11.08


P. S. Anjana



<http://w3rmt.csir.res.in>

Fax : ++ 91- (0) 471 - 2491712
Phone : 471- 2515294 (O), 471- 2446901 (R)
Email : mailadils@yahoo.com
mts@csrrltd.res.nic.in

Council of Scientific & Industrial Research

**NATIONAL INSTITUTE OF INTERDISCIPLINARY
SCIENCE AND TECHNOLOGY**

THIRUVANANTHAPURAM - 695 019, INDIA

Dr. M. T. SEBASTIAN
Deputy Director

CERTIFICATE

This is to certify that this thesis entitled “INVESTIGATIONS ON CERIA BASED DIELECTRIC CERAMIC MATERIALS FOR WIRELESS COMMUNICATION” is an authentic record of the investigations carried out by Ms. P. S. Anjana at the Materials and Minerals Division of National Institute for Interdisciplinary Science and Technology (Formerly Regional Research Laboratory) (CSIR), Thiruvananthapuram, India, under my supervision and guidance. This thesis or any part thereof has not been submitted elsewhere for the award of any other degree.

Dr. M. T. Sebastian
(Supervisor)

Thiruvananthapuram

11/11/08

The fact that the matter appears to be that, other things being the same, the principal requisite for success in "scientific research" is not the maturity of knowledge associated with age and experience, but the freshness of outlook which is natural attribute of youth.

Sir C. V. Raman

CONTENTS

PREFACE

ACKNOWLEDGEMENTS

CHAPTER 1 INTRODUCTION

1.1	INTRODUCTION	2
1.2	MICROWAVE DIELECTRIC RESONATORS	4
1.2.1	Introduction	4
1.2.2	An Overview of Dielectric Resonator Research	7
1.3	PHYSICS OF DIELECTRIC RESONATORS	10
1.3.1	Polarization Mechanisms in Dielectrics	10
1.3.2	Claussius Mossotti Equation	11
1.3.3	Working Principle of Dielectric Resonators	13
1.3.4	Resonance	14
1.3.5	DR in a Circuit	16
1.3.6	Modes and Mode Nomenclature	17
1.4	TYPES OF DIELECTRIC RESONATORS	19
1.5	MATERIAL REQUIREMENTS FOR DR APPLICATIONS	20
1.5.1	High Relative Permittivity (ϵ_r)	20
1.5.2	High Quality Factor (Low Dielectric Loss)	21
1.5.3	Small Temperature Coefficient of Resonant Frequency (τ_f)	23
1.6	FACTORS AFFECTING MICROWAVE DIELECTRIC PROPERTIES	24
1.6.1	Effect of Humidity	25
1.6.2	Effect of Porosity	26
1.7	APPLICATIONS OF DIELECTRIC RESONATORS	27
1.7.1	Dielectric Resonator Oscillators (DRO)	28
1.7.2	Dielectric Resonator Antennas (DRA)	29
1.7.3	Dielectric Resonator Filters (DRF)	30
1.8	LOW TEMPERATURE COFIRED CERAMICS (LTCC)	31
1.8.1	Introduction	31
1.8.2	Brief Historical Review	33

1.9	MATERIAL SELECTION AND REQUIREMENTS FOR LTCC	34
1.9.1	Densification Temperature Less than 950°C	35
1.9.2	Dielectric Properties (ϵ_r , Q_r , f and τ_f)	35
1.9.3	High Thermal Conductivity	37
1.9.4	Thermal Expansion	37
1.9.5	Chemical Compatibility with Electrode Material	38
1.10	GLASS-CERAMIC COMPOSITES	39
1.10.1	Introduction	39
1.10.2	Characteristics of Glasses	41
1.11	POLYMER-CERAMIC COMPOSITES	43
1.11.1	Introduction	43
1.11.2	Material Requirements for Microelectronic Packaging and Substrate Applications	44
1.11.2.1	Electrical Properties	44
1.11.2.2	Thermal and Thermomechanical Properties	45
1.11.2.3	Mechanical Properties	45
1.11.2.4	Chemical Properties	45
1.11.3	Advantages of Polymer - Ceramic Composites	46
1.12	REFERENCES	47

CHAPTER 2
SYNTHESIS AND CHARACTERIZATION
OF DIELECTRIC CERAMICS

2.1	SYNTHESIS OF DIELECTRIC RESONATORS	56
2.1.1	Introduction	56
2.1.2	Solid State Synthesis of Ceramics	57
2.1.2.1	Powder Preparation	58
2.1.2.1.1	Select Appropriate Starting Materials	58
2.1.2.1.2	Weighing of Raw Materials	59
2.1.2.1.3	Stoichiometric Mixing	59
2.1.2.2	Calcination	61
2.1.2.3	Green Body Preparation	61
2.1.2.3.1	Grinding	61
2.1.2.3.2	Addition of Polymeric Binder	62
2.1.2.3.3	Powder Compaction	62
2.1.2.4	Sintering	63

2.1.2.4.1	Solid State Sintering	64
2.1.2.4.2	Liquid Phase Sintering (LPS)	66
2.2	SYNTHESIS OF POLYMER-CERAMIC COMPOSITES	68
2.2.1	Powder Processing Method	68
2.2.2	Sigma Blend Method	68
2.3	STRUCTURAL AND MICROSTRUCTURAL CHARACTERIZATION OF DIELECTRIC RESONATORS	69
2.3.1	X-Ray Diffraction	69
2.3.2	Scanning Electron Microscopy	70
2.3.2.1	Energy Dispersive X-ray Analyzer (EDXA)	71
2.4	MICROWAVE CHARACTERIZATION OF DIELECTRIC MATERIALS	72
2.4.1	Introduction	72
2.4.1.1	Whispering Gallery Mode Resonators	74
2.4.1.2	Split-Post Dielectric Resonator Method	75
2.4.2	Network Analyzer	77
2.4.3	Measurement of Relative Permittivity (ϵ_r)	78
2.4.4	Measurement of Unloaded Quality Factor (Q_u)	81
2.4.5	Measurement of Temperature Coefficient of Resonant Frequency (τ_f)	83
2.4.6	Cavity Perturbation Method	84
2.4.7	Radio Frequency Dielectric Measurements	86
2.4.8	Error Calculations in Dielectric Property Measurements	86
2.5	THERMAL CHARACTERIZATION	87
2.5.1	Thermogravimetric Analysis (TGA) and Differential Thermal Analysis (DTA)	88
2.5.2	Differential Scanning Calorimetry (DSC)	88
2.5.3	Thermo Mechanical Analysis (TMA)	88
2.5.4	Photopyroelectric Technique	89
2.6	REFERENCES	90

CHAPTER 3
CeO₂-AO-TiO₂ (A = Ca, Mg, Zn, Mn, Co, Ni, W) CERAMICS:
SYNTHESIS, CHARACTERIZATION AND MICROWAVE
DIELECTRIC PROPERTIES

3.1	CERIUM DIOXIDE	96
3.1.1	Introduction	96

3.1.2	Fluorite Structure	96
3.2	MILESTONES IN THE RESEARCH OF CeO ₂ CERAMICS	98
3.3	MICROWAVE DIELECTRIC PROPERTIES OF CeO ₂ -AO-TiO ₂ (A= Ca, Mg, Zn, Mn, Co, Ni, W) CERAMICS	100
3.3.1	Introduction	100
3.3.2	Experimental	101
3.3.3	Structural Analysis and Microwave Measurements	101
3.3.4	Optimization of Calcination and Sintering Temperatures	102
3.3.5	Results and Discussion	105
	3.3.5.1 Phase and Microstructural Analysis	105
	3.3.5.2 Microwave Dielectric Properties	109
3.4	EFFECT OF DOPANTS IN CeO ₂ -AO-TiO ₂ (A = Ca, Mg, Zn, Mn, Co, Ni, W) CERAMICS	114
3.4.1	Introduction	114
3.4.2	Experimental	115
3.4.3	Results and Discussion	116
3.5	SYNTHESIS, CHARACTERIZATION AND MICROWAVE DIELECTRIC PROPERTIES OF ATiO ₃ (A = Co, Mn, Ni) CERAMICS	127
3.5.1	Introduction	127
3.5.2	Experimental	128
3.5.3	Results and Discussion	128
	3.5.3.1 Phase and Microstructural Analysis	130
	3.5.3.2 Microwave Dielectric Properties	132
3.6	CONCLUSIONS	135
3.7	REFERENCES	137

CHAPTER 4

MICROWAVE DIELECTRIC PROPERTIES OF BaO-CeO₂-TiO₂ CERAMICS

4.1	SYNTHESIS, CHARACTERIZATION AND MICROWAVE DIELECTRIC PROPERTIES OF BaO-CeO ₂ -TiO ₂ CERAMICS	143
4.1.1	Introduction	143
4.1.2	Experimental	144
4.1.3	Results and Discussion	145
	4.1.3.1 Characterization and Microwave Dielectric Properties of BaO-2CeO ₂ - <i>n</i> TiO ₂ (<i>n</i> = 6.....15) Ceramics	145
	4.1.3.2 Characterization and Microwave Dielectric properties	

	of BaO- p CeO ₂ -4TiO ₂ ($p = 3, \dots, 13$) Ceramics	147
4.2	EFFECT OF DOPANTS ON THE MICROWAVE DIELECTRIC PROPERTIES OF BaO-3CeO ₂ -4TiO ₂ CERAMIC	149
4.2.1	Experimental	149
4.2.2	Results and Discussion	149
4.2.2.1	Phase and Microstructural Analysis	149
4.2.2.2	Microwave Dielectric properties	151
4.3	SYNTHESIS, CHARACTERIZATION AND MICROWAVE DIELECTRIC PROPERTIES OF (1- x)CeO ₂ - x BaTi ₄ O ₉ ($0 \leq x \leq 1$) CERAMICS	154
4.3.1	Introduction	154
4.3.2	Experimental	154
4.3.3	Results and Discussion	155
4.3.3.1	Phase and Microstructural Analysis	155
4.3.3.2	Microwave Dielectric Properties	157
4.4	LOW TEMPERATURE SINTERING AND MICROWAVE DIELECTRIC PROPERTIES OF 0.5CeO ₂ -0.5BaTi ₄ O ₉ CERAMICS	160
4.4.1	Introduction	160
4.4.2	Experimental	160
4.4.3	Results and Discussion	161
4.4.3.1	Phase Analysis	161
4.4.3.2	Microstructural Analysis	162
4.4.3.3	Microwave Dielectric Properties	164
4.5	CONCLUSIONS	168
4.6	REFERENCES	170

CHAPTER 5
LOW TEMPERATURE SINTERING AND MICROWAVE
DELECTRIC PROPERTIES OF Ce₂(WO₄)₃
AND Ba₂CeV₃O₁₁ CERAMICS

5.1	SYNTHESIS, CHARACTERIZATION AND MICROWAVE DIELECTRIC PROPERTIES OF TWO NOVEL DIELECTRIC CERAMICS	175
5.1.1	Introduction	175
5.1.2	Experimental	176
5.1.3	Results and Discussion	177
5.1.3.1	Phase and Microstructural Analysis	179
5.1.3.2	Microwave Dielectric Properties	181

5.2	LOW TEMPERATURE SINTERING AND MICROWAVE DIELECTRIC PROPERTIES OF $\text{Ba}_2\text{CeV}_3\text{O}_{11}$ AND $\text{Ce}_2(\text{WO}_4)_3$ CERAMICS	183
5.2.1	Introduction	183
5.2.2	Experimental	184
5.2.3	Results and Discussion	184
	5.2.3.1 Density and Microstructural Analysis	184
	5.2.3.2 Microwave Dielectric Properties	188
5.3	CONCLUSIONS	191
5.4	REFERENCES	193

CHAPTER 6
MICROWAVE DIELECTRIC PROPERTIES OF
 $\text{Ce}_x\text{RE}_{1-x}\text{O}_{2.8}$ (RE = La, Nd, Sm, Eu, Gd, Dy, Er,
Tm, Yb and Y), $0 \leq x \leq 1$ CERAMICS

6.1	INTRODUCTION	197
6.2	EXPERIMENTAL	199
6.3	RESULTS AND DISCUSSION	200
	6.3.1 Phase Analysis	200
	6.3.2 Microstructural Analysis	202
	6.3.3 Microwave Dielectric Properties	204
6.4	CONCLUSIONS	207
6.5	REFERENCES	209

CHAPTER 7
CERIA BASED COMPOSITES FOR ELECTRONIC
PACKAGING AND SUBSTRATE APPLICATIONS

7.1	CERIA-GLASS COMPOSITES FOR LOW TEMPERATURE COFIRED CERAMIC APPLICATIONS	213
7.1.1	Introduction	213
7.1.2	Experimental	215
7.1.3	Results and Discussion	216
	7.1.3.1 Sintering of Glass Fluxed Ceria	216
	7.1.3.2 Phase Analysis	219
	7.1.3.3 Microstructural Analysis	220

7.1.3.4	Density and Microwave Dielectric Properties	223
7.2	POLYMER-CERIA COMPOSITES FOR MICROWAVE SUBSTRATE APPLICATIONS	230
7.2.1	Introduction	230
7.2.2	Experimental	233
7.2.3	Theoretical Modeling	235
7.2.4	Results and Discussion	239
7.2.4.1	Densification and Microstructural Analysis	239
7.2.4.2	Thermal Analysis	243
7.2.4.3	Dielectric Properties	247
7.3	CERIA-La_{0.5}Sr_{0.5}CoO_{3-δ} COMPOSITES FOR GIANT PERMITTIVITY APPLICATIONS	258
7.3.1	Introduction	258
7.3.2	Experimental	259
7.3.3	Results and Discussion	260
7.3.3.1	Densification of CeO ₂ -LSCO Composites	260
7.3.3.2	Phase and Microstructural Analysis	261
7.3.3.3	Dielectric Properties	263
7.4	CONCLUSIONS	267
7.5	REFERENCES	270
	CHAPTER 8	
	CONCLUSIONS AND FUTURE CHALLENGES	281
	LIST OF PATENTS AND PUBLICATIONS	290

PREFACE

Microwave dielectric materials designed for wireless communications have been a booming area of growth recently. Microwave dielectric materials play a key role in global society with a wide range of applications from terrestrial and satellite communication including software radio, GPS and DBS TV to environmental monitoring via satellites that enable effective communication between people and machines. In order to meet the specifications of the current and future systems, improved or new microwave components based on dielectric materials and new designs are required. The recent advances in materials development has led to the revolutionary changes in wireless communication technology. This revolution is apparent on a daily basis in the ever increasing number of cell phone users. In a new ubiquitous wireless age, therefore, the science and technology of microwave and millimeter wave materials must be activated further.

Dielectric Resonators (DRs) are inevitable component in microwave telecommunication devices and are extensively used as filters, oscillators and dielectric resonator antennas (DRAs). To meet the requirements for use in such practical applications, the materials should possess stringent properties like (a) high relative permittivity (ϵ_r) for miniaturization, (b) high unloaded quality factor (Q_u) or low dielectric loss for better selectivity and (c) low temperature coefficient of resonant frequency (τ_f) for frequency stability with thermal variations of the circuit.

Low Temperature Cofired Ceramic (LTCC) plays a decisive role as a base material in the development of complex miniaturized circuits. LTCC technology enables fabrication of 3-dimensional ceramic modules and substrates with embedded silver or copper electrodes which makes this technology very attractive for variety of micro- and millimetre wave applications. The important requirements for LTCC materials are (a) low sintering temperature ($<960^\circ\text{C}$) to co-fire with inexpensive metals such as silver, (b) permittivity in the range 4-14 for substrates and 15-100 for resonators and internal

capacitors, (c) low dielectric loss or high Q_u (>1000) and (d) low temperature coefficient of resonant frequency ($\tau_f < 10 \text{ ppm}^\circ\text{C}$).

Millimetre wave communication sector now presents new challenging performance requirements. Ceramic filled polymeric materials are used as base substrate for microelectronic packaging. Materials for electronic packaging should be temperature stable with low ϵ_r , low dielectric loss, high thermal conductivity and thermal expansion coefficient matching to that of silicon chips.

This thesis entitled **“INVESTIGATIONS ON CERIA BASED DIELECTRIC CERAMIC MATERIALS FOR WIRELESS COMMUNICATION”** is the outcome of a detailed investigation made on the synthesis, characterization and microwave dielectric properties of ceria based ceramics and tailoring their dielectric properties by different techniques. Accordingly these results are classified into 8 chapters in the thesis.

Chapter 1 gives a general introduction about low loss dielectric resonator materials, low temperature cofired ceramic materials and ceramic filled polymer composites for microwave and millimeter wave applications. The scientific and technological aspects, material requirements and applications of the above said dielectric ceramics are also discussed.

Chapter 2 illustrates the experimental method of conventional solid-state ceramic route for the synthesis of DR and LTCC materials. This chapter also explains the processing techniques adopted for the preparation of polymer composites. The information about instrumental techniques used for the structural, microstructural and dielectric characterization of DR, LTCC and polymer composites have also been summarised.

Chapter 3 outlines a general introduction about fluorite structure and presents the synthesis, characterization and microwave dielectric properties of $\text{CeO}_2\text{-}0.5\text{AO-}0.5\text{TiO}_2$ ($A = \text{Mg, Zn, Ca, Mn, Co, Ni, W}$) ceramics. The synthesizing conditions are optimized for best dielectric properties. These ceramics systems consisting of fluorite CeO_2 and ATiO_3 have relative permittivities (ϵ_r) in the range 17.0 to 65.5 and quality factor Q_{ur} up to 50000 GHz. The τ_f ranges from 399 ppm°C to -62 ppm°C . The effect of various

dopants on the dielectric properties of these ceramics have been investigated. Addition of Cr_2O_3 and WO_3 to $\text{CeO}_2\text{-}0.5\text{CaO-}0.5\text{TiO}_2$ and $\text{CeO}_2\text{-}0.5\text{MgO-}0.5\text{TiO}_2$ system respectively improved the dielectric properties. This chapter also reports the microwave dielectric properties of ATiO_3 ($A = \text{Co, Mn, Ni}$) ceramics for the first time. The microwave dielectric properties of ATiO_3 ($A = \text{Co, Mn, Ni}$) ceramics are reported for the first time as: ϵ_r in the range 19 to 25, Q_{uxf} from 13900 to 62500 GHz and τ_f of about $-50 \text{ ppm}^\circ\text{C}$.

The fourth chapter presents the preparation, characterization and microwave dielectric properties of $\text{BaO-}2\text{CeO}_2\text{-}n\text{TiO}_2$ ($n = 6\text{...}15$) and $\text{BaO-}p\text{CeO}_2\text{-}4\text{TiO}_2$ ($p = 3\text{...}13$) ceramics. $\text{BaO-}2\text{CeO}_2\text{-}n\text{TiO}_2$ ($n = 6\text{...}15$) ceramics are multiphase compounds containing CeO_2 , $\text{Ba}_2\text{Ti}_9\text{O}_{20}$ and TiO_2 while $\text{BaO-}p\text{CeO}_2\text{-}4\text{TiO}_2$ ($p = 3\text{...}13$) ceramics consists of CeO_2 and BaTi_4O_9 phases. The effect of different dopants on the microwave dielectric properties of $\text{BaO-}3\text{CeO}_2\text{-}4\text{TiO}_2$ ceramics is also studied. Addition of CuO to $\text{BaO-}3\text{CeO}_2\text{-}4\text{TiO}_2$ ceramic lowered the preparation temperature with improvement in microwave dielectric properties. Low melting point compounds such as B_2O_3 and CuO is added to lower the sintering temperature of $0.5\text{CeO}_2\text{-}0.5\text{BaTi}_4\text{O}_9$. $0.5\text{CeO}_2\text{-}0.5\text{BaTi}_4\text{O}_9\text{+}12 \text{ wt}\% \text{ B}_2\text{O}_3\text{+}1 \text{ wt}\% \text{ CuO}$ ceramic sintered at 950°C for 4 hours shows $\epsilon_r = 20.6$, $Q_{uxf} = 17000 \text{ GHz}$ and $\tau_f = 48 \text{ ppm}^\circ\text{C}$ and can be considered as a possible candidate for LTCC applications,.

Chapter 5 reports for the first time the microwave dielectric properties of two new cerium based ceramics - $\text{Ce}_2(\text{WO}_4)_3$ and $\text{Ba}_2\text{CeV}_3\text{O}_{11}$ for microwave substrate applications. The $\text{Ce}_2(\text{WO}_4)_3$ and $\text{Ba}_2\text{CeV}_3\text{O}_{11}$ ceramics sintered at 1000 and $1025^\circ\text{C}/4\text{h}$ have relative permittivities of 10.8 and 14.9 with quality factors of 10500 and 12700 GHz and temperature coefficient of resonant frequencies, -39 and $-14 \text{ ppm}^\circ\text{C}$ respectively. The $0.2 \text{ wt}\% \text{ ZBS}$ added $\text{Ce}_2(\text{WO}_4)_3$ ceramic sintered at 900°C and $1 \text{ wt}\% \text{ ZBS}$ glass added $\text{Ba}_2\text{CeV}_3\text{O}_{11}$ ceramic sintered at 825°C are $\epsilon_r = 11.3$ and 15.1 , $Q_{uxf} = 20200$ and 20300 GHz and $\tau_f = -39$ and $-21 \text{ ppm}^\circ\text{C}$ respectively. The $0.2 \text{ wt}\% \text{ ZBS}$ added $\text{Ce}_2(\text{WO}_4)_3$ and $1 \text{ wt}\% \text{ ZBS}$ glass added $\text{Ba}_2\text{CeV}_3\text{O}_{11}$ ceramic are possible candidates for LTCC applications.

The influence of rare earth substitutions in Ce site of CeO₂ ceramics are outlined in Chapter 6. Ceramic compositions in Ce_{1-x}RE_xO_{2-δ} (RE = La, Pr, Nd, Sm, Eu, Gd, Tb, Dy, Er, Tm, Yb and Y), 0 ≤ x ≤ 1 have been prepared and the solubility of different rare earth and yttrium ions in ceria is studied. The microwave dielectric properties of Ce_{1-x}RE_xO_{2-δ} (RE = La, Nd, Sm, Eu, Gd, Dy, Er, Tm, Yb and Y) for different compositions from 0 ≤ x ≤ 1 are reported. The best properties are obtained for Ce_{0.9}Eu_{0.1}O_{1.95} (ε_r = 25.4, Q_{uxf} = 70300 GHz, τ_f = -64 ppm/°C); Ce_{0.8}Dy_{0.2}O_{1.9} (ε_r = 26.2, Q_{uxf} = 70150 GHz, τ_f = -57 ppm/°C) and Ce_{0.3}Sm_{0.7}O_{1.65} (ε_r = 19.7, Q_{uxf} = 79450 GHz, τ_f = -51 ppm/°C).

Ceria based composites for microwave substrate and electronic packaging applications are described in Chapter 7. The first section of this chapter discusses the effect of glass additives on the sintering temperature, density and microwave dielectric properties of ceria for LTCC applications. CeO₂ mixed with 20 wt% B₂O₃ (sintered at 900°C) shows ε_r = 13.2, Q_{uxf} = 24200 GHz, τ_f = -46 ppm/°C and that of CeO₂ added with 10 wt% BBSZ (sintered at 950°C) has ε_r = 22.4, Q_{uxf} = 12000 GHz, τ_f = -57.2 ppm/°C. It is found that silver does not react with ceria mixed with 20 wt% B₂O₃ and 10 wt% BBSZ. The second section of Chapter 7 deals with the polytetrafluoroethylene (PTFE) and high density polyethylene (HDPE) based ceria composites for electronic packaging applications. The dielectric, thermal and mechanical properties of both PTFE and HDPE composites are studied in relation to filler concentration. For 0.6 volume fraction (V_f) loading of the ceramic, the PTFE composite has ε_{eff} = 5 and tan δ = 0.0064 (at 7 GHz), thermal conductivity (k_c) = 1.85 W/m°C, coefficient of thermal expansion (α_c) = 22.9 ppm/°C and Vickers' microhardness of 17 kg/mm². The 0.5 V_f of HDPE-CeO₂ composite has ε_{eff} = 6.9 and tan δ = 0.0085 (at 7 GHz), k_c = 3.22 W/m°C, α_c = 78.5 ppm/°C and Vickers' microhardness of 28 kg/mm². Due to the reasonably good dielectric, thermal and mechanical properties of HDPE composite (0.5 V_f) compared to PTFE composites, 0.5 V_f HDPE-CeO₂ composite can be considered as a possible candidate for microwave substrate applications. The last section of Chapter 7 explains the giant permittivity of CeO₂-La_{0.5}Sr_{0.5}CoO_{3-δ} (LSCO) composites. The relative permittivity is maximum (ε_r > 10⁵) at 0.4 V_f of LSCO at a sintering temperature of 1150°C in CeO₂-

La_{0.5}Sr_{0.5}CoO_{3-δ} (LSCO) composites. CeO₂-LSCO composites can replace the present ceramic-metal composites used in electromechanical and embedded passive devices due to its high relative permittivity.

The conclusions drawn from the present investigations are summarized in Chapter 8. The major achievements of the thesis and scope for future work are also highlighted. The preparation and characterization of LTCC tapes, fabrication of DRAs of different geometries and fabrication of substrates for antenna and printed circuit board applications are proposed for future work.

*******ACKNOWLEDGEMENTS*******

I present this report, in the name of God, the Almighty, who kindly showers HIS unperturbed concern, grace and blessings throughout my life.

I wish to express my deepest sense of gratitude to the man who inspired and guided me to the art of experimenting and creative thinking; Dr. M. T. Sebastian, (Scientist 'G', National Institute for Interdisciplinary Science and Technology, Thiruvananthapuram), my guide and supervisor. Among all the responsibilities and duties, he found time to share his expertise and knowledge, and I am deeply indebted to him for his gentle and inspiring guidance, forbearance, constant encouragement and support, and above all for creating an original thinking and building up a 'dream work culture' in the lab.

I am grateful to Prof. T. K. Chandrasekhar, Director, National Institute for Interdisciplinary Science and Technology (NIIST), Thiruvananthapuram, for kindly providing the facilities. My sincere gratitude is also due to Dr. B. C. Pai (Acting Director, NIIST, Thiruvananthapuram) for his encouragement during the period of my research.

I have been privileged throughout the period of my research work to have the advice and help of Dr. Manoj Raama Varma (Scientist E-II, NIIST, Thiruvananthapuram). I am very grateful to Dr. Jose James (Scientist F, NIIST, Thiruvananthapuram) for his help during my work with fruitful scientific discussions.

I am indebted to Dr. K. G. K. Warriar (Head, Materials and Minerals Division, NIIST, Thiruvananthapuram), Dr. U. Shyama Prasad, Dr. Peter Koshy, Dr. C. Pavitran and Mr. P. Prabhakar Rao (Scientists, MMD, NIIST, Thiruvananthapuram) for their help given during the course of this work. I am thankful to Dr. J. D. Sudha (Polymer Section, NIIST) for all the help rendered by her during my research work.

I wish to express my heartiest thanks to Prof. P. Mohanan (Department of Electronics, Cochin University of Science and Technology (CUSAT), Kochi) for dielectric measurements and Prof. Jacob Philip (Director, Sophisticated Testing and Instrumentation Centre, CUSAT, Kochi) for thermal conductivity measurements of the present study.

I have been privileged to collaborate with Prof. Neil Mc N Alford and Dr. Anna Karin Axelsson and extend my sincere thanks for the recording and analysis of Raman, EDXA and microwave measurements of dielectrics discussed in this thesis.

I want to record thanks to Mr. P. Chandran, Mr. P. Gurusamy, Mr. K. V. Oonnikrishnan Nair and Mr. P. Mukundan for extending the XRD, SEM and thermal measurement facility for this research work. I am thankful to all the office and library staff at NIIST for all the help and cooperation.

The creative suggestions and valuable advice given by my seniors in the lab, Dr. N. Santha, Dr. L. A. Khalam (Sel. Grade Lecturer, Iqbal College, Thiruvananthapuram), Dr. K. P. Surendran (University of Aviero, Portugal), Dr. P. V. Bijumon (Research in Motion, Canada), Dr. I. N. Jawahar (Lecturer, Kerala University) and Dr. H. Sreemoolanadhan (Scientist, VSSC) are thankfully remembered.

I would like to thank all my colleagues and friends in the Materials and Minerals Division of NIIST especially Mr. G. Subodh, Mr. Sumesh George, Ms. T. S. Sasikala, Mr. Tony Joseph, Mr. Dhanesh Thomas, Ms. P. Nisha, Mr. M. A. Sanoj, Ms. C. P. Resmi, Ms. K. S. Deepa, Mr. Jithesh and Mr. S. Biju for their support, love and positive criticism. I am very much indebted to Ms. Sherin Thomas, who has done a lot of favours throughout my research work. They have provided a harmonious research atmosphere, which is absolutely necessary for being creative. I am also thankful to Mr. P. C. Rajath Varma, Ms. R. Rejini, Ms. B. R. Priya Rani, K. S. Sandhya, Ms. Renjini, Mr. Suresh and Mr. Bala who helped me in many ways during my research work.

The favours rendered by Ms. M. N. Suma, Mr. V. Deepu (Department of Electronics, CUSAT), Ms. V. Viji and Ms. Uma (STIC, CUSAT) are greatly acknowledged.

The research fellowship from Council of Scientific and Industrial Research, Government of India, New Delhi, is gratefully acknowledged.

My husband, Dr. N. Gopakumar and my beloved son Neeraj Narayan have shown indefinable patience, love and support during the long and demanding years of hectic research activity. They stood with me in my thick and thin, provided lot of encouragements when it needed me most and their affection, understandability and adjustability throughout these years helped me in the successful and comfortable completion of this work.

I owe an unlimited debt of gratitude to my parents and other family members who have enlighten my paths with their invaluable advice, support and encouragement that contributed a lot to shape my career. I also like to express my deepest sense of gratitude to my parents-in-law for the timely help and moral support.

Last but not least, I want to express my appreciation to all those who have helped me in many ways for the successful completion of this work. I remember that the care and support from all these people gave me the confidence, their encouragement means so much to me throughout those countless hard-working days and nights.

P. S. Anjana

Chapter 1

INTRODUCTION

This chapter gives an overview of introduction and progress of research in dielectric resonators (DR) and low temperature cofired ceramics (LTCC). Historical evolution of dielectric resonators and LTCC research to the forefront of wireless communication applications are discussed. This chapter also gives a general introduction about the scientific and technological aspects of polymer-ceramic composites for substrate applications. The fundamental physical aspects and working principle of dielectric resonators as well as the requirements of the material to act as efficient resonators are described. The practical applications of DRs such as filters, oscillators, antennas etc. are briefly discussed. The important characteristics required for a material for LTCC, electronic packaging and substrate applications are also discussed in detail.

“Material developments underpin advances in almost every industrial sector and are therefore vital to the economic well being of a country.”

1.1 INTRODUCTION

Wireless communications, together with its applications and underlying technologies, is among today's most active areas of technology development. Wireless is a term used to describe telecommunications in which electromagnetic waves carry the signal over part of the entire communication. Wireless communication started around 1897 with Marconi's successful demonstration of wireless telegraphy. The explosive growth of the wireless industry is a driving force behind innovation in fields ranging from telecommunications to environmental research. The wireless technology development is being driven primarily by the transformation of what has been largely a medium for supporting voice telephony into a medium for supporting other services, such as transmission of video, images, text and data. Common examples of wireless equipment in use today are cellular phones and pagers, Global Positioning Systems (GPS), cordless computer peripherals, cordless telephone sets and satellite television. The telecommunication industry is one of the largest industries worldwide, with more than 1.5 trillion dollars in annual revenues for services and equipment. There are about 2.5 billion mobile phone subscribers worldwide. Mobile phone networks allow communication from cell to cell via antennas located on masts and associated base stations. Within a cellular network, the average base station coverage is a diameter of 35 and 18 km at 900 and 1800 MHz, respectively. Each base station houses microwave (MW) resonators that are used to carry signals of a specific frequency and remove (filter) spurious signals and sidebands that interfere with the quality of the transmitted/received frequency band.

The continuing evolution of the ceramic materials and the associated materials technologies is accelerating rapidly with each new technological development supplying more data to the knowledge bank. The successful development and commercialization of high performance ceramic materials has become a focal point of attention at a national level in various countries. *Ceramic* has been defined as “*a nonmetallic solid that is*

prepared from powdered materials, is fabricated into products through the application of heat and displays characteristic properties such as hardness, strength, low electrical conductivity and brittleness."¹ Ceramic materials display a wide range of properties that facilitate their use in many different product areas. **Advanced ceramics** are considered to be those "*functional or structural ceramics with materials excellence, used in high tech applications*". Electroceramics has been consolidated in the last decade as one of the most attractive areas in materials science because of both the improvement of basic knowledge and its technological impact. One of the major achievements of electronic ceramics is the recognition of dielectric materials as energy storage devices, in oscillators and filters for the microwaves carrying the desired information. The performance of electroceramic materials depends on the complex interplay between processing, chemistry, structure at many levels and device physics.

In contrast to many other areas of advanced ceramics, electronic ceramics are represented by an established industrial sector producing high volumes of components. Whilst relatively mature, production volumes are in general growing at annual rates of greater than 10% and in many areas technological development is driven hard by the current market pressures. Recently released industry news in U. S. states that till 1990's 62 % of the total ceramic industry was led by electronic ceramics, 26% by structural ceramics and 12% by ceramic coatings. But at the end of last year electronic ceramic industry witnessed an exponential growth to occupy almost 80% of the total ceramic industry owing to the wide application of electroceramic materials in telecommunication devices.

Fig. 1.1 shows the relative size of the major markets for ceramic-based electronic components on a worldwide basis. It is estimated that the world market for these components is in excess of 10 billion US \$ per annum. Strong drivers in the market place are component size reduction, increased performance and reduced cost. The main competition in most sectors comes from Western Europe, Japan, USA, China, Korea and Taiwan.

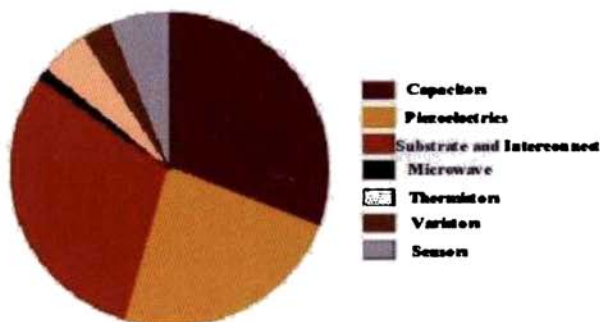


Fig. 1.1 Relative size of electronic ceramic world market sectors (after Ref. 3)

Since early 1950's, microwave technology has been used extensively by the broadcast and cable television industries, as well as in other wireless communication applications. Today, microwaves are employed by telecommunications industries in the form of both terrestrial relays and satellite communications. Frequencies from 0.3-30 GHz are usually called "microwaves". Frequencies above about 30 MHz can pass through the ionosphere and so are available for communicating with satellites and other extra-terrestrial sources. Because of their high frequencies, microwaves have the advantage of being able to carry more information than ordinary radio waves and are capable of being beamed directly from one point to another. Most of the microwave-based device systems are located in the frequency range 300 MHz to 300 GHz as shown in Fig. 1.2.² Frequencies from about 100 MHz to 2 GHz are used for communicating with low earth orbit satellites (LEOs) and 6-24 GHz are useful frequencies for geostationary satcoms. With continuing advances in microwave devices, more systems are being developed for millimeter portion of the microwave band.

1.2 MICROWAVE DIELECTRIC RESONATORS

1.2.1 Introduction

The production of low loss ceramic dielectric resonators has emerged as one of the most rapid growth areas in the electronic manufacturing with the current worldwide explosion in the development of microwave based communication technologies.

According to the statistical reports, the number of mobile phone subscribers worldwide will rise to 3 billion this year and 4 billion by 2010.³

The revolutionary utilization of microwave as a communication media, especially for the satellite communication and land mobile radio systems, has prevented the crowding of channels at radio frequencies. As a consequence, the miniaturization and reduction of the weight of the oscillators and filters were pointed out as the important objectives of innovation. The advances in semiconductor devices, electromagnetic simulators, and nonlinear circuit analysis techniques have made many new microwave component designs possible.

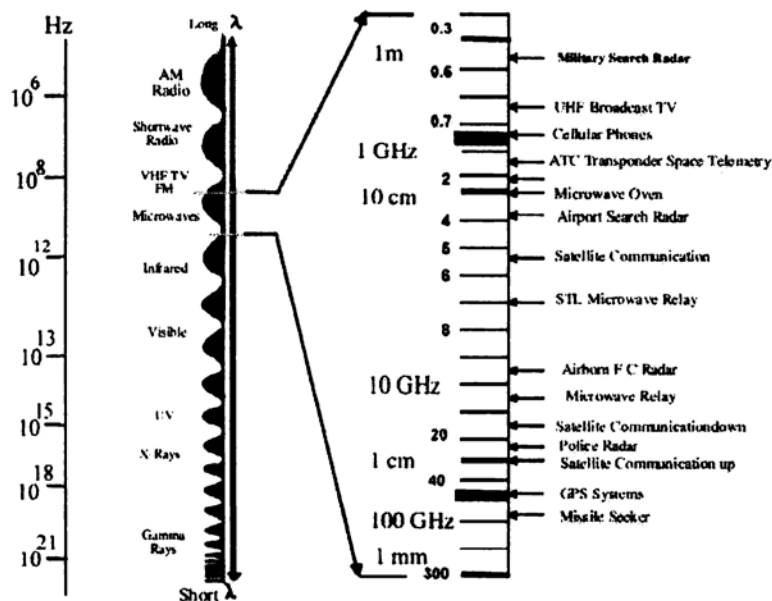


Fig. 1.2 Microwave spectrum and applications (after Ref. 2)

A microwave circuit works when a part of it vibrates or “resonates” at a specific frequency. Where selectivity to that frequency is paramount, e.g. narrow bandwidth applications, low loss temperature-stable dielectric ceramics having a high relative permittivity are utilized. The size of the resonator at any particular frequency depends on

the inverse of the square root of the relative permittivity (ϵ_r) of the material, and thus larger the ϵ_r , the size of the ceramic component may be decreased still maintaining a specific resonant frequency. Further to optimize the signal intensity and the number of channels possible within a given frequency range, the dielectric loss ($\tan \delta$) of the resonator should be low. i.e., the unloaded quality factor, Q_u ($Q_u = 1/\tan \delta$) should be high enough (>2000) to lower the insertion loss and steeper the cut off frequency. Higher Q_u values reduce the risk of cross talk and noise within a given frequency range. To be useful in practical applications, the resonant frequency of the dielectric ceramic should be constant against ambient temperature variation in the microwave circuitry. When the wanted frequency is extracted and detected it is necessary to maintain a strong signal. It is self evident that a material with a significantly non-zero τ_f is useless in a MW circuit as it cannot maintain its resonant frequency, as the base station operating temperature changes.^{4,5}

The quartz resonators were unattractive at microwave frequencies due to small signal to noise ratio with frequency multiplication. When Microwave Integrated Circuits (MIC) were developed in early seventies it was difficult to find devices which could perform these functions but with weight and size features suitable for integration in a miniature circuit. Metallic cavity resonators were tried but were bulky and non-integrable for MIC. Later on microstrip resonators emerged which had poor thermal stability and high dielectric loss. Thus the miniaturization was possible in communication circuits by compromising on the quality factor and temperature stability. All these problems were alleviated with the advent of Ceramic Microwave Dielectric Resonators. *A Dielectric Resonator (DR) is an electromagnetic component, which is a ceramic puck that exhibits resonance with useful properties for a narrow range of frequencies.* DRs are advantageous in terms of compactness, light weight, stability and relatively low cost of production.⁶ In addition, temperature variation of the resonant frequency of dielectric resonators can be engineered to a desired value to meet circuit designer's requirements. The principle of their operation is the ability of the dielectric/air interface to reflect electromagnetic (EM) radiation, and thus the material can sustain a

standing electromagnetic wave within its body. However, the physics of the standing wave in a dielectric is complex due to the fact that EM radiation has both magnetic and electric components.⁷

1.2.2 An Overview of Dielectric Resonator Research

Guided electromagnetic wave propagation in dielectric media received widespread attention in the early days of research in microwaves. In 1894 Lord Rayleigh⁸ discovered that dielectric structures can guide electromagnetic waves, and that fields of these waves extend partially into surrounding space. Surprisingly, substantial efforts in this area predate 1920 and include famous scientists of the era like, Sommerfield, Bose and Debye.⁹ In 1935, in his U. S. patent entitled “Transmission of Guided waves” Southworth¹⁰ disclosed that “The wave guiding structure may take a variety of forms: of which typical is a guide consisting of a rod of dielectric material having high ϵ_r and the specific dielectric guide he considered was a cylindrical specimen of TiO_2 (rutile). The term dielectric resonator first appeared in 1939, when Ritchmyer¹¹ of Stanford University showed that, unmetallised dielectric piece in the form of ‘toroids’ can function as microwave resonators. However, his theoretical investigations failed to generate significant interest and practically nothing happened in this area for over 25 years. During the second quarter of the last century, a lot of work has been done^{12,13,14} on the resonance properties of symmetrical structures like sphere, hemisphere, toroidal ring rectangular blocks etc. However, the first reported work on the adaptability of a high relative permittivity dielectric rod to generate standing wave resonance phenomena was proposed by Schlicke.¹⁵ In 1953, Schlicke reported the application of super-high relative permittivity materials ($\epsilon_r \sim 1000$) as capacitors in low radio frequencies. The theoretical aspects of dielectric rod resonators has aroused a lot of academic interest as the solution of Maxwell’s equation for a cylindrical system is straightforward both for the case of isotropic and anisotropic media.^{16,17} The simple but accurate measurement method for dielectric properties at microwave frequency were developed by Hakki and Coleman using Network Analyzer and Parallel Metal Plate sample holder.¹⁸ Kobayashi improved

this method to measure the loss factor more accurately.¹⁹ These inventions for measurement techniques accelerated the progress of new material development.

During 1960's, Silverman *et al.*²⁰ measured and discussed the mechanism of the dielectric loss of SrTiO₃ crystal at microwave frequencies and Spitzer *et al.*²¹ investigated the far infrared dispersion of SrTiO₃. In early 1960s, researchers from Columbia University, Okaya and Barash reported single crystal TiO₂ resonators. Their papers^{22,23} provided the first analysis of modes and dielectric resonator design parameters. Nevertheless the DR was still far from practical applications.

The first microwave filter, using TiO₂, was proposed by Cohn²⁴ and his co-workers at the Rantec Corporation. Rutile ceramics were used for experiments that had an isotropic relative permittivity of the order of 100. However, its poor temperature stability (+450 ppm/°C) prevented the development of practical components. The research and development work of temperature stable dielectric materials for microwave application started around 1970's. A real breakthrough in the dielectric ceramic industry occurred when the first temperature-stable, low loss barium tetratitanate ceramics were developed by Masse *et al.*²⁵ Konishi²⁶ and Plourde²⁷ developed stacked resonator using dielectric disks having opposite sign of temperature coefficients of resonant frequency. Later, a modified barium tetratitanate with improved performance was reported from Bell Laboratories.²⁸ These positive results led to actual implementations of DRs as microwave components. The materials, however were in scarce supply and thus were not commercially available. The next major breakthrough came from Japan when the Murata Manufacturing Company produced (Zr, Sn)TiO₄ ceramics.²⁹ They offered adjustable compositions so that the temperature coefficient could be varied between +10 and -22 ppm/°C. These components became commercially available at reasonable prices. Afterwards, the experimental and theoretical work as well as the use of DRs expanded rapidly and the search for temperature stable high relative permittivity materials with low dielectric loss has been one of the most challenging problems in Materials Science.

Technological improvements in DRs have contributed to considerable advancements in wireless communications.^{30,31,32,33,34,35,36} This has injected tremendous

interest in the research of DR materials. A simple representation of the trend can be obtained from Fig. 1.3 showing the number of research papers published/patents filed in this area versus year starting from 1980. It can be seen from the figure that last decade has witnessed dramatic increase in the research of DRs, which can be attributed to the revolutionary progress in wireless communication and information access devices in which DRs find immense applications. A good number of reviews are available describing the properties and applications of DRs.^{37,38,39,40,41,42,43}

The dielectric materials with relative permittivity from 20 to 95 are now available for practical use.² These materials should be selected considering the balance between the requirements for various applications and their properties such as ϵ_r (which decide the size of the device), Q_u value and τ_f . Currently available materials² for practical purposes which possess excellent dielectric properties include, $\text{MgTiO}_3\text{-CaTiO}_3$,²⁷ $\text{Ba}[(\text{Sn}, \text{Mg})_{1/3}\text{Ta}_{2/3}]\text{O}_3$,⁴⁴ $\text{Ba}(\text{Mg}_{1/3}, \text{Ta}_{2/3})\text{O}_3$,⁴⁵ $(\text{Zr}, \text{Sn})\text{TiO}_4$,⁴⁶ $\text{Ba}_2\text{Ti}_9\text{O}_{20}$,⁴⁷ $(\text{Ba}, \text{Sr})\text{O-RE}_2\text{O}_3\text{-TiO}_2$,⁴⁸ $\text{Ba}[(\text{Zn}_{0.7}\text{Co}_{0.3})_{1/3}\text{Nb}_{2/3}]\text{O}_3$ etc. Materials with $5 \leq \epsilon_r \leq 140$ and $Q_u \times f > 60000$ GHz and near zero τ_f have been developed.¹⁹ It is noteworthy that still DR materials are needed with a wide variety of dielectric properties to meet the ever-growing demand in various wireless devices. Hence search is continuing to find new materials as well as tailoring the properties of existing materials.

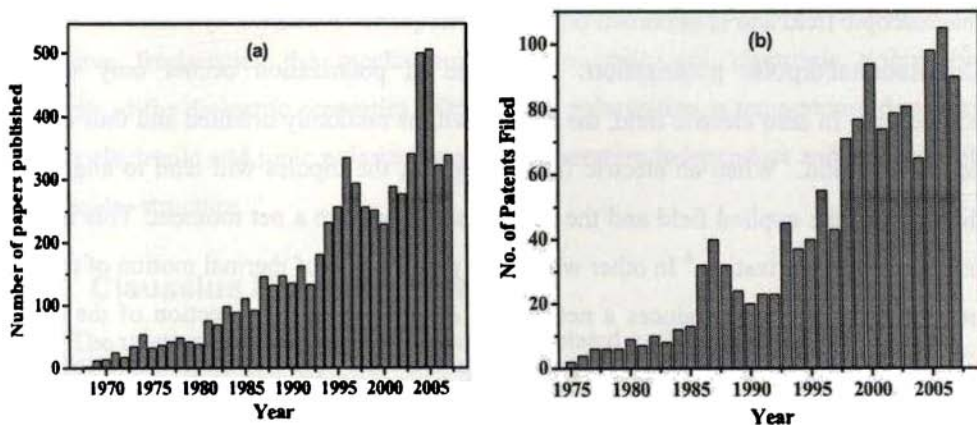


Fig. 1.3 Schematic representation of number of (a) research papers published and (b) patents filed in recent years in DRs (after Ref. 2)

1.3 PHYSICS OF DIELECTRIC RESONATORS

1.3.1 Polarization Mechanisms in Dielectrics

Dielectric polarization is the displacement of charged particles under the action of the electric field so that there is a net electric dipole moment per unit volume in atoms, ions or molecules of the material. At the microscopic level, several dielectric mechanisms can contribute to dielectric behavior. They are interfacial, dipolar, ionic and electronic. Dipole orientation and ionic conduction interact strongly at microwave frequencies. Atomic and electronic mechanisms are relatively weak, and usually constant over the microwave region. Each dielectric mechanism has a characteristic “cutoff frequency.” As frequency increases, the slow mechanisms drop out in turn, leaving the faster ones to contribute to ϵ_r . The loss factor ($\tan \delta$) will correspondingly peak at each critical frequency. The magnitude and “cut off frequency” of each mechanism is unique for different materials.

Space charge/interfacial polarization: Space charge or interfacial polarization occurs when charge carriers are present which can migrate an appreciable distance through a dielectric and which becomes piled up at physical barriers such as grain boundary, interphase boundary etc. This type involves a longer-range ion movement, which give rise to a higher relative permittivity. This process always results in a distortion of the macroscopic field and is important only at low frequencies which may extend to 10^3 Hz.

Orientalional/dipolar polarization: This type of polarization occurs only in polar substances. In zero electric field, the dipoles will be randomly oriented and thus carry no net polarization. When an electric field is applied, the dipoles will tend to align in the direction of the applied field and the materials will acquire a net moment. This is called orientational polarization.⁶ In other words, the perturbation of thermal motion of the ionic or molecular dipoles, produces a net dipolar orientation in the direction of the applied field. Two mechanisms can be operative in this case. (a) In linear dielectrics (non-ferroelectrics) dipolar polarization results from the motion of the charged ions between the interstitial positions in ionic structures parallel to the applied field direction. The

mechanism is active in the 10^3 - 10^6 Hz range. (b) Molecules having permanent dipole moment may be rotated about an equilibrium position against an elastic restoring position. Its frequency of relaxation is very high of the order of $\sim 10^{11}$ Hz. The dipolar polarization contributes to the relative permittivity in the sub-infrared range of frequencies.

Ionic polarization: Ionic polarization is due to a relative displacement of the atomic components of the molecule in the presence of an electric field. In this case the material should have an ionic character. The built in internal dipoles cancel each other and are unable to rotate. The applied external field displaces the ions slightly from their rest positions and thereby inducing net dipoles. The mechanism contributes to the relative permittivity at infrared frequency range ($\sim 10^{12}$ - 10^{13} Hz).

Electronic polarization: The electronic polarization arises from the displacement of electron cloud with respect to the nucleus. This occurs at high frequencies of about 10^{16} GHz. Electronic polarization is present in all materials and, it does not contribute to conductivity or dielectric loss in most dielectrics. The relative permittivity at optical frequencies arises almost entirely from the electronic polarizability. Electronic polarization is responsible for the optical refractive index, η and is a part of relative permittivity in all materials.

Fig. 1.4 shows the variation of dielectric loss and permittivity with frequency. At microwave frequencies the mechanisms due to ionic and electronic polarisation contribute to the dielectric properties. Orientation polarization is temperature dependent whereas electronic and ionic polarizations are temperature independent and are functions of molecular structure.

1.3.2 Claussius Mossotti Equation

The relative permittivity of an insulator is related to the polarizability of atoms comprising it. The permittivity ϵ_r can be calculated theoretically using Clausius Mossotti equation for cubic or isotropic materials⁴⁹

$$\frac{\varepsilon_r - 1}{\varepsilon_r + 2} = \left(\frac{4\pi}{3} \right) \left(\frac{\alpha_D}{V_m} \right) \quad (1.1)$$

Rearranging we get

$$\varepsilon_r = \frac{3V_m + 8\pi\alpha_D}{3V_m - 4\pi\alpha_D} \quad (1.2)$$

where V_m is the molar volume and α_D is the sum of the dielectric polarizabilities of individual ions. The V_m of the dielectric material can be obtained from X-ray diffraction studies. Based on the additivity rule, Shannon states that the molecular polarizabilities α_D of a complex material can be broken up into the molecular polarizabilities of simpler compounds by⁵⁰

$$\alpha_D(A_2A'O_4) = 2\alpha_D(AO) + \alpha_D(A'O_2) \quad (1.3)$$

where A are the cations. Furthermore, it is possible to break up the molecular polarizabilities of complex compounds into ions according to

$$\alpha(A_2A'O_4) = 2\alpha(A^{2+}) + \alpha(A^{4+}) + 4\alpha(O^{2-}) \quad (1.4)$$

The dielectric polarizabilities of several ions are reported by Shannon.⁵⁰ The calculated ε_r usually agree well with porosity-corrected experimental values for well-behaved ceramics.⁵⁰ It may be noted that deviations from calculated values can occur due to deviations from cubic symmetry, and also the fact that the sample is ceramic and not a single crystal. Presence of ionic or electronic conductivity, H₂O or CO₂ in channels, rattling of ions, presence of dipolar impurities or ferroelectric behavior also cause deviations from the calculated values.⁵⁰ The deviations in the reported values of dielectric polarizability and even a small error in determining the cell volume can significantly affect the calculated value of the permittivity. Vineis *et al.* reported⁵¹ that a more correct value of the dielectric polarizability of La is 4.82 instead of 6.12 reported by Shannon.⁵⁰ The ε_r depends on the dielectric polarizability of the constituent ions and the crystal structure.

Differentiating equation (1.1)^{52,53}

$$\frac{1}{(\epsilon_r - 1)(\epsilon_r + 2)} \left(\frac{\delta \epsilon_r}{\delta T} \right)_P = -\frac{1}{3V_m} \left(\frac{\delta V_m}{\delta T} \right)_P + \frac{V_m}{\alpha_D} \left(\frac{\delta \alpha_D}{\delta V_m} \right)_T - \frac{1}{3V_m} \left(\frac{\delta V_m}{\delta T} \right)_P + \frac{1}{3\alpha_D} \left(\frac{\delta \alpha_D}{\delta T} \right)_{V_m} \quad (1.5)$$

The first term represents the thermal expansion and its effect produces a decrease in the concentration of the dipoles. The minus sign indicates that its contribution is negative. The number of polarizable ions per unit volume decreases as the temperature increases. The second term represents the possibility that the polarization will increase with increasing volume in which ions are able to move as the temperature increases. This contribution is positive unless $(\delta V/\delta T)_P$ becomes negative which is unlikely. The third term represents the direct dependence of polarizability on temperature, the volume remaining constant. In general this contribution is negative since ϵ_r decreases with increase of temperature. Bosman and Havinga⁵² reported that for low ϵ_r materials the permittivity increased with increasing temperature whereas for high ϵ_r materials the permittivity decreased with temperature. The ϵ_r decreased with increase of pressure for all the materials they measured.

1.3.3 Working Principle of Dielectric Resonators

A piece of dielectric with high relative permittivity can confine microwave energy at a few discrete frequencies through total multiple internal reflections, provided that the energy is fed in the appropriate direction. The electromagnetic wave moving from the electrically dense high dielectric region to the electrically thin air meets very high impedance at the dielectric-air interface and reflects back to the dielectric itself. As the relative permittivity increases the impedance offered by the boundary also increase to allow better confinement of energy within the dielectric body. (See Fig. 1.5).

The reflection coefficient approaches unity when the relative permittivity approaches infinity. The trapped electromagnetic waves will form standing waves to generate resonance. A high relative permittivity material can confine most of the standing electromagnetic wave within its volume. If the transverse dimensions of the dielectric are

comparable to the wave length of the microwave, then certain field distributions or modes will satisfy Maxwell's equations and boundary conditions⁵⁴ and only those modes satisfying this condition will be excited. The frequency of the generated resonating modes depends on the dimensions and relative permittivity of the dielectric specimen.

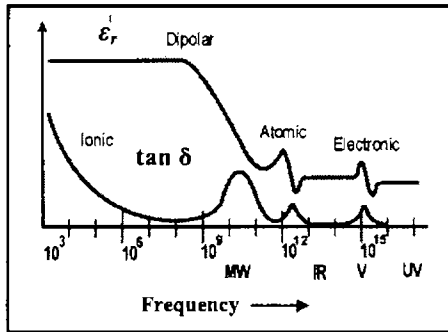


Fig. 1.4 Frequency response of dielectric mechanisms (courtesy en.wikipedia.org/wiki/Dielectric_spectroscopy)

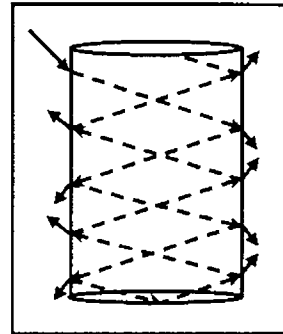


Fig. 1.5 Sketch of total multiple internal reflections in DR

For microwaves the free space wavelength (λ_0) is of the order of a few centimeters and on entering the material with ϵ_r in the range 20-100, the wavelength (λ_d) inside the dielectric will be in millimeters. The electromagnetic fields outside the dielectric sample decay rapidly. One can prevent radiation losses by placing the DR in a small metallic enclosure. Since only a small radiation field sees the metallic surface, the resulting conduction loss will be too small and can be neglected.⁵⁵

1.3.4 Resonance

A bulk dielectric material excited for resonance using microwave energy is equivalent to a parallel *LCR* resonant circuit. Hence the alternating field will have inductive, capacitive and resistive components. All the three components, capacitor (*C*), inductor (*L*) and ohmic resistance (*R*) in the circuit have a common voltage $v(t) = |V| \cos \omega t$. From the fundamental rules of resonant electrical circuits, the electric energy stored in the capacitor is given as⁵⁶

$$W_e(t) = \frac{1}{2} C [v(t)]^2 = \frac{1}{2} C |V|^2 \cos^2(\omega t) \quad (1.6)$$

and magnetic energy stored in the inductor is

$$W_m(t) = \frac{1}{2} L [i(t)]^2 = \frac{|V|^2}{2\omega^2 L} \sin^2(\omega t) \quad (1.7)$$

The stored electric energy is thus proportional to \cos^2 function and the stored magnetic energy is proportional to \sin^2 function of time. As functions of time, the stored energies $W_e(t)$ and $W_m(t)$ fluctuate between zero and their maximum values $W_{e,max}$ and $W_{m,max}$. The average values W_e and W_m are equal to one half of the corresponding maximum values. At resonance, capacitive and inductive reactances become equal and opposite to vanish. Hence the impedance of the circuit equals the ohmic resistance and maximum energy storage takes place within the body of the dielectric resonator.

At this condition

$$\omega = \omega_{res} = \frac{1}{\sqrt{LC}} \quad (1.8)$$

The maximum stored energy W_{max} will be the sum of the stored energy in capacitor (W_e) and inductor (W_m). Since the average energy values are equal to one half of their peak values,

$$W_{max} = 2W_e = 2W_m = W_e + W_m \quad (1.9)$$

In terms of the average stored energies, definition of Q at resonance becomes⁵⁷

$$Q = \left[\frac{\omega(W_e + W_m)}{P_d} \right]_{\omega=\omega_{res}} \quad (1.10)$$

If the operational frequency is not equal to the resonant frequency, the peak of the stored electric energy is not equal to the peak of the stored magnetic energy. Therefore the definition of Q is not unique at any frequency other than ω_{res} .

A microwave resonator has infinite number of resonant modes, each of them corresponding to a particular resonant frequency, at which the electric stored energy is equal to the magnetic one. In the narrow band of frequencies around each of the resonant frequencies, the cavity impedance is equal to the impedance of a simple LCR resonant

circuit, characterized by the Q factor of that particular resonant mode.⁵² Fig. 1.6 shows the schematic diagram of a DR coupled to TE_{018} and TM_{018} mode.

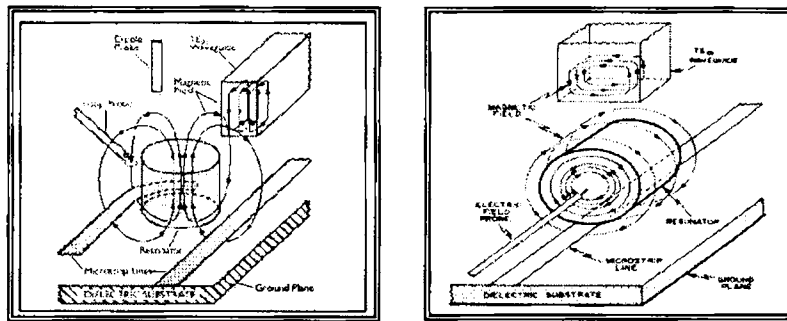


Fig. 1.6 Dielectric Resonator coupled to (a) TE_{018} mode and (b) TM_{018} mode (after Ref. 38)

1.3.5 DR in a Circuit

DR is usually placed near a microstrip line in microstrip circuits. The equivalent circuit consists of a parallel resonance circuit and an ideal transformer, which models the coupling between DR and the microstrip line (having transformation ratio n)

The Fig 1.7 shows a schematic representation of a DR coupled to a microstrip line. The parallel equivalent impedance in series with the microstrip line may be written as

$$Z = \left[\frac{n^2}{R_o} + j \left(2\pi f_o n^2 C_o - \frac{n^2}{2\pi f_o L_o} \right) \right]^{-1} \quad (1.11)$$

where f_o is the resonance frequency and n is given by

$$n = \sqrt{\frac{Q_l R_o}{Q_u (Z_g + Z_l)}} \quad (1.12)$$

where Q_l and Q_u are the loaded and unloaded quality factors of the DR respectively. Using Eqn. 1.7, the expressions for ohmic resistive, capacitive and inductive parts of the DR equivalent circuit may be obtained as

$$\frac{R_o}{n^2} = \frac{Q_u (Z_g + Z_l)}{Q_l} \quad (1.13)$$

$$n^2 C_o = \frac{1}{2\pi f_o} \frac{Q_l}{(Z_g + Z_l)} \quad (1.14)$$

$$\frac{L_o}{n^2} = \frac{1}{2\pi f_o} \frac{(Z_g + Z_l)}{Q_l} \quad (1.15)$$

The loaded quality factor Q_l is expressed⁵⁸ as

$$Q_l = \frac{2\pi f_o (Z_g + Z_l) W_m}{E^2} \quad (1.16)$$

where W_m is the stored magnetic energy in the DR and E is the voltage induced into the microstripline which is computed using

$$E = \int_l \vec{E} \cdot d\vec{l} \quad (1.17)$$

The unloaded quality factor depends on the elements of the equivalent circuit

$$Q_u = \frac{R_o}{2\pi f_o L_o} = 2\pi f_o C_o R_o \quad (1.18)$$

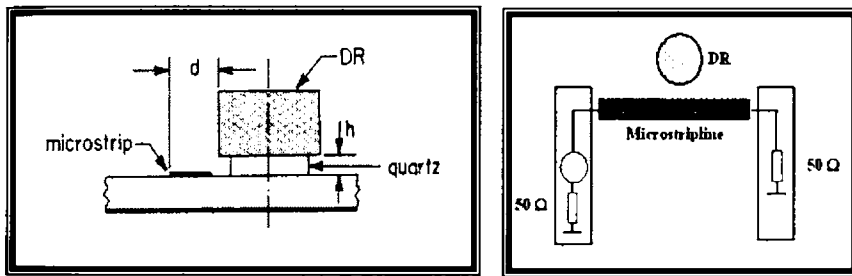


Fig. 1.7 DR as circuit element coupled to a microstripline (left) and its equivalent circuit (right) (after Ref. 38)

1.3.6 Modes and Mode Nomenclature

A microwave resonator has infinite number of resonant modes, each of them corresponding to a particular resonant frequency, at which the electric stored energy is equal to the magnetic one. The excited modes can be classified into three distinct types: TE , TM and hybrid. The fields for TE and TM modes are axisymmetric whereas hybrid modes are azimuthally dependent. The hybrid modes can again be categorized into HE and EH . According to the mode nomenclature described by Kobayashi *et al.*,^{59,60} the variation of fields along the azimuthal, radial and Z -direction inside the resonator, are denoted by adding mode indices as subscripts to each family of modes. This

nomenclature is historically based on the mode nomenclature of cylindrical dielectric waveguides. The TE , TM , HE and EH modes are classified as $TE_{nmp+\delta}$, $TM_{nmp+\delta}$, $HE_{nmp+\delta}$ and $EH_{nmp+\delta}$ respectively. The first index denotes the number of full-period field variations in azimuthal direction, the index m ($m = 1, 2, 3, \dots$) denotes the order of variation of the field along the radial direction and the index $p+\delta$ ($p = 0, 1, 2, \dots$) denotes the order of variation of the fields along the Z -direction.

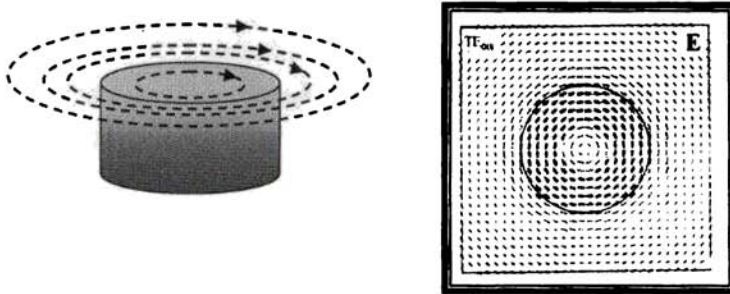


Fig. 1.8 Electric field distribution of $TE_{01\delta}$ mode in equatorial plane (after Ref. 38)

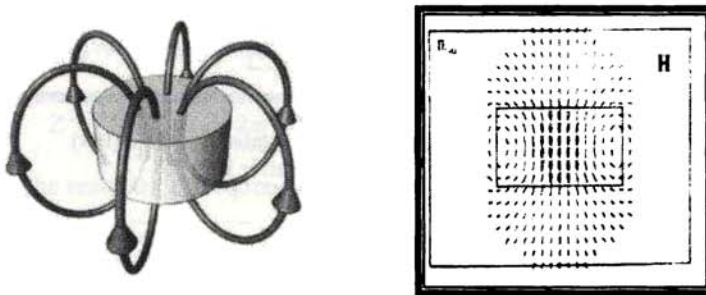


Fig. 1.9 Magnetic field distribution of $TE_{01\delta}$ in the meridian plane (after Ref. 38)

The resonant mode most often used in shielded microwave circuits is $TE_{01\delta}$. It is a transverse electrical mode having azimuthal symmetry $\partial/\partial\phi = 0$, and less than a half cycle variation in field in the z -direction. Here, the third index, denotes the fact that the dielectric resonator is shorter than one-half wavelength. The actual value of δ depends on the relative permittivity of the resonator and the substrate, and on the proximity to the top

and bottom conductor plates. Fig. 1.8 shows the typical field distributions for $TE_{01\delta}$ mode and Fig. 1.9 shows the typical field distributions for $TE_{01\delta}$ mode of a cylindrical dielectric resonator. The magnitude of the electrical field component is zero at the centre of the resonator and has a maximum value at around $x = 2r/3$ where r is the radius of the disk. Outside the resonator, the field decays exponentially. The field variation as a function of radial distance remains the same in different planes parallel to the equatorial plane.⁶¹

1.4 TYPES OF DIELECTRIC RESONATORS



Fig. 1.10 Different types of Dielectric Resonators (courtesy www.ntktech.com/product_detail.asp?productid=91)

The shape of a DR is usually a solid cylinder but can also be tubular, spherical and parallelepiped (Fig. 1.10). The resonant frequency of modes can be tuned by inserting metal or ferrite screws into the central hole of a ring resonator. Similar techniques are used to avoid interference of unwanted modes with the desired mode in a DR by suppressing the modes and thereby reducing the dielectric loss. The mode spectrum and resonant frequencies of DRs greatly depend on the aspect ratio (diameter D /length L). The dimensions of the specimen are important to achieve wide separation of modes. The proper aspect ratios are 1.0 to 1.3 and 1.9 to 2.3. In practice the specimen diameters in the range 7 to 25 mm have been found most suitable.

1.5 MATERIAL REQUIREMENTS FOR DR APPLICATIONS

Due to the development in microwave communication systems, how to design the high quality devices is very important. In order to achieve minimum dimension for the devices and for the systems to work with high efficiency and stability, microwave designers require dielectric materials with apt properties. The advantage of using dielectric materials is that they have the potential for miniaturization. For the ceramic to be usable as a dielectric resonator/filter, three key properties need to be optimized and are described in the following section.

1.5.1 High Relative Permittivity (ϵ_r)

A Dielectric Resonator (DR) can confine electromagnetic waves through total multiple internal reflections at the dielectric-air interface. If the DR is resonating at a frequency f_o , then the maximum wavelength it can have is related to the relative permittivity of the material by the following equation:

$$f_o \approx \frac{c}{\lambda D \sqrt{\epsilon_r}} \approx \frac{c}{D \sqrt{\epsilon_r}} \quad (1.19)$$

where c is the velocity of light in vacuum and λ is the wavelength of the standing wave along the diameter (D) of a resonator. Consequently, if the permittivity is increased, the size of the resonator may be decreased while still maintaining a specific resonant frequency. In the microwave frequency range, ionic polarization is the main factor contributing towards the relative permittivity. Hence materials containing ions with large ionic polarizabilities are needed for sufficiently high ϵ_r . According to classical dispersion theory, the crystal is approximated as a system of damped oscillators having an appropriate frequency and dipole moment. The real and imaginary parts of the complex relative permittivity (ϵ' , ϵ'') as functions of ω (where $\omega = 2\pi\nu$) are given by

$$\epsilon'(\omega) = \epsilon_\infty + \sum_j \frac{4\pi\rho_j(\omega_j^2 - \omega^2)\omega_j^2}{(\omega_j - \omega^2)^2 + (\gamma_j\omega)^2} \quad (1.20)$$

where $4\pi\rho_j$ is the oscillator strength, ω_j is the resonant angular frequency of the j^{th} oscillator, ϵ_∞ is the relative permittivity caused by electronic polarization at higher

frequencies and γ_j is the damping constant which is given by the width of the peak. The summation is over the j resonances in the spectrum. Each resonance is characterized by its dispersion parameters. For $\omega_j \gg \omega$,

$$\varepsilon'(\omega) = \varepsilon_\infty + \sum_j 4\pi\rho_j \quad (1.21)$$

The above equation shows that relative permittivity is independent of frequency in the microwave frequency region. Using Far-Infrared spectroscopy, the reflectance as well as transmittance can be recorded. From the reflection band, ε_r is calculated using Krammer-Kronig Analysis⁶² and classical dispersion theory. The method gives an indirect estimation of the relative permittivity. In the microwave frequency region ε_r is measured from the resonance spectra using the resonance method which is explained in the next chapter.

1.5.2 High Quality Factor (Low Dielectric Loss)

The figure of merit for assessing the performance or quality of a resonator is Q -factor. It is the efficiency of a resonant circuit to confine electromagnetic energy. Fields inside a resonator store energy at the resonant frequency where equal storage of electric and magnetic energies occur. It is a measure of energy loss or dissipation per cycle as compared to the energy stored in the fields inside the resonator. Q factor is defined by⁶³

$$Q = \frac{\text{Maximum Energy Stored per cycle}}{\text{Average Energy Dissipated per cycle}}$$

$$Q = \frac{2\pi W_0}{PT} = \frac{\omega_0 W_0}{P} \quad (1.22)$$

where W_0 is the stored energy, P is power dissipation, ω_0 is resonant radian frequency and period $T = \frac{2\pi}{\omega_0}$. In the case of bulk ceramics energized by electromagnetic wave, quality factor is roughly the inverse of dielectric loss of the material. For an electrically resonant system, the Q factor represents the effect of electrical resistance and, for electromechanical resonators such as quartz crystals it represents the mechanical friction.

In microwave communications, Quality factor is determined as the resonant frequency (f_o) divided by the bandwidth, Δf , measured at 3dB below the maximum height at resonance.

$$Q = \frac{\omega_o}{\Delta\omega} = \frac{f_o}{\Delta f} \quad (1.23)$$

It is therefore a direct measure of the ability of the resonating body to select a given frequency. The dielectric Q factor Q_d for homogeneous dielectric material is given by

$$Q_d = \frac{1}{\tan \delta} \quad (1.24)$$

When a resonant circuit or cavity is used as a load in a microwave circuit, several different Q factors can be defined. First Q accounts for internal losses, which is the unloaded Q factor (Q_u). Next external quality factor (Q_e), accounts for external losses. When the resonator is used or attached to some external circuit there arises the loaded Q factor (Q_L) which is the overall Q factor and includes both internal and external losses.

For cavity resonators, power loss by conductors, dielectric fills and radiation can contribute to unloaded Q . The conductor loss is due to the contact between the metallic cavity and DR, radiation loss is due to the evanescent field decaying out from the DR surface and dielectric loss is the intrinsic loss of the material.

$$\frac{1}{Q_u} = \frac{1}{Q_c} + \frac{1}{Q_d} + \frac{1}{Q_r} \quad (1.25)$$

where Q_c is the conduction Q factor, Q_d is the dielectric Q factor and Q_r the radiation Q factor. When the resonator is connected to load

$$\frac{1}{Q_L} = \frac{1}{Q_e} + \frac{1}{Q_o} \quad (1.26)$$

where Q_L is the loaded Q factor, Q_e the external Q factor and Q_o the unloaded Q factor. It should also be noted that in the case of an isolated DR, $Q_d = Q_u$ as a general convention. However, the quality factor of a DR can only be measured as the loaded value (Q_L) by keeping in an external circuit. Hence it is necessary to have a relation between the two forms of quality factor (Q_u and Q_L) and is represented as

$$Q_u = Q_L(1 + \beta) \quad (1.27)$$

where β is termed as the coupling coefficient given by

$$\beta = \frac{P_e}{P_u} \quad (1.28)$$

P_e is the power loss due to external factors and P_u is the sum of that due to conductor, dielectric and radiation.

Classical dispersion theory⁶⁴ predicts that at microwave frequencies, relative permittivity is independent of frequency and $\tan \delta$ is proportional to frequency (f), since

$$\tan \delta = (\gamma / \omega_T^2) f \quad (1.29)$$

where γ is the damping factor and ω_T is the resonant frequency of the optical mode of the lattice vibration. Hence Q_u decreases with increasing frequency. Hence $Q_u \omega f$ is often quoted while comparing ceramics.

1.5.3 Small Temperature Coefficient of Resonant Frequency (τ_f)

The coefficient of temperature variation of resonant frequency (τ_f) is a measure of the “drift” of resonant frequency with respect to the temperature. The frequency of standing wave is given by Eqn. (1.30). When temperature changes, then the resonant frequency f_0 changes due to the variation in ϵ_r and L length of the dielectric material. Differentiating this equation with respect to temperature gives

$$\frac{1}{f_0} \cdot \frac{\delta f_0}{\delta T} = \frac{-1}{L} \cdot \frac{\delta L}{\delta T} - \frac{1}{2} \cdot \frac{1}{\epsilon_r} \cdot \frac{\delta \epsilon_r}{\delta T} \quad (1.30)$$

where $\frac{1}{f_0} \cdot \frac{\delta f_0}{\delta T}$ is the temperature coefficient of resonant frequency (τ_f), $\frac{1}{L} \cdot \frac{\delta L}{\delta T}$ is the linear expansion coefficient (α_L) and $\frac{1}{\epsilon_r} \cdot \frac{\delta \epsilon_r}{\delta T}$ is the temperature coefficient of permittivity (τ_ϵ).

Substituting these values in the above equation, the expression for τ_f becomes

$$\tau_f = -\left(\alpha_L + \frac{\tau_\epsilon}{2}\right) \quad (1.31)$$

The temperature coefficient of resonant frequency (τ_f) is the parameter which indicates the thermal stability of the resonator. The τ_f can be defined mathematically in terms of resonant frequency and temperature as,

$$\tau_f = \frac{1}{f_0} \times \frac{\Delta f}{\Delta T} \quad (1.32)$$

where f_0 is the resonant frequency and Δf is the variation of resonant frequency with a change in temperature ΔT .

The value of τ_f should be near to zero for practical applications. It is self-evident that a material with a significantly non-zero τ_f is useless in a microwave circuit as it cannot maintain its resonant frequency as the base station operating temperature changes. In reality, a small non-zero value of τ_f is required to compensate for thermal expansion of the microwave cavity and other components in the circuit.

1.6 FACTORS AFFECTING MICROWAVE DIELECTRIC PROPERTIES

Microwave dielectric properties are influenced by a number of factors, such as permittivity⁶⁵, onset of phase transitions^{66,67}, processing conditions, raw material impurities^{68,69} and order/disorder behavior and porosity.^{32,70} The following section discusses the factors that control their properties.

The optimization of quality factor is essential to maximize commercial exploitation of the available bandwidth. It is the least understood of the three key parameters (ϵ_r , $Q_u \times f$, τ_f) and is composition, processing, structure and microstructure dependent. The dielectric loss is the result of a combined contribution of the degree of crystal structure imperfection, microstructural inhomogeneity and interaction of phonons. Ceramics with microstructural inhomogeneities such as relaxation of space charges or dipoles which lie either between matrix grains and inclusions, or at grain boundaries have higher losses (low Q_u). Such inhomogeneities may arise due to secondary phases, impurity segregation, incomplete densification etc. It is found that the quality factor of a

ceramic is increased with increase in bulk density, provided the densification is promoted by solid state diffusion mechanism. Hence glassy phase formation may be avoided during sintering to get high quality factor. Because of the natural difficulties involved in getting ceramics with reproducible in microstructures, it is essential that the ceramic is at least composed of a single phase with homogeneous microstructure to have as high Q_u as possible.

The structural factors that are involved in loss mechanism include lattice defects, distortion of symmetry, mass of ions, cation ordering etc. The dielectric loss tangent of microwave dielectrics ($\tan \delta$) is brought about by the effect of anharmonic terms in the potential energy on the mean separation of a pair of atoms and is increased by lattice imperfections in the crystal. The dielectric loss caused by the anharmonic terms increases at higher temperatures. The random distribution of ions also is considered to be a kind of imperfection in the atomic ordering. The Q factor of the ordered ceramics would be much greater than the less ordered ceramics. Any type of defects such as grain boundaries, stacking faults, chemical or structural disorder, point defects, planar defects, line defects, inclusions, secondary phases, twinning, porosity etc. contribute losses. In the microwave region, the intrinsic loss is mainly due to the interaction of the applied field with phonons. This leads to dampening of the phonon modes of fundamental lattice.

1.6.1 Effect of Humidity

The $\tan \delta$ increases with increasing porosity due to collection of moisture in the pores. Humidity effects on low frequency dielectric properties of porous materials have been studied.^{71,72} Jonscher⁷³ identified low frequency loss mechanism in porous materials in the presence of moisture, and Tinga *et al.*⁷⁴ studied the effect in some materials at microwaves. It is clear that the relaxation process centered at low frequency is responsible for high dielectric loss over a wide frequency range extending into the microwave range. The humidity effects on low frequency dielectric properties of porous materials have been associated to the liberation of ions tightly bound in the dry condition. In contact with an adsorbed water film, these ions become free to move over extended

regions. This mechanism would produce an interfacial polarization process giving rise to a low frequency peak. Charge carriers could also be produced by an electrochemical process of dissociation of water into a proton and a hydroxyl ion.⁷⁵

1.6.2 Effect of Porosity

(a) Relative permittivity

The dielectric is a composite system of two dielectrics (dielectric material and porosity) with different relative permittivities. Consider the dielectric as parallel layers of two dielectrics having volume fractions V_1 and V_2 and relative permittivities ϵ_1 ($\epsilon_1 = \epsilon_m$, dielectric phase) and ϵ_2 ($\epsilon_2 = 1$, porosity) respectively. There are two possible configurations

(a) Electric field is perpendicular to the plane of the plates.⁷⁶ Then

$$\epsilon' = \epsilon_m - P(\epsilon_m - 1) \quad (1.33)$$

(b) If electric field is perpendicular to the plane of the plates,

$$\epsilon' = \frac{\epsilon_m}{P(\epsilon_m - 1) + 1} \quad (1.34)$$

Maxwell⁸⁰ derived a realistic model of spherical particles of relative permittivity ϵ_d in a dielectric matrix ϵ_m . The relative permittivity of the mixture is given by

$$\epsilon' = \frac{V_m \epsilon_m \left(\frac{2}{3} + \frac{\epsilon_d}{3\epsilon_m} \right) + V_d \epsilon_d}{V_m \left(\frac{2}{3} + \frac{\epsilon_d}{3\epsilon_m} \right) + V_d} \quad (1.35)$$

If the spheres are pores and applying a linearized approximation⁷⁷ for $\epsilon_m - \epsilon' \ll \epsilon_m$, then the above equation becomes

$$\epsilon' = \epsilon_m \left(1 - \frac{3P(\epsilon_m - 1)}{2\epsilon_m + 1} \right) \quad (1.36)$$

(b) Dielectric loss ($\tan \delta$)

The complex permittivity of a material is given by

$$\epsilon = \epsilon' - i\epsilon'' \quad (1.37)$$

Real component ϵ' is relative permittivity and imaginary component ϵ'' describes the dissipation of the electric field.

$$\text{Dielectric loss tangent, } \tan \delta = \frac{\epsilon''}{\epsilon'} \quad (1.38)$$

$$\text{Quality factor, } Q = \frac{1}{\tan \delta} \quad (1.39)$$

The loss increases with porosity and an additional term to loss is introduced. Plot of $\tan \delta$ against porosity on a log-log plot suggested a straight line which would give a dependence of the form,

$$\tan \delta = (1 - P) \tan \delta_o + AP^n \quad (1.40)$$

$\tan \delta_o$ is the loss tangent of fully dense material which depends on the amount of material present i.e., it should depend on the porosity. The above equation can be put in the form of law of mixtures as

$$\tan \delta = (1 - P) \tan \delta_o + P(AP^{n-1}) \quad (1.41)$$

The loss may be related to the surface area of the pore volume, S

$$\tan \delta = (1 - P) \tan \delta_o + P(A'S) \quad (1.42)$$

From sintering theory, surface area of the pores varies with porosity as

$$S \propto \left(\frac{P}{1-P} \right)^{2/3} \quad (1.43)$$

Substituting the above equation in equation. (1.42), we get ⁷⁸

$$\tan \delta = (1 - P) \tan \delta_o + A'P \left[\frac{P}{1-P} \right]^{2/3} \quad (1.44)$$

1.7 APPLICATIONS OF DIELECTRIC RESONATORS

Functioning as important components in communication circuits, DRs can create and filter frequencies in oscillators, amplifiers and tuners. DRs find applications in low noise block converters for digital broadcasting systems, microwave filters, security systems, telemetry, detectors, auto cruise control of radar systems, wireless communication equipments, cellular base stations, global positioning systems, satellite

multiplexing filter devices, high stability dielectric resonator oscillators, microwave duplexers, etc. All these applications of DRs may be categorized based on their ability to determine and stabilize the frequency of a microwave oscillator or as a resonant element in a microwave filter.

1.7.1 Dielectric Resonator Oscillators (DRO)

Dielectric Resonator Oscillators (DROs) are used widely in today's electronic warfare, missile, radar, communication systems and other signal receiving and/or transmitting systems. Their popularity has been attributed to their high- Q , low loss, and conveniently sized devices for various applications in the RF and microwave fields.

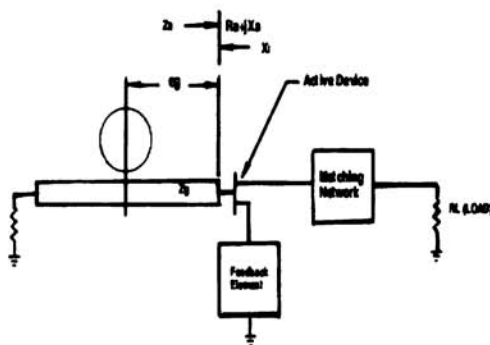


Fig. 1.11 Schematic diagram of the series feedback DRO (courtesy www.gedlm.com/DRO/DRO.asp)



Fig. 1.12 Diagram of the series feedback DRO (courtesy www.emfsystems.com/500.htm)

The DROs are characterized by low phase noise, compact size, frequency stability with temperature, ease of integration with other hybrid MIC circuitries, simple construction and the ability to withstand harsh environments. These characteristics make DROs a natural choice both for fundamental oscillators and as the sources for oscillators that are phase-locked to reference frequencies, such as crystal oscillators. The oscillation frequency of a dielectric resonator oscillator depends on its dimensions and on the electromagnetic properties of its environment. Fig. 1.11 shows the schematic diagram of the series feedback DRO. A GaAs FET or a Si-bipolar transistor is chosen as the active

device for the oscillator portion of the DRO circuit. The Si-bipolar transistor is generally selected for lower phase noise characteristics, while the GaAs FET is required for higher frequencies. Fig. 1.12 shows a commonly used series feedback DRO.

1.7.2 Dielectric Resonator Antennas (DRA)

Dielectric resonator antennas (DRA) are attractive as alternative to microstrip antennas in microwave communication. Dielectric resonator placed over the ground plane can serve as an effective radiator since the electromagnetic waves extends beyond the geometrical boundary of the cavity.⁷⁹ Dielectric Resonators (DRs) are preferred because they are easy to fabricate and offer more degree of freedom to control the resonant frequency and quality factor.⁸⁰ The Dielectric resonator Antennas (DRA) have attracted the antenna designers in microwave and millimeter band due to its features like high radiation efficiency, low temperature coefficient of frequency, zero conductor losses, mechanical simplicity, large impedance bandwidth,⁸¹ simple coupling schemes to all commonly used transmission line,⁸² and more resistant to proximity detuning when placed close to another object. The use of low-loss materials and the small influence of conductor losses permit to achieve high radiation efficiency. The bandwidth can be controlled over a wide range by the choice of dielectric constant, and the geometric parameters of the resonator. DRs with $30 < \epsilon_r < 60$ is ideally suitable for antenna applications, so that a compromise can be made between size, operating frequency and other antenna radiation characteristics.⁸³ Coaxial probe, direct microstrip line feed, printed coplanar waveguide, soldered-through probe, conformal-strip feed and rectangular wave guide are the different techniques employed to excite a DRA.⁸⁴ Dielectric resonators of any shape may be used for antenna design but geometries like rectangles, cylinders, rings, and hemispheres are predominantly used. Fig. 1.13 shows a coaxial probe fed semispherical DRA. It would be highly desirable to mount the antenna in a Surface Mount Process (SMP). This would substantially reduce the costs of the antenna placement onto the PCB of the mobile device. Conventional antennas are usually connected exterior to the mobile device which can lead to reliability problems.

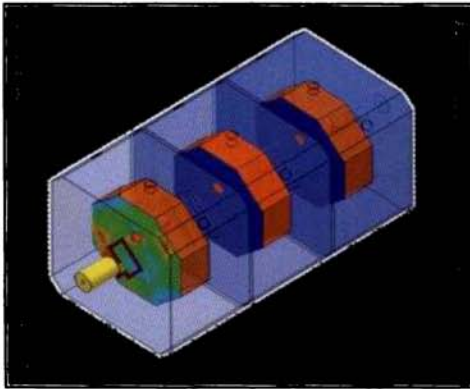


Fig. 1.13 Coaxial probe fed semispherical DRA (courtesy www.ifh.ee.ethz.ch/~fvtd/)

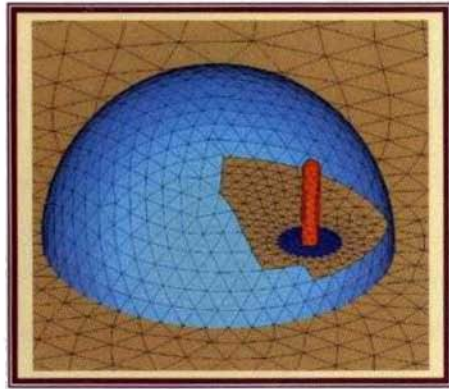


Fig. 1.14 Dielectric Resonator Filter (courtesy www.actspower.com/html/solutions.html)

1.7.3 Dielectric Resonator Filters (DRF)

Microwave filters are key components in all communication devices including satellite and mobile systems. Development of communication networks including cellular systems present highly demanding requirements on base station filters, in terms of their selectivity, out of band rejection and pass band insertion losses. The frequency allocations for duplex systems require highly selective filters and large rejections on one side of the pass band.⁸⁵ Traditional filter technology is based on metallic cavities which are intrinsically performance limited, large in size and comparatively costly to manufacture. A new generation of filters using low-loss and thermally stable ceramic resonators offer improved performance together with cost and size advantages, are expected to capture an increasing market share.⁸⁶ The requirements of the dielectric resonator for filters and low phase noise oscillators are high Q, small size, low insertion loss, high temperature stability, and low cost. There are several possible operating modes like transverse electric (TE) and transverse magnetic (TM), dual hybrid electromagnetic and triple TE and TM modes for dielectric resonator filters. These modes have an impact on the filter size, unloaded Q and spurious performance.⁸⁷ Two types of DR filters are most commonly used. The most preferred mode of operation when designing DR filter is

$TE_{01\delta}$ mode providing low loss and good spurious free performance.⁸⁸ Also an elliptic function response can be realized by this type of filter to further reduce the loss and volume.⁸⁹ Other type is the dual mode filter, operating in the HE_{11} mode, providing low loss, smaller volume and elliptic function realizations. Fig. 1.14 shows a commonly used DRF. The major disadvantage of DR band pass filters is that the necessary encapsulation in a metal case to minimize radiation loss makes them bulky, especially for medium and low frequencies.

1.8 LOW TEMPERATURE COFIRED CERAMICS (LTCC)

1.8.1 Introduction

In recent years, miniaturization of electronic components and devices for wireless and mobile applications has been stepped up. It seems currently this tendency will continue and may get even stronger in the future. Low Temperature Cofired Ceramics (LTCC) have become an attractive technology for electronic components and substrates that are compact, light, and offer high-speed and functionality for portable devices such as cellular phones, personal digital assistants (PDA) and personal computers used for wireless communication. The size, cost and performance of integration, packaging and interconnection technologies are critical factors for the success of a microwave product.⁹⁰ In both military and commercial applications, lower weight and smaller size requirements are necessitating increased density in electronics packaging. Cross-talk noise between lines and electric signal delay are suppressed by positioning the electric-signal wiring on low- ϵ_r material layers. Downsizing or lowering the profile of substrates (eg. decrease number of capacitance layers) can be achieved by forming internal capacitors on high- ϵ_r material layers. One way to achieve greater density is through integration of numerous components within a single package. Fig. 1.15 shows the schematic diagram of LTCC. LTCC has the unique ability to integrate a broad variety of components such as inductors, capacitors and filters into a very compact arrangement.

The benefits of LTCC technology are cost efficiency for high volumes, high packaging density, reliability, the ability to utilise highly conductive and inexpensive

metallization, good dielectric thickness control, high print resolution of conductors, low permittivity dielectric material, environmental stability, compact structures, integration etc.^{91,92} Integrating resistors and capacitors into the LTCC substrate eliminates any solder joints and wire bonds. Because of the excellent insulation provided by the thin layers of ceramic material, circuits can be alternately stacked, allowing digital, analog and microwave assemblies to be embedded in the same LTCC structure. This eliminates the need for separate housings and provides significant space and weight reductions. The low sintering temperature provided by the LTCC technology is the key issue enabling its advantageous utilization for today's packaging concepts in microelectronic and microsystems and in microwave modules. This technology enables fabrication of 3-dimensional ceramic modules with embedded silver or copper electrodes, and LTCCs with relative permittivity from about 3 up to over 100 have been developed showing low dielectric loss. These advantages make the LTCC technology suitable for the high frequency circuits required for high-speed data communications. LTCC 3 layer Ball Grid array is shown in Fig. 1.16. Although there are also other high-density, multilayer substrate technologies available, such as organic laminates, LTCC has a unique set of combined characteristics, which makes it a more attractive alternative as the frequencies shift into the microwave region.

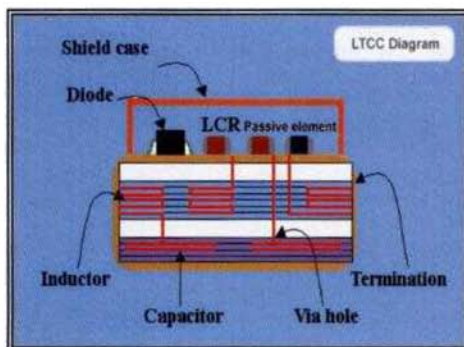


Fig. 1.15 Schematic diagram of LTCC
(courtesy www.im-tech.com/tech/lctt.html)

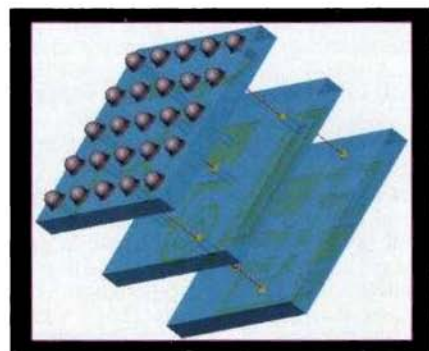


Fig. 1.16 LTCC 3 layer Ball Grid array
(courtesy <http://www.minicaps.com/lccc3d.html>)

1.8.2 Brief Historical Review

In just a handful of years, the packaging and interconnect technology known as low-temperature cofired ceramics (LTCCs) has entered the mainstream of electronics design. LTCCs, which were mostly relegated to the realm of low-volume military applications, are now being applied in high-volume consumer designs, especially in the wireless arena. The origin of multilayer ceramic substrate technology is at RCA Corporation in the late 1950's and the bases of current process technologies (green sheet fabrication technology and multilayer laminate technology using the doctor blade method) were discovered at this time.^{93,94,95} Progress was made using these technologies with IBM taking the lead, and the circuit board for IBM's mainframe computer commercialized in the early 1980's was the inheritance.^{96,97,98} Since this multilayer board was cofired at the high temperature of 1600°C with the alumina insulating material and conductor material (Mo, W, Mo-Mn), it is called High Temperature Cofired Ceramic. From the middle of the 1980's, efforts to increase the speed of mainframe computers accelerated, and as the key to increasing computer performance, further improvements are made to multilayer ceramic substrates for high density mounting applications. Fine wires were used in order to increase wiring density in circuit boards for high density mounting. But attenuation of signal occurs due to the electrical resistance of the wiring. Hence it is necessary to use materials with low electrical resistance (like Cu or Au). In addition, with the flip chip method of connecting bare LSI components directly, poor interconnection may result if the thermal expansion of the board is not close to that of the silicon (3.5 ppm/°C). Hence an insulating material with low thermal expansion (ceramic) is desirable. Further, to achieve high speed transmission of signals, it is necessary that the ceramic has a low dielectric constant. In the early 1990's, many Japanese and American electronics and ceramics manufacturers had developed multilayer boards (LTCC) that met these requirements.⁹⁹ Among them, Fujitsu and IBM were the first to succeed with commercial applications of multilayer substrates using copper wiring material and low dielectric constant ceramics. From the latter half of the 1990's to the

present, the focus of applications has shifted to high frequency wireless for the electronic components, modules and so on used in mobile communication devices. For the multilayer circuit board, the low thermal expansion of ceramics was its biggest merit for the purpose of high density mounting of LSI components. For high frequency applications, its low transmission loss is its key feature, and the low dielectric loss of ceramic gives it an advantage over other materials.

During the late 1980's, U.S. and Japanese manufacturers of computers and ceramic materials conducted extensive research and development of LTCC technology that is now crucial to present day and future communication technologies. During the past 15 years scientists world over have developed a large number of new dielectric LTCCs (about 400) for high frequency applications with low sintering temperature or improved the properties of known materials. About 1000 papers and about 500 patents are filed in the area of LTCC materials and related technologies. For details of the LTCC materials, the reader is referred to the recent review by Sebastian and Jantunen.¹⁰⁰ Next-generation electronics systems will demand the performance, reliability, lighter weight and affordability that LTCC technology can provide.

1.9 MATERIAL SELECTION AND REQUIREMENTS FOR LTCC

LTCC is among the most advanced approaches to miniaturization of electronic packaging. In the development of LTCC applications, several material properties need to be taken into account. The electrical properties of the dielectric and the conductor materials are the basic issue, but designers should also be aware of the effects of the thermomechanical properties, production costs and variation range of each parameter.¹⁰¹ There are two limiting factors, which prevent us from getting low loss of designed components. One is related to the conductivity losses in the circuitry and the other to the losses occurring in the glassy phase of the glass-ceramic composite substrate. The important characteristics required for an LTCC material are:¹⁰⁰

1.9.1 Densification Temperature Less than 950°C

For the fabrication of multilayer devices, it is important to develop microwave ceramics that have a densification or sintering temperature less than 950°C since the common electrode material Ag melts at 961°C. In the glass ceramic composites, the main phase is a dielectric material having a high sintering temperature. When sintering composites of glass-ceramic, the liquification of the glass is the key mechanism, where the glass penetrates the three dimensional mesh structure formed by ceramic particles, facilitating the wetting of each ceramic particle surface with glass melt. Therefore in order to improve the sintered density of glass-ceramic composites, it is necessary to control the softening point of the glass material, as well as its volume and powder particle size to increase its fluidity. Ceramic has the effect of an impediment hindering the flow of the glass and hence using ceramic with a large particle size and thus a small specific surface area is beneficial for improving the sintered density. It should be noted that any densification or crystallisation of the composite at lower temperatures, such as below 800 °C, is undesirable as this can prevent the evaporation of the organics and solvents used in conductive pastes and binder and plasticizers causing residual carbon traces in the microstructure.^{102,103} Any residual carbon that may form during binder decomposition if left in the LTCC would adversely affect the dielectric properties. This means that the densification of the ceramic should start above this temperature.⁸⁷

1.9.2 Dielectric Properties (ϵ_r , Q_{uxf} and τ_f)

Permittivity, dielectric loss and temperature dependence are the most important electrical properties in material selection, especially for high frequency applications. These properties enable the construction of microwave filters with convenient size and impedance matching, low insertion loss, steep cut-off of the performance curve and operational stability against ambient temperature change.

Low relative permittivity materials with $\epsilon_r = 4 - 14$ are used for substrate layers while high permittivity materials are used mainly for capacitor layers. In the case of

ceramic packages, the relative permittivity of the ceramic over and within the metal lines are deposited or embedded governs the propagation delay, t_d , which is given by¹⁰⁴

$$t_d = \frac{l\sqrt{\epsilon_r}}{c} \quad (1.45)$$

where l is the line length, ϵ_r is the relative relative permittivity of the substrate and c is the speed of light. Thus substrates with low relative permittivity are required to increase the speed of the signal.⁸⁷ LTCC compositions with higher permittivity values ($\epsilon_r > 20$) have been developed, to enable miniaturised, embedded capacitors, inductors, filters and antennas.⁸⁸ In this case one must, however, pay more attention to the component fabrication, since smaller dimensions means higher processing accuracy especially in the alignment of different layers. However, one advantage is that the permittivities of the commercial LTCCs are very stable, and batch to batch variations are generally less than 2%.

The prediction of the exact insertion loss of a microwave component is complicated. The main losses in the frequency range 4-44 GHz are conductor losses, but the relative importance of dielectric and roughness losses increases as a function of frequency. In LTCC multilayer structures, high conductive metallisations are an important benefit. The square resistances of recommended silver pastes are about 2 – 3.5 $m\Omega^2$ with a fired line thickness of 10-15 μm . Lower dielectric losses of LTCC than FR-4 at microwave and millimetre frequencies result in lower loss signal connections and higher Q values.

The temperature dependence of the resonance frequency is important because filters and resonators based on noncompensated dielectric materials need additional mechanical and electrical design to ensure satisfactory electrical performance of the device over its operating temperature.^{105,106} The coefficient of temperature variation of the resonant frequency (τ_f) value of 10 ppm/ $^{\circ}\text{C}$ causes a 0.11 % shift of the resonant frequency (5.5 MHz at 5.2 GHz) within the temperature range -30 $^{\circ}\text{C}$ to +80 $^{\circ}\text{C}$. Though novel LTCC materials with zero τ_f (e.g. Heraeus CT2000, $\tau_f \leq 10$ ppm/ $^{\circ}\text{C}$) have been developed, the component designer must be aware that the structure itself may affect its

τ_f

1.9.3 High Thermal Conductivity

The thermal conductivity of LTCC materials should be moderately good. The removal of heat generated by the device during operation is critical for the efficient functioning of the package. It is therefore necessary to maintain the temperature below 100°C for efficient and reliable operation of the device. The heat removal has become even more critical in recent years because of the ever-growing need to fabricate high density and high power devices that can operate at high speed. Advancement in technology and the continuing trends toward miniaturization of devices in the future will place even more stringent requirements on heat dissipation characteristics of the packaging LTCC. The thermal conductivity of an LTCC is 2 W/mK, versus 0.5 W/mK for organic materials. A common method to improve thermal dissipation is to use a heat spreader, but a more advantageous alternative provided by LTCC technology is to place metallic via arrays (thermal conductivity 50 W/mK) under high power components.¹⁰⁷

1.9.4 Thermal Expansion

A specific requirement of LTCC comes from the coefficient of thermal expansion (CTE), which should be chosen to match closely the value of the mounting board and chip. A thermal expansion mismatch would give rise to failure of area solder connections between the chip and the substrate. The thermal expansion match with silicon is important since systems based on silicon chips with a high device density are mounted on LTCC substrates. If the LTCC module is mounted on silicon, CTE should be about 4 ppm/°C while on alumina it should be 7-9 ppm/°C and on PCB 12-20 ppm/°C.¹⁰³

The other important material aspect of microwave modules is its thermomechanical properties. They include many properties that affect the reliability of the designed components. LTCCs must meet a number of mechanical requirements, such as high fracture strength, Young's Modulus and low surface roughness.

1.9.5 Chemical Compatibility with Electrode Material

The LTCC should not react with the conductive material used. The formation of additional phases in the ceramic should be minimised since the reaction of the composites with the conducting electrode, degrades the performance of the microwave modules. A critical issue in manufacturing LTCC microelectronics is the precise and reproducible control of shrinkage on sintering. In the screen-printing of the conductive patterns, instead of pure metals, pastes containing conductive particles in glassy or fritless additives, are used. Thus when developing LTCC materials, one has to take into account reactions not only with the conductive material like silver but also with other additives of the conductor paste. Table 1.1 shows the some of the properties of commercial LTCC materials from data sheets compared with alumina and FR-4.

Table 1.1 Properties of commercial LTCC materials, alumina and FR-4 (after Ref. 2.)

Property	Commercial LTCC	Alumina (96 %) Coors	FR-4
Permittivity commonly at 1 MHz	3.8-9.2	9.2	5.5
Loss tangent commonly at 1 MHz	0.0007-0.006	0.003	0.022
Microwave insertion (loss/dB/m) at 10 GHz	4.7-23.6	-	-
Coefficient of Thermal Expansion (ppm/ ^o C)	4.5-7.5	7.1	12-16
Thermal conductivity (W/mK)	2.0 – 4.5	21	0.2
Youngs modulus (GPa)	80-150	314	24
Flexural strength (MPa)	116-320	397	430
Surface roughness (µm/in)	<1-25	<25	-
Green tapes thickness tolerance (%)	±2-±9	-	-
X,Y shrinkage (%)	9.5-15 ±0.3	-	-
Z-shrinkage (%)	10.3-25±0.5	-	-
Metallizations	Au/Ag	-	Cu

1.10 GLASS-CERAMIC COMPOSITES

1.10.1 Introduction

Multilayer microwave components have been investigated in order to miniaturize resonant devices for volume efficiency. To be a useful material for incorporation into multilayer-type elements, dielectrics must be capable of being sintered along with electrodes, a process known as cofiring. Generally, addition of low melting point compounds such as Bi_2O_3 , B_2O_3 , V_2O_5 and glass,^{108,109} chemical processing for smaller particle sizes of the starting materials¹¹⁰ and development of novel low-sintering dielectric ceramics¹¹¹ are three of the methods used to reduce the sintering temperature of the dielectrics. Of the three, liquid phase sintering using glass additives is widely employed since it is the least expensive. The two approaches to exploit glasses to obtain ceramic compositions sinterable below 1000°C are glass-ceramic composite (glass + ceramic)^{112,102} and glass-ceramics (crystallizable glass).^{113,114}

Glass-ceramic route uses a crystallisable glass that devitrifies almost completely during high temperature processing. The devitrification of glass greatly increases the viscosity of the system during firing, thereby improving the resistance to distortion.¹¹⁵ The properties of the final products were controlled by the degree of crystallization that occurred during firing. The amorphous glass phase is the main component, but it may contain a small amount of crystalline phase, which acts as a nucleating agent during firing. During firing, the glass recrystallises to low loss phases and produces a low dielectric loss ceramic body.¹¹⁶ Therefore, a thorough understanding of the crystallization kinetics and mechanism of glass-ceramic systems is needed before the processing parameters are optimized.¹¹⁷ Crystallizable cordierite by IBM¹¹² and Wollastonite by Ferro¹¹⁸ are examples for glass-ceramic system.

A mixture of low-melting glass and high-melting ceramic fillers^{113,118} is prepared and fired at elevated temperatures in the glass ceramic composite method. The properties of the final glass + ceramics are controlled by the ratio of glass to ceramics and the individual properties of the mixtures. The crystalline filler is a major determinant of

electrical properties and increase viscosity during sintering and thereby minimising distortion. It also increases the mechanical strength of the final ceramics. In this type of system, the microstructure, phases, and final properties are controlled by the sintering conditions such as heating rate, sintering temperature, and soaking time. Typical systems include the borosilicate glass (BSG) + alumina system developed by Fujitsu¹¹⁹ and the lead borosilicate glass + alumina system of Dupont.¹¹³ The approach of glass + ceramics has been widely used due to its ease in controlling densification behaviour and simplicity to tune the final properties of fired substrate and robustness in processing for large-scale manufacturing. Both the above approaches require initial glass preparation, which involves mixing raw materials to yield the chosen glass composition, melting the mixture between 900-1500°C, quenching and pulverisation. The high temperature step involves volatilisation of constituents such as Bi₂O₃, B₂O₃, and PbO, which can lead to undesirable variations in the final composition.

Densification of glass + ceramics can be described by three-stage liquid phase sintering, i.e., particle rearrangement, dissolution and precipitation and solid state sintering. Depending upon the reactivity between glass and ceramics, the densification of glass + ceramics can be classified as non-reactive, partially reactive and completely reactive systems. Little dissolution of ceramic filler in glass during firing is observed for nonreactive systems, such as borosilicate glass (BSG) + cordierite¹²⁰ in which densification is mainly achieved by particle rearrangement. For partially reactive systems such as BSG + alumina, the dissolution of ceramic filler in glass is localized and limited, and no particle growth and shape accommodation are observed. A global dissolution of ceramic filler in a low softening glass is found for completely reactive systems including BSG + high silica glass (HSG).¹²¹ The required amount of glass content added to ceramic for achieving densification decreases with increasing particle size ratio between ceramic filler and glass.¹²²

1.10.2 Characteristics of Glasses

LTCC is a glass-ceramic composite that densifies at temperatures below 900°C via viscous sintering. For this process, the glass must form a low-viscosity melt during firing.^{123,124,125} The ceramic filler is selected to optimize the dielectric, magnetic, thermal and other properties. To improve the shape stability during firing and the dielectric as well as the mechanical properties of composite, the glass amount is reduced after densification by crystallization.^{126,127,128} The amount and type of phases-crystalline and amorphous in the microstructure of the composite after sintering determine its final properties. The selection of glass materials is very important for sintering glass/ceramic composites, since the liquidation of the glass takes a dominant role in the viscous flow mechanism among the constituents. The ceramic particles in the composites dissolve slightly in the glass during sintering and the ceramic is characterized by lack of grain growth. In low temperature sintering, characteristics of glass such as fluidity, crystallization, foaming and reactions affect the sintered density.¹²⁹ The glasses consist of different oxides which all have effect on glass properties. The different oxides of glass ingredients are SiO₂, B₂O₃, PbO, BaO, MgO/ZnO, CaO, Na₂O, K₂O, Li₂O, Al₂O₃ etc. Commercial LTCC tapes are mainly low ϵ_r glass ceramics composites having typically four or five phases present and none of which should react with the electrode. SiO₂ and B₂O₃ glasses form commonly the network structures of glass. If the silica content in the glass is high, the glass has a high transition temperature, low thermal expansion, and excellent chemical durability. The SiO₂ has a high melting point and high viscosity. B₂O₃ can be added to lower the viscosity. PbO can connect SiO₄ tetrahedrons. Na₂O, PbO, K₂O, Li₂O, CaO, MgO, BaO are modifier oxides. Na₂O lowers the softening point and increases the thermal expansion coefficient and reduces chemical durability. Na₂O and Li₂O increase the ionic conductance. But Li₂O readily crystallizes. Al₂O₃ can form AlO₄ tetrahedrons and can connect to the network structure and has effect of controlling crystallization. In general, for glass/ceramic composite type LTCCs, borosilicate glass with a softening point of around 800°C is used. Table 1.2 shows the properties of some glasses used in the present study.

Table 1.2 Common LTCC glasses and their physical properties

Glass	Density (g/cm ³)	T _g (°C)	ϵ_r	Tan δ at 1 MHz	Reference
B ₂ O ₃	2.46	450	2.5	0.00550	130
ZnO:B ₂ O ₃ (50:50)	3.65	582	6.9	0.00012	133
B ₂ O ₃ :SiO ₂ (40:60)	2.23	820	4.6	0.00940	134
Al ₂ O ₃ :SiO ₂ (50:50)	2.60	850	8.1	0.00970	134
MgO-Al ₂ O ₃ -SiO ₂ (22:22:66)	2.30	1350	4.5	0.00074	134
MgO-B ₂ O ₃ -SiO ₂ (40:40:20)	3.18	950	5.0	0.00230	134
PbO-B ₂ O ₃ -SiO ₂ (40:20:40)	12.11	442	12.1	0.01000	133
BaO-B ₂ O ₃ -SiO ₂ (30:60:10)	3.40	627	7.2	0.00440	133
ZnO-B ₂ O ₃ -SiO ₂ (50:40:10)	3.55	611	6.9	0.00950	133
ZnO-B ₂ O ₃ -SiO ₂ (60:30:10)	3.60	581	7.6	0.01100	133
Li ₂ O-B ₂ O ₃ -SiO ₂ (35.14:31.66:33.2)	2.34	513	6.4	0.00360	131
B ₂ O ₃ -Bi ₂ O ₃ -SiO ₂ -ZnO (27:35:6:32)	4.30	950	8.8	0.00130	132
Li ₂ O-MgO-ZnO-B ₂ O ₃ -SiO ₂ (20:20:20:20:20)	2.75	900	6.9	0.00200	133

The ionic and electronic polarization mechanisms contribute to relative dielectric constants of glasses in the microwave frequency region. The relative dielectric constants and dielectric losses of glasses are mainly determined by the concentration of network-modifying oxides in the glasses, and show little sensitivity to the type of network forming oxides. The dominant mechanism contributing to the relative dielectric constant and dielectric losses should be the movement and oscillation of modifying ions in their respective interstices under the influence of an alternating electric field. The network formers contained in the glass materials may absorb the microwave power profoundly in high frequency region, degrading the quality factor for the material.¹³⁴ At least three types of losses for glasses have been distinguished,¹³⁵ resonance type vibrational losses at very high frequency, migration losses caused by the movement of mobile ions (mainly

alkali ions) and deformation losses by defect or deformation of the basic silicon oxide network. Resonant type vibrational losses are particularly important in the microwave region. Only the ionic polarization mechanism can cause two kinds of dielectric losses in glasses at microwave frequency:¹³⁶ (i) deformation losses and (ii) vibration losses. The deformation losses arise from movements of parts of the network. The activation energy found in the case of deformation losses is of the order of 0.1 eV. It is evident that no transport of ions can take place in this instance. These are more likely to be slight local deformations in the network or a regrouping of ions of the network. The vibration losses are caused by the damped oscillations of the network-modifying ions in their respective interstices. The vibration losses are a typical resonance phenomenon and tend to occur at a lower frequency as the temperature increases.¹³⁷

1.11 POLYMER - CERAMIC COMPOSITES

1.11.1 Introduction

Microelectronics has become a dominant influence in our lives since its introduction in the mid-1950's. The pace of this development and the development of the associated materials and processing technology has been quite astounding. The push has been along miniaturisation and packing the maximum amount of performance into the smallest space. This latest industrial revolution was originally driven by the need for very small and lightweight electronic circuits for military and aerospace applications. With the development of first the transistor and later the integrated circuit, it has now grown to be a multi-billion dollar industry, and microelectronics applications are ubiquitous. The effectiveness with which an electronic system performs its electrical functions, as well as the reliability and cost of the system, are strongly determined not only by the electrical design, but also by the packaging materials. Electronic packaging refers to the packaging of integrated circuit chips, their interconnections for signal and power transmission and heat dissipation. As the speed and power of electronics increase, the heat dissipation problems and signal delay caused by the capacitive effect of the dielectric material become greater issues that need resolving. The solution involves the

devising of innovative packaging schemes and the continuing search for more advanced materials. The actual applications of materials in electronic packaging include interconnections, printed circuit boards, substrates, encapsulants, interlayer dielectrics, die attach materials, electrical contacts, connectors, thermal interface materials, heat sinks, solders, brazes, lids and housings. Packaging materials must have low or tailorable coefficient of thermal expansion to match with the substrate, high thermal conductivity to dissipate heat, low cost and low density for weight critical systems. Conventional materials do not satisfy all these requirements.¹³⁸ One approach is to create new composite materials with properties tailored specifically for electronic packaging applications.

The development of electrical composites is motivated by the technological need for properties that are not available in individual single component materials. In modern usage, composite materials are made from a filler, particles, flakes or fibers, embedded in a matrix made of polymer, metal or glass. Nevertheless, a composite is any material consisting of two or more distinct phases. By combining two or more components it becomes possible to tailor composite materials with the required combinations of properties. The design of such electrical composites necessitates a detailed understanding of the ways in which composite properties depends upon component properties, composition and composite microstructure.¹³⁹ Composite dielectrics that derive their electrical and mechanical properties from the combination of the high performance of ceramics and the good mechanical properties of polymers are now widely used in the electronics industry, especially as substrate materials for high frequency uses.

1.11.2 Material Requirements for Microelectronic Packaging and Substrate Applications

1.11.2.1 Electrical Properties

Signal processing is critical for the operation of an electronic system, and materials along with their architecture play an important role in the propagation of signals, especially for circuits operating at high speeds and at high electrical frequency.

The electrical characteristics of the microelectronic devices, such as signal attenuation, propagation velocity and cross talk, are influenced by the dielectric properties of the packaging materials. The electrical properties in material selection include, dielectric constant, loss tangent, frequency and temperature stability, dielectric strength and electrical resistivity. An important role of packaging materials is to ensure the electrical insulation of the silicon chip and of circuit pins. Ideally, a low conductivity is needed to avoid current leakage, a low dielectric constant to minimize the capacitive coupling effects and reduce signal delay and a low loss factor to reduce electrical loss.¹⁴⁰ The temperature coefficient of the dielectric constant of microwave substrates are very important in many outdoor wireless applications for the reduction or control of temperature-induced drift in circuit operating characteristics.¹⁴¹ High electrical resistivity and dielectric strength are also required for microelectronic applications.¹⁴²

1.11.2.2 Thermal and Thermomechanical Properties

An electronic material experiences a range of steady-state temperatures, temperature gradients, rates of temperature change, temperature cycles, and thermal shocks through manufacturing, storage and operation. Thermal properties that are significant in enduring such life cycle profiles include thermal conductivity/diffusivity, specific heat capacity and coefficient of thermal expansion.

1.11.2.3 Mechanical Properties

The mechanical properties affect the material's ability to sustain loads due to vibrations, shock and thermomechanical stresses during manufacture, assembly, storage and operation. Key properties that are of importance for electronic packaging applications include the modulus of elasticity, tensile strength, Poisson's ratio, flexural modulus, fracture toughness, creep resistance and fatigue strength.¹⁴²

1.11.2.4 Chemical Properties

Chemical properties of electronic materials are important because of the need for electronic materials to survive manufacturing, storage, handling and operating

environments. The chemical properties of significance are water absorption, flammability and corrosion resistance. The electrical properties of electronic materials often change as a result of water absorption and flammability and swelling and other dimensional instabilities can occur. The corrosion leads to the formation of more stable compounds and can degrade the physical properties of the materials.¹⁴²

1.11.3 Advantages of Polymer-Ceramic Composites

Polymeric materials play a vital role in electronic substrates and microelectronic packages as a result of their ease of processing, low cost, low dielectric constant, adhesive properties, high electrically insulating properties etc. Thermally conducting, but electrically insulating, polymer-matrix composites are important for electronic substrates and microelectronic packaging applications because the heat dissipation ability limits the reliability, performance and miniaturization of electronic device. In order to provide thermally conducting and electrically insulating composites, ceramic fillers are often used. Polymer-ceramic composites offer excellent material characteristics including low temperature processibility, flexibility, high temperature resistance, outstanding solvent resistance etc.

The fundamental principles and materials requirements for dielectric resonator, low temperature cofired ceramic and electronic packaging applications are described in this chapter. The next chapter discusses the synthesizing and characterization techniques of the dielectric ceramics involved in the present work.

1.12 REFERENCES

- 1 Y-M Chiang, Dunbar Birnie III and W. D. Kingery, *Physical Ceramics - Principles for Ceramic Science and Engineering*, John Wiley & Sons, New York, (1997).
- 2 M. T. Sebastian, *Dielectric Materials for Wireless Communication*, Elsevier Science Publishers, Oxford, (2008).
- 3 <http://www.pcworld.com/article/id,127820/article.html>
- 4 W. Wersing, *Cur. Opin. Sol. State Mater. Sci.*, **1**, 715 (1996).
- 5 A. J. Moulson and J. M. Herbert, *Electroceram.*, Chapman & Hall, London, (1990).
- 6 P. C. Osbond, R. W. Whatmore and F. W. Ainger, *Br. Ceram. Soc. Proc.*, **36**, 167 (1985).
- 7 J. C. Burfoot and G. W. Taylor, *Polar Dielectrics and Their Applications*, Macmillan Press, London, (1979).
- 8 Rayleigh, *Phil. Mag.*, **43**, 123 (1892).
- 9 K. S. Packard, *IEEE Trans. Microwave Theory Tech.*, **MTT-32**, 961 (1984).
- 10 G. C. Southworth, U. S. Patent 2 106 769, (1935).
- 11 R. D. Ritchmyer, *J. Appl. Phys.*, **10**, 391 (1939).
- 12 F. Borgnis, *Ann. Physik.*, **35**, 359 (1939).
- 13 W. L. Barrow and W. W. Maher, *Proc. Inst. Radio Engrs.*, **28**, 189 (1940).
- 14 Carson, Mead and Schelkunoff, *Bell Systems Tech. J.*, **15**, 310 (1936).
- 15 H. M. Schlicke, *J. Appl. Phys.*, **24**, 187 (1953).
- 16 P. R. Longarker and C.S. Roberts, *IEEE Trans. Microwave Theory Tech.*, **MTT-11**, 543 (1963).
- 17 J. A. Armstrong, N. Blombergen, J. Ducuing and P. S. Pershan, *Phys. Rev.*, **127**, 1918 (1962).
- 18 B. W. Hakki and P.D. Coleman, *IRE Trans. Microwave Theory Tech.*, **MTT-8**, 402 (1960).
- 19 Y. Kobayashi, *IEEE Trans. Microwave Theory Tech.*, **MTT-33**, 586 (1985).
- 20 B. D. Silverman, *Phys. Rev.*, **125**, 1921 (1962).

-
- ²¹ W. G. Spitzer, R. C. Miller, D. A. Kleinman and L. E. Howarth, *Phys. Rev.*, **126**, 1710 (1962).
- ²² A. Okaya, *Proc. IRE.*, **48**, 1921 (1960).
- ²³ A. Okaya and L. F. Barash, *Proc. IRE.*, **50**, 2081 (1962).
- ²⁴ S. B. Cohn, *IEEE Trans. Microwave Theory Tech.*, **MTT-16**, 218 (1968).
- ²⁵ D. J. Masse, R. A. Purcel, D. W. Ready, E. A. Maguire and C. D. Hartwig, *Proc. IEEE.*, **59**, 1628 (1971).
- ²⁶ Y. Konishi, *Tech. Report of NHK-Nippon Hohsoh Kyokai*, 111 (1971).
- ²⁷ J. K. Plourde, *IEEE MTT-S Digest*, 1 (1977).
- ²⁸ J. K. Plourde, D. F. Linn, H. M. O'Bryan, Jr. and J. Thompson, Jr., *J. Am. Ceram. Soc.*, **58**, 418 (1975).
- ²⁹ K. Wakino, M. Katsube, H. Tamura, T. Nishikawa and Y. Ishikawa, *IEEE Four Joint Conv. Rec.*, Paper 235 (1977).
- ³⁰ J. K. Plourde, *IEEE MTT-S Digest*, **25**, 202 (1973).
- ³¹ S. Nomura, K. Toyama and K. Tanaka, *Jpn. J. Appl. Phys.*, **21**, L624 (1982).
- ³² S. Kawashima, M. Nishida, I. Ueda and H. Ouchi, *J. Am. Ceram. Soc.*, **66**, 421 (1983).
- ³³ K. Wakino, K. Minai and H. Tamura, *J. Am. Ceram. Soc.*, **67**, 278 (1984).
- ³⁴ H. Tamura, T. Konoike and K. Wakino, *J. Am. Ceram. Soc.*, **67**, C59 (1984).
- ³⁵ G. Wolfram and H. E. Goebel, *Mater. Res. Bull.*, **16**, 1455 (1981).
- ³⁶ D. Kolar, Z. Stadler, S. Gaberscek and D. Suvorov, *Ber. Dt. Keram. Ges.*, **55**, 346 (1878).
- ³⁷ W. Wersing, *Electronic Ceramics*, B. C. H. Steele (Editor), Elsevier Pub. Co. Inc., Amsterdam, (1991).
- ³⁸ D. Kajfez and P. Guillon, *Dielectric Resonators*, Noble Publishing Corp. Atlanta, (1998).
- ³⁹ J. K. Plourde and C. L. Ren, *IEEE Trans. Microwave Theory Tech.*, **MTT-29**, 754 (1981).
- ⁴⁰ R. Freer, *Silicates Industriels*, **9-10**, 191 (1993).
- ⁴¹ S. Nomura, *Ferroelectrics*, **49**, 61 (1983).

-
- 42 K. Wakino, T. Nishikawa, Y. Ishikawa and H. Tamura, *Br. Cera. Trans. J.*, **89**, 39 (1990).
- 43 K. Wakino and H. Tamura, *Ceram. Trans.*, **15**, 305 (1990).
- 44 H. Tamura, T. Konoike and K. Wakino, *Proc of 3rd U.S.-Japan Seminar Dielectric Piezoelectr. Ceram.*, 69 (1984).
- 45 H. Tamura, T. Konoike and K. Wakino, *J. Am. Ceram. Soc.*, **67**, C59 (1984).
- 46 K. Wakino, K. Minai and H. Tamura, *J. Am. Ceram. Soc.*, **67**, 278 (1984).
- 47 H. M. O'Bryan Jr., J. Thompson Jr. and J. K. Plourde, *J. Am. Ceram. Soc.*, **57**, 450 (1974).
- 48 S. Nishikawa, Y. Ishikawa, J. Hattori and Y. Ida, *J. Inst. Electron. Inf. Commun. Eng.*, **J27-C-1**, 650 (1989).
- 49 H. Frohlics, *Theory of Dielectrics*, Clarendon Press, Oxford, (1950).
- 50 R. D. Shannon, *J. Appl. Phys.*, **73**, 348 (1993).
- 51 C. Vinies, P. K. Davies, T. Negas and S. Bell, *Mater. Res. Bull.*, **31**, 431 (1996).
- 52 A. J. Bosman and E. E. Havinga, *Phys. Rev.*, **129**, 1593 (1963).
- 53 E. L. Colla, I. M. Reaney and N. Setter, *J. Appl. Phys.*, **74**, 3414 (1993).
- 54 D. Kajfez, *Q Factor, Vector Fields*, Oxford, (1994).
- 55 L. A. Trinogga, G. Kaizhou and I. C. Hunter, *Practical Microstrip Circuit Design*, Ellis Horwood, Boston, (1991).
- 56 P. J. Harrop, *Dielectrics*, Butterworth, London, (1972).
- 57 M. Sucher, *Measurement of Q in Handbook of Microwave Measurements*, M. Sucher and J. Fox (Editors), 3rd Ed., Polytechnic Press, Brooklyn, (1963).
- 58 Y. Konishi, *Proc. IEEE*, **79**, 726 (1991).
- 59 Y. Kobayashi and T. Tanaka, *IEEE Trans. Microwave Theory Tech.*, **MTT-28**, 1077 (1980).
- 60 Y. Kobayashi and M. Miura, *IEEE MTT-S Int. Microwave Symp. Dig.*, San Fransico, (1984).
- 61 S. K. Kaul, *Millimeterwaves and Optical Dielectric Integrated Circuits*, Wiley, New York, (1997).

-
- ⁶² V. L. Gurevich, and A. K. Tagantsev, *Adv. Phys.*, **40**, 719 (1991).
- ⁶³ I. J. Bahl and P. Bhartia, *Microwave Solid State Circuit Design*, Wiley, New York, (1988).
- ⁶⁴ K. Wakino, M. Murata and H. Tamura, *J. Am. Ceram. Soc.*, **69**, 34 (1986).
- ⁶⁵ P. J. Harrop, *J. Mater. Sci.*, **4**, 370 (1969).
- ⁶⁶ E. L. Colla, I. M. Reaney and N. Setter, *J. Appl. Phys.*, **74**, 3414 (1993).
- ⁶⁷ E. L. Colla, I. M. Reaney and N. Setter, *Jpn. J. Appl. Phys.*, **33**, 3984 (1994).
- ⁶⁸ T. Negas, G. Yeager, S. Bell, N. Coates and I. Minis, *Am. Ceram. Soc. Bull.*, **72**, 80 (1993).
- ⁶⁹ A. Templeton, X. Wang, S. J. Penn, S. J. Webb, L. F. Cohen and N. McN. Alford, *J. Am. Ceram. Soc.*, **83**, 95 (2000).
- ⁷⁰ D. A. Sagala and S. Nambu, *J. Am. Ceram. Soc.*, **75**, 2573 (1992).
- ⁷¹ H. L. Curtis, *Bur. Stand. (US) Bull.*, **2**, 359 (1915).
- ⁷² R. F. Field, *J. Appl. Phys.*, **17**, 318 (1946).
- ⁷³ A. K. Jonscher, *Universal Relaxation Law*, Chelsea Dielectric, London, (1996).
- ⁷⁴ W. R. Tinga, W. A. G. Voss and B. V. Blossey, *J. Appl. Phys.*, **44**, 3897 (1973).
- ⁷⁵ J. Molla, M. Gonzalez, R. Vila and A. Ibarra, *J. Appl. Phys.*, **85**, 1727 (1999).
- ⁷⁶ W. D. Kingery, H. K. Bowen and D. R. Uhlmann, *Introduction to ceramics*, 2nd Ed., Wiley, New York, (1976).
- ⁷⁷ R. Heidinger and S. Nazare, *Powder Metall. Int.*, **20**, 30 (1988).
- ⁷⁸ S. J. Penn, N. McN. Alford, A. Templeton, X. Wang, M. Xu, M. Reece and K. Schrapel, *J. Am. Ceram. Soc.*, **80**, 1885 (1997).
- ⁷⁹ S. A Long, M.W McAllister and L.C. Shen, *IEEE Trans. Anten. Prop.*, **AP-31**, 406, (1983).
- ⁸⁰ A. A Kishk, A. W. Glisson and G. P. Junker, *Prog. Electromagn. Res.*, **PIER-33**, 97 (2001).
- ⁸¹ T. A. Denidni, Y. Coulibaly and L. Talbi, *J. of Electromagn. Waves and Appl.*, **20**, 1629 (2006).

-
- 82 R Yang, Y-J. Xie, P. Wang and L. Li, *J. of Electromagn. Waves and Appl.*, **20**, 1221 (2006).
- 83 P.V Bijumon, S. K Menon, M. T Sebastian and P. Mohanan, *Microwave and Opt. Tech. Lett.*, **35**, 327 (2002).
- 84 K.W. Leung, H.Y Lo, K.K So and K.M Luk, *Microwave and Opt. Tech. Lett.*, **34**, 157 (2002).
- 85 I.C. Hunter, J. D. Rhodes and V. Dassonville, *IEEE Trans. on Microwave Theory and Tech.*, **MTT-47**, 2304 (1999).
- 86 A. R. Weily and A. S. Mohan, *Microwave and Opt. Tech. Lett.*, **18**, 149 (1998).
- 87 J. Yohannan, A. V. P. Kumar, V. Hamsakkutty, V. Thomas and K. T. Mathew, *Prog. In Electromagn. Res.Symp.*, Hangzhou, China, 120 (2005).
- 88 Fiedziuzko, S. J. , I. C. Hunter, T. Itoh, Y. Kobayashi, T. Nishikawa, S. N. Stitzer and K. Wakino, *IEEE Trans. on Microwave Theory and Tech.*, **MTT-50**, 706 (2002).
- 89 R. R. Mansour, *IEEE Microwave Mag.*, **5**, 68 (2004).
- 90 H. Jantunen, T. Kangasvieri, J. Vähäkangas and S. Leppävuori, *J. Eur.Ceram. Soc.*, **23**, 2541 (2003).
- 91 L. Devlin, G. Pearson and J. Pittock, *Proc. of the 38th IMAPS Nordic Conference*, Oslo, Norway, 96 (2001).
- 92 A. Sutono, D. Heo, Y. J. E. Chen and J. Laskar, *IEEE Trans. Microwave Theory and Tech.*, **MTT-49**, 1715 (2001).
- 93 H. W. Stetson, *Ceramics and Civilization*, **3**, 307 (1987).
- 94 W. J. Gyuvk, *U. S. Patent* No. 3, 192, 086, (1965).
- 95 H. Steson, *U. S. Patent* No. 3, 189, 978, (1965).
- 96 B. Schwartz, *Am. Ceram. Soc. Bull.*, **63**, 577 (1984).
- 97 A. J. Blodgett and D. R. Barbour, *IBM J. Res. Dev.*, **26**, 30 (1982).
- 98 C. W. Ho, D. A. Chance, C. H. Bajorek and R. E. Acosta, *IBM J. Res. Dev.*, **26**, 286 (1982).
- 99 Y. Imanaka, Low temperature Fireable Multi Layer Ceramic Circuit Board", *NIKKEI NEW MATERIALS*, 93 (1987).

- ¹⁰⁰ M. T. Sebastian and H. Jantunen, *Int. Mater. Rev.*, **53**, 57 (2008).
- ¹⁰¹ H. Jantunen, T. Kangasvieri, J. Vähäkangas, S. Leppävuori, *J. Eur. Ceram. Soc.*, **23**, 2541 (2003).
- ¹⁰² R. R. Tummala Rao, *J. Am. Ceram. Soc.*, **74**, 895 (1991).
- ¹⁰³ V. Gektin, A. Barcohen and S. Witzman, *IEEE Trans. Comp. Packag. and Manufact. Technol. Part A.*, **21**, 577 (1998).
- ¹⁰⁴ B. Schwartz, *Am. Ceram. Soc. Bull.*, **63**, 577 (1984).
- ¹⁰⁵ C. Wang and K. A. Zaki, *IEEE MMT-S Intern. Microwave Symp. Digest*, **3**, 1041 (1993).
- ¹⁰⁶ H. Jantunen and A. Turunen, *US patent* 5, 302 924 (1994).
- ¹⁰⁷ J.P. Sommer, B. Michel, U. Goebel and J. Jelonnek, *Seventh Inter Society Conference on Thermal and Thermomechanical Phenomena in Electronic systems*, IThERM, 360 (2000).
- ¹⁰⁸ H. Kagata, T. Inoue, J. Kato and I. Kameyama, *Jpn. J. Appl. Phys.*, **31**, 3152 (1992).
- ¹⁰⁹ H. T. Kim, S. H. Kim, S. Nahm, J. D. Byun and Y. Kim, *J. Am. Ceram. Soc.*, **82**, 3043 (1999).
- ¹¹⁰ Y. Xu, G. Huang and Y. He, *Ceram. Int.*, **31**, 21 (2005).
- ¹¹¹ T. Takaneka, K. Maruyama and K. Sakata, *Jpn. J. Appl. Phys.*, **30**, 2236 (1991).
- ¹¹² A. H. Kumar, P. W. McMillan and R. R. Tummala, *U. S. Patent* No. 4 301 324. (1981).
- ¹¹³ J. I. Steinberg, S. J. Horowitz and R. J. Bacher, *Advances in Ceramics*, J. B. Blum and W. R. Cannon (Editors), Am. Ceram. Soc., Weterville, OH, 31 (1986).
- ¹¹⁴ Y. Shimada, K. Utsumi, M. Suzuki, H. Takamizowa, M. Nitta and T. Watari, *IEEE Trans. Compon. Hybrids Manuf. Techn.*, **6**, 382 (1983).
- ¹¹⁵ S. Knickerbocker, A. H. Kumar and L. W. Herron, *Am. Ceram. Soc. Bull.*, **72**, 90 (1993).
- ¹¹⁶ *FERRO-TAPE-A6*, Technical publication, Ferro Coporation, Santa Barbara, CA (1996).
- ¹¹⁷ C-R. Chang and J-H. Jean, *J. Am. Ceram. Soc.*, **82**, 1725 (1999).
- ¹¹⁸ S. Nishigaki, S. Yano, J. Fukuta, M. Fukuyama, and T. Fuwa, *Proc. 85 Int. Symp. Hybrid Microelectronics (ISHM)*, 225 (1984).
- ¹¹⁹ Y. Imanaka and N. Kamehara, *J. Ceram. Soc. Jpn.*, **100**, 558 (1992).

-
- ¹²⁰ J-H. Jean and T. K Gupta, *J. Mater. Sci.*, **27**, 1575 (1992).
- ¹²¹ J-H. Jean and T. K Gupta, *J. Mater. Res.*, **9**, 486 (1994).
- ¹²² J-H. Jean and T. K Gupta, *J. Mater. Sci.*, **27**, 4967 (1992).
- ¹²³ K. G. Ewsuk, L. W. Harrison and F. J. Walezak, *Ceram. Trans. Ceram. Powd. Sci. II*, **1**, 969 (1987).
- ¹²⁴ K. G. Ewsuk, *Ceram. Trans.*, **15**, 279 (1990).
- ¹²⁵ R. M. German, *Sintering Science and Technology*, R. M. German, G. L. Messing and R. G. Cornwall (Editors), Penn State University, University Park, P. A., 259, (2000).
- ¹²⁶ J. U. Knickerbocker, *Am. Ceram. Soc. Bull.*, **72**, 1393 (1992).
- ¹²⁷ J-H. Jean and J-I Shen, *Jpn. J. Appl. Phys.*, **35**, 3942 (1996).
- ¹²⁸ M. Eberstein, W. A. Schiller, O. Dernovsek and W. Wersing, *Glastech. Ber-Glass Sci. Tech.*, **73**, 371 (2000).
- ¹²⁹ Y. Imanaka, *Multilayered Low Temperature Cofired Ceramics (LTCC) Technology*, Springer Science, U.S.A., (2005).
- ¹³⁰ K. P. Surendran, P. Mohanan and M. T. Sebastian, *J. Solid State Chem.*, **177**, 4031 (2004).
- ¹³¹ J. H. Park, Y-J. Choi and J-H. Park, *Mater. Chem. Phys.*, **88**, 308 (2004).
- ¹³² O. Dernovsek, A. Naeini, G. Preu, W. Wersing, M. Eberstein and W. A. Schiller, *J. Eur. Ceram. Soc.*, **21**, 1693 (2001).
- ¹³³ S. Renjini, S. Thomas, R. Kiran, V. R. K. Murthy and M. T. Sebastian., *Int. J. Appl. Ceram. Tech.* **5**, 1 (2008).
- ¹³⁴ L. Navias and R. L Green, *J. Am. Ceram. Soc.*, **29**, 267 (1946).
- ¹³⁵ J. O. Israd, *Int. Conf. Comp. Mater. Electron. Pack. Eng. IEEE*, 3636 (1961).
- ¹³⁶ J. M. Stevels, *Non-crystalline Solids*, V.D. Frechette (Editor), Wiley, New York, (1958).
- ¹³⁷ J. M. Wu and H. L. Huang, *J. Non Cryst. Solids*, **260**, 116 (1999).
- ¹³⁸ C. Zweben, *Materials for Electronic Packaging*, D. D. L. Chung (Editor), Butterworth-Heinemann, Boston, (1995).

-
- ¹³⁹ D. P. Almond, C. R. Bowen and D. A. S. Rees, *J. Phys. D: Appl. Phys.*, **39**, 1295 (2006).
- ¹⁴⁰ Y. Sun, Z. Zhang and C. P. Wong, *Polym.*, **46**, 2297 (2005).
- ¹⁴¹ L. M. Walpita, P. N. Chen, H. A. Goldberg, A. Harris and C. Zipp, *U.S. Patent No. 5739193* (1998).
- ¹⁴² M. G. Pecht, G. R. Agarwal, P. McCluskey, T. Dishongh, S. Javadpour and R. Mahajan, *Electronic Packaging Materials and their Properties*, CRC Press, London, (1999).

Chapter 2

SYNTHESIS AND CHARACTERIZATION OF DIELECTRIC CERAMICS

The sequential description of various steps involved in the synthesis of low loss dielectric resonator materials and polymer composites are described in this chapter. A qualitative discussion on the structural as well as microwave characterization tools to determine the relative permittivity, quality factor (dielectric loss) and temperature coefficient of resonant frequency of ceramics is given. A brief description of the instrumentation techniques used for studying the structural, microstructural, dielectric and thermal characteristics of low loss materials and polymer composites studied in the purview of this thesis is also presented.

2.1 SYNTHESIS OF DIELECTRIC RESONATORS

2.1.1 Introduction

Innovation in technology has always resulted from improvement in materials. For ceramics to be the key to such innovation, new materials must be developed and processes established for their production. As new materials and even newer technologies are developed; methods of handling, forming and finishing are required to be devised to maintain pace with this rapid rate of development. One of the most prominent examples of this rapid and accelerating technological development is the electronics industry. The 20th century has produced the greatest advancement in ceramics and materials technology since humans have been capable of conceptive thought. As the limits of metal-based systems are surpassed, new materials capable of operating under higher temperatures, higher speeds, longer life factors and lower maintenance costs are required to maintain pace with technological advancements. Metals, by virtue of their unique properties: ductility, tensile strength, abundance, simple chemistry, relatively low cost of production, ease of forming, ease of joining, etc. have occupied the vanguard position in regard to materials development. By contrast ceramics: brittle by nature, having a more complex chemistry and requiring advanced processing technology and equipment to produce, perform best when combined with other materials, such as metals and polymers which can be used as support structures.

Ceramics for today's engineering applications are synthesized using highly refined raw material, rigorously controlled composition, strictly regulated forming and sintering and are known as "*Fine or Advanced Ceramics*". Advanced ceramics possess properties which allow their use in a variety of defense and commercial applications. In comparison with metals, these materials demonstrate superior wear resistance, high temperature strength, favorable electrical properties, chemical resistance, dimensional stability, and high strength-to-weight ratios. These properties place this new group of ceramics in a most attractive position, not only in the area of performance but also cost effectiveness. Ceramics are oxides or non-oxides of metallic and non-metallic elements which are

generally compounds of electropositive and electronegative elements of the periodic table. Ceramics are polycrystalline, and grain boundaries exist which have a large influence on the physical and chemical properties. The microstructure of the ceramics contains: fine crystalline grains, grain boundaries, impurities and crystal lattice defects in the grains and grain boundaries and pores in the grain as well as in grain boundaries.¹ Technical or Engineering ceramic production is a demanding and complex procedure. Most of the synthesis methods of organic and metallic counterparts are generally not suitable for ceramics, due to the brittleness and refractory nature of ceramic materials. Ceramic fabrication techniques generally include various powder processing methods with powder synthesis, forming and sintering. The powder synthesis processes of ceramics include several techniques² like (a) solid state reaction methods (b) mechanical methods and (c) chemical methods. High purity materials and precise methods of production must be employed to ensure that the desired properties of these advanced materials are achieved in the final product.

In the mechanical methods, small particles are produced from larger ones by mechanical forces, a process known as comminution. The process of comminution involves operations such as crushing, grinding and milling. Mechanical treatment of ceramic powders can reduce particle size and enables to obtain nano-structured powders. However, this method lacks the synthesis of phase pure ceramics, which is essential for the fabrication of dielectric ceramics with optimum dielectric properties.

2.1.2 Solid State Synthesis of Ceramics

Dielectric resonator applications require bulk artefacts of dielectric material. The most realistic method of preparing ceramic powders is by solid-state reaction methods, because it is the simplest, easier and cost effective method for producing bulk ceramics. Conventional solid state synthesis techniques involve heating mixtures of two or more solids to form a solid phase product. The conventional ceramic approach basically can be broken down into four stages³ (a) powder preparation (b) high temperature calcination (c) green body preparation and (d) sintering.

Both thermodynamic and kinetic factors are important in solid state reactions since solids react together only at higher temperatures for reaction to occur at an appreciable rate.⁴ Thermodynamic considerations show whether or not a particular reaction should occur by considering the changes in free energy that are involved; kinetic factors determine the rate at which reaction occurs. In heterogeneous reactions between two solids, the actual reaction to form the product occurs at an interface. In kinetic studies of reaction rates, there are three possibilities to know the slow, rate-controlling step in a reaction. They are (1) transport of matter to the reaction interface (b) reaction at the interface and (c) transfer of matter away from the reaction interface. Rates of reaction are controlled by three factors: i) The area of contact between reacting solids which in turn depends on the surface area ii) The rate of diffusion of ions through the various phases and especially through the product phase. Two ways to increase the rate of diffusion are: (a) increase temperature (b) introduce defects by starting with reagents that decompose prior to or during reaction, such as carbonates or nitrates iii) The rate of nucleation of the product phase which can be maximized by using reactants with crystal structures similar to that of the product. Extensive reaction will not occur until the temperature reaches at least 2/3 of the melting point of one or more of the reactants.⁵

The solid-state reaction method, which is involved in the present work, involves the following steps. Since each of these steps affects the final ceramic properties they must all be understood, and a more holistic approach is required when processing ceramics compared to metals and polymers.

2.1.2.1 Powder Preparation

2.1.2.1.1 Select Appropriate Starting Materials

Fine grain powders to maximize surface area, reactive starting reagents and well defined compositions are the three criteria that must be taken into account while selecting appropriate starting materials. The oxides of the constituent cations are used in this method. In some instances, notably Ba, the oxide is not suitable because it is either unstable or highly hygroscopic. In such cases, the carbonate or nitrate is used, because

they will decompose to oxides on heating and are more reactive. The impurities are detrimental to dielectric properties and they affect reactivity of the fired ceramics too.³ Hence raw material purity of greater than 99.9% is essential for obtaining phase pure compounds.

2.1.2.1.2 Weighing of Raw Materials

The most common route is the mixed oxide route, where oxides of the constituent cations which act as reactants are weighed in stoichiometric proportions. Electronic balance of accuracy up to four decimal places is used for weighing raw materials.

2.1.2.1.3 Stoichiometric Mixing

After the dry powders have been weighed out in their stoichiometric proportion, they must be intimately mixed to increase the point of contacts between reactant oxides, which act as “product layer formation centers”. The mixing and milling eliminates agglomeration and reduces particle size. If agglomerates are present they densify more rapidly resulting in pores. During the mixing process agglomerates are broken and defects are introduced into the grains that enhance diffusion mechanism. Therefore the mixture of powders is ground well and thoroughly mixed using distilled water or acetone. Generally ball mills and vibromills (or attrition mills) are the most widely used milling tools for advanced ceramics.

(a) Ball Milling

Ball Milling is a method of grinding and mixing material, with or without liquid, in a rotating cylinder or conical mill partially filled with grinding media such as balls. In ball mills, in which tumbling action is accompanied by size reduction of particles, shear is the predominant mechanism (see Fig. 2.1(a)).⁶ The mechanical stress leads to elastic and inelastic deformation. If the stresses exceed ultimate strength of the particle, it will not only fracture the particles but also produce other physical changes in the particle.⁷ Other factors that affect mixing of particles in a ball mill are the mill speed,^{8,9} grinding media to material density ratio,¹⁰ and charge fill level, a fraction of mill's total volume

occupied by the charge.^{11,12} Most mixing experiments have been carried out at low speeds with particles of either the same size or different size but same density.^{7,13} The rate of grinding (η) depends upon the radii of the mill bottle and density of the milling media and initial particle size of the powder.¹⁴

$$\eta \approx \frac{AR^{1/2}\rho d}{r} \quad (2.1)$$

where A is the numerical constant that is specific to the mill being used, R and r are the radius of the mill and balls respectively, ρ the density of the balls and d particle size of the powder.

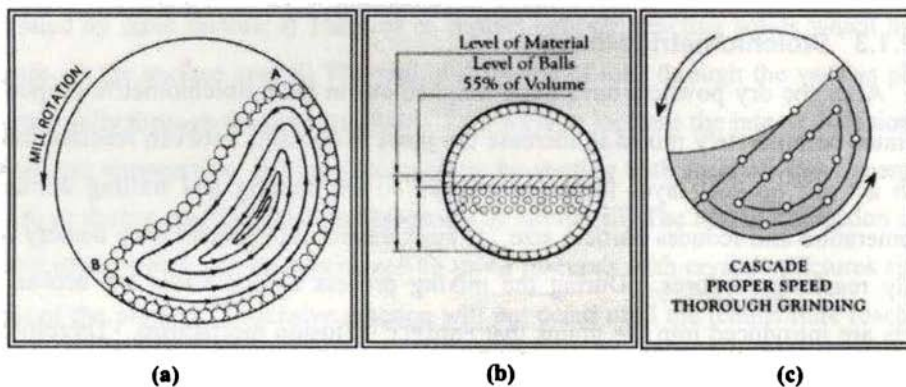


Fig.2.1 (a) Size reduction process in tumbling ball milling (b) Optimum ball-to-powder ratio and (c) Optimum speed in ideal milling conditions.

The type of mixer used can affect particle mixing and each mixer is characterized by the predominant mixing mechanism. The mechanisms of particle mixing are diffusion, shear and convection. The grinding of solid matters occurs under exposure of mechanical forces that trench the structure by overcoming of the interior bonding forces. After grinding, the state of the solid is changed: the grain size, the grain size disposition and the grain shape.¹⁵ The ball mill must operate below the critical angular frequency (F_c), at which centrifuging of media takes place and all milling effectively stops. The suspension is very viscous slurry, which effectively decreases F_c and ball milling normally operate at $0.7-0.8F_c$.

For wet milling, the balls and slurry together should occupy 50% of the mill volume with the solid content of the slurry equal to 20-40%. For dry milling, for a

quantity of balls filling about 50 % of the mill volume, the permissible charge content is 25%. As the shape of the milling media (ball) determines the product size distribution, cylindrical balls with dome ends are used to ensure uniform size distribution with narrow distribution curves.¹⁶ Fig. 2.1(b) and (c) shows the optimum ball-to-powder ratio and optimum speed in ideal milling conditions. In the present investigation, the mixture of constituent powders taken in polythethylene bottles were ball milled for sufficient duration in distilled water medium using Yttria Stabilized Zirconia (YSZ) balls (10 mm diameter and 12 mm height cylindrical balls).

2.1.2.2 Calcination

Calcination is the intermediate heat treatment of a substance below the melting or fusing point to bring about thermal decomposition or a phase transition in its the physical or chemical constitution. The modifications achieved by calcination are: coarsening, decomposition, reaction and dehydration.¹⁷ Coarsening involves crystallite growth or fusing or bonding small particles together to produce larger particles. Decomposition involves converting compositions such as carbonates and nitrates to a solid oxide and a gas.

The kinetics of solid state reactions occurring during calcination may be controlled by (i) the reaction at the interface between the reactant and the solid product, (ii) heat transfer to the reaction surface (iii) gas diffusion or permeation from the reaction surface through the porous product layer. The calcination conditions such as temperature, duration of heating and atmosphere are important factors controlling shrinkage during sintering. Though the final phases of interest may not be completely formed, the calcination yields a consistent product.

2.1.2.3 Green Body Preparation

2.1.2.3.1 Grinding

All dry powders have a tendency to agglomerate and there is a range of agglomerates in a ceramic mix. Grinding prepares the reacted material for ceramic forming. The calcined powder is ground to reduce the particle size, reduce agglomerates and mix the powder. The grinding also helps to homogenise the compositional variations

that still exist or may arise due to calcination. Generally after grinding, the powder size around 1-10 μm is advisable. If the grind is coarser, the ceramic may have large intergranular voids and low fired density. If grinding is too fine, the colloidal particles may interfere with subsequent forming operations.¹⁸ Generally, a ball mill or mortar with pestle is used. In large-scale operation, a grinding medium is chosen that suffers very little wear.

2.1.2.3.2 Addition of Polymeric Binder

Binders are particles, which form bridges between flocculated ceramic grains. The binder allows the powder particles to slide past each other to rearrange in the closest possible packing by forming temporary bonds. Binders have strong influence on the properties of granules, such as bulk density, flow rate and compaction behaviour.¹⁹ A good binder for ceramic applications should provide high green strength and appropriate elastic properties for handling and shaping during the post forming stage.²⁰ Green strength is provided by polymer-polymer and polymer-ceramic powder interactions. The two most popular binders for dry pressed ceramics are polyvinyl alcohol (PVA) and polyethylene glycol (PEG). The research trends suggest that 3-4 wt % of PVA and PEG which are water thinnable polymeric dispersions are ideal binders for fabrication of microwave dielectric ceramics.²¹ PVA binders generally provide high green strength while PEG binders provide high green density. PVA at low level of usage of the binder will not affect the dielectric properties as it will burn out at low temperatures ($\sim 400^\circ\text{C}$).

2.1.2.3.3 Powder Compaction

Powder pressing, an important stage in the ceramic processing, either uniaxially or isostatically is the most common method used for high volume production of ceramic components.^{22,23,24} The aim of powder pressing is to form a net-shaped, homogeneously dense powder compact that is nominally free of defects. A typical pressing operation has three basic steps: (i) filling the mold or die with powder (ii) compacting the powder to a specific size and shape and (iii) ejecting the compact from the die.²⁵ Die

filling/uniformity influences compaction density, which ultimately determines the size, shape, microstructure and properties of the final sintered product.^{26, 27} To optimize die filling and packing uniformity, free-flowing granulated powders are generally used. During powder pressing, the compaction pressure promotes consolidation by granule rearrangement and granule deformation. Particle coordination number, green density and compact strength all increase with increasing pressure, while volume and size of the porosity in the compact decrease.^{28,29} Friction between the powder and die wall decreases the pressure available for compaction with increasing distance from the pressing punch which in turn increases the density gradient in the compact.³⁰ Friction is influenced by the die material and its surface finish, as well as the powder and organic additives. Die-wall friction effects can be minimized with smooth surface dies and carbide tooling.³¹ Internal lubricants such as Stearic acid dissolved in Propan-2-ole, can aid processing. In the present study shaping is done using uniaxial press (Carver Inc., Wabash, U. S.)

Uniaxial pressing involves the compaction of powder into a rigid die by applying pressure in a single axial direction through a rigid punch or piston. The presses are usually mechanical or hydraulic. The pressure gradient in powder compact as a function of the distance from upper punch is given by the formula

$$P_x = P_a \exp \left[-4\mu K \frac{L}{D} \right] \quad (2.2)$$

where μ is the coefficient of friction, P_a is the applied pressure, L is the length and D is the diameter of the powder compact. When the length to diameter ratio is smaller, the pressure distribution of a powder compact is more uniform.³² In the microwave dielectric measurements, D/L ratio ≈ 2 and hence pressure distribution is more or less uniform. A pressure of 50-150 MPa is ideal in ceramic forming.

2.1.2.4 Sintering

Sintering is the process of heating a powder compact (40-60% of theoretical density) to a temperature between $\frac{1}{2}$ to $\frac{3}{4}$ of the absolute melting point by which particles are formed into a coherent body, to achieve higher strength and density. The criteria that

should be met before sintering can occur are (1) A mechanism for material transport must be present (2) A source of energy to activate and sustain this material transport must be present. The primary mechanism for transport is diffusion and viscous flow. Heat is the primary source of energy, in conjunction with energy gradients due to particle-particle contact and surface tension.¹⁷ The driving force for sintering is a decrease in the surface free energy of powdered compacts by the elimination of solid-vapor interfaces. Sintering is the bonding together of particles when heated to higher temperatures. On a microstructural scale, this bonding occurs as cohesive necks (weld bonds) grow at the points of contact between particles.³³ During sintering, neck growth by the movement of mass to the neck is desirable because it reduces the surface energy by decreasing the total surface area. This can happen by (i) reduction of the total surface area by an increase in the average size of the particles, which leads to coarsening and (ii) the elimination of solid/vapor interfaces and the creation of grain boundary area, followed by grain growth, which leads to densification.³⁴

Sintering can occur in the presence or absence of a liquid phase. In solid state sintering, densification is achieved through changes in particle shape, without particle rearrangement or the presence of the liquid. In liquid phase sintering the compositions and firing temperatures are chosen such that some liquid is formed during processing which aids compaction.³⁴

2.1.2.4.1 Solid State Sintering

Solid state sintering is the process in which fine particles, which are in contact with each other, agglomerate when heated to a suitable temperature, which results in the decrease in porosity.³⁵ The development of microstructure and densification during sintering is a direct consequence of mass transport through several possible paths and this bulk transport occurs by evaporation-condensation, surface diffusion, volume diffusion, grain boundary diffusion and viscous or creep flow.

The purpose of sintering is the reduction of compact porosity. Coble³⁵ described a sintering stage as an "interval of geometric change in which pore shape is totally defined

or an interval of time during which the pore remains constant in shape while decreasing in size." Three stages of sintering are an initial, an intermediate and a final stage (shown in Fig. 2.2(a)-(d)). During the initial stage, the interparticle contact area increases by neck growth (see Fig. 2.2(e)) and relative density increases from about 60 to 65 percent. Fig. 2.2(f) shows the SEM micrograph of neck formation in sintered alumina. The intermediate stage is characterized by continuous pore channels that are coincident with three-grain edges. During this stage the relative density increases from 65 to 90 percent by having matter diffuse toward, and vacancies away from the long cylindrical channels. The final stage begins when the pore phase is eventually pinched off and is characterized by the absence of a continuous pore channel. Individual pores are either of lenticular shape, if they reside on the grain boundaries, or rounded, if they reside within a grain. An important characteristic of this stage is the increase in pores and grain boundary mobilities, which have to be controlled if the theoretical density is to be achieved.³⁴ Solid state sintering involves movement of atoms that in turn is dependent on temperature and concentration of structural imperfections such as vacancies and interstitials. The process variables in sintering are (a) sintering temperature (b) sintering time (c) sintering atmosphere. The factors affecting solid state sintering are (a) particle size and particle size distribution (b) particle shape (c) uniformity of green microstructure (d) particle composition and (e) green density.³⁴

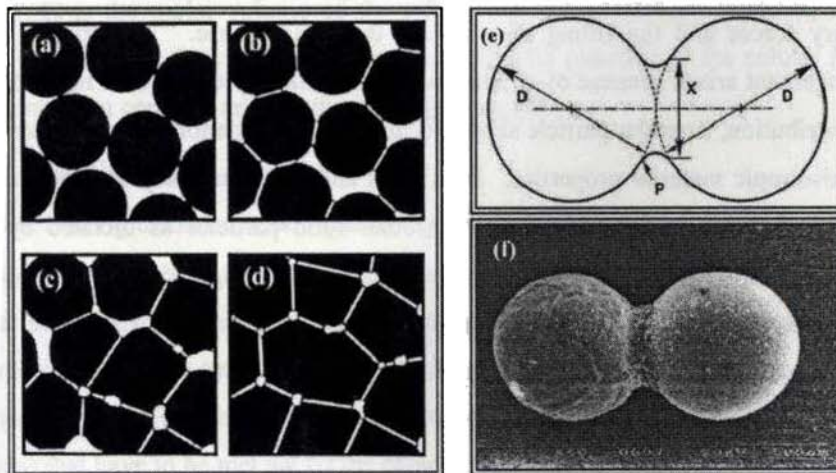


Fig. 2.2 (a) & (b) Initial stage, (c) Intermediate stage and (d) Final stage of sintering (e) Neck formation during first stage and (f) SEM picture of neck formation in sintered alumina (After Ref. 37)

2.1.2.4.2 Liquid Phase Sintering (LPS)

Liquid Phase Sintering is a subclass of the sintering process involving particulate solid along with a coexisting liquid during some part of the thermal cycle. Two major advantages of LPS over solid state sintering are it is more rapid and results in uniform densification. The disadvantages of LPS are that ceramics densified by LPS has a susceptibility to shape deformation and it may be difficult to control the sintering parameters due to additional complications from the liquid phase. The presence of a liquid phase greatly enhances grain boundary diffusion and grain boundary sliding. When solids and liquids are present together, capillary forces that result from the surface tension are generated. These forces can give rise to strong attractive forces between neighbouring particles, which when combined with the lubricating potential of the liquid, can lead to very rapid and significant particle rearrangement and densification. Upon melting, a wetting liquid will penetrate between grains and exert an attractive force, pulling them together. The combination of these forces and the lubricating effect of the liquid as it penetrates between grains leads to the following mechanisms that operate in succession:^{36,37}

a) Particle rearrangement

Initial densification results from particle rearrangement under the influence of capillary forces and the filling of pores by the liquid phase. The driving force for rearrangement arises because of an imbalance in capillary pressure as a result of particle size distribution, irregular particle shape, local density fluctuation in the powder compact and anisotropic material properties. Both solid and liquid are subject to rearrangement because of unbalanced capillary forces around solid particles as dictated by particle contact and liquid meniscus geometries that result in shearing and rotational movements of particles. As density increases, particles experience increasing resistance to further rearrangement due to crowding by neighbouring particles until the formation of a closed packing structure. Particle rearrangement is very rapid, and if during the early stages of

sintering, the liquid flows and completely fills the finer pores between the particles, 100 percent densification can result almost instantaneously.

b) Solution reprecipitation

In solution reprecipitation different solubilities of the solid in the liquid are responsible for the transport of the material from the points of solid-solid contacts to the free surfaces of the particles. When rearrangement becomes insignificant, additional densification can be achieved by dissolution of the solid at grain contacts thus resulting in the center-to-center approach of particles. The dissolved solute transfers to the uncompressed part of the grain structure by diffusion through a liquid phase followed by reprecipitation on uncompressed solid surface for a multicomponent system. There are two rate-limiting processes for solution-precipitation - diffusion controlled and interface reaction controlled material transport. The densification rate for diffusion controlled (equation (2.3)) and interface reaction controlled (equation (2.4)) material transport are

$$\frac{d(\Delta\rho/\rho_o)}{dt} = B(g) \frac{\delta D_b C_1 \gamma_v \Omega}{kT} r^{-4} \quad (2.3)$$

$$\frac{d(\Delta\rho/\rho_o)}{dt} = C(g) \frac{KC_1 \gamma_v \Omega}{kT} r^{-4} \quad (2.4)$$

where $B(g)$ and $C(g)$ are the geometrical constants, δ is the thickness of the liquid boundary, Ω is the molar volume of the solute, k is the Boltzmann constant, T is the absolute temperature, D is the grain boundary diffusion constant of the solute, K is the interface reaction constant and r is the initial particle size.

c) Solid state sintering

Once a rigid skeleton is formed, liquid phase sintering stops and solid state sintering takes over, and the overall shrinkage or densification rates are significantly reduced. Unless the liquid phase penetrates completely between solid particles, the presence of the liquid is not effective as an aid to sintering.

Based on the above discussion, for rapid densification to occur during LPS, the conditions that have to be met are (i) the composition is so chosen that the material which forms the solid phase during sintering is soluble in the liquid phase (ii) the sintering

temperature must be high enough so that an appreciable amount of liquid phase is present (iii) there must be good wetting of a liquid on solid.³⁸ Clearly, LPS of ceramics is more forgiving in terms of powder packing, more rapid, and hence more economical than the solid-state version. The presence of a glassy film at the grain boundaries can have a very detrimental effect on properties. If the properties required are not adversely affected by the presence of a liquid, then LPS is the preferred route.³⁴

2.2 SYNTHESIS OF POLYMER-CERAMIC COMPOSITES

2.2.1 Powder Processing Method

In the present study, PTFE/ceramic composites were prepared by powder processing technology. In order to create an active surface for binding with polymer, the fine powder of ceramic was mixed with acrylic acid solution for 1 hour and then dried.¹⁶ The dried powder was again treated with 2 wt% tetra butyl titanate. The use of titanate based coupling agents provides excellent mechanical and electrical properties compared to other organic functional coupling agents like silane. The evaporation of the solvent gives ceramic powders clad with coupling agents. Different volume fractions (0 to 0.6) of treated ceramics and PTFE powders were dispersed in ethyl alcohol using ultrasonic mixer for about 30 minutes. A dry powder mixture was obtained by removing the solvent at 70°C under stirring. This led to the formation of thoroughly mixed PTFE/ceramic powders. These homogeneously mixed composite powders were then compacted under uniaxial pressure of 50 MPa for 1 minute. The cylindrical and rectangular pellets thus obtained were kept at 310°C for 2hrs.

2.2.2 Sigma Blend Method

The starting materials, polyethylene and ceramic were mixed thoroughly in a kneading machine. The kneading machine consists of variable speed mixer having two counter rotating sigma blades with a gear ratio of 1:1.2 and heating facility up to 350°C (Fig. 2.3). The counter rotating sigma blades ensure fine mixing by applying high shear force on the dough-like mixture. Different volume fractions ceramics were added to the

melted polyethylene and blended at suitable temperature for 30 minutes. Thus obtained composites were thermo laminated under a pressure of 200 MPa and optimized temperature for 15 min. After thermolamination, the composites with desired shapes were polished for dielectric measurements. In the present investigation, HDPE/CeO₂ composites were prepared by sigma blend method.

2.3 STRUCTURAL AND MICROSTRUCTURAL CHARACTERIZATION OF DIELECTRIC RESONATORS

2.3.1 X-Ray Diffraction

The X-Ray diffraction method is most useful for qualitative, rather than quantitative, analysis (although it can be used for both). Qualitative analysis usually involves the identification of a phase or phases in a specimen by comparison with “standard” patterns (i.e., data collected or calculated by someone else), and relative estimation of proportions of different phases in multiphase specimens by comparing peak intensities attributed to the identified phases. Quantitative analysis of diffraction data usually refers to the determination of amounts of different phases in multi-phase samples and also the precise determination of crystal structure or crystallite size and shape.

An X-Ray diffractometer utilizes a powdered sample, an X-ray generator, a goniometer and a fixed-position detector to measure the diffraction patterns of unknowns. When Monochromatic x-rays strikes a powder sample mounted on a slide, diffraction occurs in every possible orientation of 2θ . Mount is then rotated to ensure all diffractions are obtained. The diffracted beam may be detected by electronic x-ray counters (detectors) that can measure intensities much more accurately. Computers are used to process data and make necessary complex calculations. The resulting analysis is described graphically as a set of peaks with percentage intensity on the Y-axis and goniometer angle on the X-axis. The exact angle and intensity of a set of peaks is unique to the crystal structure being examined.³⁹ A monochromator is used to ensure that a specific wavelength reaches the detector, eliminating fluorescent radiation. The resulting trace consists of a recording of the intensity against counter angle (2θ). The trace can

then be used to identify the phases present in the sample. Then use the Bragg equation to solve for the interplanar spacings (d) for all the major peaks and look up a match with JCPDS cards. (JCPDS = Joint Committee on Powder Diffraction Standards) Routinely, a 2θ range of 5 to 70 degrees is sufficient to cover the most useful part of the powder pattern. Comparing the observed data with that in the PDF allows the phases in the sample to be identified.^{40,41} In this investigation XRD spectra were recorded using CuK α radiations employing Philips X-ray Diffractometer (Model- Expert Pro), Netherlands.

2.3.2 Scanning Electron Microscopy

The Scanning Electron Microscope (SEM) is critical in all fields that require characterization of solid materials. In the present investigation SEM is used to analyze



Fig. 2.3 Kneading machine used in our lab for sigma blending technique. Inset figure shows the sigma blades

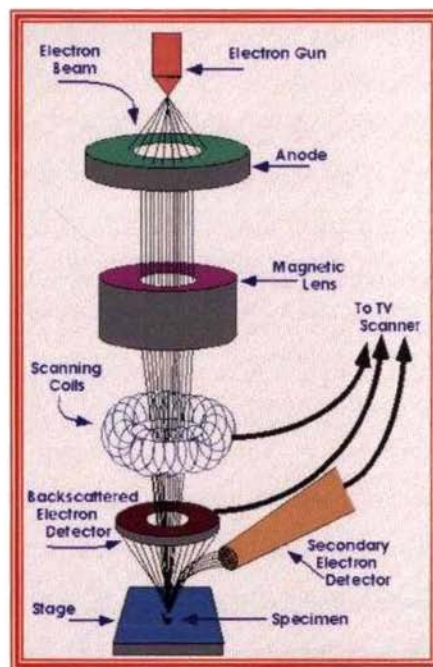


Fig. 2.4 Schematic Diagram of SEM (courtesy www.purdue.edu/REM/rs/sem.htm)

the microstructure of sintered and thermally etched surface of ceramic samples. SEM generates high-resolution images of shapes of objects (SEI) and Energy Dispersive X-ray Analysis (EDXA) is used to show spatial variations in chemical compositions. A schematic diagram of SEM is shown in Fig. 2.4. In this method, an electron beam is produced at the top of the microscope by an electron gun. The electron beam, which typically has an energy ranging from a few hundred eV to 100 keV, is focused by one or two condenser lenses into a beam with a very fine focal spot sized 0.4 nm to 5 nm. The beam passes through pairs of scanning coils or pairs of deflector plates in the electron optical column, typically in the objective lens, which deflect the beam horizontally and vertically so that it scans in a raster fashion over the sample surface. When the primary electron beam interacts with the sample, the type of signals gathered include secondary electrons, characteristic x-rays, and back scattered electrons. In SEM these signals come not only from the primary beam impinging upon the sample, but from other interactions within the sample near the surface. The SEM is capable of producing high-resolution images of a sample surface in its primary use mode, secondary electron imaging. Due to the manner in which this image is created, SEM images have great depth of field yielding a characteristic three-dimensional appearance useful for understanding the surface structure of a sample. The resolution of SEM can fall somewhere between less than 1 nm and 20 nm. An electrically conductive (usually gold) coating must be applied to electrically insulating samples. In this study we have used a Scanning Electron Microscope of Jeol JSM-5600LV, Japan for the microstructural evolution of ceramic samples prepared.

2.3.2.1 Energy Dispersive X-ray Analyzer (EDXA)

An Energy Dispersive X-ray Analyzer (EDXA) is a common accessory which gives the SEM a very valuable capability for elemental analysis. The electron beam in an SEM has energy typically between 5,000 and 20,000 electron volts (eV). The energy holding electrons in atoms (the binding energy) ranges from a few eV up to many kilovolts. Many of these atomic electrons are dislodged as the incident electrons pass

through the specimen, thus ionizing atoms of the specimen. Ejection of an atomic electron by an electron in the beam ionizes the atom, which is then quickly neutralized by other electrons. In the neutralization process an x-ray with an energy characteristic of the parent atom is emitted. By collecting and analyzing the energy of these x-rays, the constituent elements of the specimen can be determined. Its characterization capabilities are due in large part to the fundamental principle that each element of the periodic table has a unique atomic structure allowing the x-rays that are characteristic of an element's atomic structure to be uniquely distinguished from each other. There are four primary components of the EDXA setup: the beam source; the X-ray detector; the pulse processor; and the analyzer. Electron microscopes are equipped with a cathode and magnetic lenses to create and focus a beam of electrons. A detector is used to convert X-ray energy into voltage signals; this information is sent to a pulse processor, which measures the signals and passes them onto an analyzer for data display and analysis.

2.4 MICROWAVE CHARACTERIZATION OF DIELECTRIC MATERIALS

2.4.1 Introduction

Microwave materials have been widely used in a variety of applications ranging from communication devices to military satellite services, and the study of material properties at microwave frequencies and the development of functional microwave materials have always been among the most active areas in solid-state physics, materials science, and electrical and electronic engineering. In recent years, the increasing requirements for the development of high-speed, high frequency circuits and systems require complete understanding of the properties of materials functioning at microwave frequencies. All these aspects make the characterization of material properties an important field in microwave electronics. This section deals with the microwave methods applied to materials property characterization.

The dielectric properties at microwave frequency range can be measured by resonant and non-resonant methods. Non-resonant methods are often used to get a

general knowledge of electromagnetic properties over a frequency range, while resonant methods are used to get accurate knowledge of dielectric properties at a single frequency or at several discrete frequencies. Precisely measuring the dielectric properties of a material are important to predict the system performance. The generally adopted methods for characterization of dielectric properties of materials at microwave frequencies fall into (i) reflection methods (ii) transmission line methods (iii) optical methods (iv) perturbation methods (v) exact resonance methods. The choice of method will depend on the value of ϵ_r and loss factor, the amount of material available and the accuracy required. Once the resonant frequencies, Q -factors of the resonant structures and dimensions of the test samples are measured, computations have to be performed to obtain ϵ_r and loss factor.

Optical methods: Optical methods are applicable for below wavelength of one centimetre. Since this method requires large amount of material, it is not suitable for DRs.⁴²

Transmission line technique: This method has a serious disadvantage of the very small waveguide size used below 4 mm, which gives rise to practical difficulties. More over imperfections in the sample dimensions produce errors in the measurement. It was reported that the accuracy of transmission mode measurements of the dielectric properties is more in weak coupling conditions.⁴³

Reflection method: In this method, waves reflected from the dielectric are studied. When the dielectric constant becomes large, there occurs considerable error in the measurement of complex voltage reflection coefficient.⁴⁴

Perturbation Technique: The perturbation methods are highly suitable for materials of small size since the material should not alter the field configuration considerably. These techniques are suitable for relative permittivities less than 10, although this range can be extended by an exact solution of the resonator containing the specimen.⁴⁵ Hence this technique is not commonly used for DR characterization. In the present study this

technique is used to measure the dielectric properties of polymer ceramic composites which are having low relative permittivity less than 10.

Resonance method: This is the most accurate method as compared to the above-mentioned methods for the measurement of DRs. In this method, the exact resonant frequency of the resonator is measured using different techniques.⁴⁶ From the resonant characteristics, parameters like ϵ_r , Q etc are determined.

The ideal technique for the determination of the microwave dielectric properties of low loss materials is exact resonance methods, which will be discussed in detail in this chapter. Apart from this technique, alternate methods to characterize DRs such as Whispering Gallery Mode Technique and Split-Post Dielectric Resonator Method will be discussed in the following section.

2.4.1.1 Whispering Gallery Mode Resonators

Whispering Gallery Mode (WGM) Dielectric Resonators are often used in characterizing extremely low loss dielectrics, high relative permittivity materials, anisotropic dielectrics and ferrites. WGM DRs are very interesting due to (i) their relatively large dimensions even in millimeter wavelength band (ii) the quality factors are very high since they depends only on the loss tangent of the material used as the DR (iii) the radiation losses are negligible (iv) WGM resonators have good suppression of spurious modes because the propagation constant along the Z-axis is very small and the unwanted modes leak out axially and can be absorbed without perturbation (v) they offer high level of integration to planar circuits.⁴⁷ The resonant frequencies were calculated from the dimensions and relative permittivity, determined by the end-shortened method assuming $\epsilon_{11} = \epsilon_{\perp}$ where ϵ_{11} is the relative permittivity parallel to the anisotropic axis and ϵ_{\perp} , the one perpendicular to it. The modes which have high electric energy filling factor (WGM modes) will have the highest quality factor.⁴⁸

The dielectric loss tangent for the isotropic dielectric can be determined⁴⁹ using the equations

$$Q_{(E)}^{-1} = \tan\delta (P_{e_{-}} + P_{e_{+}}) + R_s / G_{(E)} \quad (2.5)$$

$$Q_{(H)}^{-1} = \tan\delta (P_{e_{-}} + P_{e_{+}}) + R_s / G_{(H)} \quad (2.6)$$

where R_s is the surface resistance of the cavity enclosing the DR.

2.4.1.2 Split-Post Dielectric Resonator Method

Split-post resonator methods are suitable for the characterization of dielectric sheet samples, including dielectric substrates for planar circuits.⁵⁰ In a split-post dielectric resonator (SPDR) method,⁵¹ the measurement fixture usually has a cylindrical structure working at a TE mode, and the resonator is split into two parts at the electric current node along a plane perpendicular to the cylinder axis. The sample under test is placed in the gap between the two parts of the resonator, and usually the sample is at the place of maximum electric field. The loading of a dielectric sheet sample changes the resonant properties of a split resonator, and the dielectric properties of the sample can be derived from the resonant properties of the resonator loaded with sample and the dimensions of the resonator and the sample.

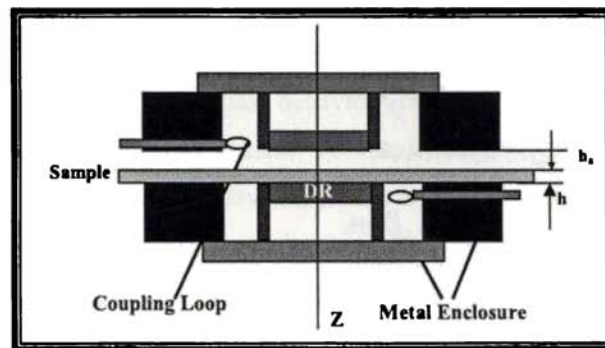


Fig 2.5 Geometry of a split-post dielectric resonator fixture for the measurement of the complex permittivity of dielectric sheet sample

The proposed geometry of a split-dielectric resonator fixture for the measurement of the complex permittivity of dielectric sheet samples is shown in Fig. 2.5. Split-post dielectric resonator usually operates with the TE_{018} mode, which has only azimuthal electric field component, so the electric field remains continuous on the dielectric

interfaces. The field distributions are affected by the introduction of the sample, which in turn changes the resonant frequency, and the unloaded Q -factor of the sample. For low-loss materials, the influence of losses on the resonant frequencies is negligible, so the real part of permittivity of the sample under test is related to the resonant frequencies and physical dimensions of the cavity and sample only. The calibration technique is used and we compare the difference of resonant frequency of the split dielectric resonator before and after the sample is inserted. The relative permittivity of the sample is an iterative solution to the following equation⁵²

$$\varepsilon_r = 1 + \frac{f_o - f_s}{hf_o K_\varepsilon(\varepsilon_r, h)} \quad (1.47)$$

where h is the thickness of the sample under test, f_o is the resonant frequency of empty resonant fixture, f_s is the resonant frequency of the resonant fixture with dielectric sample, K_ε is a function of ε_r and h . The dielectric loss tangent of the sample can be determined by

$$\tan \delta = \frac{1}{p_{es}} \left(\frac{1}{Q} - \frac{1}{Q_{DR}} - \frac{1}{Q_c} \right) \quad (1.48)$$

with

$$p_{es} = h\varepsilon_r K_1(\varepsilon_r, h) \quad (1.49)$$

$$Q_c = Q_{c0} K_2(\varepsilon_r, h) \quad (1.50)$$

$$Q_{DR} = Q_{DR0} \cdot \frac{f_o}{f_s} \cdot \frac{p_{eDR0}}{p_{eDR}} \quad (1.51)$$

where p_{es} and p_{eDR} are the electric-energy filling factors for the sample and for the split resonator respectively; p_{eDR0} is the electric-energy filling factor of the dielectric split resonator for empty resonant fixture; Q_{c0} is the quality factor depending on metal enclosure losses for empty resonant fixture; Q_{DR0} is the quality factor depending on dielectric losses in dielectric resonators for empty resonant fixture; and Q is the unloaded quality factor of the resonant fixture containing the dielectric sample. The values of p_{eDR} , p_{es} and Q_c for a given resonant structure can be calculated using numerical

techniques. In terms of sample geometry, the only requirements are that the sample must extend beyond the diameter of the two cavity sections and the sample must be flat. This provides the accuracy of a resonator technique without having to machine the sample. Typical uncertainty of the permittivity measurements of a sample of thickness h can be estimated as $\Delta\epsilon'/\epsilon = \pm(0.0015 + \Delta h/h)$ and uncertainty in loss tangent measurements $\Delta \tan \delta = 2 \times 10^{-5}$.

2.4.2 Network Analyzer

Network Analyzer is the major instrument used in this investigation for the characterization DRs. A measurement of the reflection from and/or transmission through a material along with knowledge of its physical dimensions provides the information to characterize the permittivity and permeability of the material. Network Analyzer is a swept frequency measurement equipment to completely characterize the complex network parameters in comparatively less time, without any degradation in accuracy and precision. Two types of network analyzers are available, scalar and vector network analyzers. Scalar network analyzer measures only the magnitude of reflection and transmission coefficients while the vector network analyzer measures both the magnitude and phase. Both the magnitude and phase behavior of a component can be critical to the performance of a communications system. A vector network analyzer can provide information on a wide range of these devices, from active devices such as amplifiers and transistors, to passive devices such as capacitors and filters.

A basic network analyzer is designed to show graphically, a plot of the voltage gain or loss of a network versus frequency. The network analyzer measures the magnitude, phase and group delay of two-port networks to characterize their linear behaviour. A vector network analyzer consists of a signal source, a receiver and a display. The source launches a signal at a single frequency to the material under test. The receiver is tuned to that frequency to detect the reflected and transmitted signals from the material. The measured response produces the magnitude and phase data at that frequency. The source is then stepped to the next frequency and the measurement is

repeated to display the reflection and transmission measurement response as a function of frequency (Bode response plot). The analyzer can operate in ramp or in step mode. In the ramp mode the analyzer directs the source to sweep in a linear ramp over the frequency and in the step mode, it provides maximum precision.

2.4.3 Measurement of Relative Permittivity (ϵ_r)

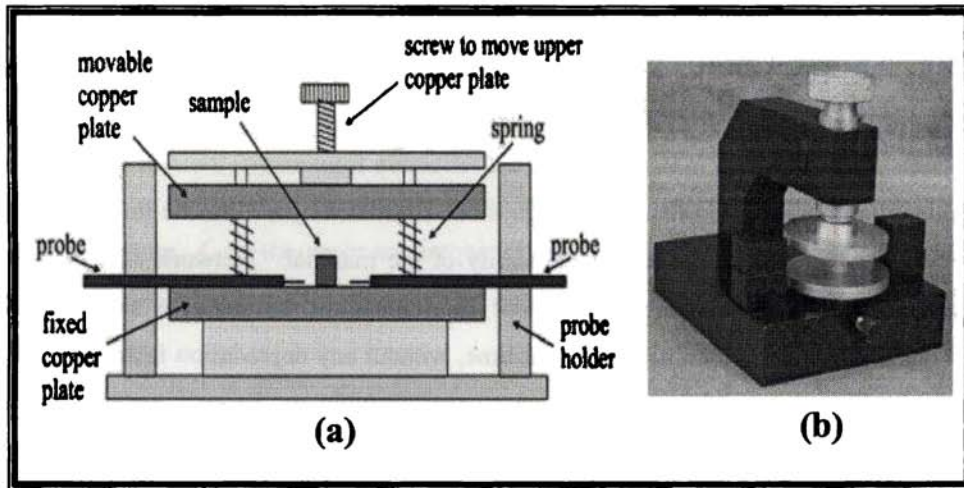


Fig. 2.6 (a) Hakki Coleman set up used for DR measurements and (b) dielectric rod kept end shorted between two mathematically infinite conducting plates

The complex permittivity of dielectric resonator is often measured by the method developed by Hakki and Coleman⁵³ and modified by Courtney.⁵⁴ This set up is shown in Fig. 2.6 (a). A cylindrical disc of material having relative permittivity ϵ_r , length L and diameter D is sandwiched between two mathematically infinite conducting plates (well polished copper plates coated with silver or gold), is shown in Fig. 2.6 (b). The TE_{011} mode is widely used in this method. If the dielectric material is isotropic then the characteristic equation for this resonant structure operating in the TE_{0ml} mode is written as

$$\alpha \frac{J_0(\alpha)}{J_1(\alpha)} = -\beta \frac{K_0(\beta)}{K_1(\beta)} \quad (2.5)$$

where $J_0(\alpha)$ and $J_1(\alpha)$ are Bessel functions of the first kind of orders zero and one respectively. The $K_0(\beta)$ and $K_1(\beta)$ are the modified Bessel functions of the second kind of order zero and one respectively. The parameters α and β depend on the geometry, the resonant wavelength inside and outside the DR respectively and dielectric properties. Thus

$$\alpha = \frac{\pi D}{\lambda_o} \left[\epsilon_r - \left(\frac{l\lambda_o}{2L} \right)^2 \right]^{1/2} \quad (2.6)$$

$$\beta = \frac{\pi D}{\lambda_o} \left[\left(\frac{l\lambda_o}{2L} \right)^2 - 1 \right]^{1/2} \quad (2.7)$$

where l = the longitudinal variations of the field along the axis, L = Length of the DR, D = Diameter of the DR, λ_o = free space resonant wave length. The characteristic equation is a transcendental equation and hence a graphical solution is necessary. Corresponding to each value of β there are infinite number of (α_n) that solves the characteristic equation. Hakki and Coleman⁵³ obtained a mode chart showing the variation of α values as a function of β and are shown in Fig. 2. 7.

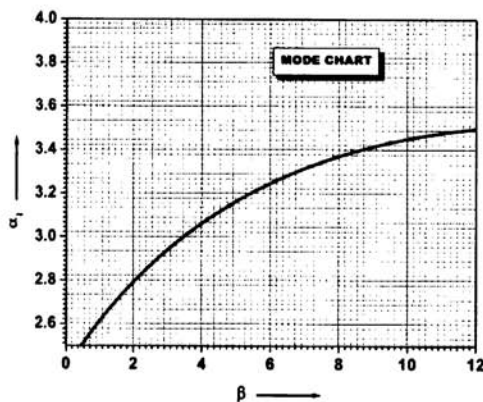


Fig. 2.7 Mode charts of Hakki -Coleman giving α_1 as functions of β .

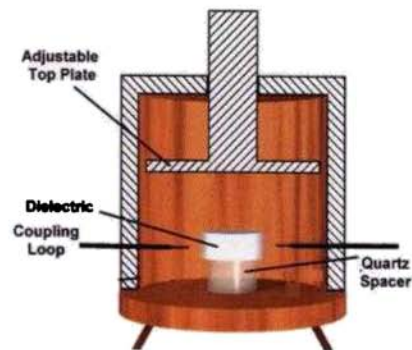


Fig. 2.8 The cavity set up for the measurement of Q-factor.

The relative permittivity of the resonator can be calculated using the mode chart parameters (α_1 and β_1), the resonant frequency (f_r) and the dimensions of the dielectric puck using the equation

$$\epsilon_r = 1 + \left[\frac{c}{\pi D f_r} \right]^2 (\alpha_1^2 + \beta_1^2) \quad (2.8)$$

Courtney⁵⁴ proposed two horizontally oriented E-field probes for coupling microwave to the dielectric resonator, which enabled to span a wide range of frequencies, since there is no cut-off frequency for coaxial lines. The TE_{011} mode is used for the measurements since this mode propagates inside the sample but is evanescent outside the geometry of DR. Therefore a large amount of electrical energy can be stored in the high Q dielectric resonators.⁵⁵ In the end shorted condition the E -field becomes zero close to the metal wall and electric energy vanishes in the air gap.⁵⁶ The TE_{011} mode is chosen for measurement because for this mode only azimuthal component of electric field exists and the error due to the air gap is practically eliminated.⁵⁷

A Vector Network Analyzer (Model 8753 ET, Agilent Technologies, Hewlett-Packard, Palo Alto, CA) is used for taking measurements at microwave frequencies. The HP 9000, 300 series instrumentation computer, interfaced with network analyzer makes the measurement quicker and accurate. The specimen is placed approximately symmetrical with the two E -probes. The resonant modes (represented by spikes in the resonance spectrum) are visualized by giving a wide frequency range by adjusting the Network Analyzer. To select the TE_{011} resonance from the several modes having non zero E_z components, the upper metal plate is slightly tilted to introduce an air gap. As the plate is tilted the entire TM modes move rapidly to the higher frequencies while the TE_{011} mode remains almost stationary. It is well known that in exact resonance technique, TE_{011} is least perturbed by the surroundings. After identifying the TE_{011} resonant frequency or central frequency (f_r), the span around f_r is reduced as much as possible to get maximum resolution. The 3 dB bandwidth of the curve decreases and a stage of saturation is reached when the width will remain the least possible. The coupling loops are fixed at

this position and the centre frequency can be noted corresponding to the maxima as f_r . By knowing the diameter ' D ' and length ' L ' of the sample β is calculated using equation (2.7). From the mode chart, the value of α_l corresponding to β_l value is noted. The relative permittivity ϵ_r is calculated using equation (2.8). The advantages of this method are very simple measurement configuration and easy access for introducing and removing the test samples. This is one of the fairly accurate and the most frequently used techniques for measurement of permittivity and this method is proposed as one of the international standards IEC techniques for measurements of the complex permittivity of low loss solids.

2.4.4 Measurement of Unloaded Quality Factor (Q_u)



Fig.2.9 Experimental set up used in our lab to measure the microwave dielectric properties

The Q -factor of microwave resonators is measured using various methods.^{58,59,60,61} However, all these methods failed to account for the practical effects such as noise, cross talk, coupling losses, transmission line delay, and impedance mismatch introduced by a

real measurement system. Inadequate accounting of these effects may lead to significant uncertainty in the measured quality factor of the DRs. Moreover the microwave loss factors of DRs are affected by many other intrinsic and extrinsic factors (See section 1.6 of Chapter 1). When Q of a DR sample is measured by the end shorted method of Courtney, the measured Q factor is affected by the conductor and radiation losses. Hence to reduce these effects, in our present study, we use a transmission mode cavity proposed by Krupka *et al.* (Fig. 2.8).⁶² Fig. 2.9 shows the experimental set up used in our laboratory to measure the dielectric properties. The specimen was placed on a low loss quartz spacer of height 8 mm inside a copper cavity of inner diameter 40 mm and height 22 mm whose inner side was finely polished and silver plated to reduce radiation loss. The use of low loss single crystal quartz spacer reduces the effect of losses due to the surface resistivity of the cavity. Samples with diameter/length (D/L) ratio of 1.8 - 2.2 is preferable to get maximum mode separation and to avoid interference from other modes. Microwaves are fed into the sample using two loop coaxial antennas, which provides a magnetic coupling to excite the transmission mode resonance spectrum of dielectric cylinder. The coupling is adjusted to be optimum (weak coupling for high Q_u and strong coupling for lossy samples). Observe S_{21} versus frequency spectrum. In principle the cavity has infinite number of modes, when excited with microwave spectrum of frequencies. $TE_{01\delta}$ mode is identified as the fundamental mode with least perturbation when the tunable top lid is adjusted properly. After identifying the desired mode, the lid is fine tuned to get maximum separation between $TE_{01\delta}$ and any nearby cavity modes, to attain maximum possible accuracy in the Q_u measurement. Measure $TE_{01\delta}$ mode frequency and the unloaded and the 3 dB bandwidth from the resonance spectrum (Fig. 2.10) to calculate the Q factor as

$$Q = \frac{f_u}{\Delta f} \quad (2.9)$$

Fig. 2.11 shows the microwave resonance spectrum of CeO_2 ($\epsilon_r=23$) in transmission configuration. The electromagnetic field could penetrate into the

conducting walls of the cavity which lowers the measured Q value of the DR. Usually the dimensions of the cavity are such that the $TE_{01\delta}$ mode of the DR is the lowest resonance. The quality factor decreases when the cavity diameter/puck diameter ratio is smaller than three. Hence the cavity normally used is 3-5 times the size of the sample. The surface resistance of copper can be calculated from the quality factor of the TE_{011} resonance of the empty cavity to apply correction to the measured Q of the sample for the loss due to cavity walls.⁶³

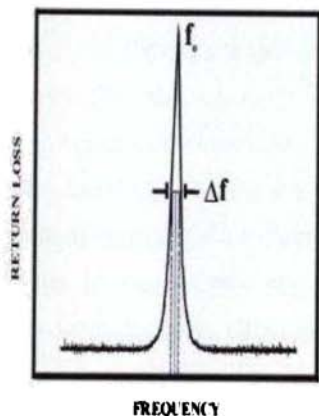


Fig. 2.10 The method of calculating Q -factor from resonant mode using equation (2.9)

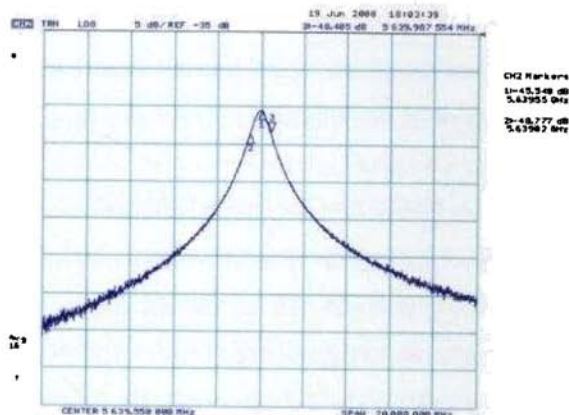


Fig. 2.11 The microwave resonance spectrum of CeO_2 ($\epsilon_r=23$) in transmission configuration

2.4.5 Measurement of Temperature Coefficient of Resonant Frequency (τ_f)

The temperature coefficient of resonant frequency (τ_f) is the parameter which indicates the stability of the resonator. The electronic devices with microwave resonators should have τ_f values as close to zero as possible. The τ_f can be measured by the cavity method used for measuring the quality factor. The use of invar cavity can minimize the inaccuracy caused due to the thermal expansion of the cavity while heating. The cavity is then kept on a hot plate and the entire system is insulated in an isothermal enclosure. The set up is then slowly heated ($\sim 1^\circ\text{C}/\text{minute}$) in the range 25 to 80°C . The probe of the

thermocouple is kept just inside the isothermal enclosure so that it does not disturb the resonant frequency. Shift in the resonant frequency of $TE_{01\delta}$ mode is noted at every 2°C increment in temperature. The variation of resonant frequency is plotted as function of temperature and the τ_f is calculated from the slope of the curve using the equation (2.10)

$$\tau_f = \frac{1}{f} \frac{\Delta f}{\Delta T} \quad (2.10)$$

The temperature coefficient of relative permittivity τ_ϵ is of considerable interest to users of dielectric substrates. This can be obtained by the parallel plate capacitor method using an LCR meter at low frequency (eg., 1 MHz) and heating the sample. From the ϵ_r noted at different temperatures the τ_ϵ can be obtained.

2.4.6 Cavity Perturbation Method

The most used technique to determine the measurement of dielectric parameters of materials depends on the measurement of either reflection coefficients or resonant frequencies. In a resonant perturbation method, the sample under test is introduced to a resonant cavity, and the electromagnetic properties of the sample are deduced from the change of resonant frequency and quality factor of the resonating cavity. Resonant perturbation method using hollow metallic cavity is called cavity perturbation method.⁶⁴ Bethe and Schwinger⁶⁵ first proposed the perturbation theory of resonant cavities. In the past cavity perturbation technique was the only method available to obtain approximate solutions but its applications were limited not only to low permittivity samples but also to a specific modes and specific samples.

Cavity perturbation methods are widely used in the study of the electromagnetic properties of dielectrics, semiconductors, magnetic materials and composite materials. It works well for the determination of the dielectric characteristics of thin sheet samples of low and medium dielectric loss.^{57,66} In the cavity perturbation technique, a small piece of the material usually in the form of a disk or sheet is placed in a metallic resonant cavity operating in a known mode. The material characteristics are estimated from the shift in the resonant frequency and change in the Q of the system.^{67,68,69} This technique was

pioneered by Slater⁷⁰ and is a suitable method for measuring the dielectric properties of materials with permittivity less than 10. The cavity perturbation method is not a swept frequency measurement since the measurement frequencies are determined by the cavity as well as the DR dimensions. Hence it can be used only for discrete frequency measurements. In this method a rectangular wave guide with a small slot at the broader wall at the middle is used and the cavity is excited with optimum iris coupling, typically the diameter of the iris is equal to the shorter dimension of the Wave Guide (WG)/2.2 can be used for the measurement of dielectric properties of the samples. The resonant frequency and quality factor of the empty cavity is determined for different cavity modes. Then the thin sheet sample is inserted and positioned at the E-field antinode. If the sample is purely dielectric the maximum electric field can be easily determined by simply moving the sample across the slit. The mode will shift to low frequency side and retraces from there. The sample is kept at the retracing position, this is the electric field maximum position. If it is slightly magnetic the permittivity can be measured only for the odd modes by keeping it at the middle of the cavity. The new resonant frequency and Q of the sample is again measured. The complex relative permittivity ($\epsilon_r = \epsilon_r' + \epsilon_r''$) of the sample is calculated using the following Equations (2.32-2.34).^{57,59,71}

$$\epsilon_r' = 1 + \left[\frac{V_c(f_0 - f_s)}{4V_s f_s} \right] \quad (2.32)$$

$$\epsilon_r'' = \frac{(\epsilon_r' - 1)}{2\epsilon_r'} \frac{f_s}{(f_0 - f_s)} \left[\frac{1}{Q_s} - \frac{1}{Q_0} \right] \quad (2.33)$$

$$\tan \delta = \frac{\epsilon_r''}{\epsilon_r'} \quad (2.34)$$

where f_0 = resonant frequency of the empty cavity, f_s = resonant frequency of the cavity with sample, V_c = Volume of the cavity and V_s = Volume of the sample, Q_0 is the quality factor of the empty cavity and Q_s is the quality factor of the cavity with sample. The experimental error was found to be less than 2% in case of permittivity and 1.3% in the

case of dielectric loss. Here also the measured Q_s and Q_o can be corrected by measuring S_{11} and S_{22} as mentioned earlier by proper calibration of the Network analyzer. It is better to use Wave guide TRL calibration for better accuracy at the ends of the waveguide to coaxial adaptor. Calibrate the Network Analyzer for full 2 port using TRL calibration. Now S_{11} and S_{22} are measured at the resonant frequency. As mentioned earlier calculate the coupling coefficients for the two ports and find the unloaded quality factors Q_u and Q_s . The main advantage of this method is the easiness of determining the permittivity and loss using simple device with moderate accuracy.

2.4.7 Radio Frequency Dielectric Measurements

LCR meters are generally used for measurement of the capacitance and dissipation factor of capacitors in the radio frequency region by the well-known parallel plate capacitor method.³⁴ One can also measure the ϵ_r and $\tan \delta$ at radio frequencies by the parallel plate capacitor method using an LCR meter for new materials. This will give an approximate idea of ϵ_r and $\tan \delta$ which in turn helps to calculate the approximate resonant frequency of the DR using the equation (1.19) of section 1.5.1, Chapter 1. The knowledge of the value of the resonant frequency further helps to know the size of the DR at a given frequency or the size of the cavity required to measure the Q-factor. In the present study, the dielectric properties at radio frequency are measured using LCR meter (HIOKI 3532-50 LCR Hi TESTER, Japan).

2.4.8 Error Calculations in Dielectric Property Measurements

The measurement of microwave dielectric properties is done with two decimal point accuracy. Usually three samples were prepared in a batch corresponding to a particular composition and the measurements were made at least twice per each specimen. The sample should be well polished to avoid the error due to surface roughness. The error in ϵ_r is calculated using the root sum of squares (RSS) method. The accuracy of ϵ_r measurement is restricted to the accuracy in measurement of resonant frequency and dimensions of the sample. The possible error in the measurement of

permittivity is of the order of 0.3%. Such an error is possible when dimensional uncertainties of the samples are in the order of 0.15%. Hence the possible errors in the measured value of relative permittivity of a sample of height (L), radius (r) and resonant frequency (f_r) given by

$$\Delta \epsilon_r = \left[\left(\frac{\partial \epsilon_r}{\partial L} \Delta L \right)^2 + \left(\frac{\partial \epsilon_r}{\partial r} \Delta r \right)^2 + \left(\frac{\partial \epsilon_r}{\partial f_r} \Delta f_r \right)^2 \right]^{1/2} \quad (2.19)$$

If the independent sources of error correspond to one standard deviation, then the error in ϵ_r will also correspond to one standard deviation.⁷² The uncertainty in quality factor using TE₀₁₈ mode cavity method with optimized enclosure is of the order of $\pm 2 \times 10^{-6}$. The errors in unloaded quality factor (Q_u) and temperature coefficient of resonant frequency (τ_f) were calculated using Root Sum Square (RSS) method by taking partial derivative of these parameters with respect to independent variables. A measurement calibration is used to eliminate the systematic (stable and repeatable) measurement errors caused by the imperfections of the system. Random errors due to noise, drift, or the environment (temperature, humidity, pressure) cannot be removed with a measurement calibration. This makes a microwave measurement susceptible to errors from small changes in the measurement system.⁷³ These errors are minimized by adopting good measurement practices, such as visually inspecting all connectors for dirt or damage and by minimizing any physical movement of the test port cables after a calibration.

2.5 THERMAL CHARACTERIZATION

Thermal analysis is “A group of techniques in which a physical property of a substance and/or its reaction products is measured as a function of temperature whilst the substance is subjected to a controlled temperature program.”⁷⁴ Three methods which provide primarily chemical rather than physical information about samples of matter are Thermogravimetry, Differential Thermal Analysis and Differential Scanning Calorimetry.

2.5.1 Thermo Gravimetric Analysis (TGA) and Differential Thermal Analysis (DTA)

In a thermo gravimetric analysis the mass of a sample in a controlled atmosphere is recorded continuously as a function of temperature or time as the temperature of the sample is increased. Thermo gravimetric methods are largely limited to decomposition and oxidation reactions and to physical processes such as vaporization, sublimation and desorption. DTA is a technique in which the difference in temperature between a substance and a reference material is measured as a function of temperature while the substance and reference material are subjected to a controlled temperature program. Information on the inorganic compounds such as dehydration, oxidation, reduction and solid-state reactions is provided by DTA.

2.5.2 Differential Scanning Calorimetry (DSC)

DSC is a thermal technique in which differences in heat flow into a substance and a reference are measured as a function of sample temperature while the two are subjected to a controlled temperature program. Both the sample and reference are maintained at nearly the same temperature throughout the experiment. The basic principle underlying this technique is that, when the sample undergoes a physical transformation such as phase transitions, more (or less) heat will need to flow to it than the reference to maintain both at the same temperature. Whether more or less heat must flow to the sample depends on whether the process is exothermic or endothermic. Differential scanning calorimetry can be used to measure a number of characteristic properties of a sample like fusion, crystallization events and glass transition temperatures (T_g), oxidation and other chemical reactions.^{75,76} In the present investigation DSC is used to determine the melting and crystallization temperature of the polymer-ceramic composite.

2.5.3 Thermo Mechanical Analysis (TMA)

In this technique (TMA), dimensional changes in a sample are the primary measured, with negligible force acting on it, while the sample is heated, cooled, or

studied at a fixed temperature. It is particularly suited to polymer materials but a wide range of materials can be examined.⁷⁷ In the present study, TMA (TMA-60H, Shimadzu, Kyoto, Japan) is used to determine the thermal expansion coefficient and softening temperature (by application of load and hemisphere-plugs) of composites. TMA is also used to confirm the softening and melting temperature of glass-ceramic composites used for low temperature cofired ceramic applications.

2.5.4 Photopyroelectric Technique

An improved photopyroelectric technique^{78,79} is used to determine the thermal conductivity of the polymer composites. A 70 mW He-Cd laser of wavelength 442 nm, intensity modulated by a mechanical chopper (model SR540) is used as the optical heating source. A PVDF film of thickness 28 μm , with Ni-Cr Coating on both sides, is used as pyroelectric detector. The out put signal is measured using a lock in amplifier (model SR 830). Modulation frequency is kept above 60 Hz to ensure that the detector, the sample and backing medium are thermally thick during measurements. The thermal thickness of the composites is verified by plotting photopyroelectric (PPE) amplitude and phase with frequency at room temperature. Thermal diffusivity (γ) and thermal effusivity (e) are also measured from PPE signal phase and amplitude⁸⁰. From the values of γ and e the thermal conductivity and specific heat capacity of the samples are obtained. In the present investigation thermal conductivity is measured for polymer-ceramic composites used for microwave substrates and electronic packaging applications.

2.6 REFERENCES

- ¹ N. Ichinose, *Introduction to Fine Ceramics, Applications in Engineering*, John Wiley and Sons, New York, (1987)
- ² D. Seagal, *Chemical Synthesis of Advanced Ceramic materials*, Cambridge University Press, Cambridge, (1991)
- ³ S. Penn and N. Alford, *Handbook of low and high dielectric constant materials and their applications phenomena, Properties and Applications*, (Editor Hari Singh Nalwa), Academic Press, (1999).
- ⁴ A. R. West, *Solid-State Chemistry and its Applications*, John Wiley and Sons., New York, (1984)
- ⁵ R. E. Carter, *J. Chem. Phys.*, **34**, 2010 (1961).
- ⁶ M. Poux, P. Fayolle, J. Bertrand, D. Bridoux and J. Bousquet, *Powder Technol.*, **68**, 213 (1991).
- ⁷ B. Beke, *Principles of Communiton*, Akademi Kiado, Budapest, (1964).
- ⁸ N. Nityanand, B. Maney and H. Henein, *Metal. Trans. B, Process Metallurgy*, **17B**, 247 (1986).
- ⁹ J. Bridgwater, *Powd. Technol.*, **15**, 215 (1976).
- ¹⁰ J. C. William, *Powd. Technol.*, **15**, 245 (1976).
- ¹¹ J. J. Mc Carthy, T. Shibrot, G. Metcalfe, J.E. Wolf and Ottino, *AIChE J.*, **42**, 3351 (1996).
- ¹² D. Brone, A. Alexander and F.J. Muzzio, *AIChE J.*, **44**, 271 (1998).
- ¹³ J. M. Ottino and D.V. Kharkhar, *Annual Rev. of Fluid Mech.*, **32**, 55 (2000).
- ¹⁴ J. G. Austin, *Powd. Technol.*, **5**, 1 (1971).
- ¹⁵ C. Chibwana and M.H. Moys, *Powd. Technol.*, **163**, 139 (2006).
- ¹⁶ H. E. Rose and R. M. E. Sullivan, *A Treatise on the Internal Mechanics of Ball, Tube and Rod mills*, Chemical Publishing, Boston, (1958).
- ¹⁷ D. W. Richerson, *Modern Ceramic Engineering, Properties, Processing, and use in design*, 3rd Ed., Taylor and Francis, London, (2006).
- ¹⁸ L. M. Sheppard, *Ceram. Ind.*, **149**, 51 (1999).

-
- ¹⁹ X. K. Wu, D. W. Whitman, W. L. Kaufell, W. C. Finch and D. I. Cumbers, *Ceram. Eng. Sci. Proc.*, **18**, 422 (1997).
- ²⁰ P. Winiewski, M. Szafran and G. Rokicki, *Key Eng. Mater., Euro Ceram.-VIII*, **264**, 428 (2000).
- ²¹ N. M. Alford, X. Wang, S. J. Penn, M. Poole and A. Jones, *Br. Ceram. Trans.*, **99**, 212 (2000).
- ²² B. J. McEntire, *Ceramics and Glasses, Engineered Materials Handbook*, 4th Ed., ASM Int., U.S.A., (1991).
- ²³ J. S. Reed, *Introduction to the Principles of Ceramic Processing*, John Wiley and Sons, New York, (1988).
- ²⁴ G. F. Austin and G. D. McTaggart, *Ceramic Fabrication Processes, Treatise on Materials Science and Techn.*, F. F. Y. Wang (Editor), 9th Ed., Academic Press, New York, (1976).
- ²⁵ S. Jill Glass and K. G. Ewsuk, *MRS Bulletin*, (1997).
- ²⁶ K. G. Ewsuk, *Characterization of Ceramics*, R. E. Loehman (Editor), Butterworth-Heinemann, Greenwich, CT, (1993).
- ²⁷ M. J. Readey and F. M. Mahoney, *Diversity into the next century, Int. SAMPE Tech. Conf. Ser., No. 27*, (Editors by R. J. Martinez, H. Arris, J. A. Emerson and G. Pike), SAMPE International, Covina, CA, (1995).
- ²⁸ A. B. van Groenou and R. C. D. Lissenburg, *J. Am. Ceram. Soc.*, **66**, 156 (1983).
- ²⁹ E. Artz, *Acta Metall.*, **30**, 1883 (1982).
- ³⁰ S. J. Glass, K. G. Ewsuk and F. M. Mahoney, *Ceramic Transactions*, (Editors T. K. Gupta, B. Hiremath and K. M. Nair), Am. Ceram. Soc., Westerville, OH, (1996).
- ³¹ R. B. Cass, K. G. Ewsuk and W. R. Blumenthal, *Ceram. Ind.*, **147**, 34 (1993).
- ³² D. F. Castro, *Sintering course*, Presented at Centro de estudios e Investigaciones Technicas de Gipuzkoa Centro de Estudios e investigaciones Technicas de Gipuzkoa, San Sebastian, (2000)
- ³³ R. M. German, *Fundamentals of sintering, in: Ceramics and Glasses, Engineered Materials Handbook*, 4th Ed., ASM Int. Ed., U.S.A., (1991)
- ³⁴ W. D. Kingery and M. Berg, *J. Appl. Phys.*, **26**, 1205 (1955).

-
- ³⁵ R. L. Coble, *J. Appl. Phys.*, **32**, 789 (1961).
- ³⁶ O-H Kwon, *Engineered Materials Handbook*, 4th Ed., ASM Int., USA, (1991).
- ³⁷ M. W. Barsoum, *Fundamentals of Ceramics*, CRC Press, New York, (2003).
- ³⁸ W. D. Kingery, *Introduction to Ceramics*, John Wiley and Sons, New York, (1960).
- ³⁹ G. E. Bacon, *X-ray and Neutron Diffraction*, Pergamon Press, Amsterdam, (1966).
- ⁴⁰ B. D. Cullity and S. R. Stock, *Elements of X-ray diffraction*, Prentice Hall, New Delhi, (2001)
- ⁴¹ D. L. Bish and J. E. Post, *Modern Powder Diffraction. Reviews in Mineralogy*, **20**, Mineralogical Association of America, Boston, (1989).
- ⁴² J. Mussil and F. Zacek, *Microwave Measurement of Complex Permittivity by Free Space Methods and Applications*, Elsevier, New York, (1986).
- ⁴³ K. Leong and J. Mazierska, *J. Supercond.*, **14**, 93 (2001).
- ⁴⁴ D. Kajfez, *Q Factor*, Vector Fields, Massachusetts, (1994).
- ⁴⁵ G. Birnbaum and J. Franeau, *J. Appl. Phys.*, **20**, 817 (1949).
- ⁴⁶ K. Wakino, *Proc. of The Second Sendai Int. Conf.*, YAGI Symposium on Advanced Technology Bridging the Gap between Light and Microwaves, 187 (1990).
- ⁴⁷ L. Rayleigh, *Phil. Mag.*, **20**, 1001 (1910).
- ⁴⁸ J. Krupka, D. Cros, M. Aubourg and P. Guillon, *IEEE Trans. Microwave Theory Tech*, **MTT-42**, 56 (1994).
- ⁴⁹ J. R. Wait, *Radio Sci.*, **2**, 1005 (1967).
- ⁵⁰ J. Krupka, S. Gabelich, K. Derzakowski and B. M. Pierce, *Meas. Sci. Tech.*, **10**, 1004 (1999).
- ⁵¹ J. Krupka, *Mater. Chem. and Phys.*, **79**, 195 (2003).
- ⁵² J. Krupka, A. P. Gregory, O. C. Rochard, R. N. Clarke, B. Riddle and J. Baker, *Eur. J Ceram. Soc.*, **21**, 2673 (2001).
- ⁵³ B. W. Hakki and P.D. Coleman, *IRE Trans. Microwave Theory Tech.*, **MTT-8**, 402 (1960).
- ⁵⁴ W. E. Courtney, *IEEE Trans. Microwave Theory Tech.*, **MTT-18**, 476 (1970).

-
- ³⁵ Y. Kobayashi, *IEEE Trans. Microwave Theory Tech.*, **MTT-28**, 1077 (1980).
- ³⁶ S. B. Cohn and K. C. Kelly, *IEEE Trans. Microwave Theory Tech.*, **MTT-14**, 406 (1966).
- ³⁷ D. L. Rebsch, D. C. Webb, R. A. Moore and J. D. Cawlishaw, *IEEE Trans. Microwave Theory Tech.*, **MTT-13**, 468 (1965).
- ³⁸ E. L. Ginzton, *Microwave Measurements*, McGraw Hill Book Co., Boston, (1957).
- ³⁹ E. J. Vanzura and J. E. Rogers: *Proc. of the IEEE Conference on Instrumentation and Measurement Technology*, Atlanta, (1991).
- ⁴⁰ T. Miura, T. Takahashi and M. Kobayashi, *IEICE Transactions on Electronics*, **E7 7-C** 900, (1994).
- ⁴¹ M. C. Sanchez, *IEE Proceedings-Part. H*, **134**, 243 (1987).
- ⁴² J. Krupka, K. Derzakowski, B. Riddle and J. B. Jarvis, *Meas. Sci. Technol.*, **9**, 1751 (1998).
- ⁴³ D. Kajfez and P. Guillon. *Dielectric Resonators*, Noble Publishing Corporation, Tucker, Georgia, U.S.A., (1998).
- ⁴⁴ L. F. Chen, C. K. Ong, C. P. NeO, V. V. Varadan and V. K. Varadan, *Microwave Electronics: Measurement and Materials Characterization*, John Wiley & Sons, England, (2004).
- ⁴⁵ H. A. Bethe and J. Schwinger, *NDRC Rep. D*, **1**, 117 (1943).
- ⁴⁶ A. Prakash, J. K. Vaid and A. Mansingh, *IEEE Trans. Microwave Theory and Tech.*, **MTT-27**, 791 (1979).
- ⁴⁷ W. Von Aubck and J. H. Rowen, *Bell System Technol. J.* **36**, 427 (1957).
- ⁴⁸ E. G. Spencer, R.C. Lecraw and F. Reggia, *Proc. IRE*, **44**, 790 (1956).
- ⁴⁹ J. O. Artman and P.E. Tannenwald, *Phys. Rev.*, **91**, 1014 (1953).
- ⁵⁰ J. Slater. *Rev. Mod. Phys.*, **18**, 441 (1946).
- ⁵¹ D. Li, C.E. Free, E. G. Pitt and P. G. Barnell, *IEEE Microwave and Wireless Comp. Lett.*, **11**, 118 (2001).
- ⁵² J. B. Jarvis, R. G. Gayer, J. H. Grosvenor Jr., M. D. Janezic, C. A. Jones, B. Riddle, C. M. Weil and J. Krupka, *IEEE Trans. Dielect. Electrical Insul.*, **5**, 571 (1998).

-
- ⁷³ Agilent Basics of Measuring the Dielectric Properties of Materials: Application Note, <http://www3.imperial.ac.uk/pls/portallive/docs/1/11949698.PDF>
- ⁷⁴ D. A. Skoog, F. J. Holler and T. Nieman, *Principles of Instrumental Analysis*. 5th Ed., New York, (1998).
- ⁷⁵ A. John Dean, *The Analytical Chemistry Handbook*, McGraw Hill Inc., New York, (1995).
- ⁷⁶ Pungor Erno and G. Horvai, *A Practical Guide to Instrumental Analysis*, 1st Ed., CRC Press, Boca Raton, New York, (1994).
- ⁷⁷ K. P. Menard, *Dynamic Mechanical Analysis; A Practical Introduction*, CRC Press, Boca Raton, (1999).
- ⁷⁸ C. P. Menon and J. Philip, *Meas. Sci. Tech.*, **11**, 1744 (2000).
- ⁷⁹ M. Marinelli, F. Murtas, M. G. Mecozzi and S. Martellucci, *Appl. Phys. A Mater. Sci. Proc.*, **51**, 387 (1990).
- ⁸⁰ M. T. Sebastian, C. P. Menon, J. Philip and R. W. Schwartz, *J. Appl. Phys.*, **94**, 3206 (2003).

Chapter 3

CeO₂-AO-TiO₂ (A = Ca, Mg, Zn, Mn, Co, Ni, W) CERAMICS: SYNTHESIS, CHARACTERIZATION AND MICROWAVE DIELECTRIC PROPERTIES

This chapter gives an introduction to cerium dioxide and fluorite structure. CeO₂-0.5AO-0.5TiO₂ (A = Mg, Zn, Ca, Mn, Co, Ni, W) dielectric ceramics have been prepared by conventional solid-state ceramic route. The structure, microstructure and elemental analysis were done by X-Ray Diffraction, Scanning Electron Microscopic and Energy Dispersive X-ray Analysis techniques. The dielectric properties of the materials were measured in the 3-6 GHz microwave frequency range. The effect of various amounts of di-, tri-, tetra-, penta- and hexavalent dopants on the microwave dielectric properties of CeO₂-0.5AO-0.5TiO₂ (A = Mg, Zn, Ca, Mn, Co, Ni, W) ceramics have been investigated. Improvement in relative permittivity, quality factor and temperature coefficient of resonant frequency was observed with the doping of small amounts of Co₃O₄, Cr₂O₃, TiO₂, CeO₂, WO₃ and MoO₃. This chapter also discusses the synthesis, characterization and microwave dielectric properties of ATiO₃ (A = Co, Mn, Ni) ceramics for the first time.

3.1 CERIUM DIOXIDE

3.1.1 Introduction

Cerium dioxide or ceria (CeO_2) is the most stable oxide of cerium. From valence state theory, cerium is supposed to have two types of oxides, cerium dioxide (CeO_2) and cerium sesquioxide (Ce_2O_3). Since CeO_2 is the most stable oxide, when the cerium oxide is mentioned, it usually refers to the tetravalent oxide. Cerium dioxide can be formed if cerium salt is calcined in oxygen rich environment.¹ Cerium oxide has three phases: Cerium dioxide (CeO_2) with the fluorite CaF_2 structure and Cerium sesquioxide (Ce_2O_3) having two structural forms, hexagonal (A-type) and cubic (C-type).² The crystal structures of the three phases of cerium oxide are shown in Fig. 3.1. Usually, cerium oxide exists as a non-stoichiometric oxide which is a mixture of Ce(III) oxide and Ce(IV) oxide, while still retaining the fluorite cubic structure. In oxygen poor conditions, Ce_2O_3 with oxygen vacancies is formed. In Ce_2O_3 , 4f states of Ce are reduced, and the valence is changed from +4 to +3.³ At room temperature, the hexagonal Ce_2O_3 crystal is unstable in air, but stable under anaerobic condition. The cubic Ce_2O_3 crystal, which can be considered as the CeO_2 crystal with ordered oxygen vacancies, is known to exist in a nonstoichiometric state in the temperature range of 1000–1200°C in hydrogen atmosphere.⁴ Cerium oxide is a highly stable, nontoxic, refractory ceramic material with a melting point of 2600°C and a density of 7.213 g/cm³. It has a face centred cubic fluorite structure with a lattice constant of 5.11 Å.⁵

3.1.2 Fluorite Structure

The general formula of crystals with the fluorite structure is MX_2 . Fig. 3.1 (a) shows the ideal cubic fluorite structure. Consider the stoichiometry of single unit cell. Each of the corner cerium ion is 1/8 inside the cell; since there are eight corners these add up to one ion inside the cell. There are six faces to a single cell, each with a cerium ion one-half inside the cell. Therefore a single cell contains four cerium ions. A single cell also contains eight oxygen ions, each one located entirely within the unit cell. Since there

are four cerium ions and eight oxygen ions inside the cell, the 1:2 stoichiometry is maintained and all the fluorite structure compounds have $Z = 4$. Fluorite tends to have mainly ionic cation-anion bonds.⁶ The fluorite structure is also adopted by several other halides and also by ZrO_2 , ThO_2 , UO_2 and PuO_2

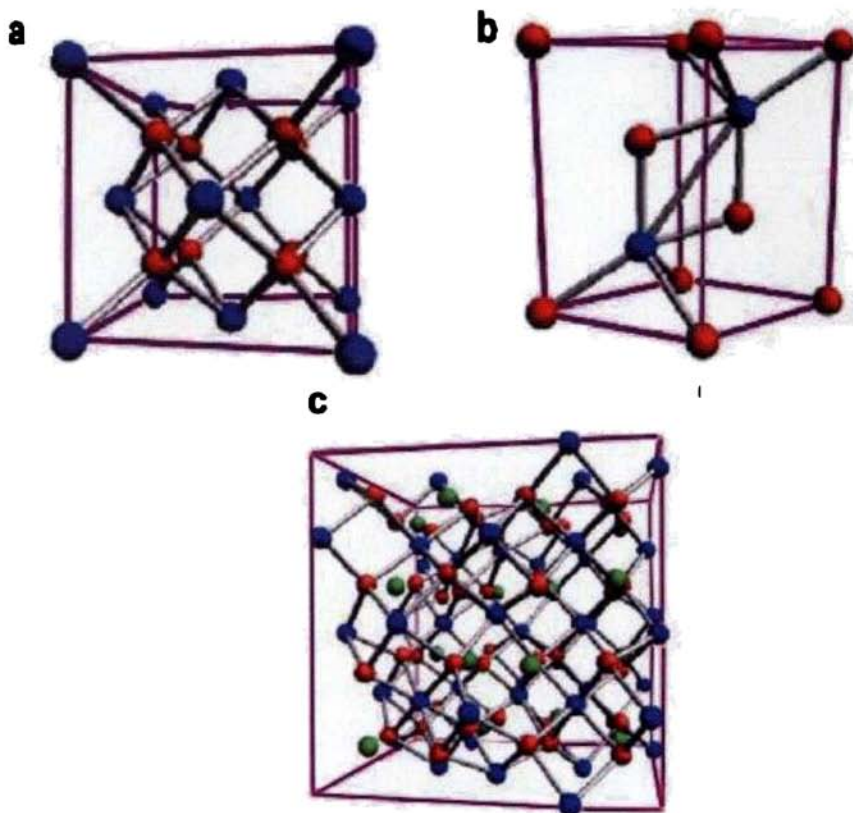


Fig. 3.1 Structures of (a) CeO_2 (Fm $\bar{3}$ m), (b) $h-Ce_2O_3$ (P3m1), and (c) $c-Ce_2O_3$ (Ia $\bar{3}$). Ce, O atoms, and O vacancies are indicated as blue, red, and green spheres respectively (after Ref. 4).

Stoichiometric ceria has a cubic fluorite crystal structure. At elevated temperatures and in reducing atmospheres, ceria can deviate from its stoichiometric composition to an oxygen-deficient composition $CeO_{2-\delta}$, by reduction of Ce^{4+} to Ce^{3+} without changing its fluorite structure (see Fig. 3.2). At 800°C, ceria can accommodate

up to ~14% oxygen vacancies, providing the opportunity to study the effects of large vacancy concentrations on a variety of properties of fluorite-structured oxides.

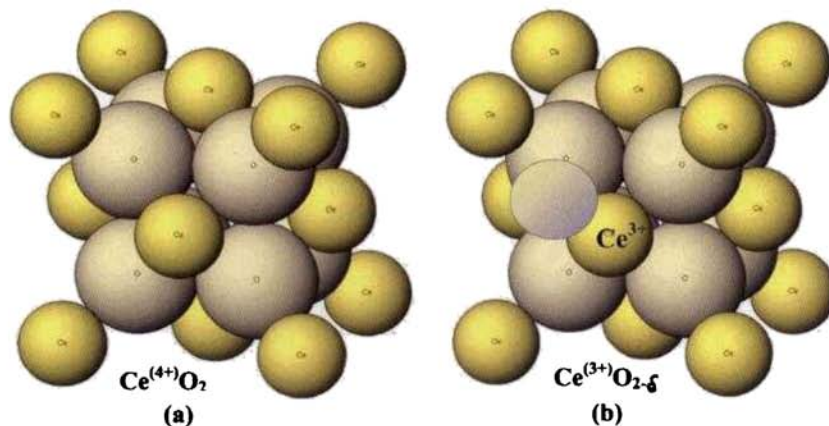


Fig. 3.2 Structure of (a) CeO_2 and (b) $\text{CeO}_{2-\delta}$ (courtesy wikis.lib.ncsu.edu/.../Fluorite/Antifluorite)

3.2 MILESTONES IN THE RESEARCH OF CeO_2 CERAMICS

Ceria is a promising insulating material with many potential applications in microelectronics and has attracted much attention in recent years. Ceria-based materials have been extensively investigated as catalysts, structural and electronic promoters of heterogeneous catalytic reactions, oxide ion conducting solid electrolytes in electrochemical cells, oxygen pumps and gas sensors.^{7,8,9,10} Ceria is also a good candidate for storage capacitors and gate insulators in DRAMS and MFIS FRAMS. Ceria nanoparticles are one of the key abrasive materials for chemical-mechanical planarization (CMP) of advanced integrated circuits. It has found applications in capacitors and buffer layers of superconducting materials.¹¹

In order to understand the properties of fine ceria particles, a large number of studies have been carried out on catalytic,^{12,13} electronic,¹⁴ lattice vibrational^{15,16} and structural properties^{17,18,19} as well as on various synthesis methods^{20,21} for ultrafine ceria particles. Ozawa²² investigated the sintering behaviour of fine CeO_2 powder and found that the accelerated sintering behaviour at 700-800°C and >1600°C is related with the

temperatures, the $Q_{i,rf}$ increases, reaches 105000 GHz at 30 K and then decreases to a minimum at ~ 100 K. Sub millimeter data shows that temperature dependence of extrinsic losses is mainly responsible for the temperature dependence of the Q factor.

Investigations on the dielectric properties of ceria revealed that it can be used as a good dielectric resonator material if temperature stability is achieved. This motivated us to investigate on the microwave dielectric properties of ceria based materials by the addition of suitable dopants and forming solid-solution with various rare earth ions. The use of ceria based composites for LTCC, packaging and substrate applications are also explored in the present study.

3.3 MICROWAVE DIELECTRIC PROPERTIES OF CeO_2 -AO- TiO_2 (A= Ca, Mg, Zn, Mn, Co, Ni, W) CERAMICS

3.3.1 Introduction

The growing importance of ceramic dielectrics for applications as microwave oscillators, filters etc. has led to great advances in the material research and development of dielectric ceramic systems. Miniaturization of microwave circuits using low loss and temperature stable dielectric ceramic resonators has spurred the wireless communication industry enormously. The stringent requirements of microwave dielectric properties prevent the use of all available DRs for practical applications and keep the development of advanced materials for wireless communication as a challenging area of research.⁴¹ The dielectric properties of CeO_2 are tailored by suitable substitution and by the formation of mixed phases having opposite τ_f . In the present work we examine the dielectric properties of CeO_2 with TiO_2 , in a novel group of ceria-titania based mixed system such as CeO_2 -0.5CaO-0.5 TiO_2 (CCaT), CeO_2 -0.5MgO-0.5 TiO_2 (CMgT), CeO_2 -0.5ZnO-0.5 TiO_2 (CZnT), CeO_2 -0.5MnO-0.5 TiO_2 (CMnT), CeO_2 -0.5CoO-0.5 TiO_2 (CCoT), CeO_2 -0.5NiO-0.5 TiO_2 (CNiT) and CeO_2 -0.5 WO_3 -0.5 TiO_2 (CWT). To further improve the dielectric properties, small amount of dopants were added to the calcined powder before sintering.

3.3.2 Experimental

The samples of $\text{CeO}_2\text{-}0.5\text{AO-}0.5\text{TiO}_2$ (A = Mg, Zn, Ca, Mn, Co, Ni, W) were prepared by the conventional solid state ceramic route as described in section 2.1.2 of Chapter 2. High purity chemicals CeO_2 (IRE, 99.9%), TiO_2 (99.8%), CaCO_3 (99+%), $\text{Mg}(\text{CO}_3)_4\text{Mg}(\text{OH})_2\cdot 5\text{H}_2\text{O}$ (99%), ZnO (99.9%), MnCO_3 (99.9+%), Co_3O_4 (99%), NiO (99%) and WO_3 (99+%) (Aldrich Chemical Company, Milwaukee, WI, USA) were used as starting powders. The powder mixture was ball milled in distilled water medium using zirconia balls in a plastic container for 24h. The slurry was dried and the reaction mixture thus obtained was calcined for 6 h at 1150°C for Ca, Mg and Zn based and at 1050°C for Mn, Co, Ni and W based ceramics respectively. The calcined powders were again ground well for 1h in an agate mortar and then mixed with 4 wt% solution of poly vinyl alcohol (PVA, 4 wt%; BDH laboratory, Poole, England, molecular weight ≈ 22000 , degree of hydrolysis $\geq 98\%$) as the binder. The slurry was dried and ground again and pressed into cylindrical disks of diameter 14 mm and height about 7 mm under a pressure of 100 MPa. The pellets were initially preheated at a rate of $5^\circ\text{C}/\text{min}$ up to 600°C and soaked for 30 minutes to expel the binder and then fired at a rate of $12^\circ\text{C}/\text{min}$ up to the sintering temperature. The sintering temperature was in the range between 1130 and 1550°C (Nabertherm Furnace, Model LHT 02/18, Lilienthal, Germany) depending on the A atom and the dwell time was 2 h. The sintered ceramic pucks were polished and their bulk density was measured using Archimedes method. The thermal and chemical stability of the sintered samples were tested by boiling the samples in distilled water for 2 h.

3.3.3 Structural Analysis and Microwave Measurements

Crystal structure and phase purity of the sintered and powdered samples were examined by X-ray diffraction patterns recorded using $\text{CuK}\alpha$ radiation with Ni filter (Philips Xpert Pro X-ray Diffractometer, Almelo, the Netherlands). The microstructures of sintered samples were recorded from the surface of finely polished samples which were thermally etched at $25\text{-}50^\circ\text{C}$ less than their respective sintering temperature for 20 minutes (Hitachi SEM S-4300, Japan). Raman spectra from the sintered pucks were

recorded using a Renishaw system 2000 microprobe with a 488 nm line of an Ar⁺ laser as exciting radiation with nominally < 4mW power incident on the sample surface. The laser line was focused onto the sample by a cylindrical microscope lens of 50 \times magnification with a spot diameter of $3 \pm 1 \mu\text{m}$. The microwave dielectric properties such as relative permittivity, unloaded quality factor and temperature variation of resonant frequency were measured using a Vector Network Analyzer (Agilent Technologies, Model No. 8753 ET, Palo Alto, California) attached with a sweep oscillator and test parameter unit employing resonance method^{44, 45, 46} as explained in Chapter 2, section 2.4.2 to 2.4.5. Dielectric properties in the range of -253 to 37°C were measured by placing the copper cavity on the cold head of a closed cycle Gifford McMahon cryocooler (“workhorse”, Cryophysics, Abingdon, UK) were a software calculated permittivity, unloaded Q and resonance frequency over temperature.

3.3.4 Optimization of Calcination and Sintering Temperatures

The calcination and sintering temperatures of $\text{CeO}_2\text{-}0.5\text{AlO}_3\text{-}0.5\text{TiO}_2$ ceramics are optimized for the best density and dielectric properties. This is done by calcining the ceramics at different temperatures and then sintering at an arbitrary temperature. Figs. 3.3-3.6 show typical example of the effect of calcination and sintering temperatures and their durations on the density and microwave dielectric properties of $\text{CeO}_2\text{-}0.5\text{ZnO-}0.5\text{TiO}_2$ (CZnT) ceramics.

First the samples are calcined at different temperatures and the density and dielectric properties of the shaped DR sample ($12.15 \times 6.12 \text{ mm}^2$) sintered at an arbitrary temperature of $1250^\circ\text{C}/2\text{h}$ is measured. It is evident from Fig. 3.3(a) and (b) that best density, ϵ_r , $Q_{ur}xf$ and τ_f are obtained for samples calcined at 1150°C . Calcination duration is also optimized by heating the powders for 2 to 8 hours at 1150°C . Fig. 3.4(a) and (b) shows the variation of density, ϵ_r , $Q_{ur}xf$ and τ_f as a function of calcination duration when sintered at 1250°C for 2h. The best density and dielectric properties are found for CZnT ceramics calcined at 1150°C for 5 hours.

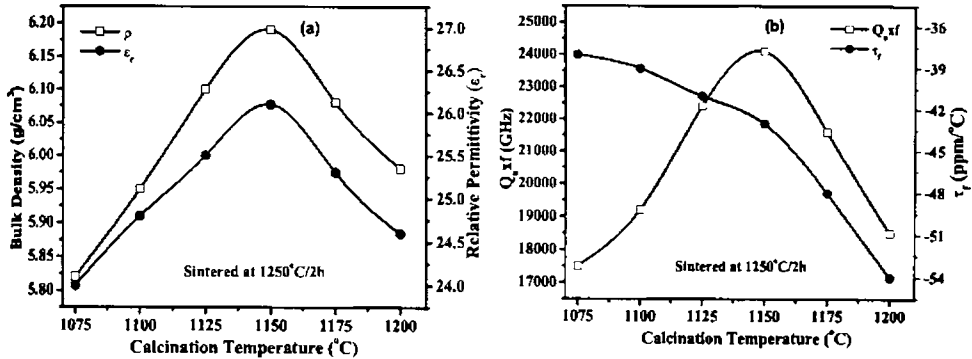


Fig. 3.3 Variation of (a) bulk density (ρ) and ϵ_r (b) Q_{rxf} and τ_r of $\text{CeO}_2\text{-}0.5\text{ZnO-}0.5\text{TiO}_2$ ceramics with calcination temperature

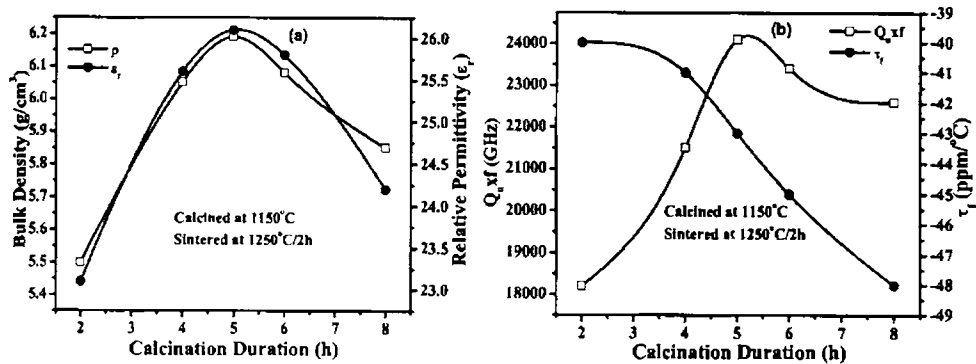


Fig. 3.4 Variation of (a) bulk density (ρ) and ϵ_r (b) Q_{rxf} and τ_r of $\text{CeO}_2\text{-}0.5\text{ZnO-}0.5\text{TiO}_2$ ceramics with calcination duration

The $\text{CeO}_2\text{-}0.5\text{ZnO-}0.5\text{TiO}_2$ samples prepared in the optimized calcination temperature (1150°C) and duration (5 hours) are sintered in the temperature range $1200^\circ\text{C-}1300^\circ\text{C}$ for 2 hours. Fig. 3.5(a) and (b) shows the variation of density, ϵ_r , Q_{rxf} and τ_r of the samples versus sintering temperature. It is found that the ceramic samples sintered at 1250°C show best density and dielectric properties. Then the sintering is carried out at 1250°C for various durations starting from 1 hour to 5 hours and found that, the bulk density and dielectric properties of the samples show best values for 2 hours of duration as shown in Fig. 3.6(a) and (b). For large duration of sintering temperatures, the density, ϵ_r and Q_{rxf} of the samples showed a decrease while τ_r has increased. This may be

due to the trapping of pores by grain growth. Abnormal grain growth may lead to dielectric loss at microwave frequencies. The best density and dielectric properties of $\text{CeO}_2\text{-}0.5\text{ZnO-}0.5\text{TiO}_2$ ceramics are for a calcination temperature of $1150^\circ\text{C}/5\text{h}$ and sintering temperature of $1250^\circ\text{C}/2\text{h}$. Similarly, the calcination and sintering temperatures and durations of $\text{CeO}_2\text{-}0.5\text{AO-}0.5\text{TiO}_2$ ($\text{A} = \text{Mg, Ca, Mn, Co, Ni, W}$) ceramics are optimized.

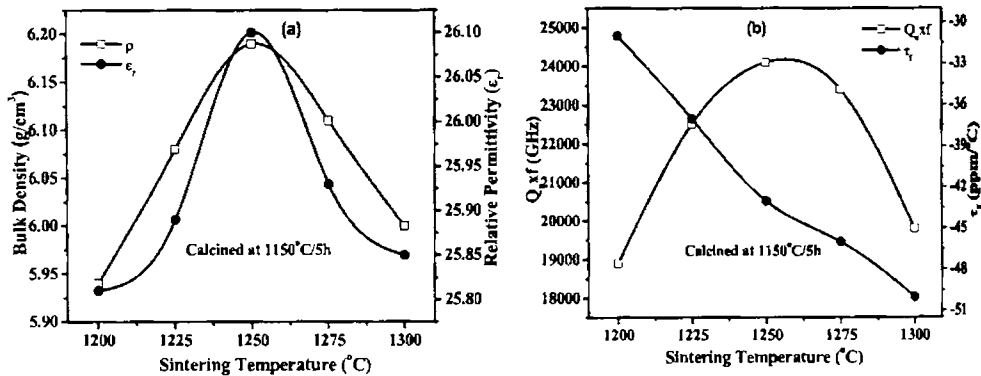


Fig. 3.5 Variation of (a) bulk density (ρ) and ϵ_r , (b) Q_{xf} and τ_f of $\text{CeO}_2\text{-}0.5\text{ZnO-}0.5\text{TiO}_2$ ceramics with sintering temperature

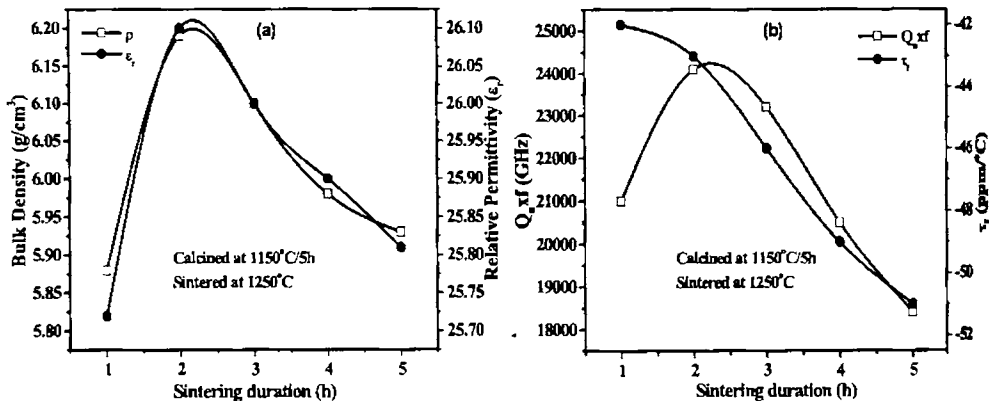


Fig. 3.6 Variation of (a) bulk density (ρ) and ϵ_r , (b) Q_{xf} and τ_f of $\text{CeO}_2\text{-}0.5\text{ZnO-}0.5\text{TiO}_2$ ceramics with sintering duration

It has been reported that in titanium based ceramics prolonged heating at high temperatures leads to reduction of Ti^{4+} to Ti^{3+} . The Ti^{3+} is semiconducting and it

presence leads to increase in the dielectric loss. Hence the titania based ceramics are usually annealed at about 1100-1300°C for oxygenation such that it is converted to Ti^{4+} . Hence prolonged annealing improves the quality factor.^{47,48,49,50} In the present case we have annealed $CeO_2-0.5ZnO-0.5TiO_2$ ceramics at a temperature of 1150°C for 4-16 hrs. No significant improvement in density or dielectric properties is observed. The density, relative permittivity and $Q_{r,f}$ decreased on annealing while τ_f increased slightly. The sintered samples are kept in boiling water for 2 h. There is no change in density, dielectric properties or in XRD pattern when boiled in water indicating excellent chemical and thermal stability of the material.

3.3.5 Results and Discussion

3.3.5.1 Phase and Microstructural Analysis

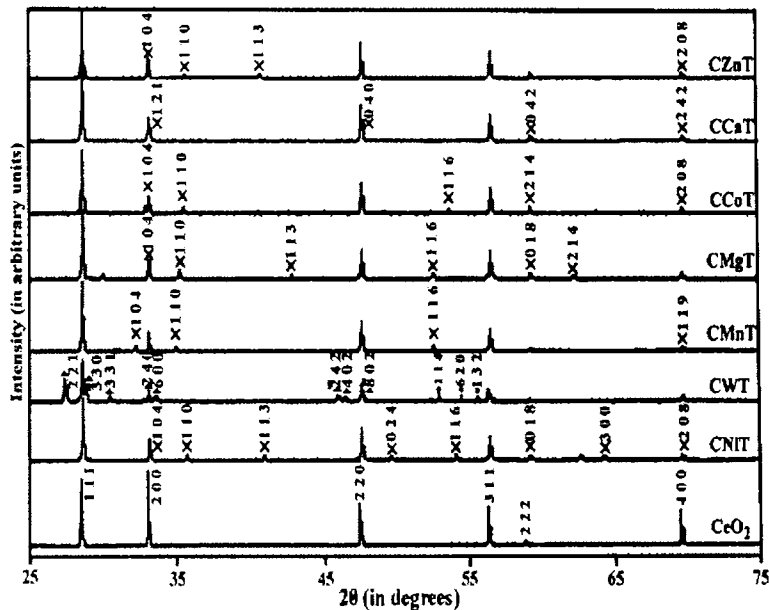


Fig. 3.7 XRD patterns of CeO_2 and $CeO_2-0.5AO-0.5TiO_2$ (A = Ca, Mg, Zn, Mn, Co, Ni, W) ceramics

The $\text{CeO}_2\text{-}0.5\text{AO-}0.5\text{TiO}_2$ ($A = \text{Mg, Zn, Ca, Mn, Co, Ni, W}$) green compacts are sintered into dense ceramics except those based on tungsten, which is difficult to sinter. Fig. 3.7 shows the X-ray diffraction patterns recorded from $\text{CeO}_2\text{-}0.5\text{AO-}0.5\text{TiO}_2$ ($A = \text{Mg, Zn, Ca, Mn, Co, Ni, W}$) dielectric ceramics using $\text{CuK}\alpha$ radiation. The powder

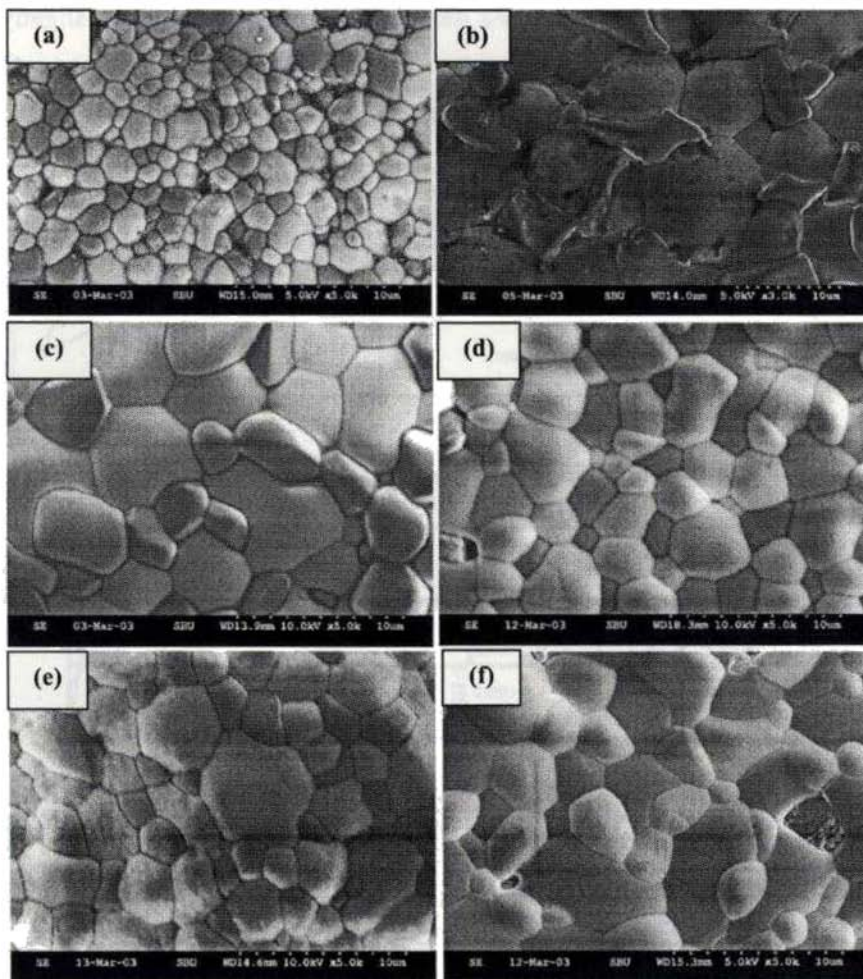


Fig 3.8 SEM micrographs of (a) $\text{CeO}_2\text{-}0.5\text{CaO-}0.5\text{TiO}_2$ (b) $\text{CeO}_2\text{-}0.5\text{MgO-}0.5\text{TiO}_2$ (c) $\text{CeO}_2\text{-}0.5\text{ZnO-}0.5\text{TiO}_2$ (d) $\text{CeO}_2\text{-}0.5\text{MnO-}0.5\text{TiO}_2$ (e) $\text{CeO}_2\text{-}0.5\text{CoO-}0.5\text{TiO}_2$ (f) $\text{CeO}_2\text{-}0.5\text{NiO-}0.5\text{TiO}_2$

diffraction patterns confirm that majority of the $\text{CeO}_2\text{-}0.5\text{AO-}0.5\text{TiO}_2$ ($A = \text{Mg, Zn, Ca, Mn, Co, Ni}$) ceramics consists of two phases namely fluorite CeO_2 and perovskite ATiO_3 . Careful analyses of the X-ray diffraction pattern show that CeO_2 peaks nearly coincide with some of the peaks of ATiO_3 ($A = \text{Mg, Zn, Ca, Mn, Co, Ni}$). In the ceramic with tungsten, $\text{CeO}_2\text{-}0.5\text{WO}_3\text{-}0.5\text{TiO}_2$, several phases are formed such as CeO_2 , Ce_2WO_6 and $\text{Ce}_2\text{Ti}_2\text{O}_7$. Bijumon *et al.*⁵¹ reported that in the case of $\text{Ce}(\text{Ti}_{0.5}\text{W}_{0.5})\text{O}_4$, which is same as the composition studied in the present case, a multiphase composite containing $\text{Ce}_2\text{Ti}_2\text{O}_7$, Ce_2WO_6 , TiO_2 and CeO_2 is formed.

Figure 3.8 shows the SEM micrographs of sintered and polished $\text{CeO}_2\text{-}0.5\text{AO-}0.5\text{TiO}_2$ ($A = \text{Ca, Mg, Zn, Mn, Co, Ni}$) ceramics revealing a highly dense product. The microstructure changes with change in the 'A' atom in $\text{CeO}_2\text{-}0.5\text{AO-}0.5\text{TiO}_2$ ($A = \text{Ca, Mg, Zn, Mn, Co, Ni}$) and it shows clearly two types of grains which are later proven to belong to CeO_2 and ATiO_3 . The average grain size of sintered pure CeO_2 is rather large ($>10\ \mu\text{m}$). In these $\text{CeO}_2\text{-}0.5\text{ATiO}_3$ composites we found much smaller CeO_2 grain sizes

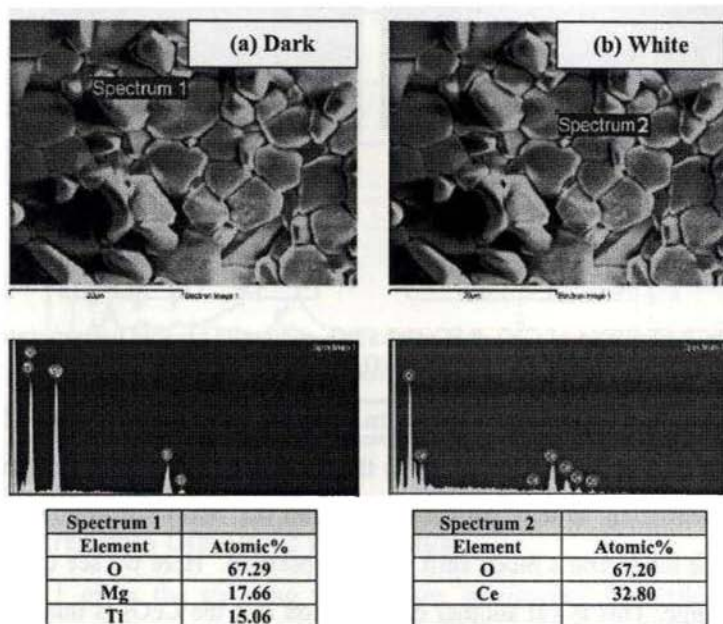


Fig. 3.9 EDXA of $\text{CeO}_2\text{-}0.5\text{MgO-}0.5\text{TiO}_2$ composite proving two separate phases of CeO_2 and MgTiO_3

varying from 2 μm in the $\text{CeO}_2\text{-}0.5\text{CaO-}0.5\text{TiO}_2$ (Fig 3.8 (a)) to 10 μm in $\text{CeO}_2\text{-}0.5\text{MgO-}0.5\text{TiO}_2$ (Fig 3.8 (b)). In all cases, the formed ATiO_3 perovskite phase has smaller grain size than CeO_2 . The CeO_2 grains are polygonal shaped with bright contrast and the smaller ATiO_3 (A = Mg, Zn, Ca, Mn, Co) grains with dark contrast and have well defined grain boundaries. EDXA analyses of $\text{CeO}_2\text{-}0.5\text{AO-}0.5\text{TiO}_2$ (A = Mg, Ca) shown in Figs. 3.9 and 3.10 respectively confirm the earlier XRD results that there are two major phases of ATiO_3 and CeO_2 . This result was dominating in all six ceramic systems except in $\text{CeO}_2\text{-}0.5\text{WO}_3\text{-}0.5\text{TiO}_2$.

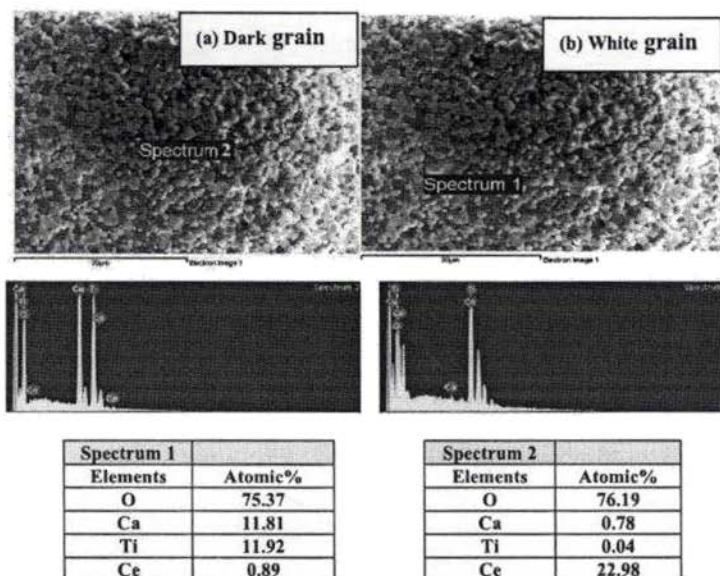


Fig. 3.10 EDXA of $\text{CeO}_2\text{-}0.5\text{CaO-}0.5\text{TiO}_2$ composite proving two separate phases of CeO_2 and CaTiO_3

Fig. 3.11 shows the Raman spectrum of $\text{CeO}_2\text{-}0.5\text{AO-}0.5\text{TiO}_2$ (A = Mg, Zn, Ca, Mn, Co, Ni, W). The mode at 463 cm^{-1} is the characteristic CeO_2 mode which is linked to the Ce-O8 vibration. If ions are substituted into the fluorite structure the line width (FWHM) of the mode and a mode shift will be observed. Here we see clearly that there is no such change. This is yet another confirmation that the CeO_2 is intact as one of the phases. Where ever possible, ATiO_3 standards were compared with the $\text{CeO}_2\text{-}0.5\text{AO-}$

0.5TiO_2 ($A = \text{Mg, Zn, Ca, Mn, Co, Ni, W}$) to prove the existence of the perovskite phase.

Raman spectra of CeO_2 and CaTiO_3 phase are shown in Fig. 3.12.

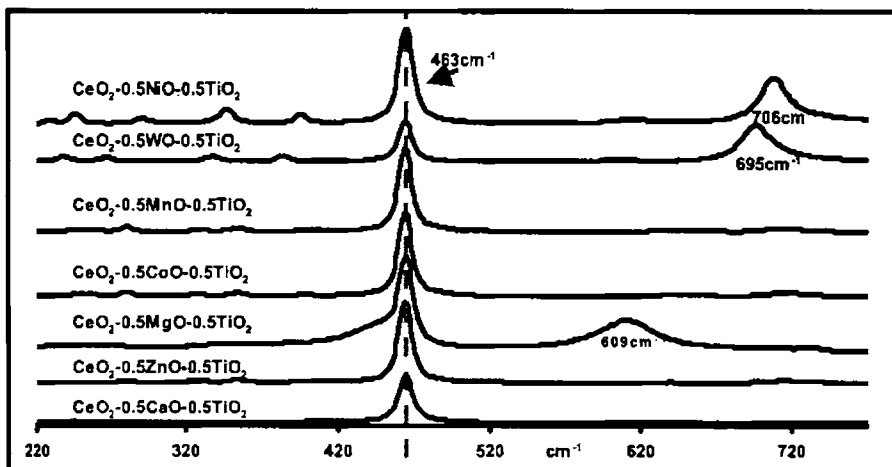


Fig. 3.11 Raman Spectra of $\text{CeO}_2-0.5\text{AO}-0.5\text{TiO}_2$ ($A = \text{Ca, Mg, Mn, Zn, Co, Ni, W}$) ceramics

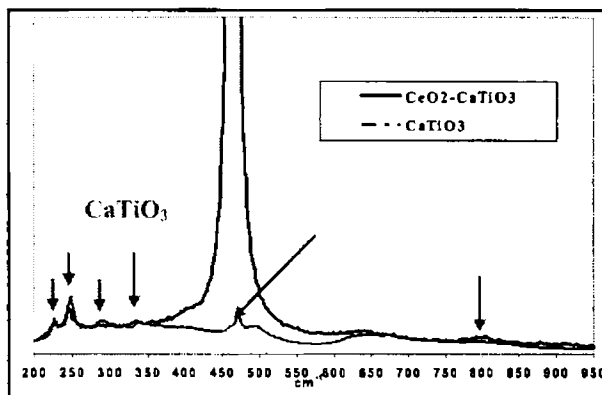


Fig. 3.12 Raman spectra of suggested CeO_2 and CaTiO_3 phase

3.3.5.2 Microwave Dielectric Properties

Table 3.1 gives the sintering temperature, microwave dielectric properties (ϵ_r , Q, f, τ_f) of $\text{CeO}_2-0.5\text{AO}-0.5\text{TiO}_2$ ($A = \text{Ca, Mg, Zn, Co, Ni, Mn, W}$) ceramics. The

different ceramics possess fairly high relative permittivity in the range 17.0 to 65.5 and quality factor Q_{uxf} from 9500 to 50000 GHz. The $\text{CeO}_2\text{-}0.5\text{CaO-}0.5\text{TiO}_2$ has the highest relative permittivity of $\epsilon_r = 65.5$ and $\text{CeO}_2\text{-}0.5\text{WO}_3\text{-}0.5\text{TiO}_2$ has the lowest at $\epsilon_r = 17.0$. The $\text{CeO}_2\text{-}0.5\text{CaO-}0.5\text{TiO}_2$ has a high τ_f of 399 ppm/°C which is due to the high positive τ_f of CaTiO_3 (800 ppm/°C) compared with other ATiO_3 (A = Mg, Zn, Co, Ni, Mn) ceramics, which have negative τ_f . $\text{CeO}_2\text{-}0.5\text{CaO-}0.5\text{TiO}_2$ and $\text{CeO}_2\text{-}0.5\text{WO}_3\text{-}0.5\text{TiO}_2$ have positive τ_f while $\text{CeO}_2\text{-}0.5\text{AO-}0.5\text{TiO}_2$ (A = Mg, Zn, Co, Ni and Mn) have negative τ_f . The sintering temperature of the $\text{CeO}_2\text{-ATiO}_3$ composite ceramics are in the range from 1130°C to 1550°C which is lower than pure CeO_2 . The low sintering temperature of $\text{CeO}_2\text{-}0.5\text{WO}_3\text{-}0.5\text{TiO}_2$ is due to the presence of low melting Ce_2WO_6 secondary phase. The $\text{CeO}_2\text{-}0.5\text{WO}_3\text{-}0.5\text{TiO}_2$ has $\epsilon_r \sim 17$, $Q_{uxf} \sim 40000$ GHz and $\tau_f \sim 7$ ppm/°C. This material is a suitable candidate for millimeter wave communications systems and microwave substrate applications.

Table 3.1 The dielectric properties of $\text{CeO}_2\text{-}0.5\text{AO-}0.5\text{TiO}_2$ (A = Mg, Zn, Ca, Mn, Co, Ni, W) ceramics

Material	Sintering Temperature (in °C) for 2 h	Density (g/cm ³)	ϵ_r	Q_{uxf} (GHz)	τ_f (ppm/°C)
$\text{CeO}_2\text{-}0.5\text{CaO-}0.5\text{TiO}_2$	1550	5.81	65.5	9500	399
$\text{CeO}_2\text{-}0.5\text{MgO-}0.5\text{TiO}_2$	1400	5.73	22.4	17500	-62
$\text{CeO}_2\text{-}0.5\text{ZnO-}0.5\text{TiO}_2$	1250	6.19	26.1	24100	-43
$\text{CeO}_2\text{-}0.5\text{MnO-}0.5\text{TiO}_2$	1200	6.07	26.3	17100	-30
$\text{CeO}_2\text{-}0.5\text{CoO-}0.5\text{TiO}_2$	1200	6.20	22.0	48750 50000*	-47
$\text{CeO}_2\text{-}0.5\text{NiO-}0.5\text{TiO}_2$	1200	5.39	18.0	25300	-58
$\text{CeO}_2\text{-}0.5\text{WO}_3\text{-}0.5\text{TiO}_2$	1130	5.45	17.0	39800 45550*	7

*measured in vacuum

The density of a mixture of two phases can be calculated using the equation

$$\rho_{mixture} = V_1\rho_1 + V_2\rho_2 \quad (3.1)$$

where V_1 and V_2 are the volume fraction, $\rho_{mixture}$ is the calculated theoretical density and ρ_1 and ρ_2 are the densities of the two components. The empirical model proposed for predicting relative permittivity of mixtures is as follows⁵²

$$\ln \varepsilon_{r,mixture} = V_1 \ln \varepsilon_{r1} + V_2 \ln \varepsilon_{r2} \quad (3.2)$$

where ε_{r1} and ε_{r2} are the relative permittivity of two materials and $\varepsilon_{r,mixture}$ is the relative permittivity of the mixed phase ceramic. To calculate the τ_f of mixtures, an empirical model was proposed as follows⁵³

$$\tau_{f,mixture} = V_1 \tau_{f1} + V_2 \tau_{f2} \quad (3.3)$$

where τ_{f1} and τ_{f2} are the temperature coefficient of resonant frequencies of the two components and $\tau_{f,mixture}$ is the resultant temperature coefficient of resonant frequency of the mixture. Table 3.2 shows the dielectric properties of CeO_2 and the perovskite ATiO_3 ($A = \text{Ca, Mg, Zn, Mn, Co, Ni}$) ceramics that we are suggesting as the secondary phase here. The details of preparation, characterization and dielectric properties of these compounds are given in section 3.5.

Table 3.2 Microwave dielectric properties of ATiO_3 ($A = \text{Ca, Mg, Zn, Mn, Co, Ni}$) and CeO_2 ceramics

Material	Theoretical density (g/cm^3)	ε_r	$Q \times f$ (GHz)	τ_f (ppm/ $^\circ\text{C}$)
CaTiO_3	4.04	170.0	12900	800
MgTiO_3	3.89	17.0	20780	-50
ZnTiO_3	5.17	21.0	19000	-50
MnTiO_3	4.60	24.3	15200	-56
CoTiO_3	4.52	19.8	37500	-49
NiTiO_3	5.10	19.7	13900	-51
CeO_2	7.20	23.0	60000	-53

By using the equations (3.1)-(3.3) and CeO_2 and ATiO_3 as the two phases, values of density, ε_r and τ_f are calculated and compared with experimental results, see Fig 3.13. The experimental values of bulk density do not show much variation from the values

calculated using mixture relation. The relative permittivity and τ_f shows very good agreement between experimental and values derived from mixture rule except in the case of CCaT ceramics. This is yet another confirmation that $\text{CeO}_2\text{-}0.5\text{AO-}0.5\text{TiO}_2$ (A = Ca, Mg, Zn, Mn, Co, Ni) ceramics is a mixture of CeO_2 and ATiO_3 phases.

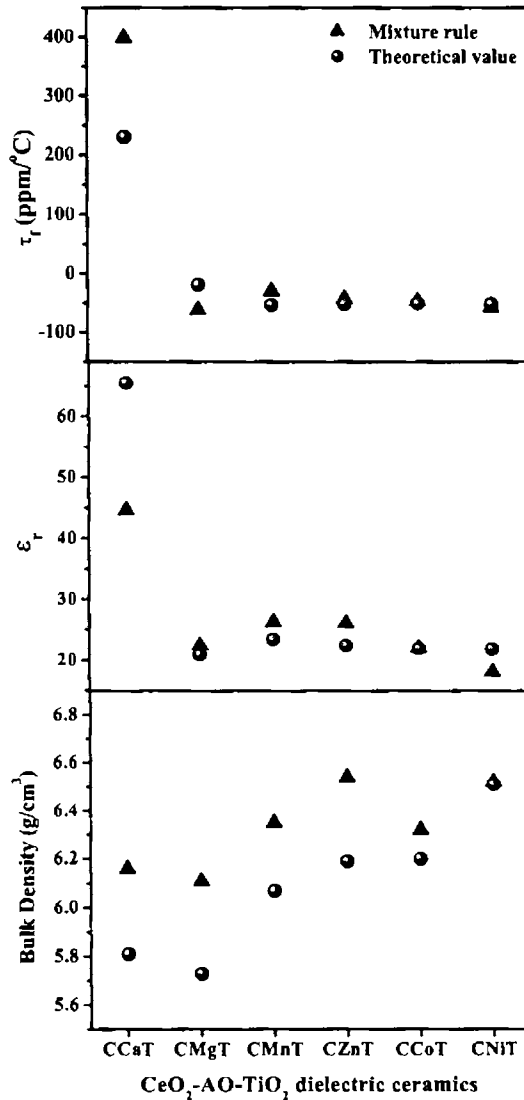


Fig. 3.13 Calculated and measured values of bulk density, ϵ_r , and τ_f for suggested $\text{CeO}_2\text{-ATiO}_3$ (A = Mg, Zn, Ca, Mn, Co, Ni) composites

Fig. 3.14 shows the variation of $Q_u x f$ as a function of temperature in the range 30-310 K. The quality factor increased considerably on cooling for $\text{CeO}_2\text{-}0.5\text{MgO}\text{-}0.5\text{TiO}_2$ and at 20 K the Q_u is as high as 98000 ($Q_u x f = 539000$ GHz) which is comparable with

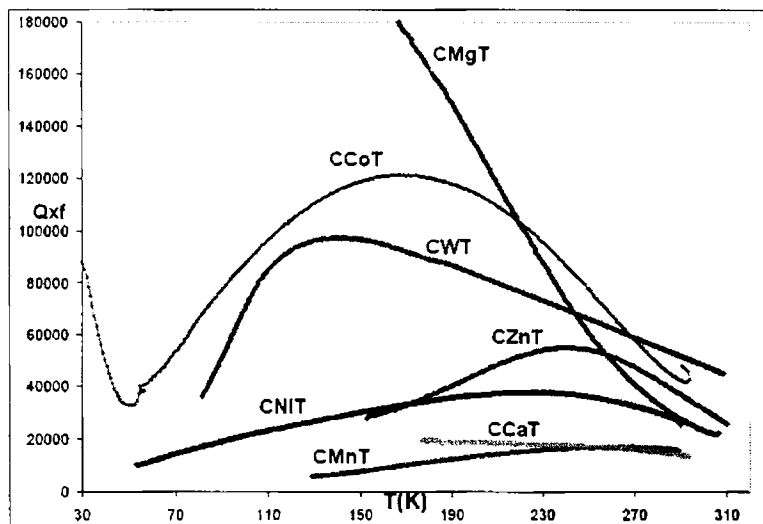


Fig. 3.14 Variation of $Q_u x f$ (GHz) over cryogenic temperatures of the $\text{CeO}_2\text{-}0.5\text{AO}\text{-}0.5\text{TiO}_2$ (A= Ca, Mg, Mn, Zn, Co, Ni, W) ceramics

undoped CeO_2 , which has a $Q_u x f$ of 580000 GHz at 20 K³⁸. In all samples, the quality factor increased initially on cooling and then on further cooling it decreased at different temperatures depending on the AO material. These points occurred at different temperatures in all materials and are also observed in undoped CeO_2 where this anomaly point is at about 190 K. The increase in the quality factor at low temperatures is due to many factors, one being the decrease of the damping of lattice vibrations (phonons). This reduces the direct interaction of the microwave field with the lattice vibrations. The decrease in quality factor and appearance of anomaly points of some of the $\text{CeO}_2\text{-}0.5\text{AO}\text{-}0.5\text{TiO}_2$ (A = Mg, Zn, Ca, Mn, Co, Ni, W) ceramics may be attributed to factors such as oxygen vacancies and other charge defects in the composites, depending on the AO. In one of the cases, $\text{CeO}_2\text{-}0.5\text{CoO}\text{-}0.5\text{TiO}_2$, the anomaly corresponds to an anomaly of the permittivity which increases at 60K when cooling, indicates a low temperature phase change.

3.4 EFFECT OF DOPANTS IN $\text{CeO}_2\text{-AO-TiO}_2$ (A = Ca, Mg, Zn, Mn, Co, Ni, W) CERAMICS

3.4.1 Introduction

Commercially available dielectric resonator materials for microwave application show high Q_u and high ϵ_r , but need to be sintered at high temperatures for longer duration to attain better densification and thereby improved performance.^{54,55,56} They often incorporate sintering aids and dopants to reduce processing temperatures and modify the dielectric properties. Densification can be promoted by the use of additives. Additives aid fabrication by allowing densification to occur at lower temperatures in shorter times or by inhibiting discontinuous grain growth and allowing pore elimination to proceed to completion. At least two theories were advanced to explain the effect of these additives. (a) Liquid phase assistance - Additive with a lower melting point is used for densification by melting and coating the ceramic particles, rapid dissolution and transfer of the base material to fill the interparticle spaces, which leads to enhanced densification. The additive has to be fairly soluble in the base ceramic and several wt% of the additive is necessary to provide sufficient liquid phase to coat all the powder particles. (b) Solid solution effect - Addition of a solute with a different valency enhances bulk material transport due to the introduction of vacancies in the ceramic. These vacancies render the diffusion coefficient extrinsic by making thermal vacancy concentration insignificant up to a certain temperature. If added in sufficient quantity, it can significantly alter the rate of material transport through the solid phase.

The best microwave dielectric properties of $\text{CeO}_2\text{-0.5AO-0.5TiO}_2$ (A = Mg, Zn, Ca, Mn, Co, Ni, W) ceramics are reported at a processing temperature in the range 1130-1550°C in the earlier section 3.3. The high sintering temperature of the ceramics also put constraints over their immediate use in practical applications. Several methods are proposed and investigated in literature, like (i) chemical synthesis^{57,58,59} (ii) using raw materials with smaller particle size⁶⁰ and (iii) liquid phase sintering⁶¹ by the addition of glassy materials, to decrease the sintering temperature and improve the dielectric

properties of low loss materials. However, each technique has got many disadvantages which precludes the industrial production of high quality DRs.⁶² Doping of ceramics with suitable dopants^{63,64,65,66,67} have been established as an effective tool for tuning the properties of microwave dielectric materials. Hence to explore the possibility of bringing down the sintering temperature and improving the densification and microwave dielectric properties, aliovalent and isovalent dopants are added to calcined $\text{CeO}_2\text{-}0.5\text{AO-}0.5\text{TiO}_2$ (A = Mg, Zn, Ca, Mn, Co, Ni, W) powders. The optimization of the synthesizing conditions is done prior to the doping. A comprehensive investigation is made to study the effect of various dopants of different ionic radii and valency on the densification, sinterability and dielectric properties of $\text{CeO}_2\text{-}0.5\text{AO-}0.5\text{TiO}_2$ (A = Mg, Zn, Ca, Mn, Co, Ni, W) ceramics.

3.4.2 Experimental

The samples of $\text{CeO}_2\text{-}0.5\text{AO-}0.5\text{TiO}_2$ (A = Mg, Zn, Ca, Mn, Co, Ni, W) were prepared by the conventional solid state ceramic route as described in section 2.1.2 of Chapter 2. The calcination was done for 5 h at 1150°C for Ca, Mg and Zn based and at 1050°C for Mn, Co, Ni and W based ceramics respectively. The resultant crispy material was ground into very fine powder. The calcined $\text{CeO}_2\text{-}0.5\text{AO-}0.5\text{TiO}_2$ (A = Mg, Zn, Ca, Mn, Co, Ni, W) precursor was divided into several batches and different wt% of dopants were added to selected weight of the parent material. The oxides to be doped were categorized based on their high temperature stable valency and depending on the A site atom, suitable dopants of various valencies were added. Accordingly different wt % of various dopants such as divalent (MgO, MnO, ZnO, NiO, CuO, CaTiO₃, SrTiO₃ & Co₃O₄), trivalent (In₂O₃, Al₂O₃, Cr₂O₃, Bi₂O₃, Fe₂O₃, Nd₂O₃, Sm₂O₃, Sb₂O₃ & La₂O₃), tetravalent (ZrO₂, SnO₂, CeO₂, TiO₂), pentavalent (V₂O₅, Ta₂O₅, Nb₂O₅) and hexavalent (WO₃ & MoO₃) were added to calcined powders of the parent materials. The resultant mixture was ground well in distilled water medium, dried and mixed with 4 wt% Poly Vinyl Alcohol (PVA) as binder. It was dried again and ground into very fine powder. Cylindrical ceramic pucks of 14 mm diameter and 6 - 7 mm height were formed under a

uniaxial pressure of 100 MPa. Doped $\text{CeO}_2\text{-}0.5\text{AO-}0.5\text{TiO}_2$ ($A = \text{Mg, Zn, Ca, Mn, Co, Ni, W}$) specimens were fired at an optimum temperature range of 950-1550°C/2h. The sintered samples were well polished to remove the surface irregularities and their densities were measured by Archimedes method. Phase purity of the materials was studied by powder X-Ray diffraction (XRD) analysis using $\text{CuK}\alpha$ radiation and microstructural analysis was done using scanning electron microscope. The dielectric properties Q_u , ϵ_r and τ_f of the materials were measured in the microwave frequency range as described in Chapter 2, section 2.4.2 to 2.4.5.

3.4.3 Results and Discussion

Depending on A-atom of $\text{CeO}_2\text{-}0.5\text{AO-}0.5\text{TiO}_2$ ($A = \text{Mg, Zn, Ca, Mn, Co, Ni, W}$) ceramics, the microwave dielectric properties are affected by dopants having different valencies and only those dopants that improved the dielectric properties are tried in different concentrations.

Sintering aids affect ceramics in many ways by changing the density, microstructure, defect structure, and possibly crystal structure. These changes brought about by the sintering aids affect the resulting dielectric properties. The density ϵ_r , Q_u and τ_f are all affected by the additives. A higher relative density results in a higher ϵ_r . The selection of proper additives, their optimum quantity and optimum processing conditions are effective in enhancing the quality factor. The parent materials, $\text{CeO}_2\text{-}0.5\text{AO-}0.5\text{TiO}_2$ ($A = \text{Mg, Zn, Ca, Mn, Co, Ni, W}$) mixtures are doped with WO_3 , MoO_3 , Sb_2O_3 , V_2O_5 , Ta_2O_5 , Nb_2O_5 , ZrO_2 , SnO_2 , CeO_2 , TiO_2 , In_2O_3 , Al_2O_3 , Cr_2O_3 , Bi_2O_3 , Fe_2O_3 , Nd_2O_3 , Sm_2O_3 , La_2O_3 , MgO , MnO , ZnO , NiO , CuO , CaTiO_3 , SrTiO_3 & Co_3O_4 to tailor their dielectric properties.

In the $\text{CeO}_2\text{-}0.5\text{CaO-}0.5\text{TiO}_2$ (CCaT) system, addition of 4 wt% Fe_2O_3 and 0.5 wt% Cr_2O_3 slightly improves the quality factor of $\text{CeO}_2\text{-}0.5\text{CaO-}0.5\text{TiO}_2$ from 9500 GHz to 13000 and 10400 GHz respectively (Table 3.3). However, addition of Cr_2O_3 , Fe_2O_3

Table 3.3 Microwave dielectric properties of doped CeO₂-0.5CaO-0.5TiO₂ ceramic sintered at 1550°C/2h

Dopant	Dopant Level (wt%)	Density (g/cm ³)	$Q_{\omega} \times f$ (GHz)	ϵ_r	τ_f (ppm/°C)
No dopant	-	5.81	9500	65.5	399
WO ₃	0.5	5.76	8585	65.3	412
MoO ₃	0.5	5.75	8430	61.4	346
Nb ₂ O ₅	0.5	6.73	2320	69.5	321
Sb ₂ O ₃	0.5	5.78	8195	61.6	345
SnO ₂	0.5	5.79	8465	62.6	362
CeO ₂	0.5	5.79	8860	63.9	310
	1.0	5.80	10200	64.4	335
	2.0	5.84	8850	63.7	356
La ₂ O ₃	0.5	5.86	8320	64.7	397
Nd ₂ O ₃	0.5	5.82	8460	64.6	362
Bi ₂ O ₃	0.5	5.78	8600	63.8	389
Cr ₂ O ₃	0.5	5.78	10400	58.2	308
	2.5	5.74	8640	47.7	152
	5.0	5.76	6460	42.2	44
	6.0	5.64	5185	37.8	32
	7.0	5.68	4525	37.5	22
	8.0	5.77	4350	35.0	0
Fe ₂ O ₃	0.5	5.80	9000	60.2	304
	2.5	5.74	10200	50.5	123
	4.0	5.74	13000	47.3	91
	5.0	5.72	9960	44.9	46
	6.0	5.72	2680	44.3	31
	6.5	5.7	1400	43.7	22
MnO	0.5	5.80	9480	60.5	329
	2.0	5.73	8850	54.0	172
	4.5	5.77	2450	46.8	92
	7.5	5.73	1100	41.7	35

and MnO improves the τ_f to 0, 22 and 35 ppm/°C from the originally 399 ppm/°C respectively. The ionic radius of Cr³⁺ (0.615 Å), Fe³⁺ (0.55 Å) and Mn²⁺ (0.67 Å) are comparable to the ionic radius of Ti⁴⁺ (0.605 Å)⁶⁸. Hence Cr³⁺, Fe³⁺ and Mn²⁺ may diffuse into the Ti⁴⁺ site. Fig. 3.15 shows the EDXA spectrum of 6.5 wt% Fe₂O₃ added CeO₂-0.5CaO-0.5TiO₂ ceramic. The presence of two types of grains CaTiO₃ and CeO₂

gives evidence for the mixture behaviour. Analysis of CaTiO_3 grain (spectrum 1) clearly shows that Fe^{3+} enters the CaTiO_3 grain and there is no presence of Fe^{3+} in the CeO_2 grain (spectrum 2). Fig. 3.16 shows the variation of τ_f with concentration of Cr_2O_3 , Fe_2O_3 and MnO dopants in the $\text{CeO}_2\text{-}0.5\text{CaO-}0.5\text{TiO}_2$ composite. The τ_f decreases with the increasing amount of Cr_2O_3 , Fe_2O_3 and MnO additives.

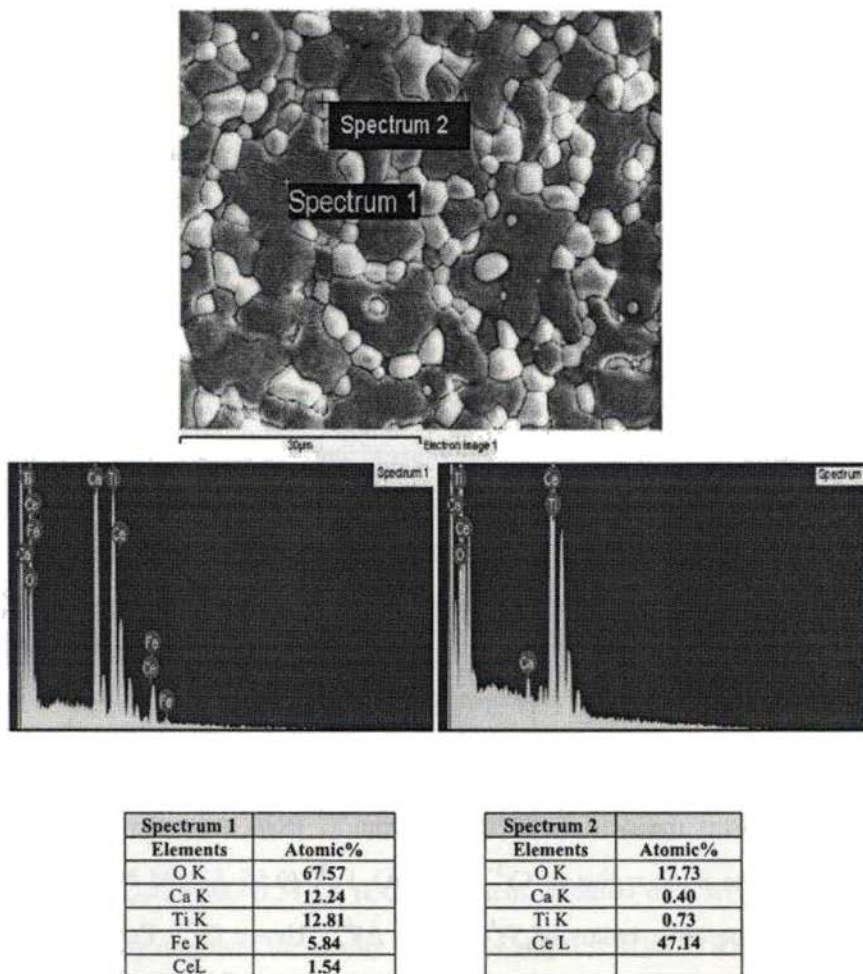


Fig. 3.15 EDXA spectrum of 6.5 wt% Fe_2O_3 added $\text{CeO}_2\text{-}0.5\text{CaO-}0.5\text{TiO}_2$ ceramics

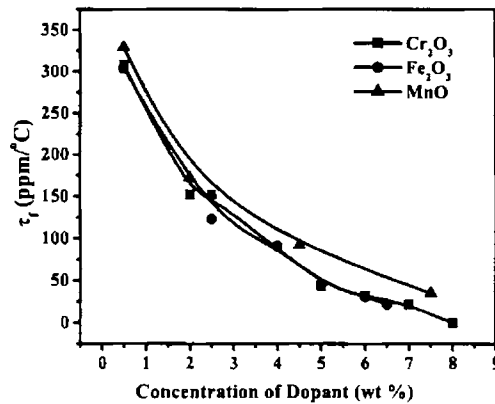


Fig. 3.16 Tuning of τ_f towards zero in the $\text{CeO}_2\text{-CaTiO}_3$ composite using different amount of Cr_2O_3 , Fe_2O_3 and MnO dopant

The $\text{CeO}_2\text{-0.5MgO-0.5TiO}_2$ (CMgT) ceramics has $\epsilon_r = 22.4$, $Q_{ixf} = 17500$ GHz and $\tau_f = -62$ ppm/°C. Addition of small amounts of WO_3 , MoO_3 , Sb_2O_3 , Fe_2O_3 and MnO (all under 2 wt%) increases the quality factor (Table 3.4). Titanium based ceramics have a Ti^{4+} oxidation state. It has been reported⁶⁹ that heating at high temperatures in air will lead to a reduction of Ti^{4+} to Ti^{3+} . This reduction is well known to increase the dielectric loss⁷⁰. Hence the addition of oxidizing agents such as WO_3 , MoO_3 , Sb_2O_3 , Fe_2O_3 and MnO may be expected to maintain a high quality factor. A quality factor $Q_{ixf} = 90000$ GHz is found by the addition of 2 wt% WO_3 to the $\text{CeO}_2\text{-0.5MgO-0.5TiO}_2$ composite with $\epsilon_r = 21.4$ and $\tau_f = -50$ ppm/°C. By adding 2 wt% $\text{WO}_3 + 0.5$ wt% TiO_2 to this system a Q_{ixf} of 87700 GHz with $\epsilon_r = 21.3$ and slightly improved $\tau_f = -48$ ppm/°C is produced. Similarly, addition of 1.2 wt% $\text{MoO}_3 + 1.2$ wt% TiO_2 gives $Q_{ixf} = 60250$ GHz. Although the quality factor is considerably improved by small amount of dopants there is not much improvement in either the relative permittivity or τ_f .

The $\text{CeO}_2\text{-0.5ZnO-0.5TiO}_2$ (CZnT) has $Q_{ixf} = 24100$ GHz, $\epsilon_r = 26.1$ and $\tau_f = -43$ ppm/°C. Addition of 8 wt% Co_3O_4 improves the quality factor of CZnT ceramics to 33100 GHz but there is a decrease in ϵ_r (Table 3.5). Co^{2+} (0.65 Å) is having an ionic radius comparable to that of Ti^{4+} (0.605 Å) and hence partial substitution of Co in Ti site may be the reason for the increase in quality factor. All other dopants such as WO_3 ,

MoO₃, Sb₂O₃, Fe₂O₃, MnO, Nb₂O₅, V₂O₅, Nd₂O₃, Cr₂O₃, ZrO₂, Ta₂O₅, La₂O₃, Bi₂O₃, SnO₂ degrade the properties of CeO₂-0.5ZnO-0.5TiO₂ ceramics. None of the dopants increase the relative permittivity or tune the τ_f .

Table 3.4 Microwave dielectric properties of doped CeO₂-0.5MgO-0.5TiO₂ ceramic sintered at 1400°C/2h

Dopant	Dopant level (wt%)	Density (g/cm ³)	$Q_{\omega} \times f$ (GHz)	ϵ_r	τ_f (ppm/°C)
No dopants	-	5.73	17500	22.4	-62
WO ₃	1.0	5.60	25600	21.6	-45
	2.0	5.64	90000	21.4	-50
	3.0	5.61	41500	21.1	-51
	4.0	5.57	27000	20.8	-48
MoO ₃	0.6	5.38	28800	20.5	-59
	1.2	5.51	33850	20.9	-56
	2.5	5.27	25000	19.2	-53
	3.0	5.40	17400	20.1	-63
Nb ₂ O ₅	1.0	5.51	3050	22.1	-54
V ₂ O ₅	1.0	5.55	13250	21.4	-51
Sb ₂ O ₃	1.2	5.71	25500	22.5	-48
	2.5	5.97	18700	22.6	-64
	5.0	5.69	14430	24.7	-39
Ta ₂ O ₅	2.0	5.75	6450	22.8	-44
SnO ₂	0.5	5.74	16900	22.4	-54
ZrO ₂	0.5	5.71	12200	22.3	-52
Bi ₂ O ₃	2.0	5.70	8350	22.9	-55
Nd ₂ O ₃	1.5	5.71	11550	22.8	-48
Cr ₂ O ₃	0.5	5.66	16700	22.1	-40
La ₂ O ₃	1.5	6.28	13100	22.3	-55
Fe ₂ O ₃	0.5	5.68	19950	22.2	-52
	1.5	5.69	13900	22.6	-58
	2.5	5.65	7020	20.1	-59
MnO	0.5	5.73	21500	22.3	-53
	1.0	5.74	18150	23.5	-51
	2.0	5.71	18620	22.5	-58
WO ₃ +TiO ₂	2.0:0.5	5.64	87700	21.3	-48
WO ₃ +TiO ₂	2.0:1.0	5.53	72600	21.2	-52
WO ₃ +TiO ₂	2.0:2.5	5.47	36400	20.3	-55
WO ₃ +CaTiO ₃	2.0:1.0	5.64	24250	22.3	-47
MoO ₃ +TiO ₂	1.2:0.6	5.51	47050	21.0	-50
MoO ₃ +TiO ₂	1.2:1.2	5.51	60250	21.3	-54
MoO ₃ +TiO ₂	1.2:2.4	5.39	29200	20.5	-60
MoO ₃ +CaTiO ₃	1.2:1.2	5.53	18950	21.6	-48

Table 3.5 Microwave dielectric properties of doped CeO₂-0.5ZnO-0.5TiO₂ ceramic sintered at 1250°C/2h

Dopant	Dopant level (wt%)	Density (g/cm ³)	$Q_w f$ (GHz)	ϵ_r	τ_f (ppm/°C)
No dopants	-	6.19	24100	26.1	-43
WO ₃	1.0	5.90	22950	24.3	-41
MoO ₃	0.5	5.87	11250	24.1	-38
Sb ₂ O ₃	1.5	6.10	8250	26.2	-37
V ₂ O ₅	1.0	5.83	8550	24.2	-36
Ta ₂ O ₅	2.0	6.11	3100	27.1	-40
Nb ₂ O ₅	0.5	6.03	5050	26.6	-33
ZrO ₂	0.5	6.12	22000	26.1	-37
SnO ₂	1.0	6.15	23800	26.1	-35
	2.5	6.10	21800	25.8	-36
Bi ₂ O ₃	2.5	5.81	3400	23.5	-45
Fe ₂ O ₃	1.0	6.11	19850	25.9	-42
La ₂ O ₃	1.5	6.16	15100	26.5	-43
Cr ₂ O ₃	1.0	6.10	13300	25.8	-43
Nd ₂ O ₃	1.5	6.13	10300	26.7	-30
Co ₃ O ₄	1.0	6.08	29700	25.4	-40
	4.0	6.00	22850	23.7	-46
	8.0	5.97	33100	22.0	-48
MnO	0.5	6.07	21400	25.7	-42

Pure CeO₂-0.5MnO-0.5TiO₂ (CMnT) ceramics has $\epsilon_r = 26.3$, $Q_w f = 17100$ GHz and $\tau_f = -30$ ppm/°C. In the case of CMnT ceramics only an excess addition of MnO (0.5 wt%) improved the quality factor to 20350 GHz (Table 3.6). The enhancement in quality factor with Mn²⁺ doping may be due to a charge compensation mechanism that takes place in dielectric resonator materials involving Ti ($Mn^{2+} + Ti^{4+} \leftrightarrow Mn^{3+} + Ti^{3+}$).⁷¹ However, addition of WO₃, MoO₃, Sb₂O₃, Nd₂O₃, Nb₂O₅ and Ta₂O₅ considerably improves the τ_f . By the addition of 3.5 wt% WO₃ and 5 wt% Nd₂O₃ the relative permittivity increases from 26.3 to 40.6 and 37.9 respectively. The τ_f is improved from -30 to 2 ppm/°C by the addition of only 1 wt% Sb₂O₃, -14 ppm/°C by the addition of 1.5 wt% Nd₂O₃ and -5 ppm/°C by 1 wt% MoO₃, 1 wt% WO₃, 0.5 wt% Nb₂O₅ and 0.5 wt% Ta₂O₅ respectively. In all the latter three cases $Q_w f$ decrease by more than fifty percentage.

Table 3.6 Microwave dielectric properties of doped CeO₂-0.5MnO-0.5TiO₂ ceramic sintered at 1200°C/2h

Dopant	Dopant level (wt%)	Density (g/cm ³)	$Q_{ur}xf$ (GHz)	ϵ_r	τ_f (ppm/°C)
No dopant	-	6.07	17100	26.3	-30
WO ₃	0.5	5.99	10000	27.2	-19
	1.0	5.96	7300	28.4	-5
	1.5	5.95	3530	35.5	60
	3.5	5.93	2660	40.6	93
MoO ₃	0.5	5.93	8000	27.2	-17
	1.0	5.85	5980	27.5	-5
	2.5	5.52	3900	27.7	11
Sb ₂ O ₃	0.5	5.99	10370	27.3	-21
	1.0	5.80	6200	29.5	2
Nb ₂ O ₅	0.5	6.00	3400	28.9	-5
Ta ₂ O ₅	0.5	6.02	3600	29.0	-5
V ₂ O ₅	0.5	5.85	6150	25.7	-26
In ₂ O ₃	1.0	6.01	11700	25.6	-38
SnO ₂	0.5	6.04	14700	26.6	-28
ZrO ₂	0.5	5.01	12000	26.3	-33
Nd ₂ O ₃	0.5	6.04	9900	27.1	-21
	1.5	6.01	8900	27.7	-14
	2.5	6.02	3230	33.4	76
	5.0	5.98	3330	37.9	88
Fe ₂ O ₃	0.5	6.00	12950	26.0	-36
Cr ₂ O ₃	0.5	6.01	1760	27.9	-21
Co ₃ O ₄	0.5	6.00	10500	24.4	-53
MnO	0.5	6.04	20350	25.4	-41
	1.0	5.98	19500	24.8	-49

The undoped CeO₂-0.5CoO-0.5TiO₂ (CCoT) ceramic sintered at 1200°C/2h has $\epsilon_r = 22$, $Q_{ur}xf = 50000$ GHz and τ_f of -47 ppm/°C. An addition of 0.5 wt% of WO₃ increases the $Q_{ur}xf$ to as high as 70000 GHz with an improvement in τ_f (from -47 to -30 ppm/°C). In a similar way, addition of TiO₂ tunes the τ_f to positive value. Addition of 10 wt% TiO₂ increases the $Q_{ur}xf$ to 62550 GHz. By combining these two dopants, 0.5 wt% WO₃ and 2 wt% TiO₂, a $Q_{ur}xf$ of 58200 GHz, $\epsilon_r = 21.2$ and $\tau_f = 5$ ppm/°C is obtained (Table 3.7). Ionic radius of W⁶⁺ (0.6 Å) and Ti⁴⁺ (0.605 Å) are similar to that of Co²⁺ (0.65 Å). Hence

substitution of W^{6+} improves the quality factor of CCoT ceramics by stabilizing the oxidation states of both Ce and Ti.

Table 3.7 Microwave dielectric properties of doped $CeO_2-0.5CoO-0.5TiO_2$ ceramic sintered at $1200^\circ C/2h$

Dopant	Dopant level (wt%)	Density (g/cm^3)	$Q_{ur}f$ (GHz)	ϵ_r	τ_f (ppm/ $^\circ C$)
No dopants	-	6.20	48750 50000*	22.0	-47
WO_3	0.5	6.05	65750*	22.0	-52
	1	6.05	70000*	21.0	-30
Sb_2O_3	0.5	6.12	37850	22.2	-53
Nb_2O_5	0.5	5.99	25500	21.8	-50
TiO_2	5	5.92	61700*	24.8	-30
	10	4.98	62550*	24.0	-15
	20	4.14	50150*	22.8	11
	30	3.94	43300*	21.0	56
	50	3.83	39250*	25.0	105
	60	3.72	56050*	25.9	151
Fe_2O_3	0.5	6.10	16100	21.2	-57
La_2O_3	0.5	6.10	36750	21.9	-54
Cr_2O_3	0.5	5.80	28950	22.5	-39
Bi_2O_3	0.5	6.01	5350	22.5	-42
Sm_2O_3	0.5	6.11	24550	21.6	-54
$SrTiO_3$	1	6.37	39700	23.0	-43
$CaTiO_3$	1	6.10	9100	23.6	-42
	10	5.62	2550	24.0	-36
WO_3+TiO_2	0.5:10	5.40	59700*	25.0	-21
WO_3+TiO_2	1:10	5.34	53150*	24.0	-12
WO_3+TiO_2	0.5:20	4.90	58200*	21.2	5

* measured in vacuum

The undoped $CeO_2-0.5NiO-0.5TiO_2$ (CNiT) ceramic sintered at $1200^\circ C$ has $\epsilon_r = 18$, $Q_{ur}f = 25300$ GHz and $\tau_f = -58$ ppm/ $^\circ C$. Addition of WO_3 , MoO_3 , Cr_2O_3 and Fe_2O_3 improves $Q_{ur}f$ slightly and addition of Ta_2O_5 , Bi_2O_3 , Fe_2O_3 and WO_3 increases ϵ_r slightly. The ionic radii of W^{6+} (0.6 Å), Mo^{6+} (0.59 Å), Cr^{6+} (0.615 Å) and Fe^{6+} (0.645 Å) are similar to that of Ti^{4+} (0.605 Å). Hence Cr^{3+} , Fe^{3+} , W^{6+} and Mo^{6+} may diffuse into the Ti^{4+}

site and improve the dielectric properties. Addition of 1 wt% MoO₃ tune τ_f from -58 to -21 ppm/°C (Table 3.8).

Table 3.8 Microwave dielectric properties of doped CeO₂-0.5NiO-0.5TiO₂ ceramic

Dopant	Dopant level (wt%)	Sintering temperature (°C) for 2h	Density (g/cm ³)	$Q_{ur}f$ (GHz)	ϵ_r	τ_f (ppm/°C)
No dopants	-	1200	5.39	25300	18.0	-58
WO ₃	0.5	1240	5.25	27150	18.7	-56
	1	1235	5.26	26750	19.8	-52
MoO ₃	0.5	1240	4.56	32500	14.0	-45
	1	1205	3.65	27300	9.8	-21
Sb ₂ O ₃	0.5	1240	6.30	23010	18.0	-45
	1	1240	4.66	24400	20.8	-40
Nb ₂ O ₅	0.5	1240	5.62	18150	21.2	-48
	1	1230	6.27	25750	18.4	-48
Ta ₂ O ₅	0.5	1240	5.76	18500	20.1	-55
Bi ₂ O ₃	0.5	1240	6.28	17300	21.0	-73
Fe ₂ O ₃	0.5	1240	4.90	26300	21.0	-56
	1	1240	4.45	23400	18.0	-51
La ₂ O ₃	0.5	1240	4.72	18150	18.0	-51
	1	1240	4.68	20150	17.4	-71
Cr ₂ O ₃	0.5	1240	5.01	27200	17.2	-56
	1	1240	6.61	26800	13.4	-54
Sm ₂ O ₃	0.5	1210	4.17	22600	14.5	-47
	1	1205	4.32	11450	12.0	-41
Nd ₂ O ₃	0.5	1170	4.35	21100	14.3	-52
	1	1210	4.66	20400	15.1	-52

The undoped CeO₂-0.5WO₃-0.5TiO₂ (CWT) ceramic sintered at 1130°C/2h has $\epsilon_r = 17$, $Q_{ur}f = 39800$ GHz and $\tau_f = 7$ ppm/°C. The $Q_{ur}f$ of CWT system shows an enhancement in $Q_{ur}f$ up to 45500 GHz when measured in vacuum. This system turns out to be the most complex composite. Addition of even a small amount of dopant (0.5 wt% decreases the quality factor and relative permittivity. Addition of 10 wt% CeO₂ improve the τ_f to 5 ppm/°C with $\epsilon_r = 16.3$ and $Q_{ur}f = 53000$ GHz (Table 3.9). In all cases undoped or doped, the CWT system has a low sintering temperature around 1130°C. The sintering temperature of CWT is decreased from 1130°C to 950°C by the addition of 0.5 wt% of 50ZnO:40B₂O₃:10SiO₂ (ZBS) glass. The 0.5 wt% ZBS added CWT has ϵ_r

17.2, $Q_{ur}xf = 10700$ GHz and $\tau_f = 32$ ppm/ $^{\circ}$ C. Hence it can be used as a possible candidate for LTCC applications.

Table 3.9 Microwave dielectric properties of doped $\text{CeO}_2\text{-}0.5\text{WO}_3\text{-}0.5\text{TiO}_2$ ceramic

Dopant	Dopant level (wt%)	Sintering Temperature ($^{\circ}$ C) for 2h	Density (g/cm^3)	$Q_{ur}xf$ (GHz)	ϵ_r	τ_f (ppm/ $^{\circ}$ C)
No dopants	-	1130	5.45	39800 45550*	17.0	7
Nb_2O_5	0.5	1130	4.57	11900	12.0	8
	1	1110	5.08	9450	11.9	13
Sb_2O_3	0.5	1130	5.34	19700 48550*	16.1	-7
	1	1110	5.56	17000 48350*	18.0	-11
Ta_2O_5	0.5	1130	4.69	16800	12	14
	1	1110	5.42	13600 33350*	14	23
TiO_2	0.5	1130	5.40	16200 55100*	16.8	12
	1	1130	5.37	14300 44900*	16	20
CeO_2	5	1110	5.64	14300 40800*	15.7	19
	10	1130	5.82	18600 53000*	16.3	5
Fe_2O_3	0.5	1130	5.65	22450 37950*	15.8	19
	1	1110	5.66	14100 38700*	16.9	18
La_2O_3	0.5	1130	5.46	19350 41050*	15.9	28
Cr_2O_3	0.5	1130	5.31	20750 41050*	15.3	19
	1	1110	5.56	20800 51500*	17.0	17
Bi_2O_3	0.5	1130	5.85	13250 18000*	17.0	20
Nd_2O_3	0.5	1130	5.4	22150 38900*	15.6	29
	1	1110	5.6	14400 20400*	16.0	36
$50\text{ZnO}:40\text{B}_2\text{O}_3:10\text{SiO}_2$	0.5	950	5.42	10700	17.2	32

* measured in vacuum

Table 3.10 Summary of microwave dielectric properties of CeO₂-AO-TiO₂ (A = Ca, Mg, Zn, Mn, Co, Ni, W) composites and their most promising dopants.

CAT-dopant	Dopant level (wt %)	$Q_{\nu}xf$ (GHz)	ϵ_r	τ_f (ppm/°C)
CCaT	-	9500	65.5	399
CCaT+Cr ₂ O ₃	8	4350	35.0	0
CMgT	-	17500	22.4	-62
CMgT+WO ₃	2	90000	21.4	-50
CZnT	-	24100	26.1	-43
CZnT+ Co ₃ O ₄	8	33100	22.0	-48
CMnT	-	17100	26.3	-30
CMnT+ MoO ₃	1	5980	27.5	-5
CCoT	-	50000*	22.0	-47
CCoT+ WO ₃	1.0	70000*	21.0	-30
CCoT+ WO ₃ /TiO ₂	0.5/20	58200*	21.2	5
CNiT	-	25300	18.0	-58
CNiT+ MoO ₃	1	27300	9.8	-21
CWT	-	45500*	17.0	7
CWT+ CeO ₂	10	53000*	16.3	5

* measured in vacuum

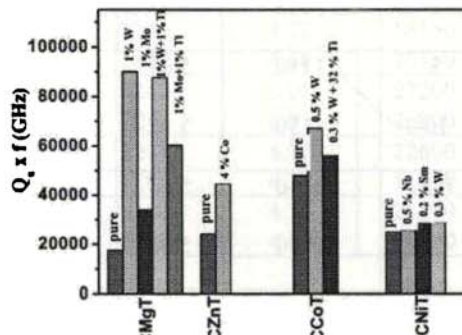


Fig. 3.17 Variation of $Q_{\nu}xf$ with dopants for CeO₂-AO-TiO₂ (A = Mg, Zn, Co, Ni) dielectric ceramics

The CeO₂-AO-TiO₂ (A = Ca, Mg, Zn, Mn, Co, Ni, W) ceramics have relative permittivity (ϵ_r) in the range 17.0 to 65.5 and quality factor $Q_{\nu}xf$ up to 50000 GHz. The τ_f ranges from 399 ppm/°C to -62 ppm/°C. Addition of different dopants improves the microwave dielectric properties as shown in Fig. 3.17 and Table 3.10. The best properties are obtained for CeO₂-0.5MgO-0.5TiO₂ doped with 2 wt% WO₃. It gives a very high $Q_{\nu}xf$ of 90000 GHz, $\epsilon_r = 21.4$ and $\tau_f = -50$ ppm/°C.

3.5 SYNTHESIS, CHARACTERIZATION AND MICROWAVE DIELECTRIC PROPERTIES OF $ATiO_3$ (A = Co, Mn, Ni) CERAMICS

3.5.1 Introduction

The structural and microstructural analysis showed that CeO_2 -0.5AO-0.5TiO₂ (A = Mg, Zn, Ca, Mn, Co, Ni) ceramics is a composite of fluorite CeO_2 and perovskite $ATiO_3$ (A = Mg, Zn, Ca, Mn, Co, Ni). A survey of literature shows that microwave dielectric properties of $ATiO_3$ (A = Mn, Co, Ni) has not been reported and this motivated us to make a systematic study of $ATiO_3$ (A = Co, Mn, Ni) ceramics.

Several studies on ABO_3 type materials have been reported with useful microwave dielectric properties.^{72,73,74} The $CoTiO_3$ prepared by solid-state reaction at high temperature has been studied for possible use as a humidity sensor and catalyst. Chu *et al.*⁷⁴ reported the gas sensitivity of nano- $CoTiO_3$ for detecting ethanol gas. Luo *et al.*⁷⁵ synthesized $ZnTiO_3$ and $(Zn_{1-x}Co_x)TiO_3$ ($x = 0.5-1$) ceramic powders at a low temperature by a sol-gel route including the Pechini process. The dielectric properties of $(Zn_{1-x}Co_x)TiO_3$ were measured at different frequencies and at $x = 0.5$, the maximum value exists for both relative permittivity and loss tangent. $MnTiO_3$ and $NiTiO_3$ nano powders were prepared and structural properties were investigated.^{76,77} The synthesis and structural details of materials having the ABO_3 form with ilmenite structure have been studied⁷⁵⁻⁷⁷ but the dielectric properties have not been reported. Non-stoichiometric $MTiO_3$ (M = Ni, Pb, Fe, Co, Mn, Cu and Zn) have been studied as functional inorganic materials with wide applications in electrodes of solid oxide fuel cells (SOFC), metal-air barriers, gas sensors and high performance catalysts.^{78,79,80} The $ATiX_3$ (A = Mg, Fe, Co, Mn, Ni) compounds (ilmenites) have a slightly distorted hexagonal closed-packed arrangement of atoms and can be regarded as an extremely distorted perovskite derived from the archetypal structure by extensive polyhedral rotation. The ilmenite structure is an ordered derivative of the corundum structure. It is adopted by $A^{2+}B^{4+}X_3$ and $A^+B^{5+}X_3$ compounds when A and B cations are similar in size and the A cation is much smaller than the X anion.⁸¹ Typically, ilmenite-type structures are formed when the Goldschmidt

tolerance factor (t) is less than 0.75, e.g. ilmenite, FeTiO_3 ($t = 0.73$) and gieselerite, MgTiO_3 ($t = 0.70$). In this chapter we report for the first time the microwave dielectric properties of a new group of ATiO_3 ($A = \text{Co, Mn, Ni}$) ceramics.

3.5.2 Experimental

The ATiO_3 ($A = \text{Co, Mn, Ni}$) dielectric ceramics were synthesized by the conventional solid state ceramic route as described in Section 2.1.2 of Chapter 2. High purity chemicals Co_3O_4 (Aldrich), MnCO_3 (Aldrich, 99.9+ %), NiO (Aldrich, 99 %) and TiO_2 (Aldrich, 99.9 %) were used as starting powders. Stoichiometric proportions of the chemicals were weighed and ball milled for 24 hours using zirconia balls in distilled water media. The slurry was dried and then calcined for 5 hours at 1075°C , 1100°C and 1025°C for Co, Mn and Ni based ceramics respectively. The well ground calcined powder ($0.1\text{-}1\ \mu\text{m}$) so obtained was then pressed into disc shaped pucks of 14 mm diameter and about 7 mm height at a pressure of about 120 MPa using a WC die. The green compacts were fired at a rate of $5^\circ\text{C}/\text{min}$ up to 600°C and soaked at 600°C for 30 minutes to expel the binder. The pellets were sintered in air at temperatures in the range between $1350 - 1475^\circ\text{C}$ depending on the A atom at a heating rate of $10^\circ\text{C}/\text{min}$. After sintering the samples were allowed to cool down to room temperature at a rate of $5^\circ\text{C}/\text{min}$. This is followed by annealing the ATiO_3 ($A = \text{Co, Mn, Ni}$) samples in air at $1250^\circ\text{C}/8\text{h}$, $1150^\circ\text{C}/8\text{h}$ and $1225^\circ\text{C}/8\text{h}$ respectively. The samples were then polished to remove surface irregularities. The densities of the samples were measured by Archimedes method. Phase purity of the materials was studied by X-ray diffraction technique using $\text{CuK}\alpha$ radiation and microstructural analysis was done using SEM techniques. The dielectric properties Q_{10} , ϵ_r and τ_f of the materials were measured in the microwave frequency range as described in Chapter 2, section 2.4.2 to 2.4.5.

3.5.3 Results and Discussion

The synthesizing conditions such as calcination temperature, sintering temperature, annealing temperature and their durations are optimized for ATiO_3 ($A = \text{Co}$,

Mn, Ni) dielectric ceramics to obtain the best density and dielectric properties. There is no change in density, dielectric properties or in XRD pattern when sintered ATiO_3 ($A = \text{Co, Mn, Ni}$) samples are boiled in water indicating excellent chemical and thermal stability of the material.

Fig. 3.18 shows the variation of percentage density with sintering temperature for ATiO_3 ($A = \text{Co, Mn, Ni}$) dielectric ceramics. The CoTiO_3 ceramic which has a black colour shows a densification of 98.5% on sintering at $1375^\circ\text{C}/2\text{h}$ and golden brown coloured NiTiO_3 shows a densification of 92% on sintering at $1475^\circ\text{C}/4\text{h}$. However, black coloured MnTiO_3 ceramic puck shows a relatively low percentage density of 89% on sintering at $1350^\circ\text{C}/2\text{h}$.

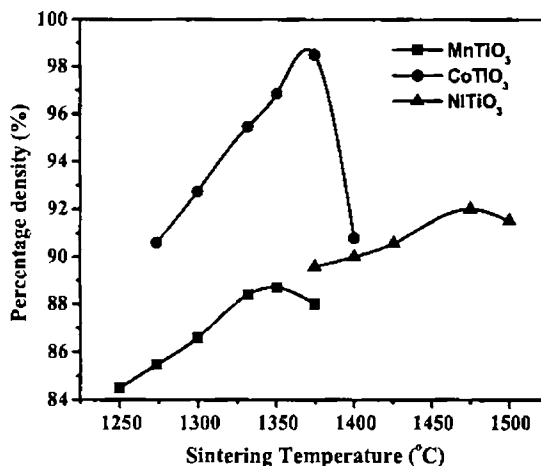


Fig.3.18 The variation of percentage density with sintering temperature for ATiO_3 ($A = \text{Co, Mn, Ni}$) ceramics

In titanium based ceramics titanium is in Ti^{4+} oxidation state. It has been reported that⁸² prolonged heating at high temperatures will lead to the reduction of Ti^{4+} to Ti^{3+} which may degrade the dielectric properties. Hence, we have annealed ATiO_3 ($A = \text{Co, Mn, Ni}$) ceramics at various temperatures and optimized their annealing temperature to get the best quality factor (Fig. 3.19). The optimized annealing temperatures are 1250°C , 1150°C and 1225°C for ATiO_3 ($A = \text{Co, Mn, Ni}$) ceramics respectively. Fig. 3.20 shows the optimization of annealing duration of ATiO_3 ($A = \text{Co, Mn, Ni}$) ceramics

and for all the three ceramics the optimized duration is 8 hours. The uniform colour of ATiO_3 ($A = \text{Co, Mn, Ni}$) samples does not change on annealing.

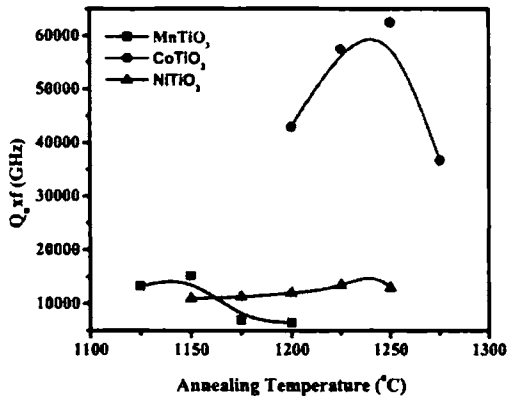


Fig. 3.19 The variation of Q_{1xf} with annealing temperature for ATiO_3 ($A = \text{Co, Mn, Ni}$) ceramics, Annealing duration is 8 hours

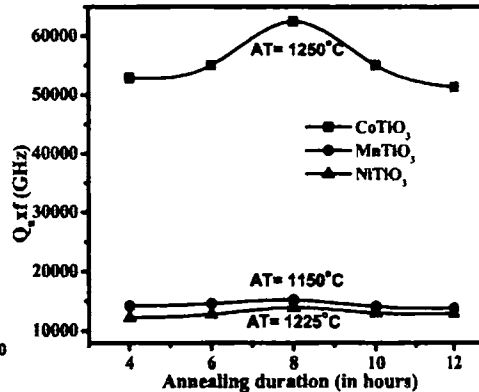


Fig. 3.20 The variation of Q_{1xf} with annealing duration for ATiO_3 ($A = \text{Co, Mn, Ni}$) ceramics, AT- Annealing temperature

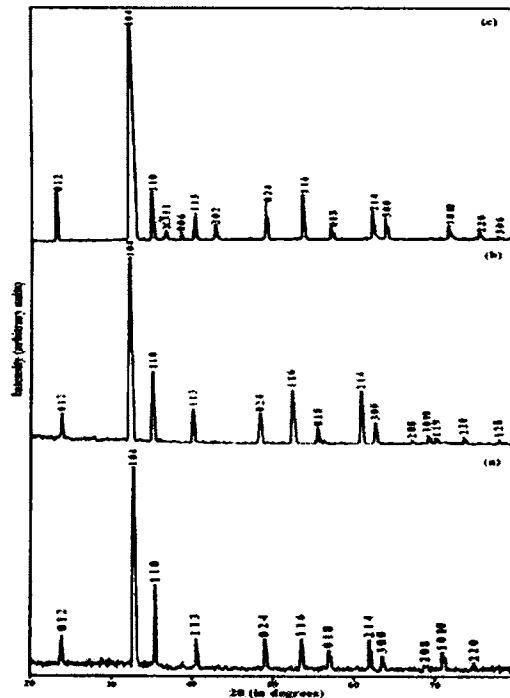
3.5.3.1 Phase and Microstructural Analysis

The XRD patterns of ATiO_3 ($A = \text{Co, Mn, Ni}$) ceramics recorded using $\text{CuK}\alpha$ radiation are shown in Fig. 3.21. The powder patterns are indexed and are comparable with JCPDS file card numbers 15-0866 (CoTiO_3), 29-0902 (MnTiO_3) and 33-0960 (NiTiO_3). XRD pattern of NiTiO_3 annealed at $1225^\circ\text{C}/8\text{h}$ is shown in Figure 3.21(c). ATiO_3 ($A = \text{Co, Mn}$) ceramics are single phase and an additional second phase of Ti_3O_5 (JCPDS card no. 23-606) is found in NiTiO_3 . Kofstad⁸³ reported that at temperatures above 1300°C all the oxides of titanium (Ti_2O , TiO , Ti_2O_3 , Ti_3O_5 , TiO_2) are formed as reaction products depending on the oxygen pressure and elapsed time of reaction. The ATiO_3 ceramics are hexagonal with space group $R\bar{3}(148)$ and having six formula units per unit cell.

The tolerance factor for ABO_3 ceramics is calculated using the following equation⁸⁴

$$t = \frac{r_A + r_O}{\sqrt{2}(r_B + r_O)} \quad (3.4)$$

where r_A , r_B and r_O are the ionic radii of the constituent ions.⁶⁸ The tolerance factors (t) of $ATiO_3$ ($A = Co, Mn, Ni$) ceramics are calculated to be 0.72, 0.73 and 0.74 respectively. Ilmenite type structures are formed when the Goldschmidt tolerance factor (t) is less than 0.75.⁸¹



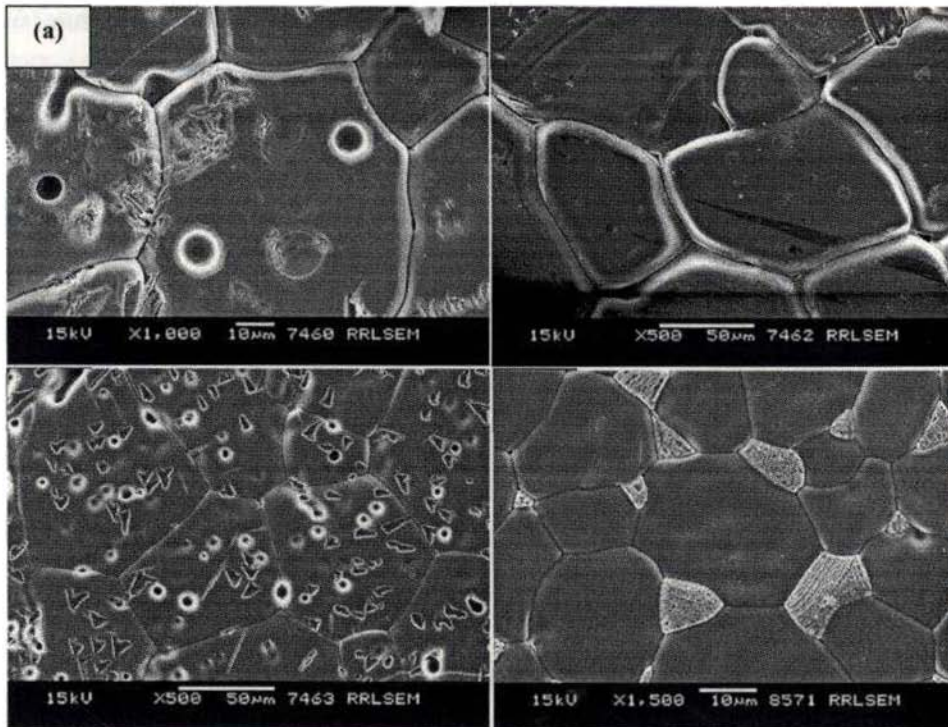


Fig. 3.22 SEM micrographs of (a) CoTiO_3 (b) MnTiO_3 (c) NiTiO_3 (d) NITiO_3 , annealed at $1225^\circ\text{C}/8\text{h}$ ceramics

3.5.3.2 Microwave Dielectric Properties

Fig. 3.23 shows the variation of microwave dielectric properties with sintering temperature of ATiO_3 ($A = \text{Co}, \text{Mn}, \text{Ni}$) ceramics. The relative permittivity and quality factor increase with sintering temperature reach a maximum value at 1375 , 1350 and 1475°C and then decrease for ATiO_3 ($A = \text{Co}, \text{Mn}, \text{Ni}$) ceramics respectively. The relative permittivity and quality factor show the same trend as that for percentage densification in ATiO_3 ($A = \text{Co}, \text{Mn}, \text{Ni}$) ceramics.

The τ_f decreases with sintering temperature for ATiO_3 ($A = \text{Mn}, \text{Ni}$) except for CoTiO_3 ceramics. Fig. 3.24 shows the variation of dielectric properties before and after annealing of ATiO_3 ($A = \text{Co}, \text{Mn}, \text{Ni}$) ceramics. Both CoTiO_3 and MnTiO_3 show a considerable increase in $Q_{\nu}xf$ whereas NiTiO_3 shows only a slight increase in the quality

factor (Fig. 3.19). The relative permittivity does not show any appreciable change with annealing but τ_f increases to the negative side.

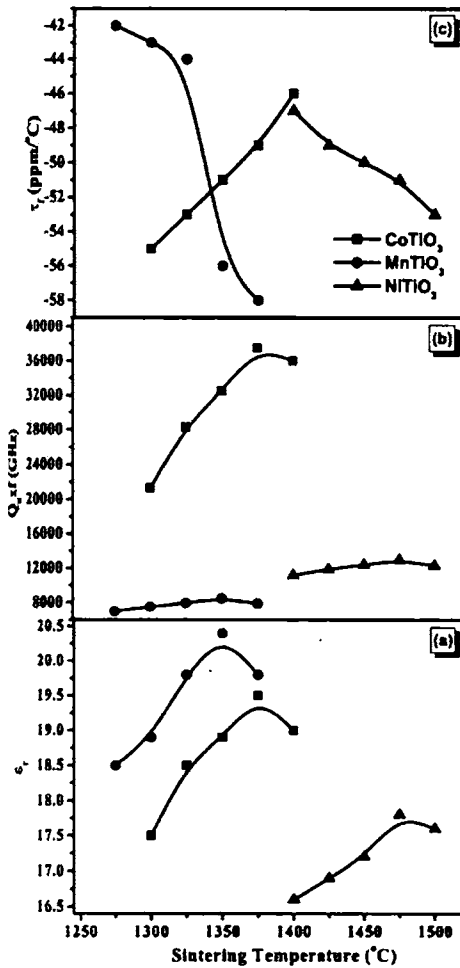


Fig. 3.23 Variation of (a) ϵ' , (b) Q_{uxf} and (c) τ_f with sintering temperature of $ATiO_3$ (A = Co, Mn, Ni) ceramics

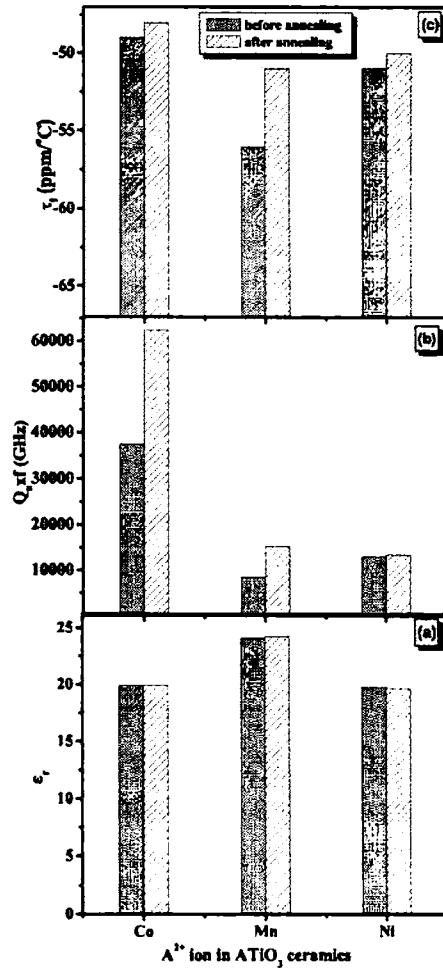


Fig. 3.24 The microwave dielectric properties (ϵ' , Q_{uxf} and τ_f) of $ATiO_3$ (A = Co, Mn, Ni) ceramics

Table 3.11 gives the optimized synthesizing conditions and microwave dielectric properties of $ATiO_3$ (A = Co, Mn, Ni) dielectric ceramics. The as-sintered $CoTiO_3$ has a Q_{uxf} of 37500 GHz which increases to 62500 GHz on annealing at 1250°C for 8h. The

MnTiO₃ ceramics annealed at 1150°C/8h has a $Q_{\omega}xf$ of 15200 GHz. The NiTiO₃ has a $Q_{\omega}xf$ of 13900 GHz when annealed at 1225°C/8h. Popov and Levitskii⁸⁵ reported that Ti in CoTiO₃ get reduced to Ti³⁺ at high temperature producing oxygen vacancies.

Table 3.11 The synthesizing conditions and dielectric properties of ATiO₃ (A = Co, Mn, Ni) dielectric ceramics

Material	CT (°C)	ST (°C)	Relative Density (%)	AT (°C)	Observed ϵ_r (ϵ_r) _o	$Q_{\omega}xf$ (GHz) (before Ann.)	$Q_{\omega}xf$ (GHz) (after Ann.)	τ_f (ppm/°C)
CoTiO ₃	1075/5h	1375/2h	98.5	1250/8h	19.5	37500	62500	-49
MnTiO ₃	1050/5h	1350/2h	89.0	1150/8h	20.4	8500	15200	-56
NiTiO ₃	1025/5h	1475/4h	92.0	1225/8h	17.8	13000	13900	-51

CT-Calcination Temperature, ST- Sintering Temperature, AT- Annealing Temperature

The presence of oxygen vacancies deteriorates the quality factor. Annealing the ceramic samples decreases the oxygen vacancies and improves the quality factor. The MnTiO₃ have poor densification and NiTiO₃ contains a second phase. Hence these materials have relatively low quality factor as compared to that of CoTiO₃. The τ_f of all the three ceramics is about -50 ppm/°C.

MnTiO₃ has the highest ϵ_r of 24.3 and CoTiO₃ and NiTiO₃ have ϵ_r of 19.8 and 19.7 respectively. The relative permittivities of ATiO₃ are corrected for porosity using the following equation derived by Penn *et al.*⁸⁶

$$(\epsilon_r)_o = (\epsilon_r)_{cor} \left(1 - \frac{3P((\epsilon_r)_{cor} - 1)}{2(\epsilon_r)_{cor} + 1} \right) \quad (3.5)$$

where $(\epsilon_r)_o$ is the measured relative permittivity of the compound which contains a fractional porosity P and $(\epsilon_r)_{cor}$ is the actual relative permittivity of the dielectric. The percentage deviation of observed ϵ_r from porosity corrected ϵ_r is maximum (16%) for MnTiO₃ due to its lower percentage density. CoTiO₃ which has a maximum percentage density (98.5%) shows only a very slight deviation (1.5%) while NiTiO₃ (92%) shows 9.6% deviation.

The ϵ_r of ATiO_3 ($A = \text{Co, Mn, Ni}$) dielectric ceramics is calculated using the following Clausius-Mossotti equation and are given in Table 3.12

$$(\epsilon_r)_{cal} = \frac{3V_m + 8\pi\alpha_D}{3V_m - 4\pi\alpha_D} \quad (3.6)$$

where α_D is the total dielectric polarizability⁸⁷ and V_m is the molar volume. The observed ϵ_r is in very good agreement with that calculated using Clausius-Mossotti equation.

Table 3.12 The dielectric polarizability and relative permittivity of ATiO_3 ($A = \text{Co, Mn, Ni}$) ceramics

Material	Porosity Corrected ϵ_r (ϵ_r) _{cor}	Claussius- Mossotti eq. ϵ_r (ϵ_r) _{cal}	$\Delta\epsilon$ (%)
CoTiO_3	19.8	20.0	1.1
MnTiO_3	24.3	26.8	9.2
NiTiO_3	19.7	17.8	11.5

The ATiO_3 ($A = \text{Co, Mn, Ni}$) ceramics have moderate relative permittivity and quality factors. However, their high negative τ_f precludes immediate use in practical applications. It may be possible to improve their τ_f by suitable doping and by solid-solution formation.

3.6 CONCLUSIONS

- Microwave dielectric ceramics based on a ceria-titania based system [CeO_2 -0.5AO-0.5TiO₂ ($A = \text{Mg, Zn, Ca, Mn, Co, Ni, W}$)] are prepared by solid-state reaction method. These ceramics systems are a composite consisting of fluorite CeO_2 and ATiO_3 with high density and interesting individual dielectric properties depending on the coexisting ATiO_3 being formed.
- The synthesizing conditions of the ceramics are optimized and dielectric properties are measured in the microwave frequency range. The ceramics have relative permittivity (ϵ_r) in the range 17.0 to 65.5 and quality factor Q_{ux} up to 50000 GHz. The τ_f ranges from 399 ppm/°C to -62 ppm/°C.

- The quality factor increases considerably on cooling for $\text{CeO}_2\text{-}0.5\text{AO-}0.5\text{TiO}_2$ ($\text{A} = \text{Mg, Zn, Ca, Mn, Co, Ni, W}$) ceramics in a manner, which is similar to pure CeO_2 . Highest Q_u is observed for the $\text{CeO}_2\text{-}0.5\text{MgO-}0.5\text{TiO}_2$ system and at 20 K reaches as high as 98000 ($Q_{uxf} = 539000$ GHz).
- The effect of dopants on the microwave dielectric properties of $\text{CeO}_2\text{-}0.5\text{AO-}0.5\text{TiO}_2$ ($\text{A} = \text{Mg, Zn, Ca, Mn, Co, Ni, W}$) ceramics are investigated. Suitable dopants of various valencies are added to tune the microwave dielectric properties. It is found that small amount of dopants could dramatically alter the dielectric properties.
- $\text{CeO}_2\text{-}0.5\text{CaO-}0.5\text{TiO}_2$ composite doped with 8 wt% Cr_2O_3 decreases the τ_f from 399 ppm/°C to zero ppm/°C. $\text{CeO}_2\text{-}0.5\text{MgO-}0.5\text{TiO}_2$ doped with 2 wt% WO_3 gives a very high Q_{uxf} of 90000 GHz.
- ATiO_3 ($\text{A} = \text{Co, Mn, Ni}$) dielectric ceramics have been synthesized by the conventional solid state ceramic route. ATiO_3 ($\text{A} = \text{Co, Mn, Ni}$) ceramics have hexagonal symmetry with $\text{R}\bar{3}$ (148) space group.
- The synthesizing conditions of ATiO_3 ($\text{A} = \text{Co, Mn, Ni}$) ceramics are optimized and annealing of these ceramics for 8 hours improves the quality factor. The relative permittivity varies from 19 to 25, Q_{uxf} from 13900 to 62500 GHz and τ_f of about -50 ppm/°C.

The synthesis, characterization and microwave dielectric properties of $\text{CeO}_2\text{-}0.5\text{AO-}0.5\text{TiO}_2$ ($\text{A} = \text{Mg, Zn, Ca, Mn, Co, Ni, W}$) ceramics are investigated in this Chapter. The effect of dopants which control the microwave dielectric properties of the ceramics are also discussed. This Chapter also reports the synthesis, characterization and microwave dielectric properties of ATiO_3 ($\text{A} = \text{Co, Mn, Ni}$) ceramics for the first time. The next Chapter discusses the $\text{BaO-CeO}_2\text{-TiO}_2$ ceramics for DR applications.

3.7 REFERENCES

- ¹ Molycorp, *Cerium: A Guide to its Role in Chemical Technology*; Molycorp, Inc.: Mountain Pass, CA, U.S.A, (1992).
- ² G. Adachi and N. Imanaka, *Chem. Rev.*, **98**, 1479 (1998).
- ³ N.V. Skorodumova, S.I. Simak, B.I. Lundqvist, I.A. Abrikosov and B. Johansson, *Phys. Rev. Lett.*, **89**, 166601 (2002).
- ⁴ T. Yamamoto, H. Momida, T. Hamada, T. Uda and T. Ohno, *Thin Solid Films*, **486**, 136 (2005).
- ⁵ D.R. Lide (Editor), *Handbook of Chemistry and Physics*, 84th Ed., CRC Press, Boca Raton, (2003)
- ⁶ Z. L. Wang, and Z. C. Kang, *Functional and Smart Materials: Structural Evolution and Structure Analysis*, Plenum Press, New York, (1998).
- ⁷ G. Li, T. Ikegami, J. H. Lee and T. Mori, *Acta Mater.*, **49**, 419 (2001).
- ⁸ S. Bernal, J. Kasper and A. Trovaralli, *Catal. Today*, **50**, 173 (1999).
- ⁹ S. Dikmen, P. Shuk and M. Greenblatt, *Solid State Ionics*, **126**, 89 (1999).
- ¹⁰ T. Sato, K. Dosaka, M. Ishitsuka, E. M. Haga and A. Okuwai, *J. Alloys Compd.*, **193**, 274 (1993).
- ¹¹ T. Nakazawa, T. Inoue, M. Satoh and Y. Yamamoto, *Jpn. J. Appl. Phys.*, **34**, 548 (1995).
- ¹² A. Tschope, W. Liu, M. F-Stephanopoulos and J. Y. Ying, *J. Catal.*, **157**, 42 (1995).
- ¹³ A. Tschope, D. Schaadt, R. Birringer and J. Y. Ying, *Nanostruct. Mater.*, **9**, 423 (1997).
- ¹⁴ S. Tsunekawa, T. Fukuda and A. Kasuya, *Surf. Sci.*, **457**, L437 (2000).
- ¹⁵ J. R. McBride, K. C. Hass, B. D. Poindexter and W. H. Weber, *J. Appl. Phys.*, **76**, 2435 (1994)
- ¹⁶ E. Spanier, R. D. Robinson, F. Zhang, S-W Chan and I. P. Herman, *Phys. Rev. B*, **46**, 245407 (2001).
- ¹⁷ S. Tsunekawa, R. Sivamohan, S. Ito, A. Kasuya and T. Fukuda, *Nanostruct. Mater.*, **11**, 141 (1999)
- ¹⁸ Z. Wu, L. Guo, H. Li, Q. Yang, Q. Li and H. Zhu, *Mater. Sci. Eng. A*, **286**, 179 (2000).

-
- ¹⁹ F. Zhang, S-W Chan, J. E. Spanier, E. Apak, Q. Jin, R. D. Robinson and I. R. Herman, *Appl Phys. Lett.*, **80**, 127 (2002).
- ²⁰ S. Tsunekawa, R. Sivamohan, T. Ohsuna, A. Kasuya, H. Takahashi and K. Tohji, *Mater. Sci Forum*, **315-317**, 439 (1999).
- ²¹ M. Hirano and E. Kato, *J. Am. Ceram. Soc.*, **83**, 786 (1999).
- ²² M. Ozawa, *Scripta Mater.*, **50**, 61 (2004).
- ²³ F. Esch, S. Fabris, L. Zhou, L. Montini, C. Africh, P. Fornasiero, G. Comelli and R. Rosie, *Science*, **309**, 752 (2005).
- ²⁴ S. Deshpande, S. Patil, S. Kuchibhatla and S. Seal, *Appl. Phys. Lett.*, **87**, 133113 (2005).
- ²⁵ P. Dutta, S. Pal and M. S. Seehra, *Chem. Mater.*, **18**, 5144 (2006).
- ²⁶ T. Baidya, A. Gayen, M. S. Hegde, N. Ravishankar and L. Dupont, *J. Phys. Chem. B*, **110**, 5262 (2006).
- ²⁷ J. Fang, X. Bi, D. Si, Z. Jiang and W. Huang, *Appl. Surf. Sci.*, **253**, 8952 (2007).
- ²⁸ Y. M. Chiang, E. B. Lavik, I. Kosacki, H. L. Tuller and J. Y. Ying, *J. Electroceram.*, **1**, 7 (1997).
- ²⁹ G. A. Kourouklis, A. Jayaraman and G. P. Espinosa, *Phys. Rev. B*, **37**, 4250 (1988).
- ³⁰ T. Yamamoto, H. Momida, T. Hamada, T. Uda and T. Ohno, *Thin Solid Films*, **486**, 136 (2005).
- ³¹ Y. Nishikawa, N. Fukushima, N. Yasuda, K. Nakayama and S. Ikegawa, *Jpn. J. Appl. Phys.*, **41**, 2480 (2002)
- ³² H. Yahiro, Y. Eguchi, K. Eguchi, H. Arai, *J. Appl. Electrochem.*, **18**, 527 (1988).
- ³³ M. Yashima, H. Arasi, M. Kakihana and M. Yoshimura, *J. Am. Ceram. Soc.*, **77**, 1067 (1994)
- ³⁴ Y. Zhang, A. Andersson and M. Muhammed, *Appl. Catal. B: Environ.*, **6**, 325 (1995).
- ³⁵ C. Lamonier, A. Bennani, A. D'Huysser, A. Aboukais and G. Wrobel, *J. Chem. Soc., Faraday Trans.*, **92**, 131 (1996).
- ³⁶ S. Imamura, M. Shono, N. Okamoto, A. Haneda and S. Ishida, *Appl. Catal. A: General*, **141**, 279 (1996).

-
- ⁷ M. N. Rahman and Y. C. Zhou, *J. Eur. Ceram. Soc.*, **240-243**, 939 (1995).
- ³⁴ N. Santha, M. T. Sebastian, P. Mohanan, N. McN. Alford, K. Sarma, R. C. Pullar, S. Kamba, A. Pashkin, P. Samukhina and J. Petzelt, *J. Am. Ceram. Soc.*, **87**, 1233 (2004).
- ³⁹ P. L. Wise, I. M. Reaney, W. E. Lee, T. J. Price, D. M. Iddles and D. S. Cannel, *J. Eur. Ceram. Soc.*, **21**, 1723 (2001).
- ⁴⁴ M. T. Sebastian, N. Santha, P. V. Bijumon, A-K. Axelsson and N. McN. Alford, *J. Eur. Ceram. Soc.*, **24**, 2583 (2004).
- ⁴¹ C-H Hsu, *Ceram. Int.*, **34**, 243 (2008).
- ⁶² D. H. Kim, S. K. Lim and C. An, *Mater. Lett.*, **52**, 240 (2002).
- ⁴³ M. T. Sebastian, *Dielectric Materials for Wireless Communication*, Elsevier Publishers, Oxford, (2008).
- ⁴⁴ B. W. Hakki and P. D. Coleman, *IRE Trans. Microwave Theory Tech.*, **MTT-8**, 402 (1960).
- ⁴⁵ W. E. Courtney, *IEEE Trans. Microwave Theory Tech.*, **MTT-18**, 476 (1970).
- ⁴⁶ J. Krupka, K. Derzakowski, B. Riddle and J. B. Jarvis, *Meas. Sci. Technol.*, **9**, 1751 (1998).
- ⁴⁷ M. Menneraye, J. Seridat and C. Jourwersma, *Glass Technol.*, **9**, 70 (1968).
- ⁴⁸ H. Ikawa, A. Iwai, K. Hiruta, H. Shimojima, K. Urabe and S. Udagawa, *J. Am. Ceram. Soc.* **71**, 120 (1988).
- ⁴⁹ Y. Zhang and P. K. Davies, *J. Am. Ceram. Soc.*, **77**, 743 (1994).
- ⁵⁰ D. Houivet, J. E. Fallah, B. Lamagnere and J-M. Haussone, *J. Eur. Ceram. Soc.*, **21**, 1727 (2001).
- ⁵¹ P. V. Bijumon, S. Soloman and M. T. Sebastian, *J. Mater. Sci. Mater. Electron.*, **14**, 5 (2003).
- ⁵² D-W Kim, J-H Park, J-H Chung and K-S Hong, *Jpn. J. Appl. Phys.*, **39**, 2696 (2000).
- ⁵³ A. E. Paladino, *J. Am. Ceram. Soc.*, **54**, 168 (1971).
- ⁵⁴ S. Nomura, K. Toyama and K. Kaneta, *Jpn. J. Appl. Phys.*, **21**, 624 (1982).
- ⁵⁵ Y. Kawashima, N. Nishida, I. Ueda and H. Ouchi, *J. Am. Ceram. Soc.*, **66**, 421 (1983).
- ⁵⁶ M. P. Seabra, M. Avdeev, V. M. Ferreira, R. C. Pullar and N. McN. Alford, *J. Eur. Ceram. Soc.*, **23**, 2403 (2003).

-
- ⁵⁷ I. Maclaren and C. B. Ponton, *J. Mater. Sci.*, **33**, 17 (1998).
- ⁵⁸ O. Renoult, J-P. Boilot, F. Chaput, R. Papiernik, L. G. Hubert-Pfalzgraf and M. Lejeune, *J. Am. Ceram. Soc.*, **75**, 3337 (1992).
- ⁵⁹ C-H. Lu and C-C. Tsai, *Mater. Sci. Eng. B*, **55**, 95 (1998).
- ⁶⁰ M-H. Liang, S-Y. Wu, C-T. Hu and I-N. Li, *Mater. Chem. Phys.*, **79**, 276 (2003).
- ⁶¹ H. M. Shirey, *M. S. Thesis*, University of Pittsburg, (2002).
- ⁶² S. Katayama, I. Yoshinaga, N. Yamada and T. Nagai, *J. Am. Ceram. Soc.*, **79**, 2059 (1996).
- ⁶³ Q. Wang, H. Rushan and Z. Z. Gan, *J. Am. Ceram. Soc.*, **75**, 2881 (1992).
- ⁶⁴ G. Rong, N. Newman, B. Shaw and D. Cronin, *J. Mater. Res.*, **14**, 4011 (1999).
- ⁶⁵ X. M. Chen and Y. J. Wu, *J. Mater. Sci. Mater. Electron.*, **7**, 369 (1996).
- ⁶⁶ M. R. Varma, R. Reghunandan and M. T. Sebastian, *Jpn. J. Appl. Phys.*, **44**, 298 (2005).
- ⁶⁷ S-Y Chen and Y-J Lin, *Jpn. J. Appl. Phys.*, **40**, 3305 (2001).
- ⁶⁸ R. D. Shannon, *Acta Crystallogr.*, **A32**, 751 (1976).
- ⁶⁹ S. Penn, N. Alford, *Ceramic Dielectrics for Microwave Applications; in Handbook of Low and High Dielectric Constant Materials and their Applications. Phenomena, Properties and Applications.* (Editor Hari Singh Nalwa), Academic Press, (1999).
- ⁷⁰ S. Nomura, K. Toyama, and K. Kaneta, *Jpn. J. Appl. Phys.*, **22**, 1125 (1983).
- ⁷¹ A. Templeton, X. Wang, S. J. Pen, S. J. Webb, Lesley, F. Cohen and N. McN Alford, *J. Am. Ceram. Soc.*, **83**, 95 (2000).
- ⁷² P. K. Davies, J. Tong and T. Negas, *J. Am. Ceram. Soc.*, **80**, 1727 (1997).
- ⁷³ S. Nomura, K. Toyama and K. Kaneta, *Jpn. J. Appl. Phys.*, **21**, L624 (1982).
- ⁷⁴ X. F. Chu, X. Q. Liu, G. Wang and G. Meng, *Mater. Res. Bull.*, **34**, 1789 (1999).
- ⁷⁵ J. Luo, X. Xing, R. Yu, Q. Xing, D. Zhang and X. Chen, *J. Alloys and Compds.*, **402**, 263 (2005)
- ⁷⁶ G. W. Zhou and Y. S. Kang, *Mater. Sci. Eng. C*, **24**, 71 (2004).

-
- ⁷⁷ D. J. Taylor, P. F. Fleig and R. A. Page, *Thin Solid Films*, **408**, 104 (2002).
- ⁷⁸ N. Dharmaraj, H. C. Park, C. K. Kim, H. Y. Kim and D. R. Lee, *Mater. Chem. Phys.*, **87**, 5 (2004).
- ⁷⁹ T. Kazuyuki, U. Yasuo, T. Shuji, I. Takashi and U. Akifumi, *J. Am. Chem. Soc.*, **106**, 5172 (1984).
- ⁸⁰ D-U Kim and M-S Gong, *Sensors and Actuators B: Chemical*, **110**, 321 (2005).
- ⁸¹ R. H. Mitchell, *Perovskites: Modern and Ancient*, Almaz Press Inc., Ontario, Canada, (2002).
- ⁸² S. Nomura, K. Toyama and K. Kaneta, *Jpn. J. Appl. Phys.*, **22**, 1125 (1983).
- ⁸³ P. Kofstad, *J. Less Com. Met.*, **12**, 449 (1967).
- ⁸⁴ R. S. Roth, *J. Res. Natl. Bur. Stand.*, **58**, 75 (1957).
- ⁸⁵ S. G. Popov and V. A. Levitskii, *J. Solid State Chem.*, **38**, 1 (1981).
- ⁸⁶ S. J. Penn, N. M. Alford, A. Templeton, X. Wang, M. Xu, M. Reece and K. Schrapel, *J. Am. Ceram. Soc.*, **80**, 1885 (1997).
- ⁸⁷ R. D. Shannon, *J. Appl. Phys.*, **73**, 348 (1993).

Chapter 4

MICROWAVE DIELECTRIC PROPERTIES OF BaO-CeO₂-TiO₂ CERAMICS

This chapter discusses the microwave dielectric properties of BaO-CeO₇-TiO₂ ceramics. The properties were found to depend on the TiO₂ and CeO₂ content in the BaO-CeO₇-TiO₂ ceramic. The influence of dopants like WO₃, MoO₃, Sb₂O₃, V₂O₅, Ta₂O₅, Nb₂O₅, ZrO₂, SnO₂, TiO₂, Fe₂O₃, Cr₂O₃, Sm₂O₃, Al₂O₃, MnCO₃, NiO, CuO & Co₃O₄ on the microwave dielectric properties of BaO-3CeO₇-4TiO₂ ceramic were also investigated. Small amount of CuO doped with BaO-3CeO₇-4TiO₂ ceramic lowered the sintering temperature from 1260 to 1050°C without degrading the microwave dielectric properties. The (1-x)CeO₇-xBaTi₄O₉ ceramics prepared by the solid-state ceramic route is a composite consisting of fluorite CeO₂ and BaTi₄O₉ phases. The density, relative permittivity and temperature coefficient of resonant frequency of mixtures predicted by the appropriate mixing relations agree well with the experimental values in (1-x)CeO₇-xBaTi₄O₉ ceramics. The effects of addition of B₂O₃ and CuO on the sintering temperature and microwave dielectric properties of 0.5CeO₇-0.5BaTi₄O₉ ceramics were also investigated.

4.1 SYNTHESIS, CHARACTERIZATION AND MICROWAVE DIELECTRIC PROPERTIES OF BaO-CeO₂-TiO₂ CERAMICS

4.1.1 Introduction

The rapid advance in wireless communication in the past decade was because of the revolutionary progress in the discovery and development of increasingly sophisticated materials. The use of these materials in the circuitry of wireless devices, microelectronic technology and in monolithic microwave integrated circuits (MMIC)^{1,2} have led to dramatic decrease in the size and weight of devices such as cellular phones in recent years. The excellent performance of the circuit is mainly controlled by the properties like relative permittivity (ϵ_r), unloaded quality factor (Q_u) and temperature variation of resonant frequency (τ_f) of the materials used. The search for new materials is in rapid progress owing to the drive for further system miniaturization and improved filtering capabilities.^{3,4,5,6} Bamberger *et al.*⁷ reported the existence of a new compound Sr₂Ce₂Ti₅O₁₆ with pseudo cubic structure in SrO-CeO₂-TiO₂ system. More recently, Subodh *et al.*⁸ reported single phase compounds in the Sr_{2+n}Ce₂Ti_{5+n}O_{15+3n} series with reasonably good dielectric properties. Hence we have made an attempt to prepare the analogous compound Ba_{2+n}Ce₂Ti_{5+n}O_{15+3n}.

The BaTi₄O₉, Ba₂Ti₉O₂₀ and BaTi₅O₁₁ in the BaO-TiO₂ binary system are low loss dielectric ceramic materials for microwave communication.^{9,10,11,12} Ceramics based on the ternary BaO-TiO₂-RE₂O₃ (RE = Rare earth) are extensively used in the manufacture of electronic components.^{13,14,15,16} Many studies proved that these ceramics contained secondary phases like BaTi₄O₉, TiO₂, RE₂Ti₂O₇ etc in addition to the major phases like Ba_{6-x}RE_{8+2x}Ti₁₈O₅₄.¹³⁻¹⁷ Although considerable amount of work has been done on the phase formation, structure, microstructure and microwave dielectric properties of BaO-TiO₂-RE₂O₃ (RE = Rare earth) ceramics, very little attention was given to Ce-based compounds. Cerium oxide (CeO₂) is an attractive insulating material because of its chemical stability, close lattice match with silicon and interesting microwave dielectric properties which is discussed in section 3.2 of Chapter 3. In contrast to most of the rare-

earth elements, which are stable in air in oxidation state 3+, cerium is most stable in oxidation state 4+. Cerium(III) oxide (Ce_2O_3) is highly unstable and ignites in air even at room temperature.^{13,14} The stability of (3+) and (4+) valence states of Ce depends on the oxygen partial pressure, temperature and crystal lattice environment. Low oxygen partial pressure and high temperature stabilize the Ce^{3+} valence state.¹⁸ Hwang *et al.*¹⁹ studied the effect of Ce substitution for Ba sites on the dielectric properties and micro structural development of BaTiO_3 . Makovec and co-workers noted that Ce is incorporated as Ce^{3+} into the Ba^{2+} site in presence of excess TiO_2 , and as Ce^{4+} into the Ti^{4+} site in the presence of BaO in the ambient atmosphere, because of the multivalency of Ce ions.^{18,20,21} It was reported that the solubility of Ce in $(\text{Ba}_{1-x}\text{Ce}_x)\text{TiO}_3$ is approximately 8 mol%, while that of Ce into Ti in the $\text{Ba}(\text{Ti}_{1-y}\text{Ce}_y)\text{O}_3$ solid solution is more than 30 mol%.²¹ Equilibrium in the ternary BaO-TiO₂-CeO₂ system was described by Guha and Kolar²² and no ternary compounds were detected. Extensive mutual solid solubility was observed between BaTiO_3 and BaCeO_3 . Kolar¹⁸ also studied the phase equilibria in the system BaO-TiO₂-Ce₂O₃. Hoffman and Waser²³ used chemical method for the preparation of BaO-CeO₂-TiO₂ compounds. Sreemoolanadhan *et al.*²⁴ reported the microwave dielectric properties of $\text{BaO}-2\text{CeO}_2-n\text{TiO}_2$ ($n = 3, 4, 5$) ceramics and obtained the symmetry of these compounds using FT Raman spectra. The microwave dielectric properties of $\text{CeO}_2-0.5\text{AO}-0.5\text{TiO}_2$ ($A = \text{Mg, Zn, Ca, Mn, Co, Ni, W}$) dielectric ceramics were discussed in the section 3.3.5.2 of Chapter 3. In this chapter we report the synthesis, characterization and the effect of TiO₂ and CeO₂ content on the structure and microwave dielectric properties of BaO-CeO₂-TiO₂ ceramics.

4.1.2 Experimental

The samples of $\text{CeO}_2\text{-BaO-TiO}_2$ were prepared by the conventional solid state ceramic route as described in Chapter 2, section 2.1.2. High purity chemicals CeO_2 (IRE, 99.99%), BaCO_3 (Aldrich, 99+%) and TiO_2 (Aldrich, 99.9%) were stoichiometrically weighed and then ball milled in distilled water medium using zirconia balls in a polyethylene container for 24 h. The slurry was dried and then calcined for 5 h at 1150°C.

The calcined powders were again ground well for 1 h in an agate mortar and then mixed with 4 wt % solution of poly vinyl alcohol (PVA) as the binder. The slurry was dried, ground and pressed into cylindrical disks of diameter 14 mm and height about 7 mm under a pressure of 100 MPa. The pellets were initially preheated at a rate of 5°C/min up to 600°C and soaked for 30 minutes to expel the binder and then fired at a rate of 10°C/min up to the sintering temperature. The samples were sintered in the temperature range between 1200-1280°C for 2 h. The sintered samples were well polished and their bulk densities were calculated by Archimedes method. Structural phases were identified by powder X-Ray diffraction (XRD) technique using CuK α radiation. Scanning electron micrographs were recorded from the surface of sintered and thermally etched samples to analyze the microstructure of the ceramics.

The dielectric properties ϵ_r , Q_u and τ_f of the materials were measured in the microwave frequency range using resonance technique as described in Chapter 2, sections 2.4.2 to 2.4.5.

4.1.3 Results and Discussion

4.1.3.1 Characterization and Microwave Dielectric Properties of BaO-2CeO₂-*n*TiO₂ (*n* = 6.....15) Ceramics

The optimized sintering temperature to get the best density and dielectric properties is 1240°C/2h for BaO-2CeO₂-*n*TiO₂ (*n* = 6....15) ceramics. The XRD patterns of BaO-2CeO₂-*n*TiO₂ (*n* = 6, 8, 10, 12, 15) ceramics recorded using CuK α radiation are shown in Fig. 4.1. XRD studies reveal that these are multiphase compounds containing a mixture of CeO₂ (ICDD Card No. 34-0394), Ba₂Ti₉O₂₀ (ICDD Card No. 35-0051) and TiO₂ (21-1276). As the value of *n* increases the intensity of rutile phase increases. This is clearly evident from the peaks of TiO₂ at 27.6, 36.2 and 54.3 degrees respectively. XRD studies indicate that the expected Ba_{2+n}Ce₂Ti_{5+n}O_{15+3n} is not formed in analogy with Sr_{2+n}Ce₂Ti_{5+n}O_{15+3n}.

The phase diagrams of BaO-RE₂O₃-*n*TiO₂ (RE = La, Nd; *n* = 3, 4, 5) compounds have been studied in detail by many researchers.^{22,23,25} Those reports showed that cerium

would not come under this phase diagram because of the +4 valence. XPS studies by Sreemoolanadhan *et al.*²⁴ showed that Ce exists as a mixture both as Ce^{3+} and Ce^{4+} in $BaO-Ce_2O_3-nTiO_2$ ($n = 3, 4, 5$) ceramics in the 4:6 stoichiometry near the sintering temperature of 1270°C. The SEM micrograph shown in Fig. 4.2 confirms that $BaO-2CeO_2-10TiO_2$ ceramic (sintered at 1240°C/2h) is a mixture of CeO_2 , $Ba_2Ti_9O_{20}$ and TiO_2 .

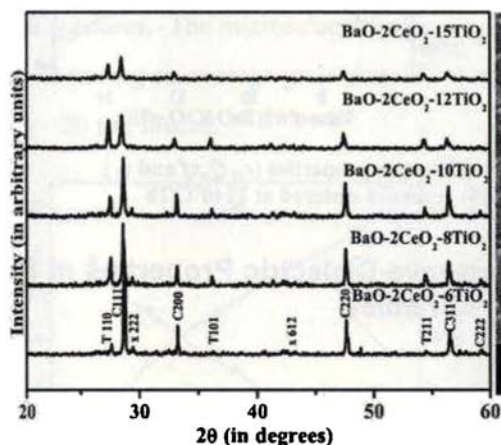


Fig 4.1 XRD patterns of $BaO-2CeO_2-nTiO_2$ ($n = 6, 8, 10, 12, 15$) ceramics. C- CeO_2 , T- TiO_2 , x- $Ba_2Ti_9O_{20}$

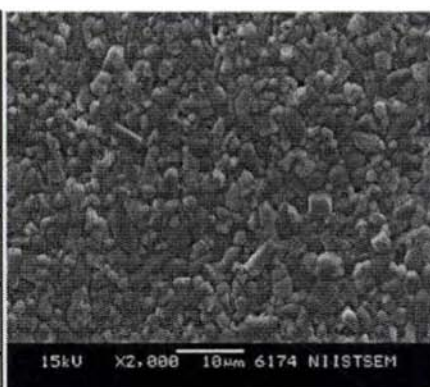


Fig. 4.2 SEM micrograph of $BaO-2CeO_2-10TiO_2$ ceramic sintered at 1240°C/2h

Fig. 4.3 shows the density and microwave dielectric properties of $BaO-2CeO_2-nTiO_2$ ($n = 6 \dots 15$) ceramics sintered at 1240°C/2h. The density is decreasing with the value of n in $BaO-2CeO_2-nTiO_2$ ($n = 6 \dots 15$) ceramics. The relative permittivity of $BaO-2CeO_2-nTiO_2$ ($n = 6 \dots 15$) ceramics varies from 41.5 to 69.9, $Q_w f$ around 25000 GHz and τ_f varies from 40 to 270 ppm/°C. The rutile phase increases with n and hence the τ_f becomes more positive with increase in the value of n in $BaO-2CeO_2-nTiO_2$ ($n = 6 \dots 15$) ceramics (τ_f of TiO_2 is +400 ppm/°C).²⁶ The relative permittivity also shows a linear increase as n increases in $BaO-2CeO_2-nTiO_2$ ($n = 6 \dots 15$) ceramics. This is also due to the increasing amount of high permittivity rutile phase ($\epsilon_r = 105$) with the value of n .²⁶

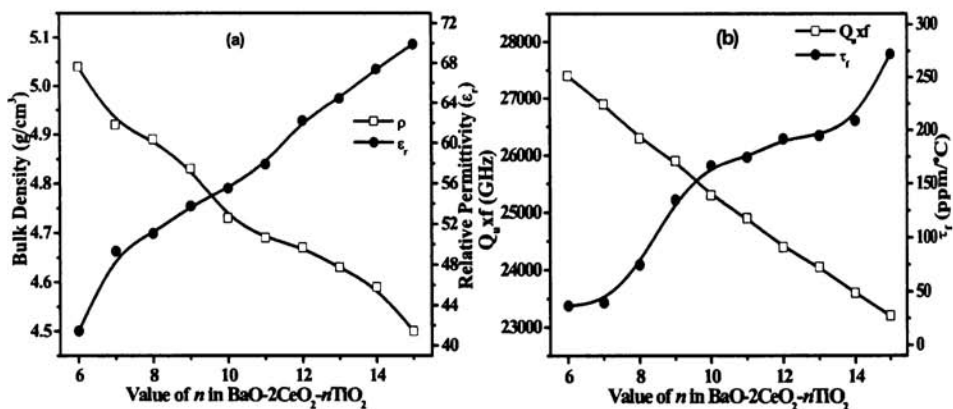


Fig. 4.3 Density (ρ) and microwave dielectric properties (ϵ_r , Q_{uxf} and τ_r) of $\text{BaO-2CeO}_2\text{-}n\text{TiO}_2$ ($n = 6 \dots 15$) ceramics sintered at $1240^\circ\text{C}/2\text{h}$

4.1.3.2 Characterization and Microwave Dielectric Properties of $\text{BaO-pCeO}_2\text{-4TiO}_2$ ($p = 3, \dots, 13$) Ceramics

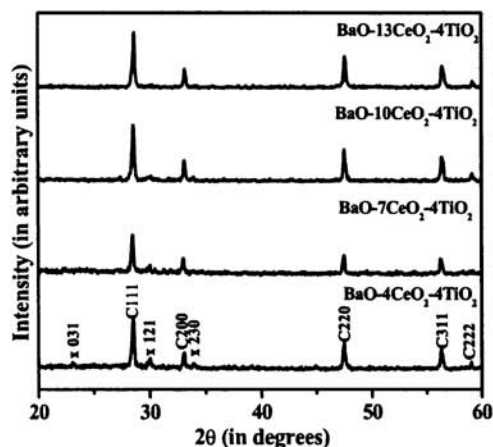


Fig. 4.4 XRD patterns of $\text{BaO-pCeO}_2\text{-4TiO}_2$ ($p = 4, 7, 10, 13$) ceramics, C-CeO_2 , $x\text{-BaTi}_4\text{O}_9$,

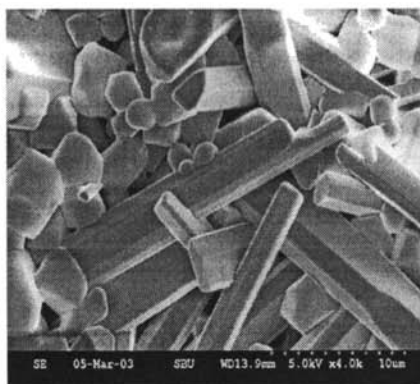


Fig. 4.5 SEM micrograph of $\text{BaO-3CeO}_2\text{-4TiO}_2$ ceramic sintered at $1260^\circ\text{C}/2\text{h}$

The optimized sintering temperature of $\text{BaO-pCeO}_2\text{-4TiO}_2$ ($p = 4, 7, 10, 13$) ceramics is $1260^\circ\text{C}/2\text{h}$ to get the best density and dielectric properties. The XRD patterns of $\text{BaO-pCeO}_2\text{-4TiO}_2$ ($p = 4, 7, 10, 13$) ceramics recorded using $\text{CuK}\alpha$ radiation are

shown in Fig. 4.4. Analysis of the XRD patterns show that the BaO- p CeO₂-4TiO₂ ($p = 4, 7, 10, 13$) ceramics is a mixture of fluorite CeO₂ (JCPDS Card No. 34-0394) and BaTi₄O₉ (JCPDS Card No. 34-0070). As the value of p increases the intensity of CeO₂ peak increases. This can be clearly seen from the XRD peaks of CeO₂ at 28.4, 33.1, 47.5, 56.3 and 59 degrees. Fig. 4.5 shows the SEM micrographs of BaO-3CeO₂-4TiO₂ ceramic sintered at 1260°C/2h. The SEM photograph indicates that the material is sintered into dense ceramics. The microstructure also shows two types of grains - CeO₂ and BaTi₄O₉. CeO₂ is having an average grain size of 2-6 μm and BaTi₄O₉ grains are elongated and are up to ~ 20 μm in size.

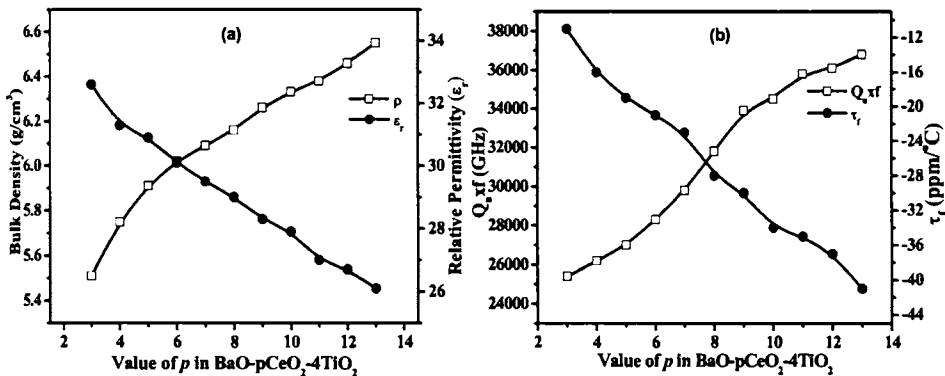


Fig. 4.6 Density (ρ) and microwave dielectric properties (ϵ_r , Q_{xf} and τ_f) of BaO- p CeO₂-4TiO₂ ($p = 3...13$) ceramics sintered at 1260°C/2h

Fig. 4.6 shows the density and microwave dielectric properties of BaO- p CeO₂-4TiO₂ ($p = 3...13$) ceramics sintered at 1260°C/2h. The density increases from 5.50 to 6.45 with the value of p in BaO- p CeO₂-4TiO₂ ($p = 3...13$) ceramics, which is due to the high density of cerium (7.21 g/cm³) compared to that BaTi₄O₉ (4.52 g/cm³). The relative permittivity of BaO- p CeO₂-4TiO₂ ($p = 3...13$) ceramics varies from 32.6 to 26.1, Q_{xf} from 25400 to 36800 GHz and τ_f varies from -11 to -41 ppm/°C. The relative permittivity decreases with the value of p due to the low ϵ_r of CeO₂ ($\epsilon_r = 23$) compared to that of BaTi₄O₉ ($\epsilon_r = 33$). The τ_f becomes more negative with increase in the value of p in BaO- p CeO₂-4TiO₂ ($p = 3...13$) ceramics. This is due to the increased amount of ceria with the value of p (τ_f of CeO₂ is -53 ppm/°C).

4.2 EFFECT OF DOPANTS ON THE MICROWAVE DIELECTRIC PROPERTIES OF BaO-3CeO₂-4TiO₂ CERAMIC

BaO-3CeO₂-4TiO₂ ceramic is selected as a representative material to study the effect of dopants since BaO-3CeO₂-4TiO₂ ceramic has fairly good dielectric properties ($\epsilon_r = 32.6$, $Q_{uxf} = 25400$ GHz (at 4.56 GHz) and $\tau_f = -11$ ppm/^oC) in its intrinsic form itself. The optimized calcination and sintering temperatures of BaO-3CeO₂-4TiO₂ ceramics are 1050^oC/5h and 1260^oC/2h for the best dielectric properties.

4.2.1 Experimental

The BaO-3CeO₂-4TiO₂ ceramic was prepared by solid state reaction method as described in section 4.1.2 of this chapter. The calcined BaO-3CeO₂-4TiO₂ powder was divided into several batches and different weight % of dopants was added to the selected weight of parent material. Different wt% of various high purity dopants such as divalent (MnCO₃, NiO, CuO & Co₃O₄), trivalent (Fe₂O₃, Cr₂O₃, Sb₂O₃, Sm₂O₃, Al₂O₃), tetravalent (ZrO₂, SnO₂, TiO₂), pentavalent (V₂O₅, Ta₂O₅, Nb₂O₅) and hexavalent (WO₃ & MoO₃) (all chemicals were of Aldrich Chemical Company, Milwaukee, USA) were added to calcined powder of the parent materials. It was then mixed well for 1 h in distilled water and dried. The resultant mixture was well ground and mixed with 3 wt% PVA. It was then again dried and cylindrical pellets of diameter 14 mm and height 6-7 mm were formed under a uniaxial pressure of 100 MPa. The green pellets were then sintered in air at 1200-1280^oC/2h. The well polished sintered pellets were then used for characterization as given in section 4.1.2 of this chapter.

4.2.2 Results and Discussion

4.2.2.1 Phase and Microstructural Analysis

X-Ray diffraction patterns of pure and CuO doped BaO-3CeO₂-4TiO₂ ceramic are shown in Fig. 4.7. 1.5 wt % CuO added BaO-3CeO₂-4TiO₂ ceramic has peaks of BaCuO₂ (ICDD Card No. 79-0838) in addition to that of CeO₂ and BaTi₄O₉. In BaO-3CeO₂-4TiO₂ + 2.5 wt % CuO added ceramic, Ba₂CuO₃ phase (ICDD Card No. 80-0425)

is present in addition to BaCuO_2 , CeO_2 and BaTi_4O_9 . Many of the peaks of BaCuO_2 is overlapping with that of BaTi_4O_9 .

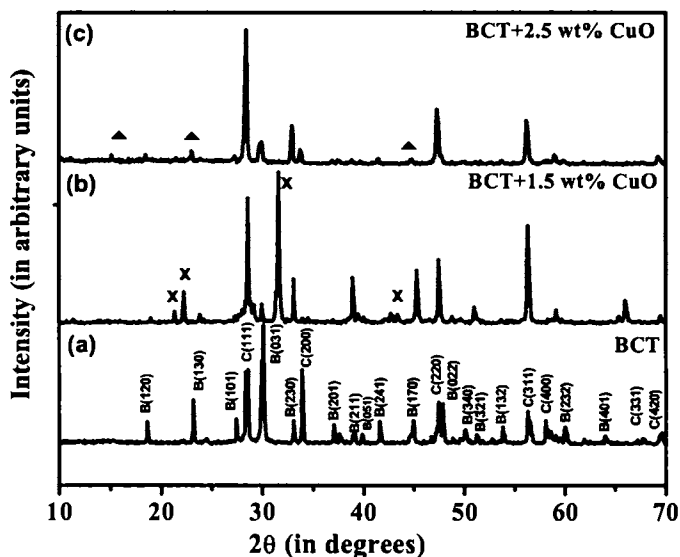


Fig. 4.7 XRD patterns of (a) $\text{BaO-3CeO}_2\text{-4TiO}_2$ (BCT) ceramic sintered at $1260^\circ\text{C}/2\text{h}$ (b) $\text{BCT} + 1.5 \text{ wt}\% \text{ CuO}$ sintered at $1050^\circ\text{C}/2\text{h}$ and (c) $\text{BCT} + 2 \text{ wt}\% \text{ CuO}$ sintered at $1100^\circ\text{C}/2\text{h}$, x- BaCuO_2 , ^- Ba_2CuO_3 , C- CeO_2 , B- BaTi_4O_9

SEM micrographs of 1.5 wt% and 2 wt% CuO doped $\text{BaO-3CeO}_2\text{-4TiO}_2$ ceramic is shown in Fig. 4.8(a) and (b) respectively. The CeO_2 and BaTi_4O_9 grains are of size about 2-5 μm and 10-20 μm in pure $\text{BaO-3CeO}_2\text{-4TiO}_2$ ceramic (see Fig. 4.5). SEM picture confirms the presence of BaCuO_2 phase in 1.5 wt% CuO added $\text{BaO-3CeO}_2\text{-4TiO}_2$ ceramic. The small round shaped grains with size 0.2-0.5 μm are of BaCuO_2 . The size of CeO_2 and BaTi_4O_9 grains is decreased to 1-3 μm and 1-2.5 μm respectively when $\text{BaO-3CeO}_2\text{-4TiO}_2$ ceramic is doped with 1.5 wt% CuO. This is due to the low sintering temperature of CuO doped $\text{BaO-3CeO}_2\text{-4TiO}_2$ ceramic. $\text{BaO-3CeO}_2\text{-4TiO}_2 + 2 \text{ wt}\% \text{ CuO}$ ceramic shows Ba_2CuO_3 phase (marked in Fig. 4.8(b)) of size 0.1-0.3 μm in addition to CeO_2 , BaTi_4O_9 and BaCuO_2 grains. The size of CeO_2 , BaTi_4O_9 and BaCuO_2 grains

increased to 2-3.5 μm , 4-5 μm and 0.5-1 μm . This is due to the higher sintering temperature of $\text{BaO-3CeO}_2\text{-4TiO}_2 + 2 \text{ wt}\% \text{ CuO}$ ceramic (1125°C).

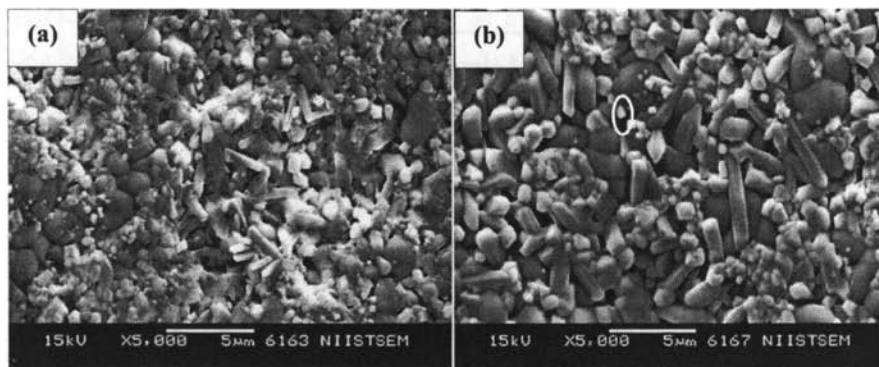


Fig. 4.8 SEM micrographs of (a) $\text{BaO-3CeO}_2\text{-4TiO}_2$ (BCT) + 1.5 wt% CuO sintered at 1050°C/2h and (b) BCT+2 wt% CuO sintered at 1125°C/2h

4.2.2.2 Microwave Dielectric Properties

The microwave dielectric properties of $\text{BaO-3CeO}_2\text{-4TiO}_2$ ceramic and the effect of dopants are given in Table 4.1. The microwave dielectric properties of the sintered $\text{BaO-3CeO}_2\text{-4TiO}_2$ ceramic has a relative permittivity (ϵ_r) of 32.60, quality factor (Q_{ux}) 25400 GHz (at 4.56 GHz) and the temperature variation of resonant frequency (τ_f) -11 ppm/°C. The quality factor is found to increase with the addition of 0.5 wt% WO_3 , MoO_3 , Sb_2O_3 , V_2O_5 , Ta_2O_5 , Nb_2O_5 , Fe_2O_3 , Cr_2O_3 , Al_2O_3 , Co_3O_4 and CuO. Further addition of these dopants decreased the quality factor. There is not much variation in the relative permittivity and τ_f with the addition of dopants.

Fig. 4.9 shows the variation of density, relative permittivity, sintering temperature and Q_{ux} with different wt% of CuO. The density of $\text{BaO-3CeO}_2\text{-4TiO}_2$ ceramic first increases and then starts decreasing with CuO addition. Small amount of CuO (0.5 wt%) enhances the density by liquid phase sintering.²⁷ The sintering temperature decreases from 1260°C and reaches a minimum of 1050°C for 1.5 wt% CuO and then starts

Table 4.1 Microwave dielectric properties of doped BaO-3CeO₂-4TiO₂ dielectric ceramic

Dopant	Dopant Level (wt %)	Density (g/cm ³)	$Q_{\omega} \times f$ (GHz)	ϵ_r	τ_f (ppm/°C)	Sintering Temperature (°C) for 2h
No dopant	-	5.51	25400	32.6	-11	1260
WO ₃	0.5	5.46	27250	32.0	-12	1260
	1	5.47	20450	32.5	-9	1250
MoO ₃	0.5	5.48	26200	32.2	-11	1260
	1	5.43	20400	31.8	-10	1250
Ta ₂ O ₅	0.5	5.54	29750	32.6	-13	1260
	1	5.51	19860	32.8	-10	1260
V ₂ O ₅	0.5	5.51	29200	32.1	-12	1250
	1	5.49	28140	32.0	-12	1250
Sb ₂ O ₃	0.5	5.51	28200	32.1	-13	1260
	1	5.52	20360	32.8	-9	1260
Nb ₂ O ₅	0.5	5.50	31200	32.4	-12	1260
	1	5.50	20720	32.7	-9	1260
TiO ₂	0.5	5.54	24050	32.8	-13	1255
SnO ₂	0.5	5.54	24900	32.8	-13	1255
ZrO ₂	0.5	5.53	24450	32.7	-12	1255
Al ₂ O ₃	0.5	5.50	31100	32.5	-13	1255
	1	5.44	11620	32.4	-9	1255
Fe ₂ O ₃	0.5	5.52	26100	32.6	-12	1255
	1	5.46	17460	32.6	-10	1255
Cr ₂ O ₃	0.5	5.53	27330	32.7	-14	1255
	1	5.51	19100	32.5	-10	1255
Sm ₂ O ₃	0.5	5.53	17220	32.7	-11	1255
Co ₃ O ₄	0.5	5.52	26350	32.6	-12	1255
	1	5.44	9870	21.7	-12	1255
MnCO ₃	0.5	5.51	17970	32.7	-11	1255
NiO	0.5	5.54	23800	32.6	-11	1255
CuO	0.5	5.55	28230	32.8	-12	1175
	1	5.38	29410	31.6	-11	1100
	1.5	5.21	32200	30.0	-12	1050
	2	5.19	25000	29.6	-13	1125

increasing with CuO addition. The decrease in sintering temperature is due to the low melting phase BaCuO₂. The relative permittivity also shows the same trend as that of density. The quality factor increases with the addition of CuO reaches a maximum at 1.5 wt% ($Q_{\omega} \times f = 32200$ GHz) and then starts decreasing. The BaCuO₂ phase formed with the

addition of CuO may be low loss and this enhances the quality factor with CuO doping. The decrease in quality factor of 2 wt% CuO doped BaO-3CeO₂-4TiO₂ may be due to the formation of lossy Ba₂CuO₃ secondary phase. The τ_f remains almost the same with CuO addition (see Table 4.1). ϵ_r and τ_f of 1.5 wt% CuO doped BaO-3CeO₂-4TiO₂ ceramic are 30 and -12 ppm/°C respectively. Thus suitable doping can improve the microwave dielectric properties with a lowering of preparation temperature and BaO-3CeO₂-4TiO₂+ 1.5 wt% CuO can be used as an ideal candidate for LTCC applications using copper electrode.

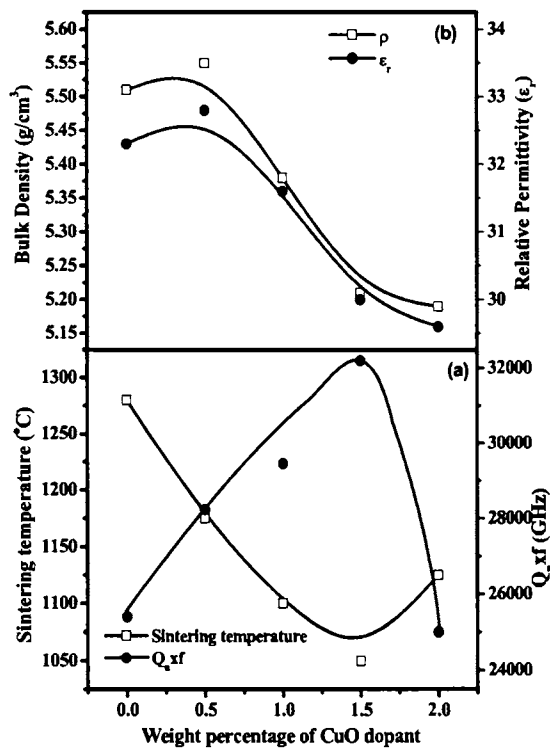


Fig. 4.9 Variation of (a) Sintering temperature and Q^*xf (b) Bulk Density (ρ) and Relative Permittivity of BaO-3CeO₂-4TiO₂ ceramic with CuO dopant

4.3 SYNTHESIS, CHARACTERIZATION AND MICROWAVE DIELECTRIC PROPERTIES OF $(1-x)\text{CeO}_2-x\text{BaTi}_4\text{O}_9$ ($0 \leq x \leq 1$) CERAMICS

4.3.1 Introduction

$\text{BaO-pCeO}_2\text{-4TiO}_2$ ($p = 3, \dots, 13$) ceramics consists of two phases - CeO_2 and BaTi_4O_9 . The present work is a systematic study of $(1-x)\text{CeO}_2-x\text{BaTi}_4\text{O}_9$, to confirm the mixture behaviour of $\text{BaO-pCeO}_2\text{-4TiO}_2$ ($p = 3, \dots, 13$) ceramics with interesting microwave dielectric properties.

The dielectric properties of CeO_2 have been discussed in the section 3.2 of Chapter 3. Temperature stable compositions are obtained when suitable dopants were added to CeO_2 .^{28,29} The studies of O' Bryan *et al.*³⁰ and Masse *et al.*³¹ first demonstrated that barium titanates, including BaTi_4O_9 , could be superior microwave resonator materials. Subsequently, large number of investigations have been carried out in this area.^{32,33} The BaTi_4O_9 phase was first reported by Satton³⁴ and the crystal structure of this phase was identified as orthorhombic. Mhaisalkar *et al.*³⁵ reported that BaTi_4O_9 has ϵ_r of 38, Q_r of 22700 GHz and $\tau_f + 15$ ppm/ $^\circ\text{C}$.^{36,37} Choy and Han³⁸ synthesized BaTi_4O_9 by pechini's method and the sintered ceramics have good dielectric properties. Temperature stable ceramics were obtained with the addition of MnO_2 and CuO dopants.³⁹ The present investigation gives evidence to the mixture nature of $(1-x)\text{CeO}_2-x\text{BaTi}_4\text{O}_9$ ceramics by comparing the experimental results with those obtained by mixture rules.

4.3.2 Experimental

The samples of BaTi_4O_9 ceramics were prepared by the conventional solid-state ceramic route as described in Chapter 2, section 2.1.2. High purity chemicals (Aldrich Chemical Co., Milwaukee, U.S.A) BaCO_3 (99+%) and TiO_2 (99.9%) were used as starting powders. Stoichiometric proportions of the chemicals were weighed and ball milled for 24 hours using zirconia balls in distilled water media. The slurry was dried and then calcined for 5 hours at 1050°C . The finely ground calcined BaTi_4O_9 powder and CeO_2 (IRE, 99.99%) powder were stoichiometrically weighed and mixed in appropriate

proportion to get $(1-x)\text{CeO}_2\text{-}x\text{BaTi}_4\text{O}_9$ ($0 \leq x \leq 1$) ceramics. It was then mixed with 4 wt % PVA, dried and then pressed into disc shaped pucks of about 14 mm diameter and about 7 mm height at a pressure of about 100 MPa using a tungsten carbide die. The green compacts were fired in air at temperatures 1260 -1650°C and the dwell time was 2 hours. The samples were then polished to remove surface irregularities and used for characterization.

4.3.3 Results and Discussion

The synthesizing conditions such as calcination temperature, sintering temperature and their durations are optimized for $(1-x)\text{CeO}_2\text{-}x\text{BaTi}_4\text{O}_9$ ($0 \leq x \leq 1$) dielectric ceramics to obtain the best density and dielectric properties.

4.3.3.1 Phase and Microstructural Analysis

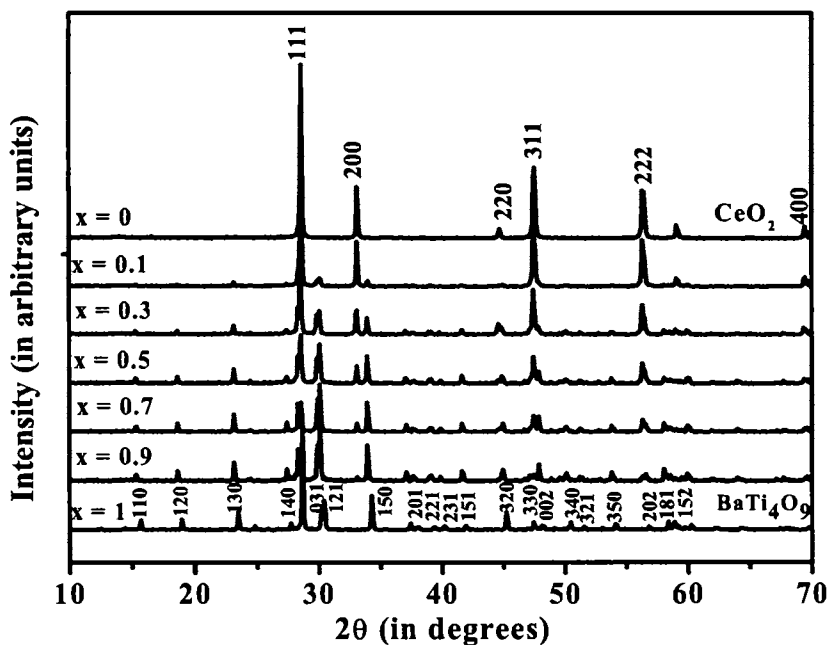


Fig. 4.10 Powder X-ray diffraction patterns of $(1-x)\text{CeO}_2\text{-}x\text{BaTi}_4\text{O}_9$ ceramics

The XRD patterns of $(1-x)\text{CeO}_2-x\text{BaTi}_4\text{O}_9$ ($0 \leq x \leq 1$) ceramics recorded using $\text{CuK}\alpha$ radiation are shown in Fig. 4.10. Analysis of the XRD patterns shows that the ceramics is a mixture of fluorite CeO_2 (ICDD Card No. 34-0394) and BaTi_4O_9 (ICDD Card No. 34-0070). Pure CeO_2 has a cubic fluorite structure with space group $\text{Fm}\bar{3}\text{m}(225)$ and BaTi_4O_9 is orthorhombic with space group $\text{Pnmm}(59)$. The lattice parameter for CeO_2 is $a = 5.4645(5) \text{ \AA}$ and for BaTi_4O_9 are $a = 6.2894(4) \text{ \AA}$, $b = 14.5635(2) \text{ \AA}$, $c = 3.7719(3) \text{ \AA}$. It is evident from Fig. 4.10 that the intensity of XRD peaks corresponding to BaTi_4O_9 in the mixture is increasing with the value of x .

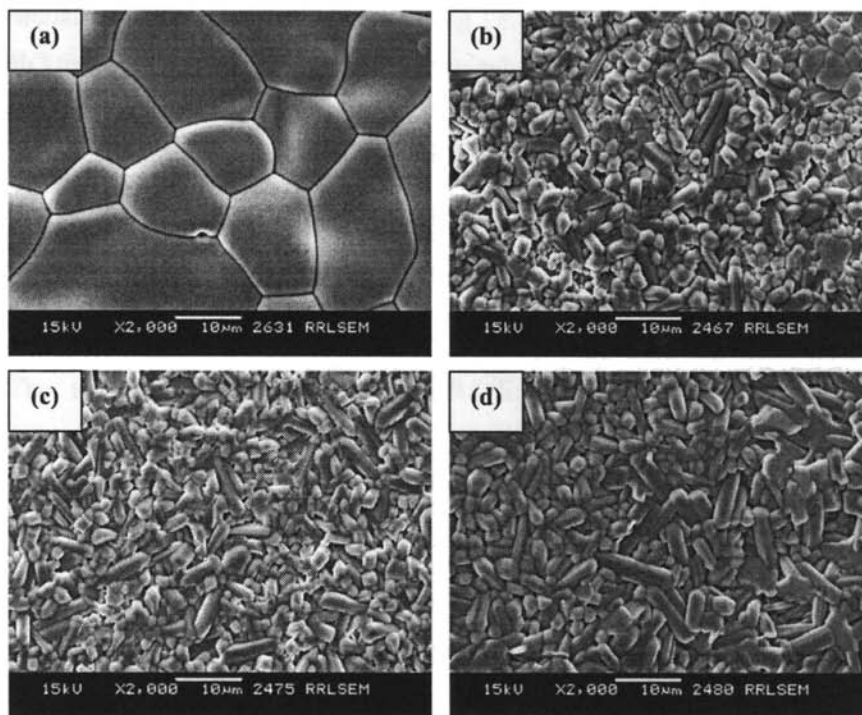


Fig. 4.11 SEM micrographs of (a) CeO_2 sintered at $1650^\circ\text{C}/2\text{h}$ (b) $0.7\text{CeO}_2 - 0.3 \text{BaTi}_4\text{O}_9$, sintered at $1260^\circ\text{C}/2\text{h}$ (c) $0.3\text{CeO}_2 - 0.7 \text{BaTi}_4\text{O}_9$, sintered at $1260^\circ\text{C}/2\text{h}$ (d) BaTi_4O_9 , sintered at $1300^\circ\text{C}/2\text{h}$

Fig. 4.11(a)-(d) shows the scanning electron micrographs of sintered, polished and thermally etched $(1-x)\text{CeO}_2-x\text{BaTi}_4\text{O}_9$ ($x = 0, 0.25, 0.75, 1$) revealing the formation of

dense ceramics. The two end members have distinct microstructures. Pure CeO_2 ($x = 0$) has faceted grains of large size up to $25 \mu\text{m}$ while BaTi_4O_9 ($x = 1$) exhibits elongated grains of about $8\text{-}10 \mu\text{m}$. In the mixture region ($x = 0.5$) a heterogeneous microstructure with both elongated and faceted grains are formed and the grain size of CeO_2 decreased to $2.5\text{-}5 \mu\text{m}$. This decrease in grain size of CeO_2 is due to the lower sintering temperature.

4.3.3.2 Microwave Dielectric Properties

The CeO_2 sintered into 94% of its theoretical density (7.21 g/cm^3) and BaTi_4O_9 up to 93% of its theoretical density (4.52 g/cm^3). Fig. 4.12 shows the variation of bulk density of $(1-x)\text{CeO}_2\text{-}x\text{BaTi}_4\text{O}_9$ as a function of BaTi_4O_9 content. The density decreased with increasing amount of BaTi_4O_9 from 6.78 to 4.23 g/cm^3 . The density of the mixture is calculated according to the equation

$$\rho_{\text{mixture}} = V_1\rho_1 + V_2\rho_2 \quad (4.1)$$

where ρ_{mixture} is the calculated theoretical density of mixtures and ρ_1 and ρ_2 are the densities of CeO_2 and BaTi_4O_9 , respectively. The density of $(1-x)\text{CeO}_2\text{-}x\text{BaTi}_4\text{O}_9$ ($0 \leq x \leq 1$) ceramics calculated by mixture rule is also shown in Fig. 4.12.

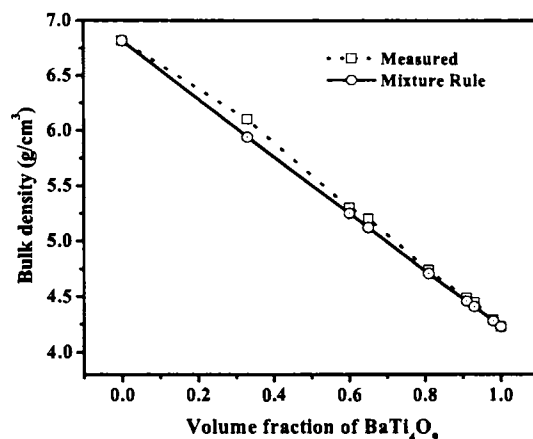


Fig. 4.12 Variation of experimental and calculated density with BaTi_4O_9 in $(1-x)\text{CeO}_2\text{-}x\text{BaTi}_4\text{O}_9$ ceramics

The microwave dielectric properties of $(1-x)\text{CeO}_2\text{-}x\text{BaTi}_4\text{O}_9$ ($0 \leq x \leq 1$) ceramics are shown in Fig. 4.13. Fig. 4.13(a) shows the variation of relative permittivity of CeO_2 with BaTi_4O_9 addition. CeO_2 has a relative permittivity of 23 and that of BaTi_4O_9 is 36.7. The relative permittivity of a mixture can be calculated using the general Maxwell-Wagner formula⁴⁰

$$\epsilon_{\alpha}^r = \sum V_i \epsilon_{ri}^{\alpha} \quad (4.2)$$

where V_i and ϵ_{ri} are the volume fraction and relative relative permittivity of the i^{th} material and α is a constant which depends on the type of mixing rule.

$\alpha = 1$ (serial mixing model)

$\alpha = -1$ (parallel mixing model)

$\alpha = 0$ (logarithmic mixing model)

Using the rule of mixtures, the relative permittivity of the mixture is calculated and is plotted as a function of BaTi_4O_9 , as shown in Fig. 4.13(a). Serial mixing rule fits best with the experimental values compared to parallel and logarithmic ones. The relative permittivity increases with the addition of BaTi_4O_9 , which is expected due to the higher relative permittivity of BaTi_4O_9 .

The temperature variation of resonant frequency, τ_f for experimental and calculated values of $(1-x)\text{CeO}_2\text{-}x\text{BaTi}_4\text{O}_9$ ($0 \leq x \leq 1$) ceramics is plotted in Fig. 4.13(b). The τ_f of the mixture phases can be computed using a general mixture rule⁴¹

$$\tau_{f, \text{mixture}} = V_1 \tau_{f_1} + V_2 \tau_{f_2} \quad (4.3)$$

The τ_f deviates from the mixture rule for values $0.3 < x < 0.7$. The deviation of ϵ_r and τ_f from the predicted mixing relations is due to the dissimilar microstructural shapes of CeO_2 and BaTi_4O_9 in this region.⁴²

The variations of unloaded quality factor of the various mixture phases with increasing BaTi_4O_9 content are plotted in Fig. 4.13(c). The $Q_{ur}xf$ of end member compositions, CeO_2 and BaTi_4O_9 , are 53000 GHz and 19500 GHz respectively. The quality factor shows a sudden drop at $x = 0.1$ and then gradually decreases with increase in BaTi_4O_9 content. The small amount of BaTi_4O_9 may contribute to the significant

decrease in $Q_u xf$ because BaTi_4O_9 possess a lower quality factor as compared to CeO_2 . It must be noted that the microwave quality factor, which depends greatly on the synthesizing conditions, porosity, grain morphology, densification etc., doesn't show any specific relationship with the rule of mixtures.^{43,44,45}

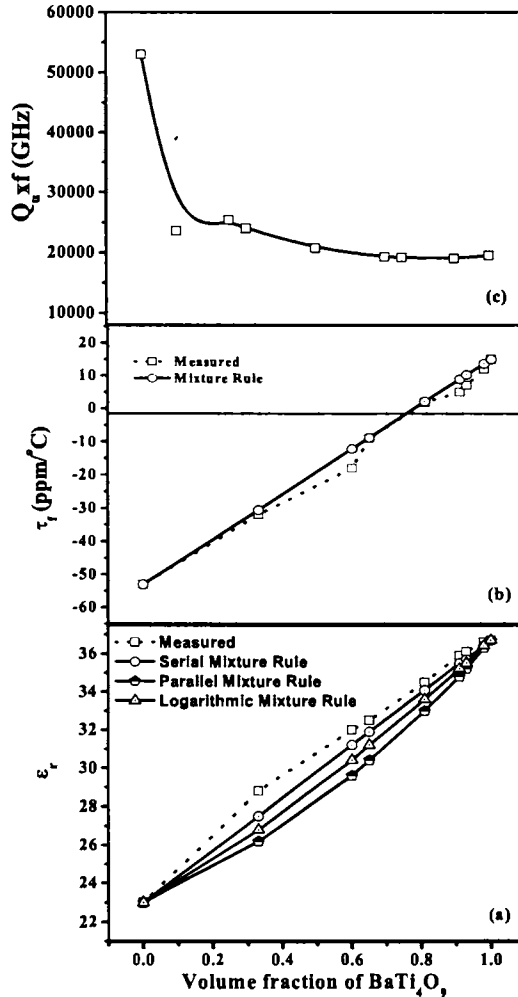


Fig. 4.13 Variation of microwave dielectric properties (ϵ_r , τ_f , $Q_u xf$) of $(1-x)\text{CeO}_2-x\text{BaTi}_4\text{O}_9$ ceramics with BaTi_4O_9

The variation in structure, microstructure and microwave dielectric properties of $(1-x)\text{CeO}_2-x\text{BaTi}_4\text{O}_9$ ($0 \leq x \leq 1$) ceramics confirm the mixture behaviour of $\text{BaO}-p\text{CeO}_2-4\text{TiO}_2$ ($p = 3, \dots, 13$) ceramics.

4.4 LOW TEMPERATURE SINTERING AND MICROWAVE DIELECTRIC PROPERTIES OF 0.5CeO₂-0.5BaTi₄O₉ CERAMICS

4.4.1 Introduction

Low-temperature co-fired ceramics (LTCCs) have been widely investigated because of their extensive applications for the multilayer microwave components which can miniaturize the microwave devices. In the multilayer structures, the sintering temperature of the dielectric materials has to be reduced below 950°C so as to co-fire with highly conductive embedded electrode such as Ag (the melting point of Ag is about 961°C).⁴⁶ But a high sintering temperature of > 1200°C is required to obtain dense 0.5CeO₂-0.5BaTi₄O₉ (CBT) ceramics. The different methods used to reduce the sintering temperature of dielectrics are: (1) addition of low melting point compounds such as Bi₂O₃, B₂O₃, V₂O₅ and glass^{47,48,49} and (2) use of starting materials with smaller particle sizes which can be obtained by chemical processing.⁵⁰

Several studies of the effect of glass on the densification and dielectric properties of BaTi₄O₉ ceramics are reported in the literature.³¹⁻³³ Kim *et al.*⁴⁴ reported BaTi₄O₉ ceramics with good microwave dielectric properties: $\epsilon_r = 33$, $Q_{ur}xf = 27000$ at 9 GHz and $\tau_f = +7$ ppm/°C with zinc borosilicate glass addition by sintering at 900°C/2h. Yang *et al.*⁵¹ investigated lowering the sintering temperature of BaTi₄O₉ ceramics by adding MgO-CaO-Al₂O₃-SiO₂ glass. Wet chemical methods were also used to lower the sintering temperature of BaTi₄O₉ ceramics. Weng *et al.*⁵² produced BaTi₄O₉ ceramics of $\epsilon_r = 35.6$, $Q_{ur}xf = 42600$ at 6 GHz and $\tau_f = +12$ ppm/°C by the polymeric precursor method and sintered at 1250°C. The present section discusses the effect of low melting point compounds, B₂O₃ and CuO on the sintering temperature, microstructure and microwave dielectric properties of temperature stable 0.5CeO₂-0.5BaTi₄O₉ ceramics.

4.4.2 Experimental

The BaTi₄O₉ ceramics were prepared by the conventional solid-state ceramic route as described in Chapter 2, section 2.1.2. It was then mixed with CeO₂ powder in the ratio

1:1. High purity chemicals CeO_2 (IRE, 99.99%), TiO_2 (99.9%) and BaCO_3 (99+%) (Aldrich Chemical Co., Milwaukee, U.S.A) were used as starting powders. To the mixed $0.5\text{CeO}_2\text{-}0.5\text{BaTi}_4\text{O}_9$ ceramic, different amounts of B_2O_3 and CuO was added. To check the reactivity of glass-ceramic with Ag, 20 wt% Ag powder was added. It was then ground well, mixed with 4 wt% PVA, dried and then pressed into cylindrical pucks of 14 mm diameter and 6-7 mm height at a pressure of about 100 MPa. The green compacts were then sintered in air at temperatures in the range $900\text{-}1260^\circ\text{C}/2\text{h}$. The samples were well polished and used for structural, microstructural and microwave dielectric characterization.

4.4.3 Results and Discussion

The synthesizing conditions such as sintering temperature and its duration are optimized for low temperature sintered $0.5\text{CeO}_2\text{-}0.5\text{BaTi}_4\text{O}_9$ dielectric ceramics to obtain the best density and dielectric properties.

4.4.3.1 Phase Analysis

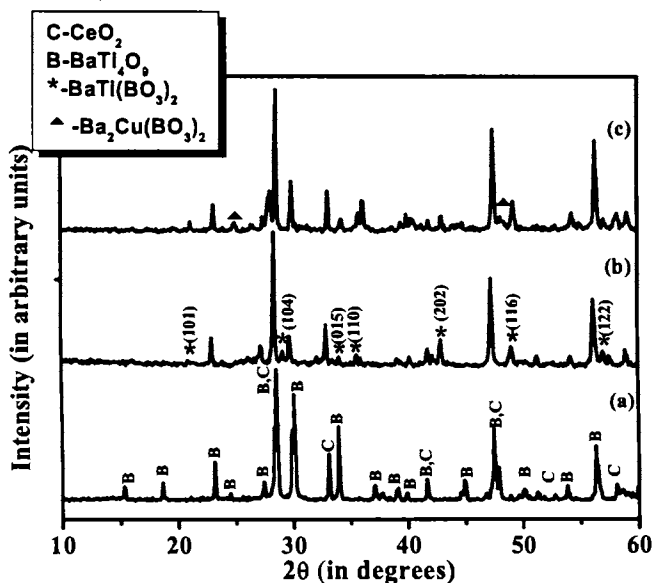


Fig. 4.14 Powder X-ray diffraction patterns of (a) $0.5\text{CeO}_2\text{-}0.5\text{BaTi}_4\text{O}_9$, (b) 12 wt % B_2O_3 added $0.5\text{CeO}_2\text{-}0.5\text{BaTi}_4\text{O}_9$, (c) 12 wt % B_2O_3 + 1 wt % CuO added $0.5\text{CeO}_2\text{-}0.5\text{BaTi}_4\text{O}_9$ ceramic

Fig. 4.14 shows the XRD of CBT ($0.5\text{CeO}_2\text{-}0.5\text{BaTi}_4\text{O}_9$), 12 wt% B_2O_3 added CBT and 12 wt% B_2O_3 + 1 wt% CuO added CBT ceramic. The XRD peaks corresponding to $\text{BaTi}(\text{BO}_3)_2$ [JCPDS Card No. 35-0825] secondary phase are present in addition to the peaks of the main phases CeO_2 and BaTi_4O_9 in 12 wt% B_2O_3 added CBT ceramic. New XRD peaks corresponding to the secondary phases $\text{BaTi}(\text{BO}_3)_2$ and $\text{Ba}_2\text{Cu}(\text{BO}_3)_2$ ⁵³ appeared on the XRD pattern of 12 wt% B_2O_3 + 1 wt% CuO added CBT ceramic (Fig. 4.14 (b) and (c)).

4.4.3.2 Microstructural Analysis

SEM micrograph of pure CBT and 12 wt% B_2O_3 added CBT ceramic sintered at 1025°C is shown in Fig. 4.15(a) and (b). The SEM micrograph of 12 wt% B_2O_3 added CBT reveals that it is a mixture of CeO_2 , BaTi_4O_9 , and $\text{BaTi}(\text{BO}_3)_2$ phases. The uniform grain growth is observed for sample sintered at 1025°C. The effectiveness of sintering aids depends on several factors such as sintering temperature, viscosity, solubility and glass wettability.⁵⁴ The main requirement of liquid phase sintering is that the liquid phase should wet the grains of the ceramics. Generally, the chemical reaction between sintering aids and ceramics can provide the best wetting condition,⁵⁵ however, a chemical reaction results in the formation of the secondary phase. SEM picture of 12 wt% B_2O_3 added CBT ceramic confirms the presence of $\text{BaTi}(\text{BO}_3)_2$ secondary phase.

Figs. 4.15(c) and (d) show the microstructures of 12 wt% B_2O_3 + 1 wt% CuO added CBT ceramic sintered at temperatures 950 and 1000°C respectively. Microstructures show typical characteristics of LTCC, where ceramics are distributed in the matrix of dense glass.⁵⁶ SEM pictures confirm the formation of a low temperature phase $\text{Ba}_2\text{Cu}(\text{BO}_3)_2$ when 1 wt% CuO is added to 12 wt% B_2O_3 added CBT ceramic. The CuO itself cannot considerably decrease the sintering temperature of the B_2O_3 added CBT ceramic.⁵⁷ $\text{Ba}_2\text{Cu}(\text{BO}_3)_2$ phase exists as the liquid phase and assists the sintering of CBT ceramics. $\text{Ba}_2\text{Cu}(\text{BO}_3)_2$ melted during the sintering and aided in the densification of CBT ceramic. The essential element of liquid-phase sintering is the presence of a low-temperature phase that must be able to directly or indirectly accelerate a reaction with the

matrix phase.⁵⁸ The densification of 12 wt% B_2O_3 + 1 wt% CuO added CBT ceramic is maximum at a sintering temperature of 950°C. The increase in sintering temperature enhance the porosity due to the evaporation of liquid phase as illustrated in Fig. 4.15(d), in which these relatively large pores seem to result from the coalescence of originally small pores.⁵⁹ The presence of micropores can also be due to the internal stress associated with the crystallization of high temperature phase as well as due to the coefficient of thermal expansion mismatch among different phases.⁵⁶ The increase in porosity leads to the decrease in density of the sintered body.

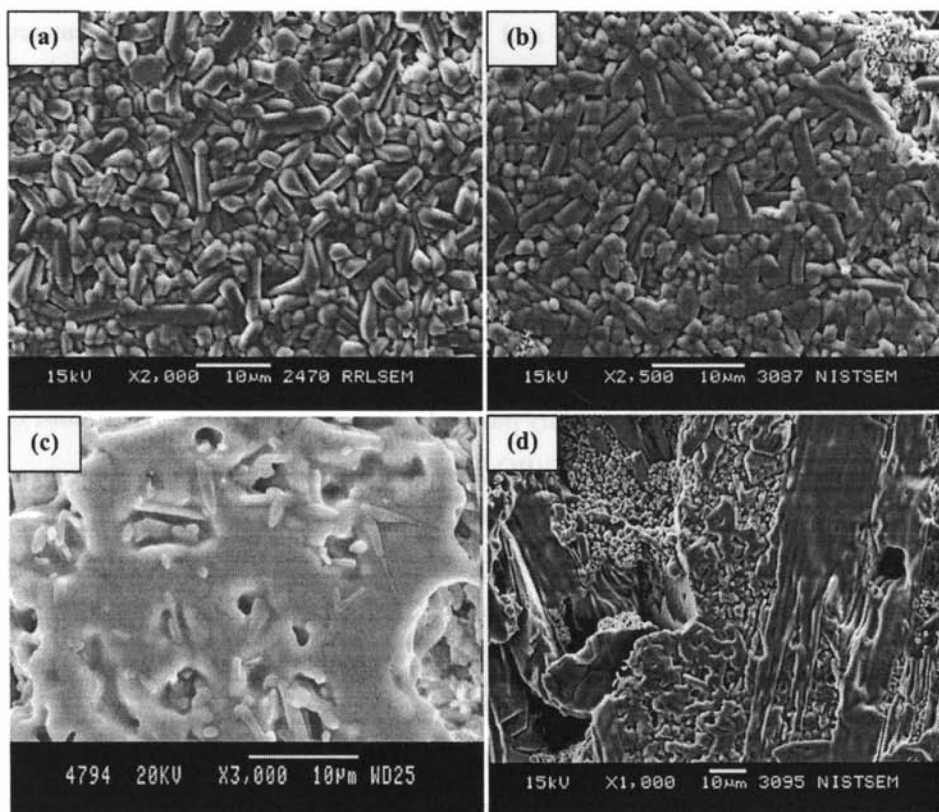


Fig. 4.15 SEM micrographs of (a) $0.5CeO_2 - 0.5BaTi_4O_9$, sintered at 1260°C/2h (b) 12 wt% B_2O_3 added $0.5CeO_2 - 0.5BaTi_4O_9$, ceramic sintered at 1025°C/4h (c) 12 wt% B_2O_3 + 1 wt% CuO added $0.5CeO_2 - 0.5BaTi_4O_9$, ceramic sintered at 950°C/4h (d) 12 wt% B_2O_3 + 1 wt% CuO added $0.5CeO_2 - 0.5BaTi_4O_9$, ceramic sintered at 1000°C/4h

4.4.3.3 Microwave Dielectric Properties

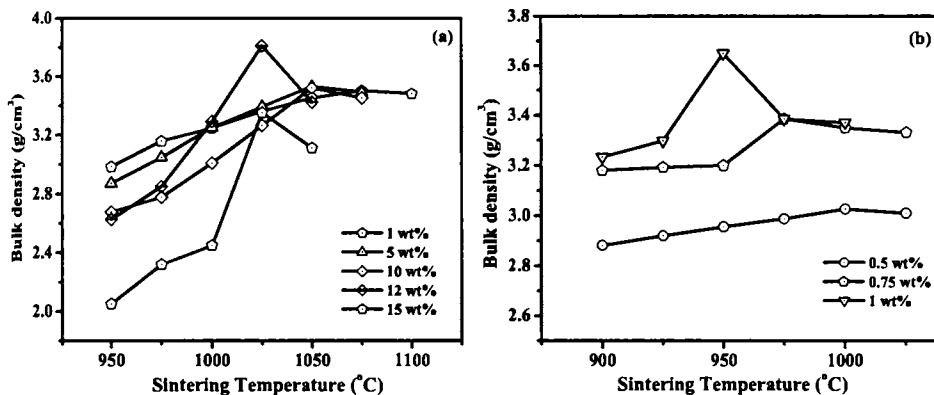


Fig. 4.16 Variation of bulk density (a) with B₂O₃ content in 0.5CeO₂-0.5BaTi₄O₉ ceramic (b) with CuO in 12 wt% B₂O₃ added 0.5CeO₂-0.5BaTi₄O₉ as a function of sintering temperature

The bulk densities of CBT ceramic with various amount of B₂O₃ addition at different sintering temperatures are shown in Fig 4.16(a). Densities of B₂O₃ added ceramic is lower than that of CBT due to the formation of BaTi(BO₃)₂ phase which has a lower density (4.21 g/cm³). For various amount of B₂O₃ addition (1-15 wt%) density increases and then decreases with sintering temperature. For 1, 5, 10, 15 wt% B₂O₃ addition maximum densities obtained are at sintering temperatures 1075, 1050, 1050, 1025°C respectively. Maximum density of 3.81 g/cm³ is obtained for 12 wt% B₂O₃ added CBT ceramic at 1025°C. In order to reduce the sintering temperature further different amount of CuO (0.5, 0.75, 1 wt%) is added to 12 wt% B₂O₃ added CBT and the variation of density with sintering temperature is plotted (Fig. 4.16(b)). The densities of CuO added specimens first increases reaches a maximum value and then decreases. Maximum density of 3.65 g/cm³ is obtained for 1 wt% CuO added sample at a sintering temperature of 950°C.

Fig. 4.17(a) shows the variation of relative permittivity with sintering temperature for different amount of B₂O₃ added CBT samples. The relative permittivity depends on

the density and phase constituents. The ϵ_r of B_2O_3 added samples is very much less than that of pure CBT. This is due to the lower relative permittivity of $BaTi(BO_3)_2$ phase. $BaTi(BO_3)_2$ sintered at $1000^\circ C$ has $\epsilon_r = 11.5$ and $Q_{ur}xf = 23000$ GHz.⁶⁰ With 1-15 wt% B_2O_3 addition, the ϵ_r increases with sintering temperature reaches a maximum value and then decreases. The relationship between relative permittivity and sintering temperature shows the similar trend as the relationship between density and sintering temperature. Maximum ϵ_r (25.2) is obtained for 12 wt% B_2O_3 added CBT sample sintered at $1025^\circ C$. The maximum ϵ_r for 1, 5, 10, 15 wt% B_2O_3 added CBT samples at their optimum sintering temperatures are 20.5, 22.8, 22.9 and 18.6 respectively. The variation of relative permittivity with sintering temperature for CuO added CBT + 12 wt% B_2O_3 ceramic is shown in Fig. 4.17(b). Maximum ϵ_r of 16.2, 17.7 and 20.6 are found for 0.5, 0.75 and 1 wt% CuO added samples when sintered at temperatures 1000, 975 and $950^\circ C$ respectively. The decrease in relative permittivity with sintering temperature is due to the formation of porous microstructure (Fig. 4.15(d)) and low bulk density (Fig. 4.16(b)).

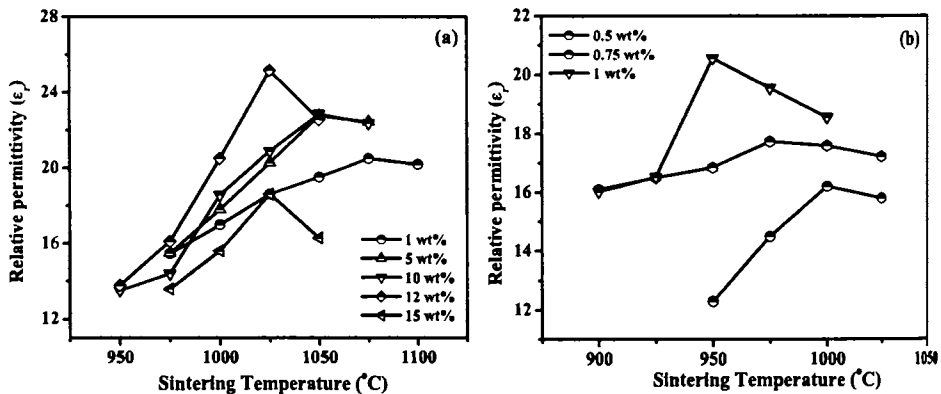


Fig. 4.17 Variation of ϵ_r (a) with B_2O_3 content in $0.5CeO_2-0.5BaTi_4O_9$ ceramic (b) with CuO in 12 wt% B_2O_3 added $0.5CeO_2-0.5BaTi_4O_9$

Fig. 4.18(a) shows the variation of the temperature coefficient of resonant frequency for different weight percentage of B_2O_3 added CBT ceramics. The τ_f increases with the addition of higher amount of B_2O_3 which is due to the formation of $BaTi(BO_3)_2$

phase. The τ_f of 12 wt% B_2O_3 added specimen is found to be 90 ppm/°C. When CuO of varying amount is added to 12 wt% B_2O_3 added CBT ceramic, the rate of increase of τ_f is reduced (Fig. 4.18(b)). The τ_f increases gradually with increasing CuO content. The τ_f of CBT + 12 wt% B_2O_3 + 1 wt% CuO is decreased to 48 ppm/°C from 90 ppm/°C for CBT + 12 wt% B_2O_3 ceramic.

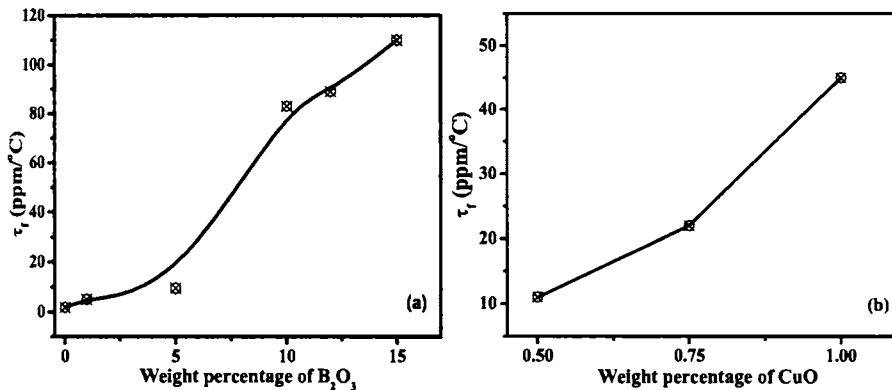


Fig. 4.18 Variation of τ_f (a) with B_2O_3 content in $0.5CeO_2-0.5BaTi_4O_9$ ceramic (b) with CuO in 12 wt% B_2O_3 added $0.5CeO_2-0.5BaTi_4O_9$,

Fig. 4.19(a) shows the variation of Q_{urxf} with sintering temperature for different weight percentages of B_2O_3 added CBT ceramics. The Q_{urxf} values of CBT ceramics are strongly dependent on both sintering temperature and amount of B_2O_3 addition. With increasing sintering temperature, Q_{urxf} value is found to increase to a maximum value and thereafter decreases. A similar result was reported by Zhang *et al.*⁵⁹ when ZnO- B_2O_3 - SiO_2 glass was added to ZnO- TiO_2 ceramics. For CBT ceramics with 1, 5, 10 wt% B_2O_3 addition and sintered at 1075, 1050, 1050°C, maximum Q_{urxf} values are 9500, 16650 and 19100 GHz respectively. With 12 and 15 wt% B_2O_3 addition the sintering temperature is lowered to 1025°C with Q_{urxf} values 20600 and 15200 GHz. The maximum Q_{urxf} at low temperature is due to the increase in density and the maximum Q_{urxf} value corresponds to the maximum density. The Q_{urxf} did not vary much from the pure CBT specimen due to the similar Q_{urxf} of $BaTi(BO_3)_2$ phase ($Q_{urxf} = 23000$ GHz).⁵⁰ The variation of Q_{urxf} with sintering temperature for different weight percentages of CuO to CBT + 12 wt% B_2O_3

ceramic is plotted in Fig. 4.19(b). The $Q_{ur}xf$ value increased with sintering temperature reaches a maximum value and then decreases. The sintering temperatures for 0.5, 0.75, 1 wt% CuO added CBT + 12 wt% B_2O_3 ceramics are 1000, 975, 950°C with maximum $Q_{ur}xf$ values 20620, 18100, 17000 GHz respectively. For LTCC applications, the sintering temperature should be less than the melting point of silver (960°C) and hence 1 wt% CuO added CBT + 12 wt% B_2O_3 ceramic is suitable for LTCC.

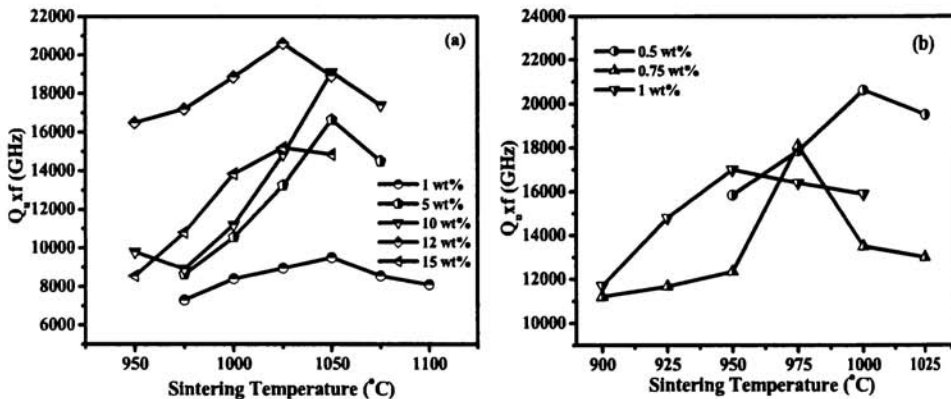


Fig. 4.19 Variation of $Q_{ur}xf$ (a) with B_2O_3 content in $0.5CeO_2-0.5BaTi_4O_9$ ceramic (b) with CuO in 12 wt% B_2O_3 added $0.5CeO_2-0.5BaTi_4O_9$ ceramic

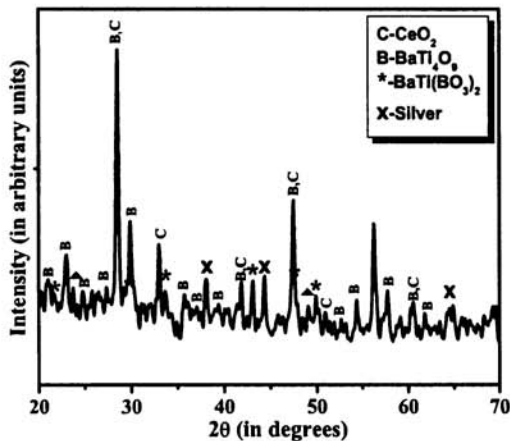


Fig. 4.20 X-ray diffraction patterns of 20 wt% silver added $0.5CeO_2-0.5BaTi_4O_9$ + 12 wt% B_2O_3 + 1 wt% CuO ceramic sintered at 950°C/4h

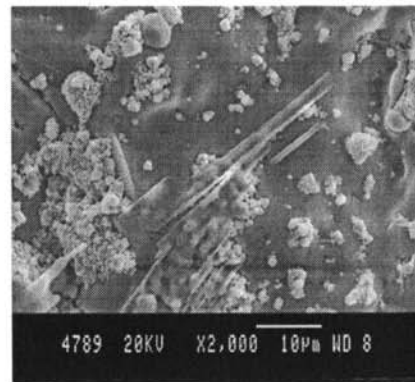


Fig. 4.21 SEM micrograph of 20 wt% silver added $0.5CeO_2-0.5BaTi_4O_9$ + 12 wt% B_2O_3 + 1 wt% CuO ceramic sintered at 950°C/4h

For practical applications, the silver electrode has to be attached to the LTCC. For successful application, the silver electrode material should not react with the ceramic. In order to study the reactivity of silver with the B_2O_3 and CuO added ceramic, 20 wt% Ag is added to CBT + 12 wt% B_2O_3 + 1 wt% CuO ceramic. Figs. 4.20 and 4.21 show the X-ray powder diffraction pattern and the SEM picture of the above silver added composition respectively. The powder diffraction patterns of Ag were indexed based on JCPDS File Card Number 4-783. It is evident from these figures that silver remains unreacted with the ceramic-glass composite, which is one of the requirements of LTCC. Although the BaO-CeO₂-TiO₂ compositions are mixture of CeO₂, TiO₂ and BaTi₄O₉ phases, they have good microwave dielectric properties. It may be noted that many compositions currently in the market are mixtures of a few phases.

4.5 CONCLUSIONS

- BaO-2CeO₂-*n*TiO₂ (*n* = 6...15) ceramics are multiphase compounds containing CeO₂, Ba₂Ti₉O₂₀ and TiO₂ and they do not form the expected Ba_{2+n}Ce₂Ti_{5+n}O_{15+3n} compounds in analogy with Sr_{2+n}Ce₂Ti_{5+n}O_{15+3n}. The ϵ_r increases from 41.5 to 69.9, $Q_{\nu} \times f$ decreases from 27400 to 23200 GHz and τ_f increases from 40 to 272 ppm/°C with the value of *n* in BaO-2CeO₂-*n*TiO₂ (*n* = 6...15) ceramics due to the increasing amount of rutile.
- BaO-*p*CeO₂-4TiO₂ (*p* = 3...13) ceramics consists of CeO₂ and BaTi₄O₉ phases. The ϵ_r decreases from 32.6 to 26.1, $Q_{\nu} \times f$ increases from 25400 to 36800 GHz and τ_f increases to the negative side from -11 to -41 ppm/°C with the value of *p* in BaO-*p*CeO₂-4TiO₂ (*p* = 3...13) ceramics due to the increasing amount of ceria.
- BaO-3CeO₂-4TiO₂ ceramic doped with 1.5 wt% CuO sintered at 1050°C/2h has $\epsilon_r = 30$, $Q_{\nu} \times f = 32200$ GHz and $\tau_f = -12$ ppm/°C and can be used as an ideal candidate for LTCC applications with copper electrode.

- $(1-x)\text{CeO}_2-x\text{BaTi}_4\text{O}_9$ ($0 \leq x \leq 1$) ceramics are prepared by the solid-state ceramic route. X-ray diffraction patterns and SEM analysis indicate that $(1-x)\text{CeO}_2-x\text{BaTi}_4\text{O}_9$ ($0 \leq x \leq 1$) ceramics are of a two phase composite consisting of fluorite CeO_2 and BaTi_4O_9 . The $0.5\text{CeO}_2-0.5\text{BaTi}_4\text{O}_9$ samples sintered at $1260^\circ\text{C}/2\text{h}$ exhibit excellent microwave dielectric properties: $\epsilon_r = 34.5$, $Q_{\mu}xf = 20750$ GHz (at 4.2 GHz) and $\tau_f = 2$ ppm/ $^\circ\text{C}$.
- The density, relative permittivity and temperature coefficient of resonant frequency of mixtures predicted by the appropriate mixing relations agree well with the experimental values for $(1-x)\text{CeO}_2-x\text{BaTi}_4\text{O}_9$ ($0 \leq x \leq 1$) ceramics.
- The addition of B_2O_3 and CuO significantly lowered the sintering temperature of $0.5\text{CeO}_2-0.5\text{BaTi}_4\text{O}_9$ ceramic to 950°C . The $0.5\text{CeO}_2-0.5\text{BaTi}_4\text{O}_9 + 12$ wt% $\text{B}_2\text{O}_3 + 1$ wt% CuO and sintered at 950°C for 4 hours shows $\epsilon_r = 20.6$, $Q_{\mu}xf = 17000$ GHz (at 5.7 GHz) and $\tau_f = 48$ ppm/ $^\circ\text{C}$.
- Silver remains unreacted with the $0.5\text{CeO}_2-0.5\text{BaTi}_4\text{O}_9+12$ wt% B_2O_3+1 wt% CuO composite, which is one of the requirements of LTCC.

The present Chapter discusses the microwave dielectric properties and low temperature sintering of $\text{BaO-CeO}_2\text{-TiO}_2$ ceramics using low melting point compounds. The forthcoming Chapter describes the synthesis, characterization and microwave dielectric properties of two new ceramics based on cerium.

4.6 REFERENCES

- ¹ W. Wersing, *Electronic ceramics*, B. C. H. Steele (Editor), Elsevier, Amsterdam, (1991)
- ² S. J. Fiedziuszko, I. C. Hunter, T. Itoh, Y. Kobayashi, T. Nishikawa, S. N. Stitzer and K. Wakino, *IEEE Trans. Microwave Theory Tech.*, **MTT 50**, 706 (2002).
- ³ K. P. Surendran, M. R. Varma, P. Mohanan and M. T. Sebastian, *J. Mater. Res.*, **17**, 2561 (2002).
- ⁴ P. V. Bijumon, S. Solomon, P. Mohanan and M. T. Sebastian, *J. Mater. Sci. Mater. Electron.*, **14**, 5 (2003).
- ⁵ H. J. Lee, K. S. Hong and S. J. Kim, *Mater. Res. Bull.*, **32**, 847 (1997).
- ⁶ R. Ubic, I. M. Reaney and W. E. Lee, *Int. Mater. Rev.*, **43**, 205 (1993).
- ⁷ C. E. Bamberger, T. J. Haverlock and O. C. Kopp, *J. Am. Ceram. Soc.*, **77**, 1659 (1994).
- ⁸ G. Subodh, J. James, M. T. Sebastian, R. Paniago, A. Dias and R. L. Moreira, *Chem. Mater.*, **19**, 4077 (2007).
- ⁹ K. W. Kirby and B. A. Wechsler, *J. Am. Ceram. Soc.*, **74**, 1841 (1991).
- ¹⁰ D. E. Rase and R. Roy, *J. Am. Ceram. Soc.*, **38**, 102 (1955).
- ¹¹ T. Negas, R. S. Roth, H. S. Parker and D. Minor, *J. Solid State Chem.*, **9**, 297 (1974).
- ¹² Jr. H. M. O'Bryan and Jr. J. Thomas, *J. Am. Ceram. Soc.*, **57**, 450 (1974).
- ¹³ P. Laffez, G. Desgardin and B. Raveau, *J. Mater. Sci.*, **27**, 5229 (1992).
- ¹⁴ H. Ohsato, J. Sugino, A. Komura, S. Nishigaki and T. Okuda, *Jpn. J. Appl. Phys.*, **38**, 5625 (1999).
- ¹⁵ R. Ratheesh, H. Sreemoolanadhan, M. T. Sebastian and P. Mohanan, *Ferroelectrics*, **211**, 1 (1998).
- ¹⁶ S. Solomon, N. Santha, I. N. Jawahar, H. Sreemoolanadhan, M. T. Sebastian and P. Mohanan, *J. Mater. Sci. Mater. Electron.*, **11**, 595 (2000).
- ¹⁷ H. Ohsato, *J. Eur. Ceram. Soc.*, **21**, 2703 (2001).
- ¹⁸ D. Kolar, *Mater. Res. Symp. Proc.*, **453**, 425 (1997).

-
- ¹⁹ J. H. Hwang and Y. H. Han, *Jpn. J. Appl. Phys.*, **39**, 2701 (2000).
- ²⁰ D. Hennings, B. Schreinemacher and H. Schreinemacher, *J. Eur. Ceram. Soc.*, **13**, 81 (1994).
- ²¹ D. Makovec, Z. Samardaija and D. Kolar, *J. Solid State Chem.*, **123**, 30 (1996).
- ²² J. P. Guha and D. Kolar, *J. Am. Ceram. Soc.*, **56**, 5 (1973).
- ²³ C. Hoffmann and R. Waser, *Ferroelectrics*, **201**, 127 (1997).
- ²⁴ H. Sreemoolanadhan, M. T. Sebastian, R. Ratheesh, R. Blachnik, M. Woehlecke, B. Schneider, M. Neumann and P. Mohanan, *J. Solid State Chem.*, **177**, 3995 (2004).
- ²⁵ L. P. Mudrodubova, K. E. Lisker, B. A. Totenberg, T. F. Limar and A. N. Borsch, *Ser. Radiodet. Radiokomp*, **1**, 3 (1982).
- ²⁶ M. T. Sebastian, *Dielectric Materials for Wireless Communication*, Elsevier Science Publishers, Oxford, (2008).
- ²⁷ M. T. Sebastian and H. Jantunen, *Int. Mat. Rev.*, **53**, 57 (2008).
- ²⁸ M. T. Sebastian, N. Santha, P. V. Bijumon, A-K. Axelsson and N. McN. Alford, *J. Eur. Ceram. Soc.*, **24**, 2583 (2004).
- ²⁹ D. H. Kim, S. K. Lim and C. An, *Mater. Lett.*, **52**, 240 (2002).
- ³⁰ Jr. H. M. O'Bryan, Jr. J. Thomas and J. K. Plourde, *J. Am. Ceram. Soc.*, **57**, 450 (1974).
- ³¹ D. J. Masse, R. A. Pucel, D. W. Readey, E. A. Magnire and C. P. Hartig, *Proc. IEEE*, **59**, 1628 (1971).
- ³² D. E. Rase and R. Roy, *J. Am. Ceram. Soc.*, **41**, 102 (1955).
- ³³ T. Negas, G. Yeager, S. Bell, N. Coats and I. Minis, *J. Am. Ceram. Bull.*, **72**, 80 (1993).
- ³⁴ W. O. Satton, *J. Chem. Phys.*, **19**, 33 (1951).
- ³⁵ S. G. Mhaisalkar, D. W. Readey and S. A. Akbar, *J. Am. Ceram. Soc.*, **74**, 1894 (1991).
- ³⁶ D. J. Masse, R. A. Pucel, D. W. Readey, E. A. Magnire and C. P. Hartig, *Proc. IEEE*, **59**, 1628 (1971).
- ³⁷ S. G. Mhaisalkar, W. E. Lee and D. W. Readey, *J. Am. Ceram. Soc.*, **72**, 2154 (1989).
- ³⁸ J. Choy and Y. Han, *J. Am. Ceram. Soc.*, **78**, 1169 (1995).

-
- ³⁹ Y-C Liou, K-H Tseng and T-C Chung, *J. Eur. Ceram. Soc.*, **27**, 3027 (2007).
- ⁴⁰ W. D. Kingery, H. K. Bowen and R. Uhlmann, *Introduction to Ceramics*, 2nd Ed., John Wiley & Sons Ltd., New Jersey, (1976).
- ⁴¹ A. E. Paladino, *J. Am. Ceram. Soc.*, **54**, 168 (1971).
- ⁴² D-W. Kim, H-J. Youn, K. S. Hong and C. K. Kim, *Jpn. J. Appl. Phys.*, **41**, 3812 (2002).
- ⁴³ K. P. Surendran, N. Santha, P. Mohanan and M. T. Sebastian, *Eur. Phys. J. B*, **41**, 301 (2004).
- ⁴⁴ W. S. Kim, T. H. Kim, E. S. Kim and K. H. Yoon, *Jpn. J. App. Phy.*, **37**, 5367 (1998).
- ⁴⁵ P. Liu, E. S. Kim and K. H. Yoon, *Jpn. J. App. Phy.*, **40**, 5769 (2001).
- ⁴⁶ O. Dernovsek, A. Naeini, G. Preu, W. Wersing, M. Eberstein and W. A. Schiller, *J. Eur. Ceram. Soc.*, **21**, 1693 (2001).
- ⁴⁷ H. Kagata, T. Inoue, J. Kato and I. Kameyama, *Jpn. J. Appl. Phys.*, **31**, 3152 (1992).
- ⁴⁸ W. C. Tzou, C. F. Yang, Y. C. Chen and P. S. Cheng, *J. Eur. Ceram. Soc.*, **20**, 991 (2000).
- ⁴⁹ H. T. Kim, S. H. Kim, S. Nahm, J. D. Byun and Y. Kim, *J. Am. Ceram. Soc.*, **82**, 3043 (1999).
- ⁵⁰ Y. Xu, G. Huang and Y. He, *Ceram. Int.*, **31**, 21 (2005).
- ⁵¹ C. F. Yang, *Jpn. J. App. Phy.*, **38**, 3576 (1999).
- ⁵² M. H. Weng, T. J. Liang and C. L. Huang, *J. Eur. Ceram. Soc.*, **22**, 1693 (2002).
- ⁵³ M-H Kim, J-B Lim, J-C Kim, S Nahm, J-H Paik, J-H Kim and K-S Park, *J. Am. Ceram. Soc.*, **89**, 3124 (2006).
- ⁵⁴ W. D. Kingery, *J. Appl. Phys.*, **30**, 301 (1959).
- ⁵⁵ J. H. Jean and S. C. Lin, *J. Am. Ceram. Soc.*, **83**, 1414 (2000).
- ⁵⁶ Y. J. Seo, D. H. Shin and Y. S. Cho, *J. Am. Ceram. Soc.*, **89**, 2352 (2006).
- ⁵⁷ M- H Kim, S. N. Nahm, W-S Lee, M-J Yoo, N-K Kang, H-T Kim and H-J Lee, *Jpn. J. Appl. Phy.*, **44**, 3091 (2005).

-
- ⁵⁸ M. Valant, D. Suvorov, R. C. Pullar, K. Sarma and Mc. N. Alford, *J. Eur. Ceram. Soc.*, **26**, 2777 (2006).
- ⁵⁹ Q. L. Zhang, H. Yang, J. L. Zou and H. P. Wang, *Mater. Lett.*, **59**, 880 (1995).
- ⁶⁰ W. Huang, K. S. Liu, L-W. Chu, G-H. Hsuie and I. N. Lin, *J. Eur. Ceram. Soc.*, **23**, 2559 (2003).

Chapter 5

LOW TEMPERATURE SINTERING AND MICROWAVE DIELECTRIC PROPERTIES OF $\text{Ce}_2(\text{WO}_4)_3$ AND $\text{Ba}_2\text{CeV}_3\text{O}_{11}$ CERAMICS

This chapter reports for the first time the microwave dielectric properties of two new ceramics based on cerium - $\text{Ce}_2(\text{WO}_4)_3$ and $\text{Ba}_2\text{CeV}_3\text{O}_{11}$. These two materials have been synthesized by conventional solid state ceramic route. The influence of glasses such as B_2O_3 , $\text{ZnO-B}_2\text{O}_3$, $\text{BaO-B}_2\text{O}_3\text{-SiO}_2$, $\text{ZnO-B}_2\text{O}_3\text{-SiO}_2$ and $\text{PbO-B}_2\text{O}_3\text{-SiO}_2$ on the sintering temperature and microwave dielectric properties of $\text{Ce}_2(\text{WO}_4)_3$ and $\text{Ba}_2\text{CeV}_3\text{O}_{11}$ ceramics have also been investigated. Addition of small amount of glasses improved the properties of $\text{Ce}_2(\text{WO}_4)_3$ and $\text{Ba}_2\text{CeV}_3\text{O}_{11}$ ceramics. The results of this research established low temperature synthesis of $\text{Ce}_2(\text{WO}_4)_3$ and $\text{Ba}_2\text{CeV}_3\text{O}_{11}$ ceramics with improved microwave dielectric properties for dielectric substrate and possible Low Temperature Cofired Ceramic (LTCC) applications.

5.1 SYNTHESIS, CHARACTERIZATION AND MICROWAVE DIELECTRIC PROPERTIES OF TWO NOVEL DIELECTRIC CERAMICS

5.1.1 Introduction

The developments of microwave dielectric materials for applications in communication systems, such as cellular phones, wireless local area networks, direct broadcasting satellite (DBS) and global positioning systems, have evolved in an unprecedented path for the last decade.^{1,2} An increasing effort has been directed towards attaining the miniaturization of components with the multilayer microwave integrated circuits (MIC), i.e., integration of passive components such as inductors, capacitors, resistors and line resonators into the substrate which carries the integrated circuits.^{3,4} Moreover, the extension of the carrier frequency from industrial, scientific and medical (ISM) bands to the millimeter wave range is expected in the near future as the research on ultrahigh-speed communication systems is currently underway. These substrate materials need to have a low ϵ_r value, in order to minimize the cross-coupling effect with conductors, and a high quality factor (Q_rxf) value to increase their selectivity. A near zero temperature coefficient of resonant frequency is also required in order to ensure the stability of the frequency against temperature changes. Though extensive research has been made on single phase DR materials using cerium, very few reports has been made on its microwave dielectric properties.^{5,6,7} Hence we tried to prepare new single phase cerium compounds having good microwave dielectric properties and low sintering temperature that can be used for Dielectric Resonator and substrate applications

Several researches on compound formation in rare earth tungstates have been reported.^{8,9,10} Mc Carthy *et al.*¹¹ prepared and identified many compounds: $R_2O_3/WO_3 = 3/1$ (La-Lu, Y), $5/2$ (Gd-Ho, Y), $7/4$ (Nd-Lu, Y) and $1/1$ (Nd-Lu, Y) etc. The system based upon Ce_2O_3 is difficult because of the instability of Ce_2O_3 . Yoshimura *et al.*¹² identified the stable phases in the system $Ce_2O_3-WO_3$. The subsolidus phase relation was also discussed for the ternary system $CeO_2-Ce_2O_3-WO_3$. Borchardt¹³ reported that $Ce_2O_3.3WO_3$ was only one compound which was produced by the reaction between CeO_2

and WO_3 in air. The microwave dielectric properties of $\text{CeO}_2\text{-WO}_3\text{-TiO}_2$ ceramics has been reported in section 3.3 of Chapter 3 as $\epsilon_r = 17$, $Q_{\mu}xf = 45550$ GHz in vacuum and $\tau_f = 7$ ppm/ $^{\circ}\text{C}$. The $\text{Ce}_2(\text{WO}_4)_3$ has a monoclinic crystal structure¹², though the microwave dielectric properties of the ceramic have not been reported to date.

A considerable amount of work has been done on the phase formation and structure of $\text{AO-V}_2\text{O}_5$ ($A = \text{Ba, Mg, Zn}$) and Ce-V-O compounds.^{14,15,16,17,18,19} Tsipis *et al.*²⁰ reported the stability and oxygen ion conductivity of zircon-type $\text{Ce}_{1-x}\text{A}_x\text{VO}_4$ ($A = \text{Ca, Sr}$). A comparison between the Raman spectra of $\text{Ce}_{1-x}\text{Ca}_x\text{VO}_{4-0.5x}$ and $\text{Ce}_{1-x}\text{Bi}_x\text{VO}_4$ in which Ca^{2+} and Bi^{3+} are substituted for Ce^{3+} in CeVO_4 has been reported by Hirata *et al.*²¹ In the $\text{AO-V}_2\text{O}_5$ ($A = \text{Ba, Mg, Zn}$) binary system, $\text{A}_3(\text{VO}_4)_2$ ($A = \text{Ba, Mg, Zn}$) are low loss dielectric ceramic materials for microwave communication.^{22,23,24} Chapter 4 discusses the microwave dielectric properties of $\text{BaO-CeO}_2\text{-TiO}_2$ system. Although considerable research has been done on $\text{BaO-V}_2\text{O}_5$ and $\text{CeO}_2\text{-V}_2\text{O}_5$ system, very little attention has been paid on the $\text{BaO-CeO}_2\text{-V}_2\text{O}_5$ system and its dielectric properties.

The present investigation reports for the first time two new dielectric ceramics based on cerium having low relative permittivity - $\text{Ba}_2\text{CeV}_3\text{O}_{11}$ and $\text{Ce}_2(\text{WO}_4)_3$.

5.1.2 Experimental

The $\text{Ce}_2(\text{WO}_4)_3$ and $\text{Ba}_2\text{CeV}_3\text{O}_{11}$ ceramics were prepared by the conventional solid-state ceramic route as described in Chapter 2, section 2.1.2. High purity chemicals CeO_2 (Treibacher, 99.9%), BaCO_3 (Aldrich, 99+%), V_2O_5 (Aldrich, 98+%) and WO_3 (Aldrich, 99+%) were used as the starting powders. Stoichiometric proportions of the chemicals were weighed and ball milled for 24 hours using zirconia balls in distilled water media. The slurry was dried and then calcined at $925^{\circ}\text{C}/8\text{h}$ and $725^{\circ}\text{C}/5\text{h}$ for $\text{Ce}_2(\text{WO}_4)_3$ and $\text{Ba}_2\text{CeV}_3\text{O}_{11}$ ceramics respectively. The calcined powder was then ball milled for 24 hours. The finely ground calcined powder so obtained was then pressed into disc shaped pucks of 20 mm diameter and about 10 mm height at a pressure of about 120 MPa using a WC die. The green compacts were fired at a rate of $5^{\circ}\text{C}/\text{min}$ up to 600°C and soaked at 600°C for 30 minutes to expel the binder. The pellets were sintered

in air at temperatures in the range 950-1050°C and the dwell time was 4 hours. After sintering the samples were allowed to cool down to room temperature at the rate of 3°C/min. The samples were then polished to remove surface irregularities. The Ba₃V₄O₁₃ which formed as a secondary phase along with the Ba₂CeV₃O₁₁ ceramic was also prepared separately using the same method mentioned above at a calcination temperature of 625°C/5h and a sintering temperature of 700°C/4h.

The sintered samples were well polished and their bulk densities were found by Archimedes method. Structural phases were identified by powder X-Ray diffraction (XRD) technique using CuK α radiation. Scanning electron micrographs were recorded from the surface of sintered thermally etched samples to analyze the microstructure of the ceramics. The microwave dielectric properties were measured employing resonance method^{25,26,27} as described in sections 2.4.2 to 2.4.5 of Chapter 2.

5.1.3 Results and Discussion

The synthesizing conditions such as calcination temperature, sintering temperature and their durations are optimized for Ce₂(WO₄)₃ and Ba₂CeV₃O₁₁ ceramics to obtain the best density and dielectric properties. The samples are having good thermal and chemical stability as explained in section 3.3.4 of Chapter 3.

Figs. 5.1(a) and 5.2(a) show the variation of density with calcination temperature for Ce₂(WO₄)₃ and Ba₂CeV₃O₁₁ ceramics respectively. The density increases and reaches a maximum at a calcination temperature of 925 and 725°C and then decreases for Ce₂(WO₄)₃ and Ba₂CeV₃O₁₁ ceramics respectively. The variation of density with sintering temperature for Ce₂(WO₄)₃ and Ba₂CeV₃O₁₁ ceramic are shown in Figs. 5.1(b) and 5.2(b) respectively. The densities range from 4.88 to 5.89 g/cm³ and 4.18 to 4.35 g/cm³ for Ce₂(WO₄)₃ and Ba₂CeV₃O₁₁ ceramic respectively. Maximum density of 5.89 g/cm³ (for Ce₂(WO₄)₃) and 4.35 g/cm³ (for Ba₂CeV₃O₁₁) is obtained at a sintering temperature of 1000 and 1025°C respectively. The density decreased with further increase in sintering temperature. The maximum densification of 87% is obtained for

$\text{Ce}_2(\text{WO}_4)_3$ ceramics at a sintering temperature of 1000°C (theoretical density = 6.77 g/cm^3).²⁸

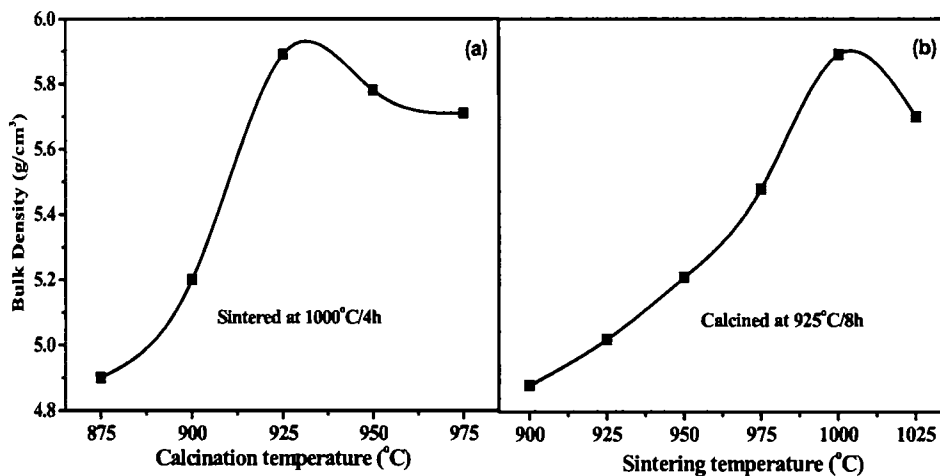


Fig. 5.1 Variation of bulk density of $\text{Ce}_2(\text{WO}_4)_3$ ceramic with (a) Calcination temperature and sintered at 1000°C for 4 hours (b) samples calcined at $925^\circ\text{C}/8\text{h}$ and sintered at different temperatures for 4 hours

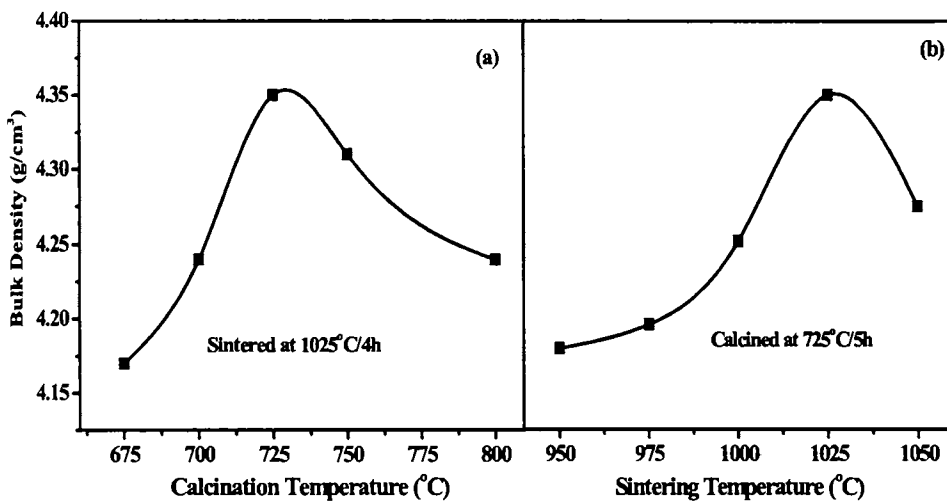


Fig. 5.2 Variation of bulk density of $\text{Ba}_2\text{CeV}_3\text{O}_{11}$ ceramic with (a) Calcination temperature and sintered at 1025°C for 4 hours (b) samples calcined at $725^\circ\text{C}/5\text{h}$ and sintered at different temperatures for 4 hours

5.1.3.1 Phase and Microstructural Analysis

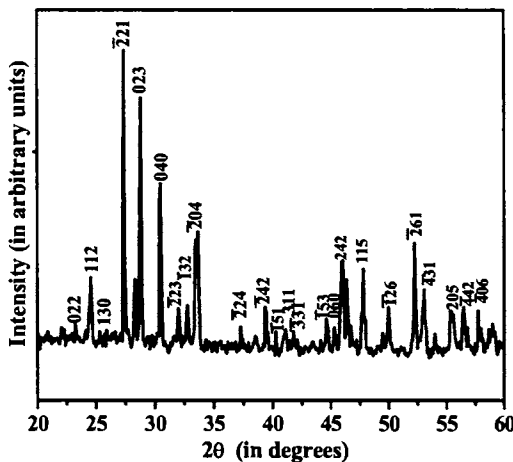


Fig. 5.3 X-Ray diffraction pattern of $\text{Ce}_2(\text{WO}_4)_3$ ceramic sintered at $1000^\circ\text{C}/4\text{h}$

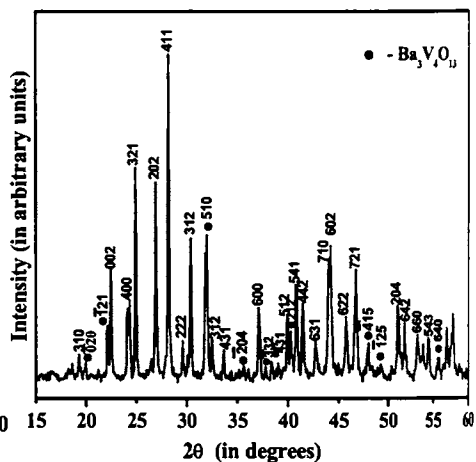


Fig. 5.4 X-Ray diffraction pattern of $\text{Ba}_2\text{CeV}_3\text{O}_{11}$ ceramic sintered $1025^\circ\text{C}/4\text{h}$

Figs. 5.3 and 5.4 show the powder X-ray diffraction pattern of $\text{Ce}_2(\text{WO}_4)_3$ ceramic and $\text{Ba}_2\text{CeV}_3\text{O}_{11}$ ceramic sintered at 1000 and 1025°C for 4 hours respectively. The powder pattern of $\text{Ce}_2(\text{WO}_4)_3$ ceramic exhibits a single phase nature with monoclinic symmetry in agreement with ICDD file card numbers 31-0340. All peaks are indexed and the unit cell parameters are $a = 7.828 \text{ \AA}$, $b = 11.730 \text{ \AA}$ and $c = 11.600 \text{ \AA}$. The XRD profile in Fig. 5.4 shows that $\text{Ba}_2\text{CeV}_3\text{O}_{11}$ ceramic is the main crystalline phase, in association with a second phase $\text{Ba}_3\text{V}_4\text{O}_{13}$ [ICDD File No. 36-1466]. The powder pattern of $\text{Ba}_2\text{CeV}_3\text{O}_{11}$ is compared with the JCPDS file No. 45-0093. $\text{Ba}_3\text{V}_4\text{O}_{13}$ has a space group $12/a$ with lattice parameters $a = 15.07 \text{ \AA}$, $b = 8.941 \text{ \AA}$ and $c = 10.16 \text{ \AA}$.

SEM micrographs of $\text{Ce}_2(\text{WO}_4)_3$ and $\text{Ba}_2\text{CeV}_3\text{O}_{11}$ ceramic sintered at 1000 and 1025°C for 4 hours are shown in Figs. 5.5 and 5.6 respectively. The SEM studies on $\text{Ce}_2(\text{WO}_4)_3$ ceramic show that the densification is poor and the average grain size is about 10-25 μm . Small cracks are seen on the microstructure and this is the cause for poor densification in $\text{Ce}_2(\text{WO}_4)_3$ ceramic. $\text{Ba}_2\text{CeV}_3\text{O}_{11}$ ceramic sintered at 1025°C exhibits dense microstructure and has two types of grains which are identified as of

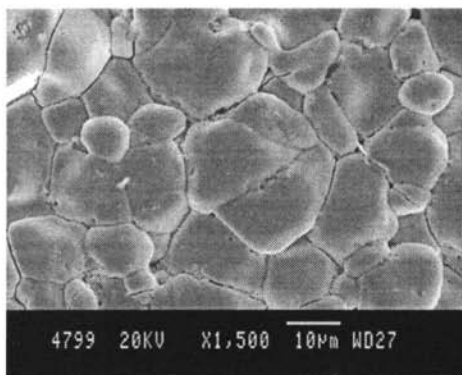


Fig. 5.5 SEM micrographs of $\text{Ce}_2(\text{WO}_4)_3$ ceramic sintered at $1000^\circ\text{C}/4\text{h}$

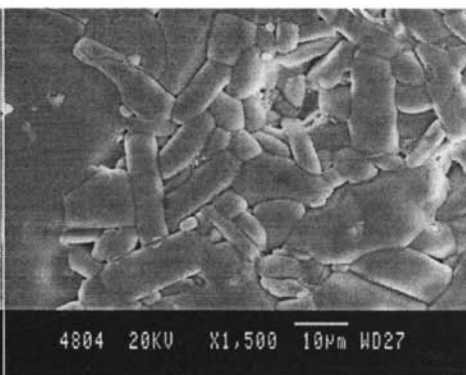


Fig. 5.6 SEM micrographs of $\text{Ba}_2\text{CeV}_3\text{O}_{11}$ ceramic sintered $1025^\circ\text{C}/4\text{h}$

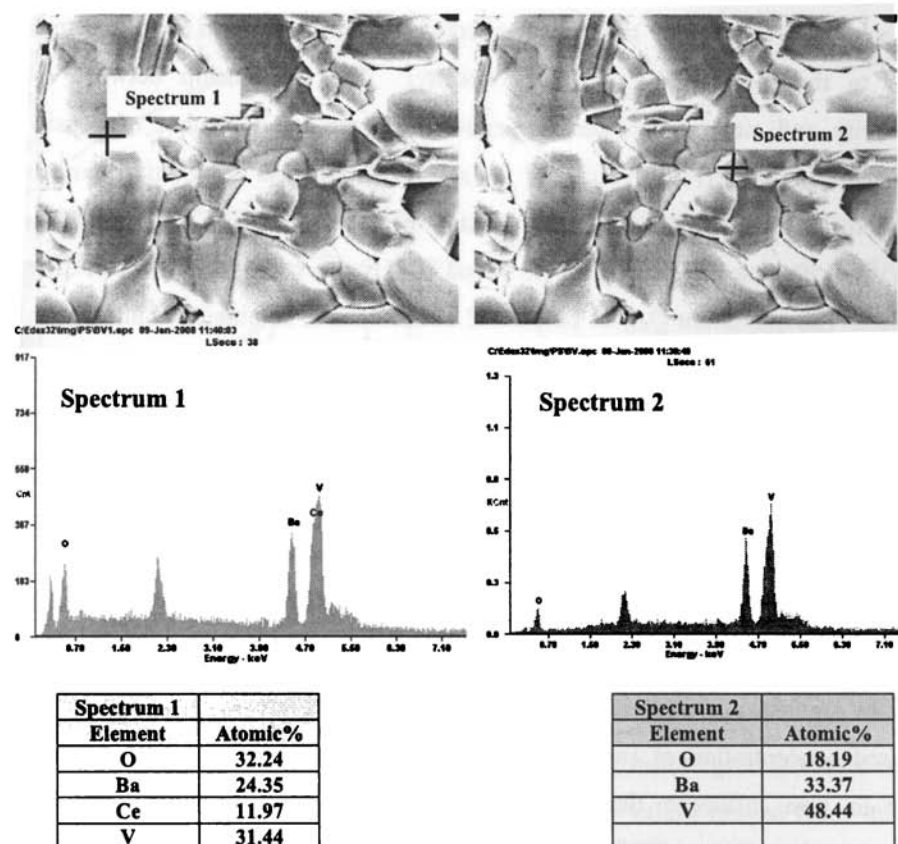


Fig. 5.7 EDXA spectrum of $\text{Ba}_2\text{CeV}_3\text{O}_{11}$ ceramic sintered at $1025^\circ\text{C}/4\text{h}$

$\text{Ba}_2\text{CeV}_3\text{O}_{11}$ and $\text{Ba}_3\text{V}_4\text{O}_{13}$. The average size of $\text{Ba}_2\text{CeV}_3\text{O}_{11}$ grain is about 10-25 μm . Small round shaped grains of size about 2 μm are of $\text{Ba}_3\text{V}_4\text{O}_{13}$. EDXA analysis of $\text{Ba}_2\text{CeV}_3\text{O}_{11}$ ceramic shown in Fig. 5.7 confirms the earlier XRD result on the presence of the secondary phase $\text{Ba}_3\text{V}_4\text{O}_{13}$.

5.1.3.2 Microwave Dielectric Properties

The variation of microwave dielectric properties of $\text{Ce}_2(\text{WO}_4)_3$ and $\text{Ba}_2\text{CeV}_3\text{O}_{11}$ ceramics with sintering temperature are shown in Figs. 5.8 and 5.9 respectively. The relative permittivity increases with sintering temperature up to a maximum of 10.8 (for $\text{Ce}_2(\text{WO}_4)_3$) and 14.9 (for $\text{Ba}_2\text{CeV}_3\text{O}_{11}$ ceramic) at 1000 and 1025°C respectively and decrease on sintering further at higher temperatures. The increase in relative permittivity is due to the increase in percentage density. The relationship between relative permittivity and sintering temperature show the same trend as that of density and sintering temperature (Figs. 5.8(a) and 5.9(a)). With increase in sintering temperature, $Q_{\text{ur}}\text{xf}$ increase, reach a maximum value and thereafter decrease for $\text{Ce}_2(\text{WO}_4)_3$ and $\text{Ba}_2\text{CeV}_3\text{O}_{11}$ ceramics. The variation in ϵ_r and $Q_{\text{ur}}\text{xf}$ is also consistent with that of density variation. The maximum $Q_{\text{ur}}\text{xf}$ of 10500 and 12700 GHz is obtained by sintering at 1000 and 1025°C for $\text{Ce}_2(\text{WO}_4)_3$ and $\text{Ba}_2\text{CeV}_3\text{O}_{11}$ ceramics respectively. At low sintering temperatures, the microwave quality factors are low due to the poor density and when the sintering temperature increase above 1025°C abnormal grain growth occur which degrade the quality factor (Figs. 5.8(b) and 5.9(b)). Inhomogeneous grain growth at high sintering temperatures increases the number of lattice imperfections and the dielectric loss increase.²⁹ The most important grain characteristics for microwave dielectric properties are the average grain size, the grain size distribution, the grain morphology and the grain orientation. Several studies revealed that the presence of a liquid phase, an increased concentration of structural defects, closed porosity etc. cause grain growth which in turn influence the dielectric properties.^{30,31,32} The increase in sintering temperature from 740 to 820°C of $\text{Bi}_{12}\text{TiO}_{20}$ increases the mean grain size from ≈ 10 to ≈ 20 μm .³³ Penn *et al.*³⁰ reported that the dielectric loss of alumina is increased when the

grain size exceeds 3–4 μm . In alumina, when pure powder compacts are sintered, some grains grow extensively to enormous size with pores trapped within those large grains.^{34,35} Molla *et al.*³⁶ reported that moisture trapped in the pores increases the dielectric loss. The microstructures of the ceramic bodies proved that sintering at higher temperatures result in abnormal grain growth and corresponding microcracks occur in a polycrystalline ceramic. The internal stress and crack formation are responsible for the deterioration of dielectric properties when abnormal grain growth occurs.³⁷

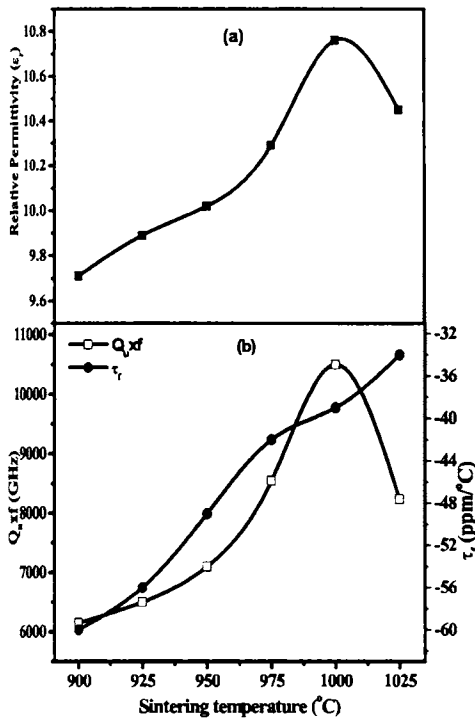


Fig. 5.8 Variation of microwave dielectric properties of $\text{Ce}_2(\text{WO}_4)_3$ ceramic sintered at $1000^\circ\text{C}/4\text{h}$ (a) ϵ_r , (b) Q_wxf and τ_f

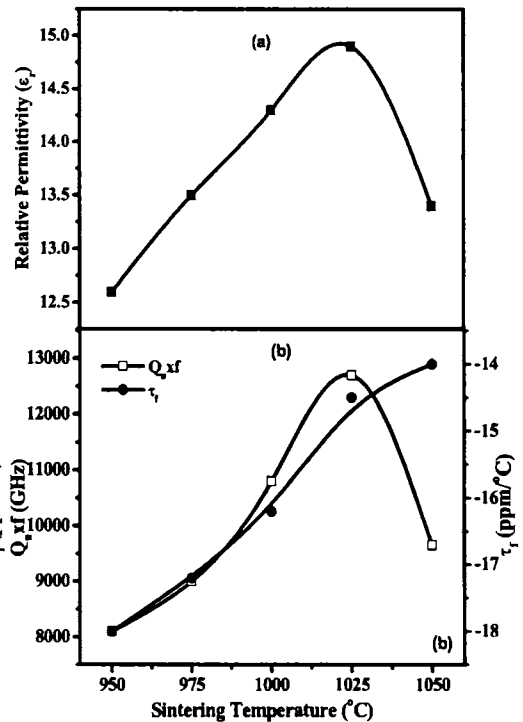


Fig. 5.9 Variation of microwave dielectric properties of $\text{Ba}_2\text{CeV}_3\text{O}_{11}$ ceramic sintered at $1025^\circ\text{C}/4\text{h}$ (a) ϵ_r , (b) Q_wxf and τ_f

Fig. 5.8(b) and 5.9(b) shows the influence of the sintering temperature on the τ_f values of $\text{Ce}_2(\text{WO}_4)_3$ and $\text{Ba}_2\text{CeV}_3\text{O}_{11}$ samples. The τ_f values ranged from -60 to -34 ppm/°C and -18 to -14 ppm/°C for the $\text{Ce}_2(\text{WO}_4)_3$ and $\text{Ba}_2\text{CeV}_3\text{O}_{11}$ samples sintered in the temperature range of 900–1025°C and 950–1050°C respectively.

The $\text{Ba}_3\text{V}_4\text{O}_{13}$ which formed as a secondary phase along with $\text{Ba}_2\text{CeV}_3\text{O}_{11}$ ceramic has been separately prepared as a single phase material. The $\text{Ba}_3\text{V}_4\text{O}_{13}$ sintered at $700^\circ\text{C}/4\text{h}$ has a percentage density of 94, relative permittivity (ϵ_r) = 12, quality factor ($Q_{ur}xf$) = 22500 GHz and $\tau_f = -67 \text{ ppm}^\circ\text{C}$.

5.2 LOW TEMPERATURE SINTERING AND MICROWAVE DIELECTRIC PROPERTIES OF $\text{Ba}_2\text{CeV}_3\text{O}_{11}$ AND $\text{Ce}_2(\text{WO}_4)_3$ CERAMICS

5.2.1 Introduction

In LTCC technology, the dielectrics are needed to cofire with electrode metal such as silver, depending on the requirement of the small delay time of the signal and low power consumption.³⁸ Most of the commercial low loss dielectric materials used for high-frequency applications show high quality factors and relative permittivities, but have a high sintering temperature above 1300°C . The commonly used two methods to reduce the sintering temperature of dielectric ceramics are addition of low melting glasses^{39,40} or low melting point materials^{41,42} and chemical processing.⁴³ The first method has been commonly found effective to decrease the firing temperature in spite of slight degradation of microwave dielectric properties of ceramics. Intensive research is being carried out on liquid phase sintering using low loss glass additives because of the potential they offer and being the least expensive.^{44,45,46,47,48,49} The $\text{Ce}_2(\text{WO}_4)_3$ and $\text{Ba}_2\text{CeV}_3\text{O}_{11}$ ceramics synthesized has high sintering temperature of 1000 and 1025°C respectively and hence they cannot be cofired with silver electrode (melting point is 961°C) for LTCC applications. Hence their sintering temperatures need to be lowered for LTCC applications. This can be achieved by the addition of low melting and low loss glasses.

In this section we report the utilization of small levels of B_2O_3 and borosilicate glasses to the $\text{Ce}_2(\text{WO}_4)_3$ and $\text{Ba}_2\text{CeV}_3\text{O}_{11}$ ceramics in an attempt to prepare ceramics with a sintering temperature less than 950°C that could have potential applications as cofired circuit components.

5.2.2 Experimental

The $\text{Ce}_2(\text{WO}_4)_3$ and $\text{Ba}_2\text{CeV}_3\text{O}_{11}$ ceramics were prepared by the conventional solid-state ceramic route as described in section 5.1.2. The glass powders used in this investigation were B_2O_3 (abbreviated as B), $\text{ZnO-B}_2\text{O}_3$ (ZB), $\text{BaO-B}_2\text{O}_3\text{-SiO}_2$ (BBS), $\text{ZnO-B}_2\text{O}_3\text{-SiO}_2$ (ZBS) and $\text{PbO-B}_2\text{O}_3\text{-SiO}_2$ (PBS). For synthesizing glasses, high purity (Aldrich, 99.9 %) oxides/carbonates were weighed stoichiometrically and mixed for two hours in an agate mortar with pestle using distilled water as the medium. It was then melted in a platinum crucible above their deformation temperature (see Table 1.2 in Chapter 2), quenched and powdered. The calcined $\text{Ce}_2(\text{WO}_4)_3$ and $\text{Ba}_2\text{CeV}_3\text{O}_{11}$ powder is subsequently mixed with different weight percentages of various glasses. The mixed powders were then dried and PVA was added as a binder. It was then ground well and granulated before pressing into pellets. The pellets were sintered at temperatures in the range 850-1000°C in air for 4 hours. The bulk densities of the sintered samples were measured using Archimedes method. The structure of the samples were characterized using X-ray diffraction, microstructure using SEM, elemental analysis using EDXA and microwave characterization using resonance technique described in section 2.4.2 to 2.4.5 in Chapter 2.

5.2.3 Results and Discussion

5.2.3.1 Density and Microstructural Analysis

The samples are having good thermal and chemical stability as explained in section 3.3.4 of Chapter 3. Glasses such as B_2O_3 (B), $\text{ZnO-B}_2\text{O}_3$ (ZB), $\text{BaO-B}_2\text{O}_3\text{-SiO}_2$ (BBS), $\text{ZnO-B}_2\text{O}_3\text{-SiO}_2$ (ZBS) and $\text{PbO-B}_2\text{O}_3\text{-SiO}_2$ (PBS) are added to $\text{Ce}_2(\text{WO}_4)_3$ and $\text{Ba}_2\text{CeV}_3\text{O}_{11}$ to lower the sintering temperature. Figs. 5.10 and 5.11 show the variation of density with sintering temperature of 0.2 wt% different glass added $\text{Ce}_2(\text{WO}_4)_3$ and $\text{Ba}_2\text{CeV}_3\text{O}_{11}$ ceramic respectively. The density of glass fluxed ceramic increases with sintering temperature, reaches a maximum and then decreases. For all glass doped $\text{Ba}_2\text{CeV}_3\text{O}_{11}$ ceramics, density is maximum at 975°C. Maximum density of 6.23 g/cm³

(for $Ce_2(WO_4)_3$) and 4.58 g/cm^3 (for $Ba_2CeV_3O_{11}$) is obtained for 0.2 wt% PBS added $Ba_2CeV_3O_{11}$ ceramic at a sintering temperature of 925 and 975°C respectively. The high density obtained for PBS glass fluxed ceramic is due to the high density of PBS glass compared to other glasses used in the present study. Optimized densities of B, ZB, BBS and ZBS added $Ce_2(WO_4)_3$ and $Ba_2CeV_3O_{11}$ ceramics are 6.08 and 4.36, 5.91 and 4.39, 6.19 and 4.38, 5.90 and 4.37 g/cm^3 respectively. The slight increase in density with the addition of 0.2 wt% B, ZB, BBS, ZBS and PBS glass could be attributed to the liquid phase sintering, which promotes rapid densification.

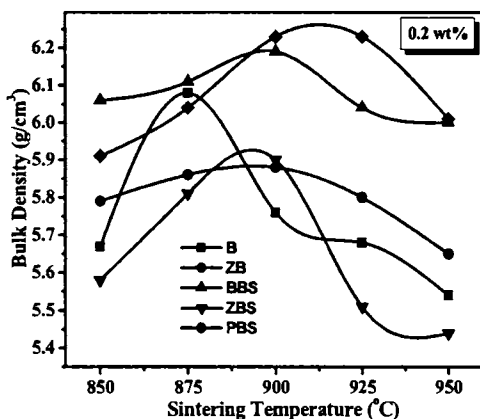


Fig. 5.10 Variation of density of 0.2 wt% of different glass fluxed $Ce_2(WO_4)_3$ ceramic

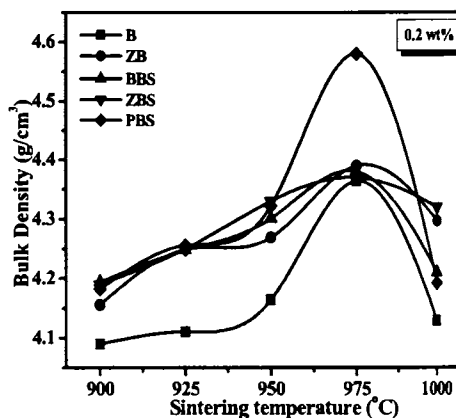


Fig. 5.11 Variation of density of different wt% ZBS glass fluxed $Ba_2CeV_3O_{11}$ ceramic

Fig. 5.12 shows the comparison of densities of 0.2 and 0.5 wt% ZB and ZBS glass fluxed $Ce_2(WO_4)_3$ ceramic. The density is decreased from 5.88 to 5.81 g/cm^3 and 5.90 to 5.85 g/cm^3 with the addition of 0.5 wt% ZB and ZBS glass respectively. The variation of density with different wt% of ZBS glass added $Ba_2CeV_3O_{11}$ ceramic in the temperature range 800 - 1000°C is shown in Fig. 5.13. The decrease in bulk density at higher sintering temperature is probably due to the inhomogeneous evaporation of the liquid phase from grain boundaries causing incomplete wetting.⁵⁰ Addition of 1 wt% ZBS glass to $Ba_2CeV_3O_{11}$ lowers the sintering temperature from 1025°C to 825°C . The addition of further amount of ZBS glass does not lower the sintering temperature. Maximum value

of density (4.46 g/cm^3) is obtained for 1 wt% ZBS glass added $\text{Ba}_2\text{CeV}_3\text{O}_{11}$ ceramic sintered at 825°C .

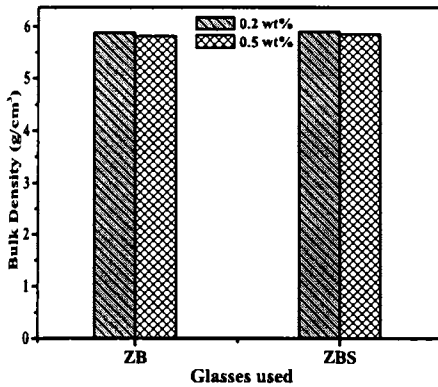


Fig. 5.12 Variation of density of 0.2 and 0.5 wt% ZB and ZBS glass fluxed $\text{Ce}_2(\text{WO}_4)_3$ ceramic

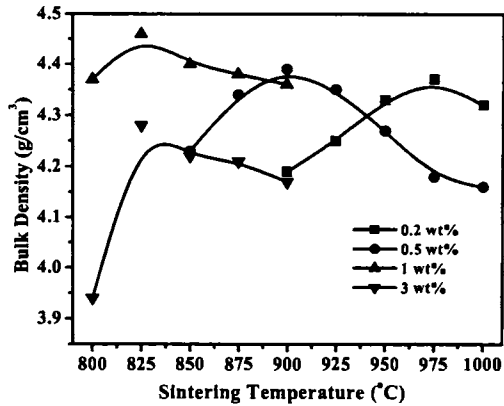


Fig. 5.13 Variation of density of 0.2 wt% of different glass fluxed $\text{Ba}_2\text{CeV}_3\text{O}_{11}$ ceramic

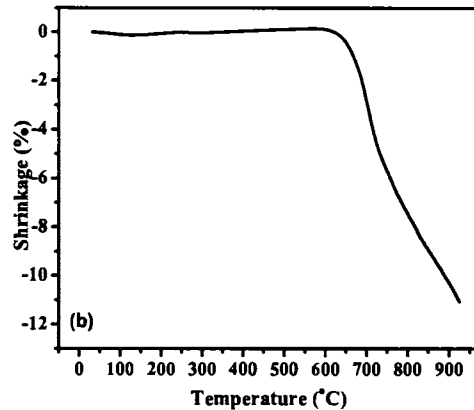
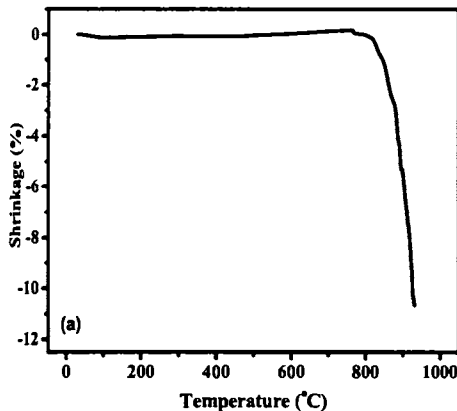


Fig. 5.14 Shrinkage curves of (a) $\text{Ce}_2(\text{WO}_4)_3$ ceramic doped with 0.2 wt% ZBS glass and (b) $\text{Ba}_2\text{CeV}_3\text{O}_{11}$ ceramic doped with 1 wt% ZBS glass

Fig. 5.14 (a) and (b) shows the shrinkage curves of $\text{Ce}_2(\text{WO}_4)_3$ ceramic doped with 0.2 wt% ZBS glass and $\text{Ba}_2\text{CeV}_3\text{O}_{11}$ + 1 wt% ZBS glass respectively. The onset of shrinkage occurs around 800 and 600°C respectively for $\text{Ce}_2(\text{WO}_4)_3$ ceramic doped with 0.2 wt% ZBS glass and $\text{Ba}_2\text{CeV}_3\text{O}_{11}$ doped 1 wt% ZBS glass respectively. The shrinkage is complete only beyond 925°C for both the samples. An 11 % shrinkage at 925°C is

observed for both $\text{Ce}_2(\text{WO}_4)_3$ ceramic + 0.2 wt% ZBS glass and $\text{Ba}_2\text{CeV}_3\text{O}_{11}$ + 1 wt% ZBS glass added ceramic.

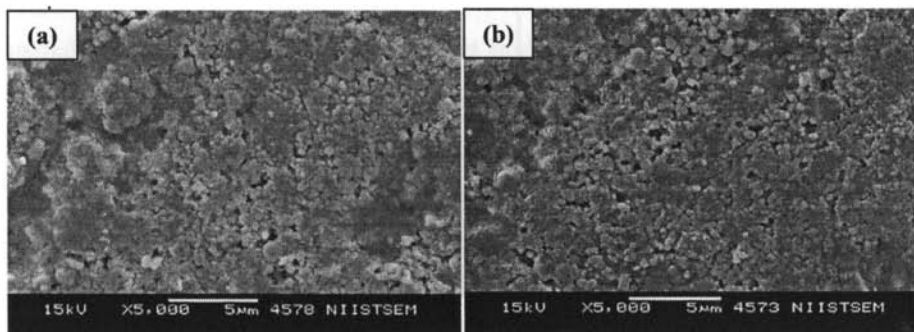


Fig. 5.15 SEM micrograph of 0.2 wt% (a) ZB and (b) ZBS glass fluxed $\text{Ce}_2(\text{WO}_4)_3$ ceramic sintered at 875°C/4h

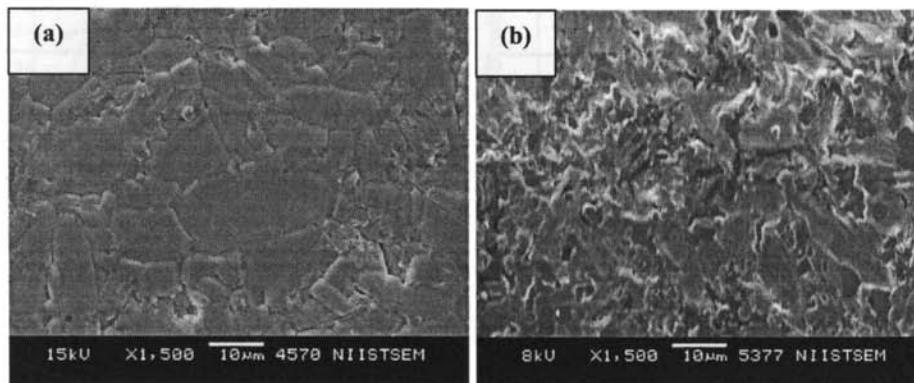


Fig 5.16 SEM micrograph of (a) 1 wt% and (b) 3 wt% ZBS glass fluxed $\text{Ba}_2\text{CeV}_3\text{O}_{11}$ ceramic sintered at 825°C/4h

Fig. 5.15 (a) and (b) shows the microstructures of 0.2 wt% ZB and ZBS glass fluxed $\text{Ce}_2(\text{WO}_4)_3$ ceramic sintered at 875°C/4h. The size of the $\text{Ce}_2(\text{WO}_4)_3$ grain decreased from 10-25 μm to 0.2-1 μm with the addition of 0.2 wt% ZB and ZBS glass (see Fig. 5.5). This decrease in size of the grain is due to the lower sintering temperature and also due to liquid phase sintering.⁵¹ SEM micrographs of 1 wt% and 3 wt% ZBS glass added $\text{Ba}_2\text{CeV}_3\text{O}_{11}$ is shown in Fig. 5.16(a) and (b). Addition of 1 wt% ZBS glass

to $\text{Ba}_2\text{CeV}_3\text{O}_{11}$ improved the sinterability of the ceramic. The presence of dense grains indicate the improvement in the sinterability due to liquid phase sintering in 1 wt% ZBS glass added $\text{Ba}_2\text{CeV}_3\text{O}_{11}$ ceramic. During sintering, low melting glass exists along the dielectric grains in liquid phase. The glass phase assists in the densification of the ceramic through liquid-phase sintering.^{52,53} Addition of 3 wt% ZBS glass increases the porosity⁵⁴ which in turn decreases the density of the ceramic.

5.2.3.2 Microwave Dielectric Properties

The $\text{Ce}_2(\text{WO}_4)_3$ and $\text{Ba}_2\text{CeV}_3\text{O}_{11}$ ceramic sintered at 1000 and 1025°C/4h has a relative permittivity of 10.8 and 14.9 with a quality factor of 10500 and 12700 GHz and temperature coefficient of resonant frequency, -39 and -14 ppm/°C respectively.

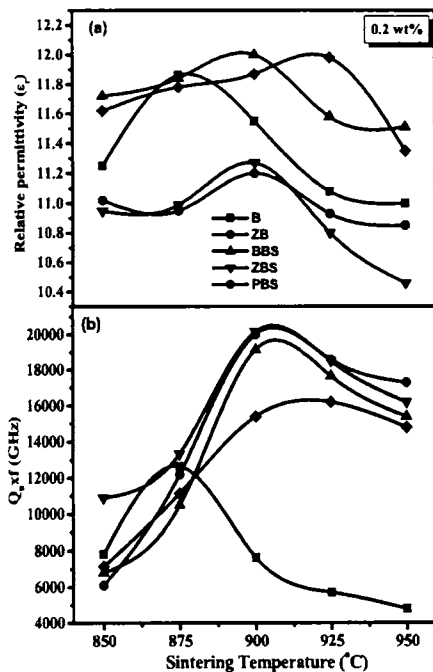


Fig. 5.17 Variation of (a) ϵ_r and (b) Q_{rxf} of 0.2 wt% glass fluxed $\text{Ce}_2(\text{WO}_4)_3$ ceramic

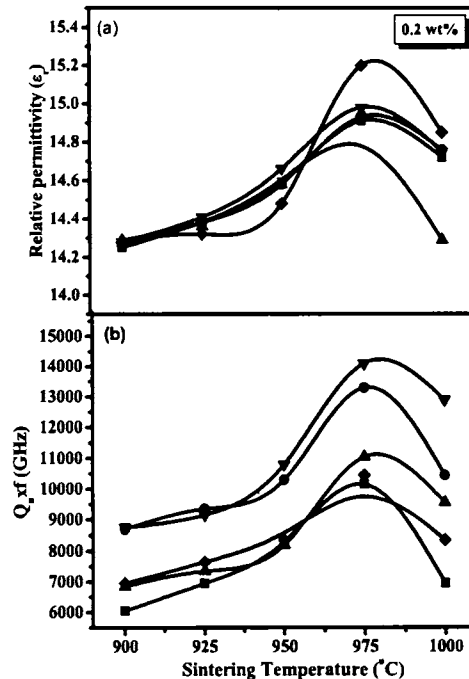


Fig. 5.18 Variation of (a) ϵ_r and (b) Q_{rxf} of 0.2 wt% glass fluxed $\text{Ba}_2\text{CeV}_3\text{O}_{11}$ ceramic

The ϵ_r and Q_{rxf} of 0.2 wt% different glass added $\text{Ce}_2(\text{WO}_4)_3$ and $\text{Ba}_2\text{CeV}_3\text{O}_{11}$ ceramic are investigated by sintering at temperatures in the range 850-1000°C, and the

results are shown in Figs. 5.17 and 5.18 respectively. The ϵ_r increases with sintering temperature reaches a maximum value and then decreases. The relationship between relative permittivity and sintering temperature shows the similar trend as the relationship between density and sintering temperature. Maximum ϵ_r of 11.9, 11.2, 12.0, 11.3 and 11.9 is obtained for 0.2 wt% B, ZB, BBS, ZBS and PBS glass added $Ce_2(WO_4)_3$ ceramic respectively. For 0.2 wt% B, ZB, BBS, ZBS and PBS glass added $Ba_2CeV_3O_{11}$ ceramic maximum ϵ_r obtained is 14.9, 14.9, 15.0, 15.0 and 15.2 respectively. The high ϵ_r of PBS glass added ceramic is due to the high ϵ_r of PBS glass.

The quality factor increases reaches a maximum and then decreases with sintering temperature for $Ce_2(WO_4)_3$ with all glasses. The quality factor increased from 10500 GHz for pure $Ce_2(WO_4)_3$ to 12650, 20000, 20150 and 16200 GHz for 0.2 wt% B, ZB, BBS, ZBS and PBS doped $Ce_2(WO_4)_3$ ceramics respectively (Fig. 5.17(b)). With the addition of 0.2 wt% of glasses to $Ba_2CeV_3O_{11}$ ceramic, the $Q_{ur}xf$ is found to increase for ZB (13300 GHz) and ZBS (14100 GHz) (Fig. 5.18(b)). The quality factor is influenced by many factors including bulk density, grain boundary, secondary phases and other defects as well as anharmonic lattice vibrations.⁵⁵ The best property is obtained for 0.2 wt% ZB and ZBS fluxed with $Ce_2(WO_4)_3$ and 0.2 wt% ZBS doped $Ba_2CeV_3O_{11}$ ceramic. Hence a detailed study on the microwave dielectric properties of different amount of ZB and ZBS glass fluxed $Ce_2(WO_4)_3$ and ZBS glass doped $Ba_2CeV_3O_{11}$ ceramic is carried out.

The variation of ϵ_r and $Q_{ur}xf$ with different wt% ZB and ZBS glass fluxed $Ce_2(WO_4)_3$ and ZBS glass fluxed $Ba_2CeV_3O_{11}$ ceramic are respectively shown in Figs. 5.19 and 5.20. The relative permittivity decreases from 11.2 to 10.9 when 0.5 wt% ZB glass is added and from 11.3 to 10.5 when 0.5 wt% ZBS is added to $Ce_2(WO_4)_3$ ceramic. It is found that relative permittivity shows a close relation with bulk density for different amount of ZBS glass fluxed $Ba_2CeV_3O_{11}$ ceramic. The quality factor decreases with the addition of ZB and ZBS glass in $Ce_2(WO_4)_3$ ceramic. Maximum quality factor of 20200 GHz and relative permittivity 11.3 is obtained for 0.2 wt% ZBS glass fluxed $Ce_2(WO_4)_3$ ceramic sintered at 900°C/4h. Maximum value of density (4.46 g/cm³), relative

permittivity (15.1) and quality factor (20300 GHz) is obtained for 1 wt% ZBS glass doped $\text{Ba}_2\text{CeV}_3\text{O}_{11}$ ceramic sintered at 825°C . Addition of further amount of ZBS glass decreases the quality factor due to the increase in porosity and the fact that glass has a higher dielectric loss.⁵⁶

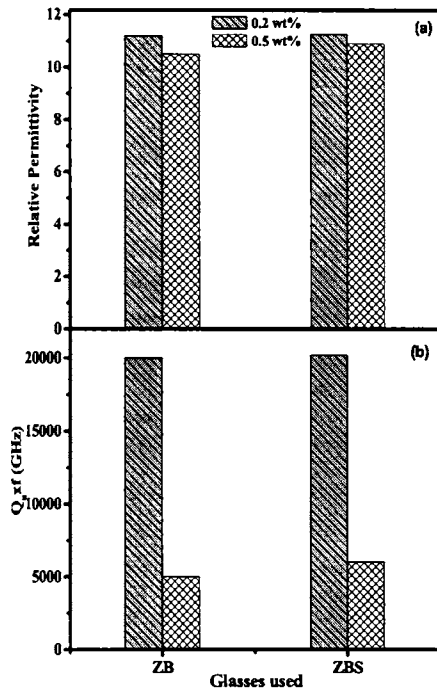


Fig. 5.19 Variation of (a) ϵ_r and (b) $Q_{\omega f}$ of 0.2 and 0.5 wt% ZB and ZBS glass fluxed $\text{Ce}_2(\text{WO}_4)_3$ ceramic

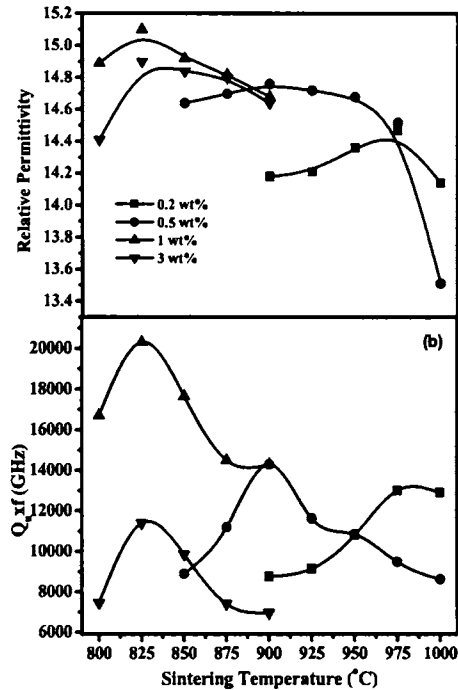


Fig. 5.20 Variation of (a) ϵ_r and (b) $Q_{\omega f}$ of different wt% ZBS glass fluxed $\text{Ba}_2\text{CeV}_3\text{O}_{11}$ ceramic

The variation in τ_f with the addition of different wt% of glass added $\text{Ce}_2(\text{WO}_4)_3$ and $\text{Ba}_2\text{CeV}_3\text{O}_{11}$ ceramics are shown in Figs. 5.21 and 5.22. In glass fluxed $\text{Ce}_2(\text{WO}_4)_3$ ceramics, τ_f is decreased with the addition of 0.2 wt% B, ZB and ZBS glass (τ_f of pure $\text{Ce}_2(\text{WO}_4)_3$ ceramic is $-39 \text{ ppm}/^\circ\text{C}$). The 0.5 wt% addition of ZB and ZBS glass to $\text{Ce}_2(\text{WO}_4)_3$ ceramic decrease the τ_f to -23 and $-25 \text{ ppm}/^\circ\text{C}$ respectively. A decrease in τ_f from -21 to $-12 \text{ ppm}/^\circ\text{C}$ is observed for 0.2 wt% PBS added $\text{Ba}_2\text{CeV}_3\text{O}_{11}$ ceramic. The τ_f of $\text{Ba}_2\text{CeV}_3\text{O}_{11}$ ceramic increases and reaches $-42 \text{ ppm}/^\circ\text{C}$ for 3 wt% ZBS addition.

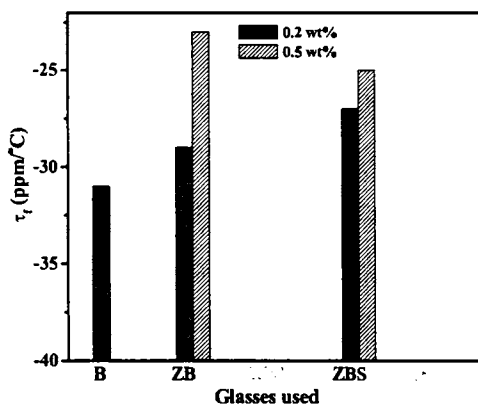


Fig. 5.21 Variation of τ_f with various glass fluxed $\text{Ce}_2(\text{WO}_4)_3$ ceramics

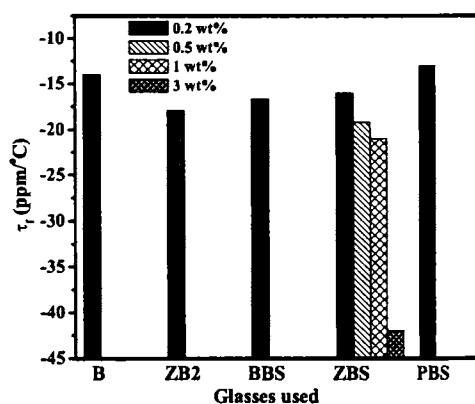


Fig. 5.22 Variation of τ_f with various glass fluxed $\text{Ba}_2\text{CeV}_3\text{O}_{11}$ ceramics

The reasonably good microwave dielectric properties of 0.2 wt% ZBS doped $\text{Ce}_2(\text{WO}_4)_3$ and 1 wt% ZBS glass added $\text{Ba}_2\text{CeV}_3\text{O}_{11}$ show that they can be used as possible candidates for LTCC substrate applications.

5.3 CONCLUSIONS

- Two new microwave dielectric ceramics based on cerium - $\text{Ce}_2(\text{WO}_4)_3$ and $\text{Ba}_2\text{CeV}_3\text{O}_{11}$ have been synthesized and their structure, microstructure and microwave dielectric properties are investigated.
- The $\text{Ce}_2(\text{WO}_4)_3$ sintered at $1000^\circ\text{C}/4\text{h}$ has a relative permittivity of 10.8 with a quality factor of 10500 GHz and temperature coefficient of resonant frequency, $-39 \text{ ppm}^\circ\text{C}$.
- It is difficult to obtain $\text{Ba}_2\text{CeV}_3\text{O}_{11}$ as a single phase material. The XRD pattern, SEM micrograph and EDXA spectrum of $\text{Ba}_2\text{CeV}_3\text{O}_{11}$ reveal that a second phase $\text{Ba}_3\text{V}_4\text{O}_{13}$ is formed along with $\text{Ba}_2\text{CeV}_3\text{O}_{11}$ ceramic.
- The $\text{Ba}_2\text{CeV}_3\text{O}_{11}$ ceramic (contain a small amount of $\text{Ba}_3\text{V}_4\text{O}_{13}$) sintered at $1025^\circ\text{C}/4\text{h}$ has a relative permittivity 14.9 with a quality factor of 12700 GHz and temperature coefficient of resonant frequency, $-14 \text{ ppm}^\circ\text{C}$.

- The $\text{Ba}_3\text{V}_4\text{O}_{13}$ which formed as a secondary phase along with $\text{Ba}_2\text{CeV}_3\text{O}_{11}$ ceramic has a percentage density of 94, relative permittivity 12, quality factor 22500 GHz and $\tau_f = -67$ ppm/ $^\circ\text{C}$ at a sintering temperature of 700 $^\circ\text{C}/4\text{h}$.
- Glasses such as B_2O_3 , $\text{ZnO-B}_2\text{O}_3$, $\text{BaO-B}_2\text{O}_3\text{-SiO}_2$, $\text{ZnO-B}_2\text{O}_3\text{-SiO}_2$ and $\text{PbO-B}_2\text{O}_3\text{-SiO}_2$ are added to $\text{Ce}_2(\text{WO}_4)_3$ and $\text{Ba}_2\text{CeV}_3\text{O}_{11}$ ceramics to lower the sintering temperature.
- The microwave dielectric properties of 0.2 wt% ZBS added $\text{Ce}_2(\text{WO}_4)_3$ ceramic and 1 wt% ZBS glass added $\text{Ba}_2\text{CeV}_3\text{O}_{11}$ ceramic sintered at 900 and 825 $^\circ\text{C}$ are $\epsilon_r = 11.3$ and 15.1, $Q_{uxf} = 20200$ and 20300 GHz and $\tau_f = -27$ and -21 ppm/ $^\circ\text{C}$ respectively.
- The 0.2 wt% ZBS doped $\text{Ce}_2(\text{WO}_4)_3$ and 1 wt% ZBS glass added $\text{Ba}_2\text{CeV}_3\text{O}_{11}$ ceramic can be used as possible candidates for LTCC applications.

This Chapter discusses the synthesis, characterization and microwave dielectric properties of two new compounds based on cerium - $\text{Ce}_2(\text{WO}_4)_3$ and $\text{Ba}_2\text{CeV}_3\text{O}_{11}$. The next Chapter gives the influence of rare earth substitution in Ce site on the structure and microwave dielectric properties of cerium oxide.

5.4 REFERENCES

- ¹ S. Nishigaki, H. Kato, S. Yano and R. Kamimura, *Am. Ceram. Soc. Bull.*, **66**, 1405 (1987).
- ² K. Wakino, K. Minai and H. Tamura, *J. Am. Ceram. Soc.*, **67**, 278 (1984).
- ³ K. Hirade, *Electron. Ceram.*, **23**, 64 (1992).
- ⁴ R. R. Tummala, *J. Am. Ceram. Soc.*, **74**, 895 (1991).
- ⁵ L. Gowri, *M. Sc. Project Report*, Regional Research Laboratory, (2004).
- ⁶ M. T. Sebastian, S. Solomon, R. Ratheesh, J. George and P. Mohanan, *J. Am. Ceram. Soc.*, **84**, 1487 (2001).
- ⁷ G. Subodh, J. James, M. T. Sebastian, R. M. Paniago, A. Dias and R. L. Moreira, *Chem. Mater.*, **19**, 4077 (2007).
- ⁸ M. M. Ivanova, G. M. Balagina and E.YA Rode, *Izv. Akad. Nauk. SSSR, Neorg. Mater.* **6**, 914 (1970).
- ⁹ L. L. Y. Chang, M. G. Scroger and B. Phillips, *J. Inorg. Nucl. Chem.*, **28**, 1179 (1966).
- ¹⁰ L. H. Brixner, A. W. Sleight and C. M. Foris, *J. Solid State Chem.*, **7**, 418 (1973).
- ¹¹ G. J. Mc Carthy, R. D. Fischer, G. G. Johnson Jr., and C. E. Gooden, *NBS Special Publication*, 364, (1972).
- ¹² M. Yoshimura, F. Sibieude, A. Rouanet and M. Foex, *J. Solid State Chem.*, **16**, 219 (1976).
- ¹³ H. J. Borchardt, *J. Chem. Phys.*, **39**, 504 (1963).
- ¹⁴ P. Susse and M. J. Buerger, *Z. Kristallog., Kristallgeometrie, Kristallphys., Kristallchem.*, **131**, 161 (1970).
- ¹⁵ A. A. Fotiev, V. V. Makarov, V. V. Volkov and L. L. Surat, *Russian J. Inorg. Chem.*, **14**, 144 (1969).
- ¹⁶ R. C. Kerby and J. R. Wilson, *Can. J. Chem.*, **51**, 1032 (1973).
- ¹⁷ V. A. Makarov, A. A. Fotiev and L. N. Serebryakova, *Russ. J. Inorg. Chem. [Engl. Transl.]*, **16**, 1515 (1971).
- ¹⁸ K. Iwasaki, H. Takizawa, K. Uheda, T. Endo and M. Shimada, *J. Solid State Chem.*, **158**, 61 (2001).

-
- ¹⁹ R. Cousin, D. Courcot, E. Abi-Aad, S. Capelle, J. P. Amoureux, M. Dourdin, M. Guelton, A. Aboukais, *Colloids and Surf. A: Physiochem. and Eng. Aspects*, **158**, 43 (1999).
- ²⁰ E. V. Tsipis, V. V. Kharton, N. P. Vyshatko, A.L. Shaula and J. R. Frade, *J. Solid State Chem.*, **176**, 47 (2003).
- ²¹ T. Hirata and A. Watanabe, *J. Solid State Chem.*, **158**, 264 (2001).
- ²² R. Umemura, H. Ogawa, A. Yokoi, H. Ohsato and A. Kan, *J. Alloys and Comp.*, **424**, 388 (2006).
- ²³ R. Umemura, H. Ogawa, A. Yokoi, H. Ohsato and A. Kan, *J. Eur. Ceram Soc.*, **25**, 2865 (2005).
- ²⁴ R. Umemura, H. Ogawa and A. Kan, *J. Eur. Ceram Soc.*, **26**, 2063 (2006).
- ²⁵ B. W. Hakki and P. D. Coleman, *IRE Trans. Microwave Theory Tech.*, **MTT-8**, 402 (1960).
- ²⁶ W. E. Courtney, *IEEE Trans. Microwave Theory Tech.*, **MTT-18**, 476 (1970).
- ²⁷ J. Krupka, K. Derzakowski, B. Riddle and J. Baker-Jarvis, *Meas. Sci. Technol.*, **9**, 1751 (1998).
- ²⁸ D. L. Perry and S. L. Philip (Editors), *Handbook of Inorganic Solids*, CRC Press, Boca Raton, New York, (1995).
- ²⁹ C-L Huang and S-S Liu, *Jpn. J. Appl. Phys.*, **46**, 283 (2007).
- ³⁰ S. J. Penn, N. Mc Alford, A. Templeton, X. Wang, M. Xu, M. Reece and K. Schrapel, *J. Am. Ceram. Soc.*, **80**, 1885 (1997).
- ³¹ A. Templeton, X. Wang, S. J. Penn, S. J. Webb, L. F. Cohen and N. Mc Alford, *J. Am. Ceram. Soc.*, **83**, 95 (2000).
- ³² R. Heidiner and S. Nazare, *Powd. Metal. Inter.*, **20**, 30 (1988).
- ³³ M. Valant and D. Suvorov, *Mater. Chem. and Phys.*, **79**, 104 (2003).
- ³⁴ R. L. Coble, U. S. Patent No. 3026210, March 20, 1962.
- ³⁵ W. Jo, D-Y Kim and N-M Hwang, *J. Am. Ceram. Soc.*, **89**, 2369 (2006).
- ³⁶ J. Molla, M. Gonzalez, R. Vila and A. Ibarra, *J. Appl. Phys.*, **85**, 1727 (1999).

-
- ³⁷ I. Yamai, T. Ota, J. Takahashi, *Ceramics Today-Tomorrow's Ceramics*, P. Vincenzini (Editor), Elsevier Science Publishers, New York, (1991).
- ³⁸ A. H. Kumar, P. W. McMillan and R. R. Tummala, U.S. Pat. No. 1 301 324 (1981).
- ³⁹ T. Takada, S. F. Wang, S. Yoshikawa, S. T. Tang and R. E. Newnham, *J. Am. Ceram. Soc.*, **77**, 1909 (1994).
- ⁴⁰ Y-C Lee and W-H Lee, *Jpn. J. Appl. Phys.*, **44**, 1838 (2005).
- ⁴¹ H. Kagata, T. Inoue, J. Kato and I. Kameyama, *Jpn. J. Appl. Phys.*, **31**, 3152 (1992).
- ⁴² H. T. Kim, S. H. Kim, S. Nahm, J. D. Byun and Y. Kim, *J. Am. Ceram. Soc.*, **82**, 3043 (1999)
- ⁴³ V. Tolmer and G. Desgardin, *J. Am. Ceram. Soc.*, **80**, 1981 (1997).
- ⁴⁴ P. V. Bijumon and M. T. Sebastian, *Mater. Sci. and Eng. B*, **123**, 31 (2005).
- ⁴⁵ S. Thomas and M. T. Sebastian, *Mater. Res. Bull.*, **43**, 843 (2008).
- ⁴⁶ K. P. Surendran, P. Mohanan and M. T. Sebastian, *J. Solid State Chem.*, **177**, 4031 (2004).
- ⁴⁷ J-A. Lee, J-H. Lee and J-J. Kim, *J. Eur. Ceram. Soc.*, **26**, 2135 (2006).
- ⁴⁸ T. Takada, S. F. Wang, Shoko Yoshikawa, S-J. Jang and R. E. Newnham, *J. Am. Ceram. Soc.*, **77**, 2485 (1994).
- ⁴⁹ M. T. Sebastian and H. Jantunen, *Int. Mat. Rev.*, **53**, 57 (2008).
- ⁵⁰ S. Y. Chen and Y. J. Lin, *Jpn. J. Appl. Phys.*, **40**, 3305 (2001).
- ⁵¹ D. L. Corker, R. W. Whatmore, E. Ringgaard and W. W. Wolny, *J. Eur. Ceram. Soc.*, **20**, 2039 (2000).
- ⁵² C. R. Chang and J. H. Jean, *J. Am. Ceram. Soc.*, **82**, 1725 (1999).
- ⁵³ H. Jantunen, R. Rautioaho, A. Uusimaki and S. Leppavuori, *J. Eur. Ceram. Soc.*, **20**, 2331 (2000).
- ⁵⁴ Q. L. Zhang, H. Yang, J. L. Zou and H. P. Wang, *Mater. Lett.*, **59**, 880 (1995).
- ⁵⁵ C. F. Yang, *Jpn. J. Appl. Phys.*, **38**, 3576 (1999).
- ⁵⁶ M. T. Sebastian, *Dielectric Materials for Wireless Communication*, Elsevier Science Publishers, Oxford, (2008).

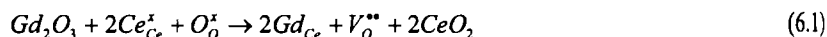
Chapter 6

MICROWAVE DIELECTRIC PROPERTIES OF $Ce_xRE_{1-x}O_{2-\delta}$ (RE = La, Nd, Sm, Eu, Gd, Dy, Er, Tm, Yb and Y), $0 \leq x \leq 1$ CERAMICS

This chapter discusses the solubility of different rare earths and yttrium ions in ceria. Ceramic compositions in $Ce_{1-x}RE_xO_{2-\delta}$ (RE = La, Pr, Nd, Sm, Eu, Gd, Tb, Dy, Er, Tm, Yb and Y), $0 \leq x \leq 1$ have been prepared by solid state ceramic route. The solubility limit of each rare earth ion in ceria has been found out using, XRD, SEM and EDXA analysis. The variation of microwave dielectric properties with the concentration of rare earth in ceria has been measured. Several high Q dielectric resonator materials were identified in $Ce_{1-x}RE_xO_{2-\delta}$ (RE = La, Nd, Sm, Eu, Gd, Dy, Er, Tm, Yb and Y), ceramics for $0 \leq x \leq 1$ which are suitable for applications in telecommunication devices.

6.1 INTRODUCTION

The development of microwave communication technology has been promoted by microwave dielectric ceramics. One of the usual method for developing new high Q or high ϵ_r microwave ceramics is by formation of solid solutions. Ceria (CeO_2) is a fluorite-structured oxide that forms extensive solid solutions with a variety of alien cations. Rare-earth (RE) substituted ceria is an important material in view of applications in oxygen concentration cells and in solid oxide fuel cells.^{1,2} RE substituted ceria is very stable and exhibits high oxygen mobility. Dense ceria based electrolytes are fabricated via solid-state reaction by heat-treating a mixture of the individual component oxide powders at $\sim 1300^\circ\text{C}$ to yield a single phase solid solution and then refiring the solid solution powder at even higher temperatures of $\sim 1700 - 1800^\circ\text{C}$.^{3,4} Common synthesis approach of nano-sized ceria and rare earth substituted ceria at lower preparation temperatures include hydrothermal and solvothermal synthesis,^{5,6,7} sol-gel synthesis,^{8,9} spray pyrolysis etc.¹⁰ When a Ce^{4+} cationic sub lattice gets substituted with a trivalent RE ion, oxygen vacancies are created in anionic sub lattice in order to compensate the effective negative charge produced by the substituent cations.^{1,11} Geometry, structure and properties of these defects resulting from the true atomic substitution not only depend on the crystal structure, electronic charge, ionic radius, electronegativity etc. of the dopant but also on its mol fraction within the host matrix. This, in turn will increase oxygen diffusion within the host lattice and drastically affects oxygen uptake and release by the system.¹² A considerable amount of work has been done on the conductivity of RE doped ceria. The appropriate doping of the cerium oxide lattice with gadolinium oxide as a dopant can be written, in the Kröger-Vink¹³ notation, as



where V_O^{**} represents oxygen vacancy. These oxygen vacancies promote the oxygen-ion migration that is characteristic of substituted ceria. It is also known that a high concentration of oxygen vacancies eventually decreases the conductivity, and increases the activation energy.¹⁴

The electrical conductivity of ceria has been extensively investigated with respect to different ions (Ca^{2+} , Y^{3+} , La^{3+} , Gd^{3+} , Sc^{3+} , Sr^{2+} , Sm^{3+})^{15,16,17} and substituent concentration.^{18,19} The ionic conductivity of ceria resulting from oxygen vacancies depends on the substituents and their amount.^{20,21,22} An increase in the amount of substituent compounds tends to form a second phase due to the solubility limit and this reduces the conductivity.²³ The critical substituent concentration to achieve the total conductivity was reported to be approximately 20 mol%, which was due to the formation of microdomains.²⁴ Balazs *et al.*²⁵ reported that the addition of 10 mol% substituents did not appear to affect the sintering properties with the exception of some rare earths. They also reported that the ionic radius of the substituent did not affect the conductivity of ceria. Of the all RE_2O_3 substituents, Sm_2O_3 and Gd_2O_3 substituted ceria was found to have the highest electrical conductivity at a fixed substitution level, since Sm_2O_3 and Gd_2O_3 doping induces the least distortion of the parent lattice.^{6,26,27} The conductivity values varies with the amount of rare earth though there is a contradiction among the literature reports regarding the exact composition having highest conductivity.^{28,29,30} Steele³⁰ reported that the ionic conductivity at 500°C of $\text{Ce}_{0.9}\text{Gd}_{0.1}\text{O}_{1.95}$ was higher than that of $\text{Ce}_{0.887}\text{Y}_{0.113}\text{O}_{1.9435}$, $\text{Ce}_{0.8}\text{Gd}_{0.2}\text{O}_{1.9}$ and $\text{Ce}_{0.9}\text{Sm}_{0.1}\text{O}_{1.95}$ respectively. Longo *et al.*³¹ reported that yttria is the most soluble rare earth oxide in ceria lattice with excellent ionic conductivity. Comprehensive studies on Y_2O_3 -substituted CeO_2 have shown its conductivity varied substantially with the substituent concentration (0.05-10 mol% Y_2O_3).^{17,25} Wang *et al.*¹⁷ showed that the change of the lattice conductivity with substituent concentration corresponds to the change in the activation energy of oxygen vacancy diffusion. The substitution of cerium oxide in the series $\text{Ce}_{1-x}\text{RE}_x\text{O}_{2-x/2}$ ($\text{RE} = \text{lanthanides}^{3+}$ or Y^{3+} , $x = 0.1, 0.2, 0.3$) produces its characteristic high oxygen-ion mobility³² and exhibits electronic or mixed ionic-electronic conduction in reducing atmospheres.^{33,34} Electronic conduction can also appear when the grain size of pure ceria is below 100 nm.^{35,36,37}

The electrical properties of heavily substituted ceria with nano-sized grains are currently under investigation in different laboratories around the world. The boundary

between ionic and electronic regime will be observed at a grain size of 20 nm at 500°C.³⁸ There are recent claims that the ionic conductivity of $Ce_{0.8}Ln_{0.2}O_{2-\delta}$ (RE = Sm, Y) increases with decreasing grain size at temperatures below 200°C.^{39,40} A clear dependence of dc conductivity with grain size for Y-substituted CeO_2 has also been reported⁴¹ while they have observed an enhancement in conductivity for Y- substituted CeO_2 ⁴² in relatively mild reducing conditions of nitrogen gas. There are also indications that a decrease in grain size induces an increase in electronic conductivity.⁴³

Mc Bride *et al.*⁴⁴ studied the relationship between the intensity of Raman peak at the high frequency side of the F_{2g} band and the content of oxygen vacancies in the solid solutions $Ce_{1-x}RE_xO_{2-\delta}$. They found that the relative intensity of this Raman peak increased with the oxygen vacancy concentration and the line width of F_{2g} mode was broadened for substituted ceria.⁴⁴ The microwave dielectric properties of ceria⁴⁵ have been discussed in section 3.2 of Chapter 3. Although considerable amount of work has been reported on the conductivity of rare earth substituted ceria, no report has been published on its dielectric properties. This has drawn our attention and stimulated us to synthesize, characterize and measure the microwave dielectric properties of rare earth substituted ceria for the first time.

6.2 EXPERIMENTAL

The $Ce_{1-x}RE_xO_{2-\delta}$ (RE = La, Pr, Nd, Sm, Eu, Gd, Tb, Dy, Er, Tm, Yb and Y), for $0 \leq x \leq 1$ ceramics were prepared by the conventional solid-state ceramic route as described in section 2.1.2 of Chapter 2. High purity chemicals of Treibacher Industries, Althofen, Austria - CeO_2 , La_2O_3 , Pr_6O_{11} , Nd_2O_3 , Sm_2O_3 , Eu_2O_3 , Gd_2O_3 , Tb_2O_3 , Dy_2O_3 , Er_2O_3 , Tm_2O_3 , Yb_2O_3 and Y_2O_3 (all having purity 99.9%) were used as the starting powders. Stoichiometric proportions of the chemicals were weighed and ball milled for 24 hours using zirconia balls in distilled water media. The slurry was dried and then calcined for 5 hours at 1100°C, ground well and again calcined at 1300°C/5h. The calcined powders were then ball milled for 24 hours. The fine powder was then pressed into disc shaped pucks of 20 mm diameter and about 10 mm height at a pressure of about 120 MPa using a

WC die. The green compacts were fired at a rate of 5°C/min up to 600°C and soaked at 600°C for 30 minutes to expel the binder. The pellets were sintered in air at temperatures in the range between 1500 – 1675°C depending on the rare earth ion and the dwell time was 4 hours. After sintering, the samples were allowed to cool down to room temperature at the rate of 3°C/min. The samples were then polished to remove surface irregularities.

The densities of the samples were measured using Archimedes method. X-ray diffraction patterns were recorded from powdered samples using CuK α radiation and SEM micrographs and EDXA were recorded from the surface of thermally etched samples. The microwave dielectric properties (ϵ_r , $Q_w f$ and τ_f) were measured employing resonance method^{46,47,48} as described in sections 2.4.2 to 2.4.5 of Chapter 2.

6.3 RESULTS AND DISCUSSION

The Ce_{1-x}RE_xO_{2- δ} (RE = La, Nd, Sm, Eu, Gd, Dy, Er, Tm, Yb and Y) for $0 \leq x \leq 1$ green compacts are sintered into dense ceramics and their sintering temperature and durations are optimized to obtain the best density and microwave dielectric properties. The ceramics prepared are having excellent chemical and thermal stability as explained in section 3.3.4 of Chapter 3. The Ce_{1-x}RE_xO_{2- δ} (RE = Pr, Tb) ceramics have no resonance and hence their properties are not investigated. Eventhough 'RE' represents rare earth, yttrium is also included here for convenience. Ce_{1-x}RE_xO_{2- δ} (RE = Eu, Er, Dy) ceramics has been studied in detail as representative of Ce_{1-x}RE_xO_{2- δ} (RE = La, Nd, Sm, Eu, Gd, Dy, Er, Tm, Yb and Y) solid solutions.

6.3.1 Phase Analysis

Fig. 6.1-6.3 show the XRD patterns of Ce_{1-x}RE_xO_{2- δ} (RE = Eu, Er, Dy); $0 \leq x \leq 1$ ceramics. The XRD patterns of pure CeO₂ (ICDD Card No. 34-0394) and Er₂O₃ (ICDD Card No. 43-1007) is also shown for comparison. The crystal structures of CeO₂ and rare earth oxides are fluorite and C-type respectively. It can be seen that the samples crystallize in a fluorite structure with the complete absence of the component oxide,

RE_2O_3 (RE = Eu, Er, Dy), which indicates the formation of complete solid solution at $x = 0.1, 0.15$ and 0.25 for Eu, Er and Dy respectively. Similar results were reported by Kuharuangrong²³ that 20 mol% Er- and 30 mol% Dy- substituted ceria exhibit the same phase and structure of CeO_2 . Trejo *et al.*⁴⁹ reported the perfect fluorite structure of $\text{Ce}_{0.9}\text{Eu}_{0.1}\text{O}_{2.5}$ cermics.

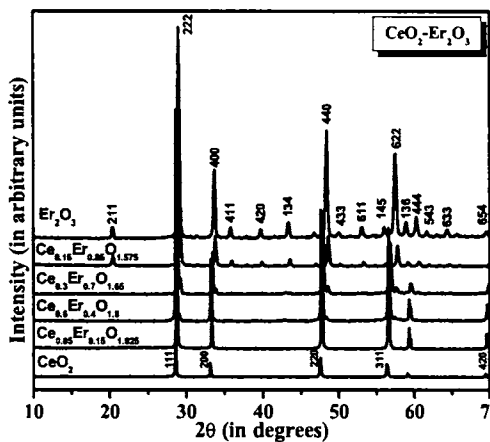


Fig. 6.1 XRD patterns of $\text{Ce}_{1-x}\text{Er}_x\text{O}_{2.5}$ ($x = 0.15, 0.4, 0.7, 0.85$) ceramics

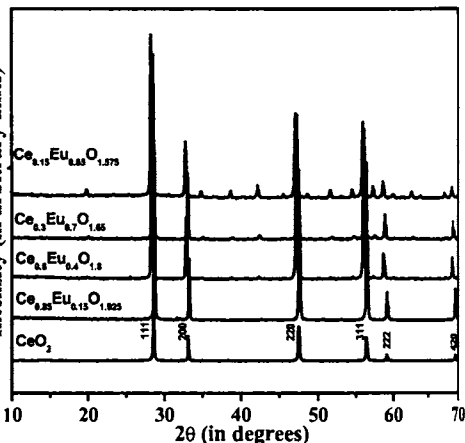


Fig. 6.2 XRD patterns of $\text{Ce}_{1-x}\text{Eu}_x\text{O}_{2.5}$ ($x = 0.15, 0.4, 0.7, 0.85$) ceramics

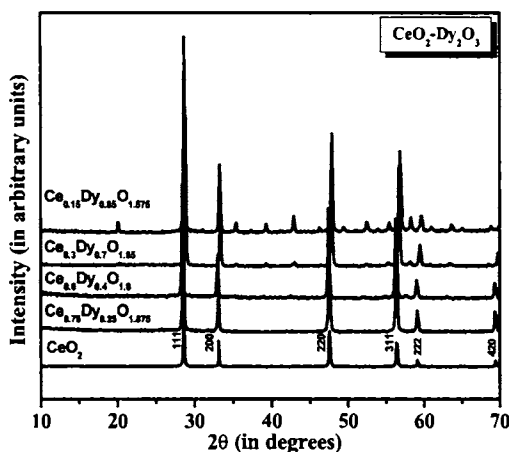


Fig. 6.3 XRD patterns of $\text{Ce}_{1-x}\text{Dy}_x\text{O}_{2.5}$ ($x = 0.25, 0.4, 0.7, 0.85$) ceramics

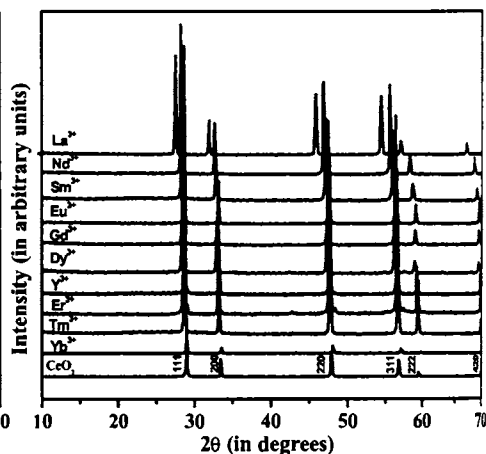


Fig. 6.4 XRD patterns of $\text{Ce}_{1-x}\text{RE}_x\text{O}_{2.5}$ (RE = Yb, Tm, Er, Y, Dy, Gd, Eu, Sm, Nd, La) ceramics in the solubility limit

For $x = 0.1-0.5$, the peaks of $Ce_{1-x}RE_xO_{2.8}$ ($RE = Eu, Er, Dy$) ceramics shift towards left and at $x = 0.7$ onwards the peaks start shifting to right side. This indicates that there is an additional solid solution formation at $x = 0.7$ in all RE ($RE = Eu, Er, Dy$) substituted $Ce_{1-x}RE_xO_{2.8}$ ceramics. After $x = 0.7$, the structure shifts towards that of RE_2O_3 in $Ce_{1-x}RE_xO_{2.8}$ ($RE = Eu, Er, Dy$) ceramics. A similar variation of XRD patterns is observed for other RE-substituted ceria ($RE = La, Nd, Sm, Gd, Tb, Tm, Yb$ and Y). The solid solubility limit of RE in ceria is determined as explained above and the XRD patterns of $Ce_{1-x}RE_xO_{2.8}$ ($RE = La, Nd, Sm, Eu, Gd, Dy, Er, Tm, Yb$ and Y) ceramics at the solubility limit in the increasing ionic radius size is shown in Fig. 6.4. The peaks of $Ce_{1-x}RE_xO_{2.8}$ ceramics shift to the left with the increasing ionic size of the substituted rare earth. No other additional diffraction peaks other than that of ceria is observed below the solubility limit of $Ce_{1-x}RE_xO_{2.8}$ ($RE = La, Nd, Sm, Eu, Gd, Dy, Er, Tm, Yb$ and Y) ceramics.

6.3.2 Microstructural Analysis

SEM micrographs of $Ce_{1-x}RE_xO_{2.8}$ ($RE = Eu, Er$); $x = 0.1, 0.7, 0.85$ ceramics is shown in Fig. 6.5(a)-(f). All these ceramics have good densification. SEM microstructure of pure CeO_2 is shown in Fig. 4.11 of section 4.3.3.1, Chapter 4. The SEM image of $Ce_{0.9}Eu_{0.1}O_{1.95}$ shows large grains of size approximately $5-12 \mu m$ and nearly circular grains. The SEM picture of $Ce_{0.3}Eu_{0.7}O_{1.65}$ also shows that it consists of large grains of size approximately $4-7 \mu m$ and very small nearly circular grains of about $0.5 \mu m$. In $Ce_{0.15}Eu_{0.85}O_{1.575}$ ceramics, two phases are clearly seen from the microstructure - large grains of size $2.5-4.5 \mu m$ and small grains of $0.5-1 \mu m$. The analysis of EDXA data given in Table 6.1 shows that both the grains seen in $Ce_{0.9}Eu_{0.1}O_{1.95}$ ceramics are having the same composition. But in $Ce_{0.3}Eu_{0.7}O_{1.75}$ and $Ce_{0.15}Eu_{0.85}O_{1.65}$ ceramics, two different solid solution phases co-exist. The SEM micrographs of $Ce_{1-x}Er_xO_{2.8}$ ($x = 0.15, 0.7, 0.85$) ceramics (Figs. 6.5(d)-(f)) are homogeneous with good densification. $Ce_{0.85}Er_{0.15}O_{1.925}$ ceramics is having well-defined grain boundaries with large grains of size $5-12 \mu m$ and small circular shaped grains. The microstructure of $Ce_{0.3}Er_{0.7}O_{1.65}$ ceramics also shows two types of grains – large grains

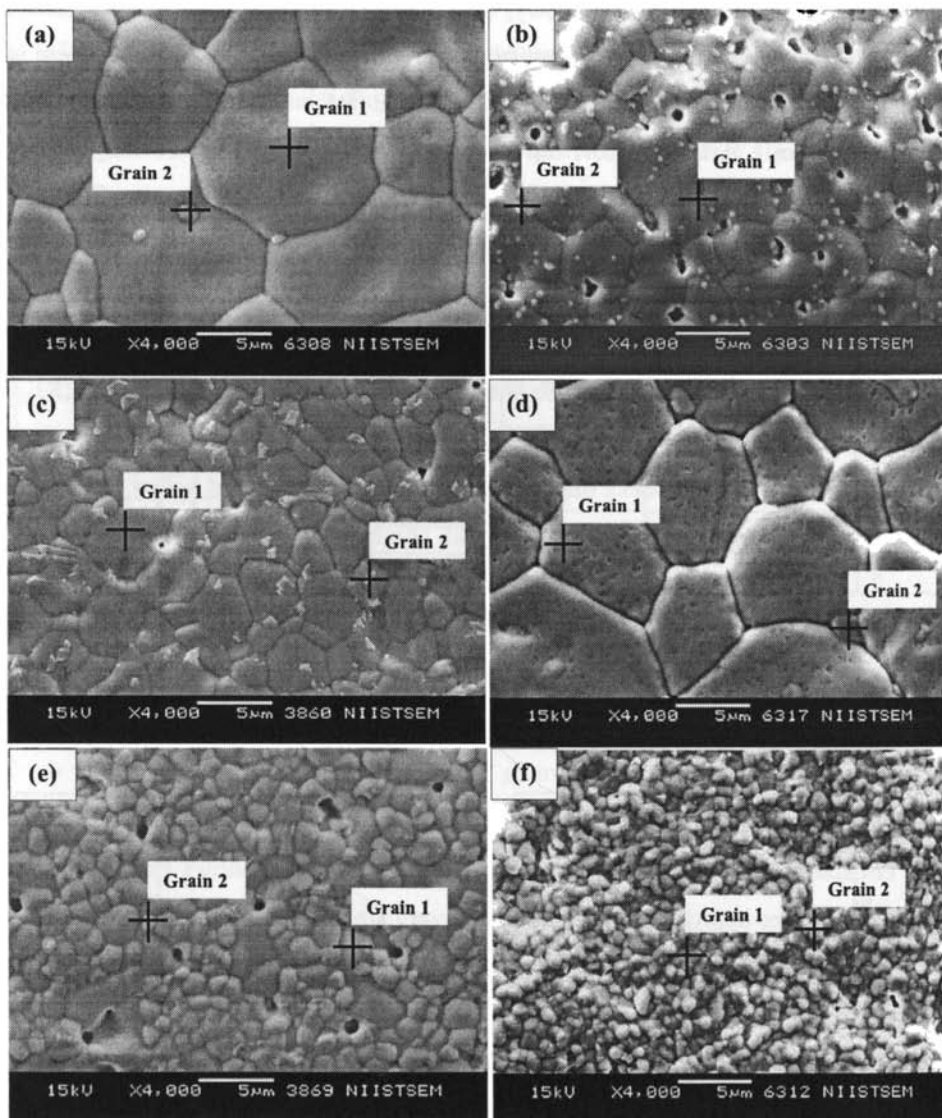


Fig. 6.5 SEM micrographs of (a) $Ce_{0.9}Eu_{0.1}O_{1.95}$ (b) $Ce_{0.3}Eu_{0.7}O_{1.65}$ (c) $Ce_{0.15}Eu_{0.85}O_{1.575}$ (d) $Ce_{0.85}Er_{0.15}O_{1.925}$ (e) $Ce_{0.3}Er_{0.7}O_{1.65}$ (f) $Ce_{0.15}Er_{0.85}O_{1.575}$ ceramics

having 1.5-3 μm and small grains having 0.5-1 μm . The $Ce_{0.15}Er_{0.85}O_{1.575}$ ceramics are having two types of grains having lighter and darker contrast. Both are having approximately same size of 0.5-2.5 μm . The EDXA data given in Table 6.2 clearly

shows that both the grains are same having the same composition and $Ce_{0.85}Er_{0.15}O_{1.925}$ is single phase. The elemental analysis of two types of grains in $Ce_{0.3}Er_{0.7}O_{1.65}$ and $Ce_{0.15}Er_{0.85}O_{1.575}$ shows that two different solid solution phases is present-one phase having the same composition as that prepared and other having different composition.

Table 6.1 EDXA data of $Ce_{1-x}Eu_xO_{2-\delta}$; ($x = 0.1, 0.7, 0.85$) ceramics

Element	$Ce_{0.85}Er_{0.15}O_{1.925}$		$Ce_{0.3}Er_{0.7}O_{1.65}$		$Ce_{0.15}Er_{0.85}O_{1.575}$	
	Grain 1	Grain 2	Grain 1	Grain 2	Grain 1	Grain 2
Ce (atomic %)	49.21	42.97	28.45	17.31	5.41	8.97
Er (atomic %)	9.71	8.15	35.04	41.82	46.51	49.63
O (atomic %)	41.08	48.88	36.51	40.87	48.08	51.40

Table 6.2 EDXA data of $Ce_{1-x}Er_xO_{2-\delta}$; ($x = 0.15, 0.7, 0.85$) ceramics

Element	$Ce_{0.9}Eu_{0.1}O_{1.95}$		$Ce_{0.3}Eu_{0.7}O_{1.65}$		$Ce_{0.15}Eu_{0.85}O_{1.575}$	
	Grain 1	Grain 2	Grain 1	Grain 2	Grain 1	Grain 2
Ce (atomic %)	48.06	44.51	27.80	21.22	22.07	26.07
Eu (atomic %)	6.01	5.10	27.56	39.65	39.81	40.14
O (atomic %)	45.92	50.39	44.64	39.13	38.12	33.79

6.3.3 Microwave Dielectric Properties

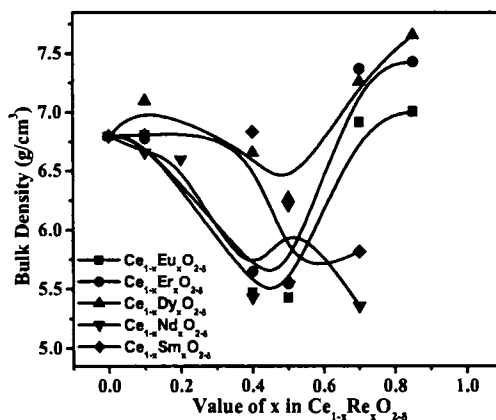


Fig. 6.6 Variation of bulk density with the composition of x in $Ce_{1-x}RE_xO_{2-\delta}$ (RE = Nd, Eu, Er, Dy, Sm) ceramics

The densities of $Ce_{1-x}RE_xO_{2.8}$ (RE = Nd, Eu, Er, Dy, Sm) ceramics for different values of x is plotted in Fig. 6.6. The density of pure ceria is 6.83 g/cm^3 . The densities of $Ce_{1-x}RE_xO_{2.8}$ (RE = Nd, Eu, Er, Dy, Sm) ceramics decrease with the value of x , reach minimum at $x = 0.5$ and start increasing from $x = 0.7$. The density is decreased to 5.47, 5.55, 6.27, 5.43 and 5.56 g/cm^3 for $Ce_{1-x}RE_xO_{2.8}$ (RE = Nd, Eu, Er, Dy, Sm) ceramics respectively. The increase in density at $x = 0.7$ is due to the formation of a new solid solution phase as evident from XRD, SEM and EDXA results.

Table 6.3 Microwave dielectric properties of $Ce_{1-x}RE_xO_{2.8}$ (RE = Nd, Eu, Er, Dy, Sm), $0 \leq x \leq 1$ solid solutions

Material	ϵ_r	$Q_{\omega}f$ (GHz)	τ_f (ppm/ $^{\circ}$ C)
$Ce_{0.6}Nd_{0.4}O_{1.8}$	19.9	34100	-55
$Ce_{0.5}Nd_{0.5}O_{1.75}$	17.0	22750	-66
$Ce_{0.3}Nd_{0.7}O_{1.65}$	18.3	44700	-63
$Ce_{0.15}Nd_{0.85}O_{1.575}$	17.2	11700	-63
$Ce_{0.9}Eu_{0.1}O_{1.95}$	25.4	70300	-64
$Ce_{0.6}Eu_{0.4}O_{1.8}$	16.8	26400	-58
$Ce_{0.5}Eu_{0.5}O_{1.75}$	16.1	24700	-52
$Ce_{0.3}Eu_{0.7}O_{1.65}$	19.0	60300	-54
$Ce_{0.15}Eu_{0.85}O_{1.575}$	16.9	64700	-39
$Ce_{0.85}Er_{0.15}O_{1.925}$	21.7	23000	-40
$Ce_{0.6}Er_{0.4}O_{1.8}$	16.3	21100	-42
$Ce_{0.5}Er_{0.5}O_{1.75}$	16.3	13950	-45
$Ce_{0.3}Er_{0.7}O_{1.65}$	17.1	15350	-41
$Ce_{0.15}Er_{0.85}O_{1.575}$	15.2	17650	-40
$Ce_{0.8}Dy_{0.2}O_{1.9}$	26.2	70150	-57
$Ce_{0.6}Dy_{0.4}O_{1.8}$	17.0	28100	-48
$Ce_{0.5}Dy_{0.5}O_{1.75}$	17.9	26300	-47
$Ce_{0.3}Dy_{0.7}O_{1.65}$	17.1	22650	-45
$Ce_{0.15}Dy_{0.85}O_{1.575}$	16.3	15200	-39
$Ce_{0.75}Sm_{0.25}O_{1.875}$	16.8	29650	-56
$Ce_{0.5}Sm_{0.5}O_{1.75}$	17.7	24050	-49
$Ce_{0.3}Sm_{0.7}O_{1.65}$	19.7	79450	-51
$Ce_{0.15}Sm_{0.85}O_{1.575}$	18.5	52050	-55

The microwave dielectric properties of $Ce_{1-x}RE_xO_{2.8}$ (RE = Nd, Eu, Er, Dy, Sm) ceramics for different values of x is given in Table 6.3. The relative permittivity decreases with the value of x , reaches minimum at $x = 0.5$ and then starts increasing from

$x = 0.7$ for $\text{Ce}_{1-x}\text{RE}_x\text{O}_{2-\delta}$ (RE = Nd, Eu, Er, Sm); $0 \leq x \leq 1$ ceramics. As the value of x increases, the relative permittivity decreases for $\text{Ce}_{1-x}\text{Dy}_x\text{O}_{2-\delta}$ ceramics. This variation in relative permittivity is due to the presence of secondary phases at $x = 0.7$ in $\text{Ce}_{1-x}\text{RE}_x\text{O}_{2-\delta}$ (RE = Nd, Eu, Er, Sm) ceramics. The variation of relative permittivity with the amount of RE is same as that of density variation in $\text{Ce}_{1-x}\text{RE}_x\text{O}_{2-\delta}$ (RE = Nd, Eu, Er, Dy, Sm) ceramics. A maximum relative permittivity of 25.4 and 26.2 is obtained for $\text{Ce}_{0.9}\text{Eu}_{0.1}\text{O}_{1.975}$ and $\text{Ce}_{0.8}\text{Dy}_{0.2}\text{O}_{1.9}$ ceramics respectively. The highest relative permittivity at the solid solubility limit is due to the high density and single phase nature of the ceramics at the particular composition.

The quality factor decreases with increase in the substitution of RE till $x = 0.5$ and then starts increasing in $\text{Ce}_{1-x}\text{RE}_x\text{O}_{2-\delta}$ (RE = Nd, Eu, Er, Sm) ceramics. The quality factor reaches a minimum of 22750, 24700, 13950 and 24050 GHz at $x = 0.5$ and then increased to 44700, 60300, 15350 and 79450 GHz at $x = 0.7$ for $\text{Ce}_{1-x}\text{RE}_x\text{O}_{2-\delta}$ (RE = Nd, Eu, Er, Sm) ceramics respectively. In $\text{Ce}_{1-x}\text{Dy}_x\text{O}_{2-\delta}$ ceramics, the quality factor decreases from 70150 GHz for $x = 0.2$ to 15200 for $x = 0.85$. A high quality factor of 70300, 70150 and 79450 GHz is obtained for $\text{Ce}_{0.9}\text{Eu}_{0.1}\text{O}_{1.975}$, $\text{Ce}_{0.8}\text{Dy}_{0.2}\text{O}_{1.9}$ and $\text{Ce}_{0.3}\text{Sm}_{0.7}\text{O}_{1.65}$ ceramics respectively. The high quality factors obtained for $\text{Ce}_{0.9}\text{Eu}_{0.1}\text{O}_{1.975}$ and $\text{Ce}_{0.8}\text{Dy}_{0.2}\text{O}_{1.9}$ ceramics is due to the single phase nature of the ceramics. A highest quality factor of 79450 GHz in $\text{Ce}_{0.3}\text{Sm}_{0.7}\text{O}_{1.65}$ ceramics may be due to the formation of low loss secondary phase. The quality factor of a particular material depends on the densification, presence of secondary phases and the solid solubility limit. The coefficient of temperature variation of resonant frequency decreases with the RE addition for $\text{Ce}_{1-x}\text{RE}_x\text{O}_{2-\delta}$ (RE = Eu, Dy, Sm) ceramics. In $\text{Ce}_{1-x}\text{RE}_x\text{O}_{2-\delta}$ (RE = Eu, Sm) ceramics, the τ_f decreases up to $x = 0.5$ and then starts increasing. In the case of $\text{Ce}_{1-x}\text{RE}_x\text{O}_{2-\delta}$ (RE = Er, Nd), τ_f increases and starts decreasing at $x = 0.7$. This change in the value at $x = 0.7$ is due to the presence of two types of solid solutions at that composition. $\text{Ce}_{0.9}\text{Eu}_{0.1}\text{O}_{1.975}$ has the highest negative τ_f of $-64 \text{ ppm}/^\circ\text{C}$ and $\text{Ce}_{0.15}\text{Eu}_{0.85}\text{O}_{1.575}$ has the minimum value of $-39 \text{ ppm}/^\circ\text{C}$. All the ceramics prepared has a high negative τ_f which precludes its immediate practical applications.

Table 6.4 Table showing the ionic radius, solubility limit and microwave dielectric properties at the solubility limit of $Ce_{1-x}RE_xO_{2-\delta}$ (RE = La, Nd, Sm, Eu, Gd, Dy, Er, Tm, Yb and Y) ceramics

Material	Ionic radius (Å) of RE^{3+} ion	Solubility limit (x)	ϵ_r	$Q \times f$ (GHz)	τ_f (ppm/°C)
$Ce_{1-x}La_xO_{2-\delta}$	1.160	0.25	19.2	14700	-64
$Ce_{1-x}Nd_xO_{2-\delta}$	1.109	0.40	19.9	17050	-55
$Ce_{1-x}Sm_xO_{2-\delta}$	1.079	0.25	16.8	29050	-56
$Ce_{1-x}Eu_xO_{2-\delta}$	1.066	0.10	25.4	70300	-64
$Ce_{1-x}Gd_xO_{2-\delta}$	1.053	0.50	14.9	15300	-62
$Ce_{1-x}Dy_xO_{2-\delta}$	1.027	0.20	26.2	70150	-57
$Ce_{1-x}Er_xO_{2-\delta}$	1.004	0.15	21.7	20300	-40
$Ce_{1-x}Tm_xO_{2-\delta}$	0.994	0.25	17.3	27850	-36
$Ce_{1-x}Yb_xO_{2-\delta}$	0.985	0.25	25.2	47800	-69
$Ce_{1-x}Y_xO_{2-\delta}$	1.019	0.50	13.9	35000	-53

Table 6.4 gives the ionic size of the substituted ion, solubility limit and microwave dielectric properties of $Ce_{1-x}RE_xO_{2-\delta}$ (RE = La, Nd, Sm, Eu, Gd, Dy, Er, Tm, Yb and Y) ceramics. Ionic radius of Ce^{4+} ion is 0.97 Å.⁵⁰ No correlation of ionic radius of substituted ion with solubility limit of $Ce_{1-x}RE_xO_{2-\delta}$ is established. It is also established that microwave dielectric properties of ceria does not depend on the ionic radius of the doped ions.

6.4 CONCLUSIONS

- The $Ce_{1-x}RE_xO_{2-\delta}$ (RE = La, Nd, Sm, Eu, Gd, Dy, Er, Tm, Yb and Y) for $0 \leq x \leq 1$ solid solutions are prepared by solid state ceramic route.
- The solid solubility limit of each rare earth ion in ceria is found out from XRD, SEM and EDXA analysis. The XRD, SEM and EDXA analysis revealed that there exists two types of solid solutions for $x = 0.7$ in $Ce_{1-x}RE_xO_{2-\delta}$ (RE = Eu, Dy, Er) ceramics.
- The microwave dielectric properties of $Ce_{1-x}RE_xO_{2-\delta}$ (RE = La, Nd, Sm, Eu, Gd, Dy, Er, Tm, Yb and Y) for different compositions from $0 \leq x \leq 1$ are measured and

found that these properties depend on the solid solution formation at different concentrations of substituted ion.

- The best properties are obtained for $\text{Ce}_{0.9}\text{Eu}_{0.1}\text{O}_{1.95}$ ($\epsilon_r = 25.4$, $Q_{uxf} = 70300$ GHz, $\tau_f = -64$ ppm/°C) $\text{Ce}_{0.8}\text{Dy}_{0.2}\text{O}_{1.9}$ ($\epsilon_r = 26.2$, $Q_{uxf} = 70150$ GHz, $\tau_f = -57$ ppm/°C) and $\text{Ce}_{0.3}\text{Sm}_{0.7}\text{O}_{1.65}$ ($\epsilon_r = 19.7$, $Q_{uxf} = 79450$ GHz, $\tau_f = -51$ ppm/°C).

This Chapter discusses the solubility and microwave dielectric properties of different compositions of rare earth and yttrium ions in ceria. The next Chapter discusses different ceria based composites for electronic packaging and substrate applications.

6.5 REFERENCES

- ¹ Y. Maki, M. Matsuda and T. Kudo, U.S. Patent No. 3 [607] 424 (1971).
- ² M. Yashima, H. Arashi, M. Kakihana and M. Yoshimura, *J. Am. Ceram. Soc.*, **77**, 1067(1994).
- ³ H. Yahiro, K. Eguchi and H. Arai, *Solid State Ionics*, **36**, 71 (1989).
- ⁴ T. Kudo and H. Obayashi, *J. Electrochem. Soc.*, **122**, 142 (1975).
- ⁵ C. S. Wright, J. Fischer, D. Thompsett and R. I. Walton, *Angew. Chem. Int. Ed.*, **45**, 2442 (2006).
- ⁶ A. B. Corradi, F. B. Bondioli, A. M. Ferrari and T. Manfredini, *Mater. Res. Bull.*, **41**, 38 (2006).
- ⁷ J. Park, J. Kim, J. Han, S. W. Nam and T. H. Lim, *J. Ind. Eng. Chem.*, **11**, 897 (2005).
- ⁸ A. Hartridge, A. K. Bhattacharya, R. E. Dunin-Borkowski and J. L. Hutchison, *J. Nanoparticle Res.*, **3**, 433 (2001).
- ⁹ W. Huang, P. Shuk and M. Greenblatt, *Solid State Ionics*, **100**, 23 (1997).
- ¹⁰ H. S. Kang, Y. C. Kang, H. Y. Koo, S. H. Ju, D. Y. Kim, S. K. Hong, J. R. Sohn, K. Y. Jung and S. B. Park, *Mater. Sci. Eng. B-Solid State Mater. Adv. Technol.*, **127**, 99 (2006).
- ¹¹ K. Matsui, H. Suzuki, M. Ohgai and A. Arashi, *J. Ceram. Soc. Jpn.*, **98**, 1302 (1990).
- ¹² B. P. Mandal, M. Roy, V. Grover and A. K. Tyagi, *J. Appl. Phys.*, **103**, 033506 (2008).
- ¹³ F. A. Kröger, *Chemistry of Imperfect Crystals*, North-Holland, Amsterdam, (1964).
- ¹⁴ T. Kudo and H. Obayashi, *J. Electrochem. Soc.*, **123**, 415 (1976).
- ¹⁵ D. Y. Wang and A. S. Nowick, *J. Solid State Chem.*, **35**, 325 (1980).
- ¹⁶ K. E. Adham and A. Hammou, *Solid State Ionics*, **9-10**, 905 (1981).
- ¹⁷ D. Y. Wang, D. S. Park, J. Griffith and A. S. Nowick, *Solid State Ionics*, **2**, 95 (1981).
- ¹⁸ H. Yahiro, K. Eguchi and H. Arai, *Solid State Ionics*, **21**, 37 (1986).
- ¹⁹ T. Inoue, T. Setoguchi, K. Eguchi and H. Arai, *Solid State Ionics*, **35**, 285 (1989).
- ²⁰ H. Yahiro, K. Eguchi and H. Arai, *Solid State Ionics*, **36**, 71 (1989).

-
- ²¹ H. Inaba and H. Tagawa, *Solid State Ionics*, **83**, 1 (1996).
- ²² M. Mogensen, N. M. Sammes and G. A. Tompsett, *Solid State Ionics*, **129**, 63 (2000).
- ²³ S. Kuharungrong, *J. Power Sources*, **171**, 506 (2007).
- ²⁴ T. S. Zhang, J. Ma, L. B. Kong, S. H. Chan and J. A. Kilner, *Solid State Ionics*, **170**, 209 (2004).
- ²⁵ G. B. Balazs and R. S. Glass, *Solid State Ionics*, **76**, 155 (1995).
- ²⁶ H. Yahiro, Y. Eguchi, K. Eguchi and H. Arai, *J. Appl. Electrochem.*, **18**, 527 (1988).
- ²⁷ B. C. H. Steele, *High Conductivity Solid Ion Conductors, Recent Trends and Applications*, T. Takashi (Editor), World Scientific, London, (1989).
- ²⁸ Z. Tianshu, P. Hing, H. Huang and J. Kilner, *Solid State Ionics*, **148**, 567 (2002).
- ²⁹ J. M. Ralph and J. A. Kilner, *Proc. of the Second European SOFC Forum*, B. Thorstenson (Editor), **2**, 773 (1996).
- ³⁰ B. C. H. Steele, *Solid State Ionics*, **129**, 95 (2000).
- ³¹ V. Longo and L. Podda, *J. Mater. Sci.*, **16**, 839 (1981).
- ³² E. Ruiz-Trejo, J. D. Sirman, Yu. M. Baikov and J. A. Kilner, *Solid State Ionics*, **113-115**, 565 (1998).
- ³³ K. Huang, M. Feng and J. B. Goodenough, *J. Am. Ceram. Soc.*, **81**, 357 (1998).
- ³⁴ H. L. Tuller and A. S. Nowick, *J. Electrochem. Soc.*, **126**, 209 (1979).
- ³⁵ Y.-M. Chiang, E. B. Lavik, I. Kosacki, H.L. Tuller and J. Y. Ying, *J. Electroceram.*, **1**, 7 (1997).
- ³⁶ S. Kim and J. Maier, *J. Electrochem. Soc.*, **149**, J73 (2002).
- ³⁷ A. Tschöpe, E. Sommer and R. Birringer, *Solid State Ionics*, **139**, 255 (2001).
- ³⁸ J. H. Hwang and T. O. Mason, *Z. Phys. Chem.*, **207**, 21 (1998).
- ³⁹ M. G. Bellino, D.G. Lamas and N. E. Walsøe de Reca, *Adv. Funct. Mater.*, **16**, 107 (2006).
- ⁴⁰ T. Suzuki, I. Kosacki and H. U. Anderson, *Solid State Ionics*, **151**, 111 (2002).

-
- ⁴¹ D.R.Ou, T. Mori, F.Ye, M. Takahashi, J. Zou and J. Drennan, *Acta Mater.*, **54**, 737 (2006).
- ⁴² E. Ruiz-Trejo, A. Benítez-Rico, S. Gómez-Reynoso and M. Angeles-Rosas, *J. Electrochem. Soc.*, **154**, A258 (2007).
- ⁴³ J. Rupp and L. Gauckler, *Solid State Ionics*, **177**, 2513 (2006).
- ⁴⁴ J. R. McBride, K. C. Hass, B. D. Poindexter and W. H. Weber, *J. Appl. Phys.*, **76**, 2435 (1994).
- ⁴⁵ N. Santha, M. T. Sebastian, P. Mohanan, Mc N. Alford, K. Sarma, R. C. Pullar, S. Kamba, A. Pashkin, P. Samukhina and J. Petzelt, *J. Am. Ceram. Soc.*, **87**, 1233 (2004).
- ⁴⁶ B. W. Hakki and P. D. Coleman, *IRE Trans. Microwave Theory Tech.*, **MTT-8**, 402 (1960).
- ⁴⁷ W. E. Courtney, *IEEE Trans. Microwave Theory Tech.*, **MTT-18**, 476 (1970).
- ⁴⁸ J. Krupka, K. Derzakowski, B. Riddle and J. Baker-Jarvis, *Meas. Sci. Technol.*, **9**, 1751 (1998).
- ⁴⁹ E. Ruiz-Trejo, J. Santayo-Salazar, R. Vilchis-Morales, A. Benitez-Rico, F. Gomez-Garcia, C. Flores-Morales, J. Chavez-Carvayar and G. Tavizon, *J. Solid State Chem.*, **180**, 3093 (2007).
- ⁵⁰ R. D. Shannon, *Acta Cryst.*, **A 32**, 751 (1976).

CHAPTER 7

CERIA BASED COMPOSITES FOR ELECTRONIC PACKAGING AND SUBSTRATE APPLICATIONS

This chapter reports three ceria based composites. The first section discusses the effect of glass additives on the microstructure, densification and microwave dielectric properties of cerium oxide. The results of this research established low temperature synthesis of CeO_2 ceramics with improved microwave dielectric properties for dielectric resonator and possible Low Temperature Cofired Ceramics (LTCC) applications. Cerium oxide filled polytetrafluoroethylene (PTFE) composites prepared by powder processing technique and high density polyethylene (HDPE) composites prepared by melt mixing method for microwave substrate applications are discussed in the second section of this chapter. The variation of dielectric, thermal and mechanical properties with volume fraction of filler loading is also described. The last section of the chapter discusses the $\text{CeO}_2\text{-La}_{0.5}\text{Sr}_{0.5}\text{CoO}_{3-\delta}$ composites for electromechanical applications.

7.1 CERIA-GLASS COMPOSITES FOR LOW TEMPERATURE COFIRED CERAMIC APPLICATIONS

7.1.1 Introduction

Recently, the development of low temperature co-fired ceramics (LTCC) has been getting much interest due to the application of multilayer integrated circuit (MLIC), such as chip LC filters and antennas.¹ The most important parameter for the LTCC technology is the low sintering temperature, and it enables the advantageous utilization for today's packaging concepts in microelectronic and microwave modules. Since the LTCC tapes can be sintered at low temperatures ($< 950^{\circ}\text{C}$), the embedded microwave components and transmission lines can be fabricated using highly conductive and inexpensive metals such as silver, gold or copper with low conductor loss and low electrical resistance at high-frequencies.² This is an advantage over other ceramic technologies. The LTCC is widely used for substrate, semiconductor package, passive integrated device and module applications in wireless communication.³ A low dielectric loss or high quality factor (Q_{ixf}) and a small temperature coefficient of resonant frequency (τ_f) are essential for practical applications. In addition, a low relative permittivity ($\epsilon_r < 15$) material is needed for substrate applications to avoid signal delay⁴ whereas a high relative permittivity ($\epsilon_r > 20$) is preferred for miniaturization.⁵ The sintering temperature must be less than the melting point of the electrode material such that the ceramics can be cofired with the electrode. This is an important requirement for LTCC technology. A number of strategies have been reported to lower the sintering temperature of ceramics (a) addition of low melting point glass^{6,7} or low melting point materials such as CuO , V_2O_5 , B_2O_3 ^{8,9} (b) using starting materials with smaller particle size¹⁰ and (c) development of novel glass free low-sintering dielectric ceramics.¹¹ Recent research trend suggests that, liquid phase sintering using low loss glass additives is widely employed since it is the least expensive.

Most of the known commercial ceramic materials like $\text{BaMg}_{1/3}\text{Ta}_{2/3}\text{O}_3$, $\text{BaZn}_{1/3}\text{Ta}_{2/3}\text{O}_3$, $(\text{Zr},\text{Sn})\text{TiO}_4$ etc. need sintering temperatures above 1300°C , which limits their use in LTCC applications. Many attempts were made to reduce the firing

temperature by the addition of various low melting and low loss glasses.^{12,13,14,15} CuO and V₂O₅ are well-known liquid-phase sintering promoters. But there are reports that multi-component glasses are more effective than single component glasses to lower the sintering temperature of ceramics without much degradation in the physical and dielectric properties of the matrix.^{1,16} Wu *et al.*¹⁷ reported the microwave dielectric properties of various borosilicate glasses. After conducting a detailed investigation on the dielectric properties of glasses at ultra-high frequencies, Navias *et al.*¹⁸ noted that the dielectric losses of borosilicate glasses are comparatively lower than alkali containing glasses. This is due to the fact that in the latter, alkali ions which are weakly held in the glassy network, absorb energy and eventually give rise to dielectric loss. On the other hand, borosilicate glasses^{18,19} having continuous atomic structures, with SiO₄ and BO₃ configurations joined to form (-Si-O-B-O-) linkages, will have high electrical resistance and low dielectric loss. The microwave dielectric properties of a few borosilicate glasses (BaO-B₂O₃-SiO₂, PbO-B₂O₃-SiO₂ and ZnO-B₂O₃-SiO₂) have been reported¹⁸ recently in which it was observed that the τ_f of all these glasses are negative. Several authors reported the lowering of sintering temperature of ceramics such as MgAl₂O₄ and CaZrO₃-CaTiO₃ by adding lithium based glasses such as Li₂O-MgO-ZnO-B₂O₃-SiO₂ and Li₂O-B₂O₃-SiO₂ respectively.^{20,21} Studies were also conducted on Bi₂O₃-ZnO-B₂O₃-SiO₂ glass for making it a suitable additive for LTCC applications.^{22,23}

Cerium oxide has been widely used as a substrate or buffer layer for superconducting microwave devices because of its low dielectric loss, excellent lattice matching and a good matching for thermal expansion.²⁴ The microwave dielectric properties of ceria have been discussed in section 3.2 of Chapter 3. But ceria requires high sintering temperature of above 1600°C which is time and energy consuming for industrial production.²⁵ A considerable amount of work has been done to prepare ceria by chemical methods like urea-based hydrogenous precipitation,^{26,27} solvothermal synthesis,²⁸ electrochemical synthesis,²⁹ hydrothermal synthesis³⁰ etc. The section 4.4.3.3 of Chapter 4 discusses the variation of microwave dielectric properties of B₂O₃ and CuO added 0.5CeO₂-0.5BaTi₄O₉ ceramics. Hsu *et al.*³¹ reported the dielectric properties of

B_2O_3 doped $0.98CeO_2-0.02CaTiO_3$ ceramics. A considerable number of research has been done on the interaction of glasses with low loss microwave dielectrics. However, the vitreous phase densification and dielectric loss of silicate/borate or borosilicate glasses in cerium oxide for LTCC materials, has not been reported before. This has drawn our attention and provided motivation to study the effect of glass flux on the sintering behaviour and microwave dielectric properties of ceria for LTCC applications. $B_2O_3-SiO_2$, $Al_2O_3-SiO_2$, $ZnO-B_2O_3$, $BaO-B_2O_3-SiO_2$, $ZnO-B_2O_3-SiO_2$, $MgO-B_2O_3-SiO_2$, $Li_2O-B_2O_3-SiO_2$, $PbO-B_2O_3-SiO_2$, $MgO-Al_2O_3-SiO_2$, $Bi_2O_3-ZnO-B_2O_3-SiO_2$ and $Li_2O-MgO-ZnO-B_2O_3-SiO_2$ glasses and B_2O_3 are used in the present investigation to lower the sintering temperature of CeO_2 .

7.1.2 Experimental

The glass powders used in this investigation were B_2O_3 (abbreviated as B), $B_2O_3-SiO_2$ (BS), $ZnO-B_2O_3$ (ZB), $Al_2O_3-SiO_2$ (AS), $BaO-B_2O_3-SiO_2$ (BBS), $MgO-B_2O_3-SiO_2$ (MBS), $PbO-B_2O_3-SiO_2$ (PBS), $ZnO-B_2O_3-SiO_2$ (ZBS), $2MgO-Al_2O_3-5SiO_2$ (MAS), $Li_2O-B_2O_3-SiO_2$ (LBS), $Bi_2O_3-ZnO-B_2O_3-SiO_2$ (BZBS) and $Li_2O-MgO-ZnO-B_2O_3-SiO_2$ (LMZBS). For synthesizing glasses, high purity (Aldrich Chemical Co., Milwaukee, WI, USA, >99.9 %) oxides/carbonates were weighed stoichiometrically and mixed for two hours in an agate mortar with pestle using distilled water as the medium. It was then melted in a platinum crucible above their softening temperature (see Table 1.2 of Chapter 1), quenched and powdered.

High purity CeO_2 powder (Treibacher Industries, Althofen, Austria, 99.9%) used in the present investigation was initially heated at $1000^\circ C/4h$ to remove any volatile impurities and then mixed with different weight percentages of the glasses for 2 hours. 4 wt% aqueous solution of polyvinyl alcohol (PVA) was added as a binder. The powder was uniaxially pressed into cylindrical compacts of 20 mm diameter and 9-10 mm in thickness under a pressure of about 130 MPa in tungsten carbide die. These compacts were heated at a rate of $5^\circ C/min$ up to $600^\circ C$ and soaked at $600^\circ C$ for 30 minutes to expel the binder. They were then sintered in the temperature range $900-1650^\circ C$ for 4 hours in

air at a heating rate of 10°C/min and the samples were then cooled to 1000°C at a rate of 3°C per minute. The sintering temperature was optimized for the best density of each glass ceramic composition. The polished ceramic pellets with an aspect ratio (diameter to height) of 1.8 to 2.2 which is ideal for maximum separation of the modes, were used for microwave measurements.

The bulk densities of the sintered samples were measured using Archimedes method. The powdered samples were used for analyzing the X-ray diffraction patterns using CuK_α radiation and the surface morphology was studied using SEM methods. EDXA was used for elemental analysis. The coefficient of thermal contraction of the samples was measured using a thermo mechanical analyzer (TMA-60H Shimadzu, Kyoto, Japan) in the temperature range 30°–1000°C. The dielectric properties ϵ_r , Q_w and τ_f of the materials were measured in the microwave frequency range using resonance technique^{32, 33, 34} as described in Chapter 2, sections 2.4.2 to 2.4.5.

7.1.3 Results and Discussion

7.1.3.1 Sintering of Glass Fluxed Ceria

The synthesizing conditions such as sintering temperature and their durations are optimized for glass added CeO_2 ceramics to obtain the best density and dielectric properties. There is no change in density, dielectric properties or in XRD pattern when sintered glass added CeO_2 samples are boiled in water indicating excellent chemical and thermal stability of the material.

Table 1.2 in Chapter 1 gives the physical and electrical properties of the glasses used. Twelve different glasses are added to CeO_2 initially and the variation of sintering temperature, density and microwave dielectric properties with different weight percentage of glasses (up to 5 wt%) are studied. Table 7.1 gives the sintering temperature, density and microwave dielectric properties of CeO_2 fluxed with different weight percentage of BS, AS, BBS, MBS, LBS, MAS and LMZBS glass frits. The

sintering temperature decreases with the addition of increasing amount of glass frits in ceria. The 5 wt% addition of AS and MAS glass does not further decrease the sintering temperature from 1425 and 1400°C respectively. The 0.5 wt% of glass fluxed CeO₂ gives the maximum density and best microwave dielectric properties. With higher amount of glass addition, density is decreased and microwave dielectric properties get deteriorated. Hence we did not study the effect of higher amount of BS, AS, BBS, MBS, LBS, MAS and LMZBS glass frits on the microwave dielectric properties of CeO₂. Five glasses (B₂O₃, ZB, ZBS, PBS and BZBS) were selected for further study since they showed reasonably high *Q* factor and decreased the sintering temperature.

Fig. 7.1 shows the variation of sintering temperature as a function of weight percentage of B₂O₃, ZB, ZBS, PBS and BZBS glass. The undoped ceria has a sintering temperature of 1650°C. The sintering temperature of ceria decreases with the addition of glasses, which becomes significant for glass content greater than 5 wt%. Addition of 0.2 wt% of B₂O₃, ZB, ZBS, PBS and BZBS, lowers the sintering temperature to 1625, 1600, 1575, 1600 and 1550°C respectively. Addition of 20 wt% of B₂O₃, ZB and PBS and 12 wt% of ZBS lowers the sintering temperature to about 900°C whereas addition of 10 wt% BZBS lowers the sintering temperature to 950°C. Thus the sintering temperature is significantly decreased by the addition of the above glasses. Further increase in the glass content had no effect on the sintering temperature. It is known³ that boron based glasses are more effective in lowering the sintering temperature and this is due to the low softening temperature of B₂O₃ (450°C). The lowering of sintering temperature of ceria by the addition of ZB, ZBS and PBS glass is due to their low softening temperatures (610, 582 and 442°C respectively). The sintering temperature of BZBS glass added CeO₂ could not be decreased below 950°C since the melting point of BZBS glass is 950°C.

Table 7.1 Table showing the sintering temperature, density and microwave dielectric properties of pure and glass fluxed CeO₂ ceramics

Glass Code	Amount of glass (wt%)	Sintering Temperature (°C) for 4 h	Density (g/cm ³)	ϵ_r	$Q \times f$ (GHz)	τ_f (ppm/°C)
Pure CeO ₂	0.0	1650	6.82	23.0	60200	-53
BS	0.2	1625	6.11	20.9	20000	-56
	0.5	1575	6.20	21.3	34000	-53
	1.0	1425	5.48	17.6	32250	-49
	5.0	1400	5.02	16.0	10000	-47
AS	0.2	1600	6.11	20.0	18500	-53
	0.5	1525	6.20	20.5	39650	-54
	1.0	1425	5.68	19.2	28750	-59
	5.0	1425	5.09	18.6	9500	-63
BBS	0.2	1625	5.68	14.8	8000	-46
	0.5	1525	5.77	15.5	20400	-47
	1.0	1400	4.92	15.1	15400	-48
	5.0	1250	4.67	10.8	8700	-50
MBS	0.2	1600	5.81	18.2	31000	-55
	0.5	1525	6.07	18.8	34100	-52
	1.0	1375	5.25	15.8	21350	-49
	5.0	1250	4.60	14.9	9350	-44
MAS	0.2	1600	5.92	19.5	14300	-48
	0.5	1525	6.09	20.5	32000	-50
	1.0	1400	5.57	18.2	16000	-51
	5.0	1400	5.20	13.8	6400	-53
LBS	0.2	1625	5.99	19.8	38500	-51
	0.5	1575	6.09	20.4	43600	-52
	1.0	1450	5.34	17.0	33150	-62
	5.0	1375	4.80	16.3	9450	-57
LMZBS	0.2	1625	5.94	19.7	16300	-50
	0.5	1550	6.12	20.7	37000	-55
	1.0	1400	5.30	17.0	31000	-57
	5.0	1375	4.85	14.5	8600	-59

Fig. 7.2 (a) and (b) shows the shrinkage of CeO₂+20 wt% B₂O₃ and CeO₂+10 wt% BZBS respectively. The sample sintered with B₂O₃ shrinks at a slightly lower temperature than that added with BZBS glass. The onset of shrinkage occurs below 700 and 800°C for B₂O₃ and BZBS added CeO₂ samples respectively. The shrinkage is complete only beyond 1000°C for B₂O₃ and BZBS added CeO₂ samples.

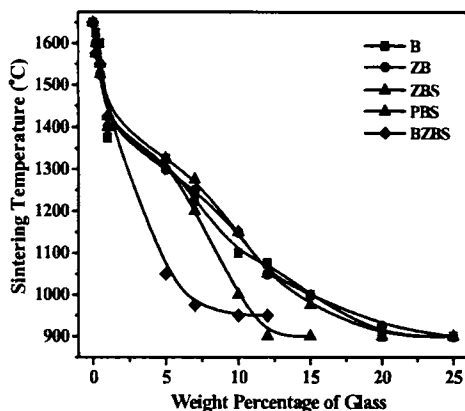


Fig. 7.1 Variation of sintering temperature as a function of weight percentage of B, ZB, ZBS, PBS and BZBS glass additives

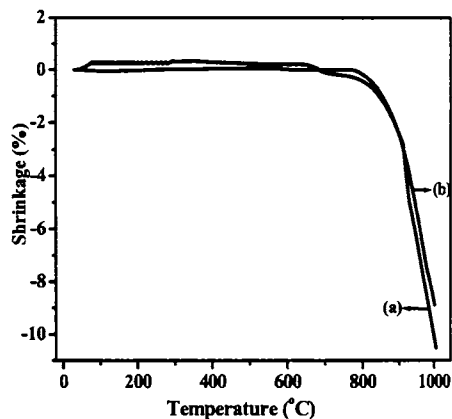


Fig. 7.2 The shrinkage curves of CeO_2 fluxed with (a) 20 wt% B_2O_3 and (b) 10 wt% BZBS

7.1.3.2 Phase Analysis

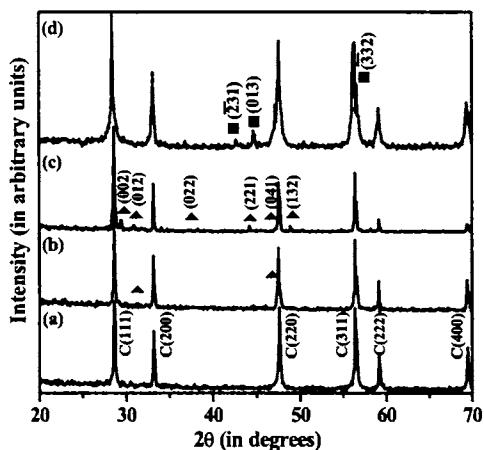


Fig. 7.3 Powder X-ray diffraction patterns of (a) 1 wt% (b) 5 wt% (c) 10 wt% BZBS and (d) 20 wt% B_2O_3 added CeO_2 ceramic, C- CeO_2 , \blacktriangle - CeBO_3 , \blacksquare - $\text{Ce}(\text{BO}_2)_3$

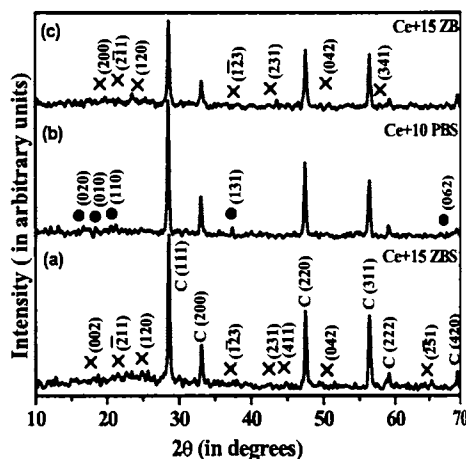


Fig. 7.4 Powder X-ray diffraction patterns of (a) 15 wt% ZB (b) 10 wt% PBS and (c) 15 wt% ZB added CeO_2 ceramic, C- CeO_2 , \times - CeZnB_2O_5 , \bullet - PbB_4O_7

Figs. 7.3 (a)-(c) show the XRD patterns of 1, 5 and 10 wt% BZBS added CeO_2 ceramics. The XRD pattern of 1 wt% BZBS added CeO_2 ceramic did not show any additional peak. New peaks of CeBO_3 [JCPDS Card No. 21-0177] are found in the XRD

pattern when further amount of BZBS (≥ 5 wt%) is added to CeO_2 . The amount of CeBO_3 has increased with increasing amount of BZBS in CeO_2 . $\text{Ce}(\text{BO}_2)_3$ phase [JCPDS Card No. 23-0877] coexists with the CeO_2 phase in the XRD pattern of 20 wt% B_2O_3 added CeO_2 ceramic (Fig. 7.3(d)). Figs. 7.4(a)-(c) show the XRD pattern of 15 wt% ZBS, 10 wt% PBS and 15wt% ZB added CeO_2 ceramic. The new peaks corresponding to CeZnB_2O_5 [JCPDS Card No. 86-1884] are found in the XRD pattern of 10 wt% ZB and 15 wt% ZBS added ceramic whereas peaks of PbB_4O_7 [JCPDS Card No. 15-078] are found in the XRD profile of 10 wt% PBS added CeO_2 ceramic.

7.1.3.3 Microstructural Analysis

The variation in microstructures of different compositions of BZBS and B_2O_3 added CeO_2 ceramic sintered at different temperatures could be observed from SEM photographs. Pure CeO_2 ceramic sintered at $1650^\circ\text{C}/4\text{h}$ exhibits a dense microstructure and has faceted grains of large size up to $40\ \mu\text{m}$ (Fig. 7.5(a)). SEM micrographs of 0.5, 5 and 10 wt% BZBS added CeO_2 ceramic sintered at 1550, 1050 and 950°C respectively are shown in Figs. 7.5(b)-(d). Figs. 7.5(e) and (f) illustrate the SEM micrographs of 0.5 and 20 wt% B_2O_3 added CeO_2 ceramic sintered at 1600 and 900°C respectively. 0.5 wt% BZBS and B_2O_3 doped CeO_2 ceramic shows a relatively dense microstructure with no secondary phases. At 5 and 10 wt% BZBS additions, elongated BZBS phase appeared in the SEM micrograph. Many of these elongated grains are found to be hollow. At the end of these tubular grains, they have hexagonal shape, hollow core with a diameter of 2-3 μm , length of about 12-25 μm and wall thickness of 0.5-1 μm . Microstructure of 10 wt% BZBS added CeO_2 ceramic shows typical characteristics of LTCC, where ceramics are distributed in the matrix of dense glass.³⁵ Presence of $\text{Ce}(\text{BO}_2)_3$ secondary phase is confirmed from the SEM picture of 20 wt% B_2O_3 added CeO_2 . Flake like grains seen in the SEM picture are of $\text{Ce}(\text{BO}_2)_3$. The main requirement for liquid phase sintering to occur is that the liquid phase should wet the grains of the ceramics. Generally, the chemical reaction between sintering aids and ceramics can provide the best wetting condition, with the formation of secondary phase.³⁶ The addition of 10 and 20 wt% BZBS

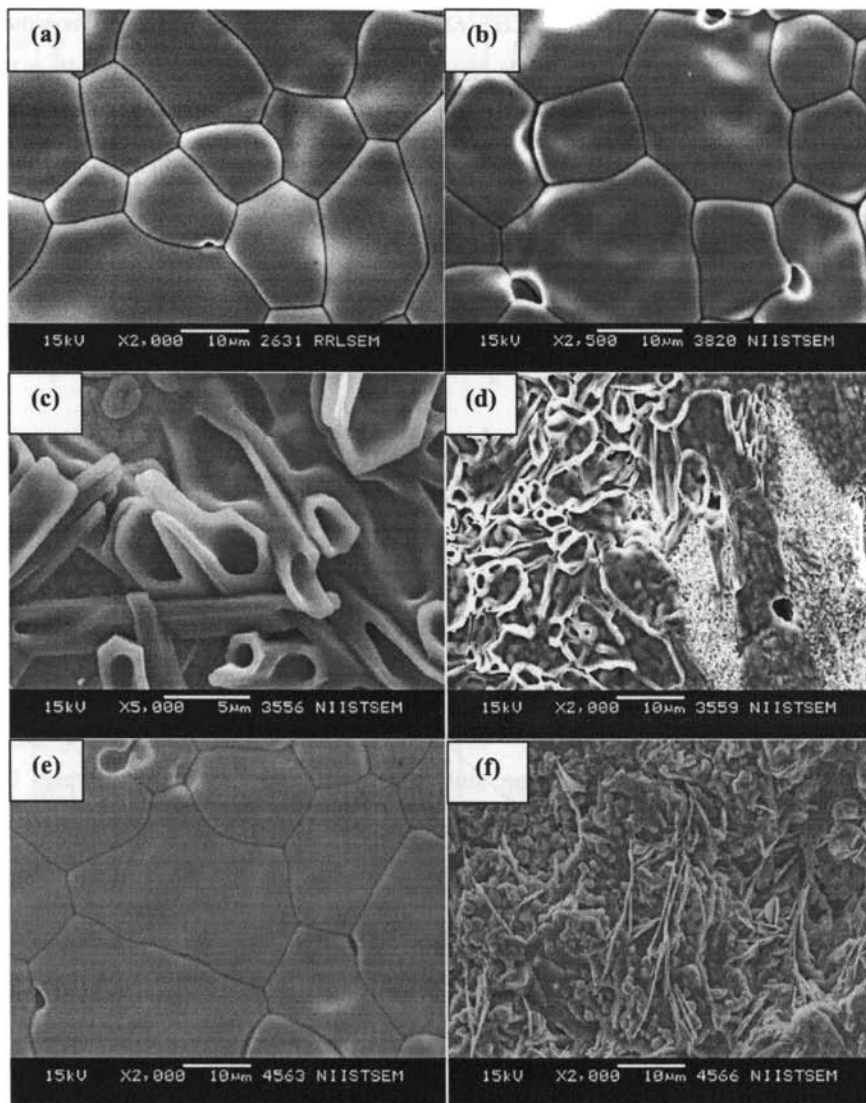


Fig. 7.5 SEM micrographs of (a) CeO_2 sintered at $1650^\circ\text{C}/4\text{h}$ (b) 0.5 wt% BZBS added CeO_2 sintered at $1550^\circ\text{C}/4\text{h}$ (c) 5 wt% BZBS added CeO_2 sintered at $1050^\circ\text{C}/4\text{h}$ (d) 10 wt% BZBS added CeO_2 sintered at $950^\circ\text{C}/4\text{h}$ (e) 0.5 wt% B_2O_3 added CeO_2 sintered at $1600^\circ\text{C}/4\text{h}$ (f) 20 wt% B_2O_3 added CeO_2 sintered at $900^\circ\text{C}/4\text{h}$

and B_2O_3 to CeO_2 enhanced the porosity and the relatively large pores seem to result from the coalescence of originally small pores.³⁷ As the weight percentage of BZBS and B_2O_3

increases, the size of ceria grain decreases. The size of CeO_2 grain is about 10-20 μm , 2-4.5 μm and 0.5-1.5 μm for 0.5, 5 and 10 wt% BZBS addition respectively. Similar trend of reduction in grain size from 20-33 μm (for 0.5 wt%) to 1-1.8 μm (for 20 wt%) is observed for B_2O_3 added ceramic. These results are in agreement with the report of Corker *et al.*³⁸ indicating that a liquid phase sintering produces a smaller grain size than a solid-state sintering process. This decrease in size of the grains with the addition of glass is also due to the low sintering temperature of glass added ceramic compared to that of pure specimen.³⁹

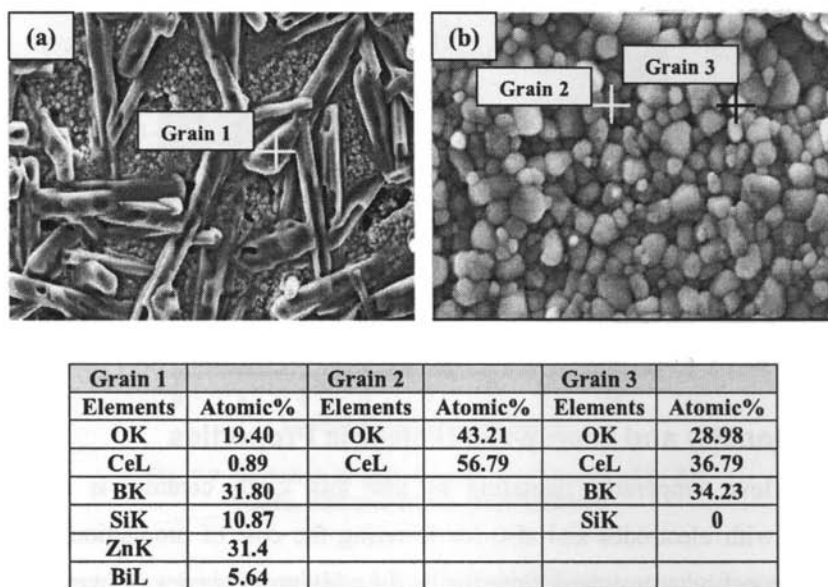


Fig. 7.6 EDXA Spectrum of 5 wt% BZBS added CeO_2 sintered at 1050°C/4h

Fig. 7.6 shows the EDXA spectrum of 5 wt% BZBS added CeO_2 ceramic. The EDXA data of elongated grain show that the cation composition is close to 5.64% Bi, 31.8% B, 10.87% Si and 31.4% Zn (the ideal is 35%, 27%, 6%, 32%). Elongated grains are of BZBS phase with some Bi^{2+} (Melting point of Bi_2O_3 is 825°C)⁴⁰ evaporated due to the high sintering temperature of 5 wt% BZBS added CeO_2 (1050°C). Fig. 7.6(b) shows the enlarged portion of the hexagonal shaped grains. The EDXA data of small round

shaped grains confirms the presence of CeBO_3 phase which is evident from XRD. Similarly, Fig. 7.7 shows the EDXA spectrum of 20 wt% B_2O_3 added CeO_2 ceramic sintered at $900^\circ\text{C}/4\text{h}$. The EDXA data shows that the cationic composition of CeO_2 grain is Ce (47.15 %) and that of flake like $\text{Ce}(\text{BO}_2)_3$ grain is Ce (20.31 %) and B (59.12 %).

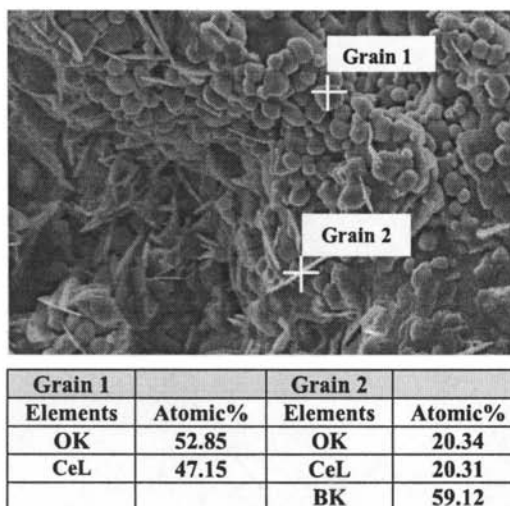


Fig. 7.7 EDXA Spectrum of 20 wt% B_2O_3 added CeO_2 sintered at $900^\circ\text{C}/4\text{h}$

7.1.3.4 Density and Microwave Dielectric Properties

The low temperature sintering of low loss CeO_2 ceramic is important for cosintering with electrodes and also for lowering the cost of production. This can be achieved through vitreous phase sintering by the addition of glasses. But excess addition of glass has been proven to degrade the dielectric properties of the ceramic although the sintering temperature is lowered. Introducing a glassy material into matrix plays a pivotal role in controlling the phase evolution and densification phenomena. As a typical case, the behavior of percentage density and microwave quality factors of CeO_2 mixed with 0.5 wt% BZBS glass as a function of sintering temperature is shown in Fig. 7.8. The density increases with sintering temperature, reaches a maximum (6.48 g/cm^3) at 1550°C and then decreases with further increase in temperature. This variation in density is due to the evaporation of the glass and the resulting trapped porosity associated with

grain growth at higher temperatures.⁴¹ The relationship between quality factor and sintering temperature shows the similar trend as the relationship between density and sintering temperature. Maximum quality factor of 69500 GHz (at 5.92 GHz) is obtained at a sintering temperature of 1550°C. At low sintering temperatures, the microwave quality factors are low due to the poor densification. The samples sintered at temperatures higher than 1550°C show a decrease in quality factor and is attributed to the lowering of density and associated porosity.

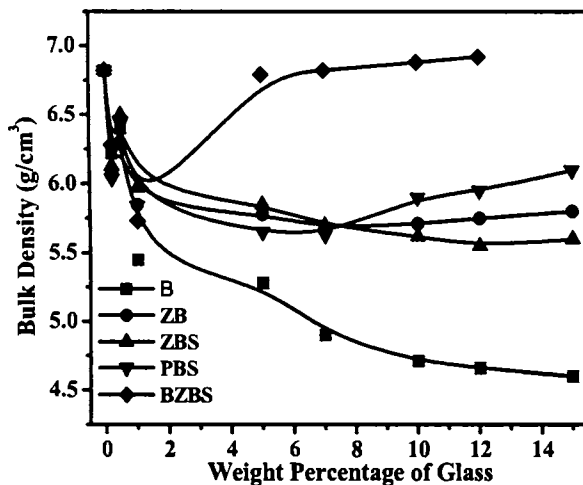


Fig. 7.9 Variation of bulk density as a function of B, ZB, ZBS, PBS and BZBS glass additives

The densities of various glass added CeO_2 at different compositions is shown in Fig. 7.9. Density of CeO_2 increases for addition of glasses up to 0.5 wt%. The density decreases as the weight percentage of glasses increases beyond 0.5 wt%. This is due to the relatively low density of the glasses as given in Table 1.2 of Chapter 1. B_2O_3 has the lowest density of 2.46 g/cm^3 and BZBS has a density of 4.34 g/cm^3 . Low contact angle, low dihedral angle and high solubility of the solid in the liquid are essential for achieving high sintered density in glass added ceramics. In such cases, the transient glassy phase formed at a lower temperature would act as a short circuit medium for grain to grain materials transport.⁴² The primary glass B_2O_3 is regarded as a typical glass network

former that has a lower glass transition temperature.⁴³ The density then starts increasing at 10, 15, 10 and 5 wt% for ZB, ZBS, PBS and BZBS glasses respectively. This increase in density is due to the formation of high density secondary phases as a result of higher weight percentage of glass addition. Maximum density of 6.92 g/cm^3 is obtained for 12 wt% BZBS added CeO_2 ceramic. Moreover, the density of $\text{Ce}(\text{BO}_2)_3$, CeZnB_2O_5 , PbB_4O_7 and CeBO_3 phases formed due to the addition of B_2O_3 , ZB, ZBS, PBS and BZBS glasses are respectively 4.43, 4.41, 5.87 and 5.46 g/cm^3 .⁴⁴ The densities of the secondary phases formed are higher than the respective glasses used (see Table 1.2 in Chapter 1).

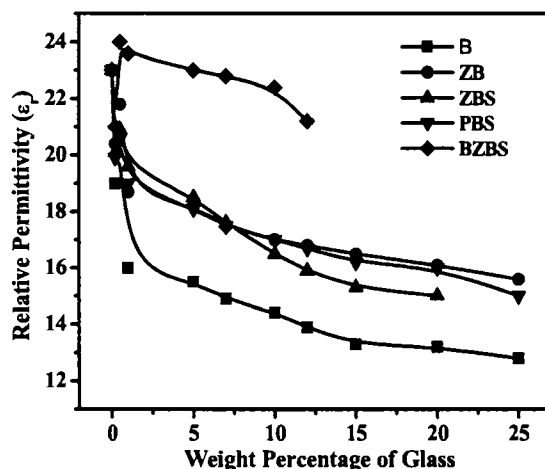


Fig. 7.10 Variation of ϵ_r as a function of B, ZB, ZBS, PBS and BZBS glass additives

The undoped CeO_2 sintered at 1650°C has $\epsilon_r = 23$, $Q_{\text{ext}}f = 60200 \text{ GHz}$ and $\tau_f = -51 \text{ ppm}^\circ\text{C}$. Fig. 7.10 shows the variation of relative permittivity with different wt% of glass added CeO_2 . The relative permittivity depends on the density and phase constituents.⁴⁵ The relative permittivity shows a maximum value for 0.5 wt% of glass added CeO_2 . The increase of the relative permittivity is attributed to improved densification due to liquid phase sintering.⁴⁶ The relative permittivity decreases with the addition of higher amount of glass frits due to the lower permittivity of glass flux compared to pure CeO_2 (see Table 1.2 in Chapter 1). The low relative permittivity of secondary phases formed due to B_2O_3 , ZB, ZBS, PBS and BZBS addition may also attribute to the decrease in permittivity. It is

generally agreed that a non wetting glassy network leads to porosity and hence the densification will be lower if the solubility of the ceramic in the liquid phase is poor. The relative permittivity of 20 wt% ZB, 12 wt% ZBS and 20 wt% PBS added ceramic sintered at 925, 900 and 900°C are 16.1, 15.9 and 16 respectively. Maximum relative permittivity (22.4) is obtained for 10 wt% BZBS added ceramic sintered at 950°C and minimum value (13.2) for 20 wt% B₂O₃ added CeO₂ ceramic sintered at 900°C. The glass forming oxide B₂O₃ have the lowest relative permittivity and most additional oxides produce increase in ϵ_r .¹⁸

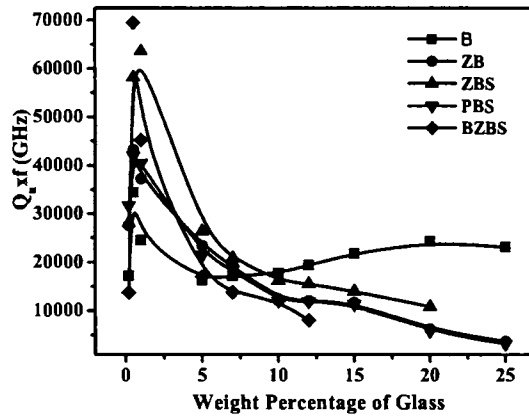


Fig. 7.11 Variation of $Q_r \times f$ as a function of B, ZB, ZBS, PBS and BZBS glass additives

The microwave dielectric properties of glass added ceramics depend on their density and presence of secondary phases.^{11,47} Fig. 7.11 shows the variation of quality factor as a function of different amount of glass additives. The maximum quality factor for the glasses at 0.5 wt% is due to the good densification obtained for this composition. 0.5 wt% BZBS glass added CeO₂ ceramic shows the highest quality factor of 69500 GHz. Small amount of glass addition increases the density and improve the microwave dielectric properties of the host material, because the liquid forming composition enables better pore elimination by enhancing the material transport.⁴⁸ The addition of more than 0.5 wt% of all glasses considerably degrades the quality factor. The addition of excess glass to a ceramic lowers the sintering temperature accompanied by significant

deterioration in the microwave dielectric properties.^{49,38} The quality factor is decreased with higher percentage of glass additives due to the formation of secondary phases. The network formers contained in the glass materials may absorb the microwave power profoundly in high frequency region, degrading the quality factor of the material.¹⁸ Moreover, the grain size of the CeO_2 ceramic decreases with the amount of B_2O_3 and BZBS glass (Figs. 7.5(a)-(f)) and hence the effective grain boundary area increases. Wersing has reported that grain boundaries, secondary phases and dislocations cause losses in real inhomogeneous ceramics.⁵⁰ These losses are caused by either dipole relaxation of impurities concentrated at the interfaces (grain boundaries) or relaxation of space charge polarization present at the interfaces.⁵¹ The quality factor of CeO_2 ceramic with 20 wt% ZB (sintered at 925°C), 12 wt% ZBS (900°C) and 20 wt% PBS (900°C) addition are 6200, 15500 and 5850 GHz respectively. The quality factor for 20 wt% B_2O_3 and 10 wt% BZBS added CeO_2 ceramic sintered at 900 and 950°C are respectively 24200 and 12000 GHz.

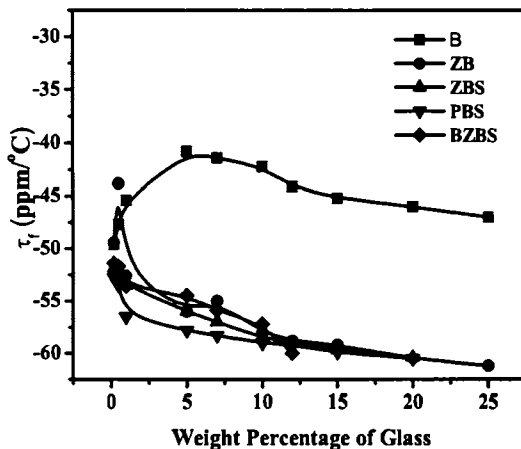


Fig. 7.12 Variation of τ_f as a function of B, ZB, ZBS, PBS and BZBS glass additives

The variation of τ_f as a function of different amount of glass additives is shown in Fig. 7.12. The τ_f of glass added CeO_2 is increasing to the negative side with the addition of glasses except B_2O_3 . This increase in τ_f to the negative side is due to the negative τ_f of

these glasses.^{17,52} With the addition of 5 wt% B_2O_3 to CeO_2 , τ_f shifts to a less negative value $-40.8 \text{ ppm}^\circ\text{C}$ from $-53 \text{ ppm}^\circ\text{C}$ for pure CeO_2 . A similar variation in τ_f value is observed for B_2O_3 doped $0.98CeO_2-0.02CaTiO_3$ ceramics.³¹ The increase in τ_f with the addition of ZB, ZBS, PBS and BZBS glasses are due to the formation of glass based secondary phases. The τ_f of 20 wt% ZB sintered at 925°C , 12 wt% ZBS and 20 wt% PBS added CeO_2 sintered at 900°C are -61 , -59 and $-61 \text{ ppm}^\circ\text{C}$ respectively. The τ_f of 20 wt% B_2O_3 and 10 wt% BZBS added CeO_2 ceramic sintered at 900°C and 950°C respectively are -46 and $-57 \text{ ppm}^\circ\text{C}$. There is no significant improvement in τ_f with the addition of glass frits to CeO_2 ceramic.

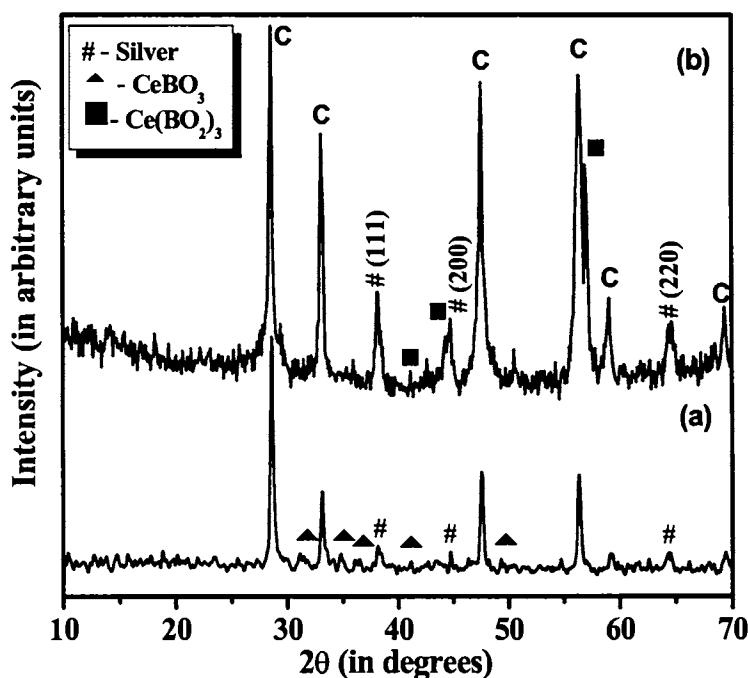


Fig. 7.13 X-ray diffraction patterns of 20 wt% silver added (a) CeO_2 fluxed with 10 wt% BZBS (sintered at $950^\circ\text{C}/4\text{h}$) and (b) CeO_2 fluxed with 20 wt% B_2O_3 (sintered at $900^\circ\text{C}/4\text{h}$)

For co-firing applications, the glass ceramic composite should not react with the common electrode materials such as silver. Figs. 7.13 and 7.14 show the XRD patterns and SEM micrographs of 20 wt% silver added CeO_2 with 10 wt% BZBS and 20 wt%

B_2O_3 sintered at 950°C and 900°C for 4 h respectively. The powder diffraction patterns of Ag were indexed based on JCPDS File Card Number 4-0783. Fig. 7.15 shows the EDXA spectrum of 20 wt% Ag added CeO_2 fluxed with 20 wt% B_2O_3 sintered at $900^\circ\text{C}/2\text{hrs}$ (Ag marked in Fig. 7.14 (b)). The EDXA data of 20 wt% silver added CeO_2 with 10 wt% BZBS (Ag marked in Fig. 7.14 (a)) is Ag (93.34 at%). It is worth to note from these figures that silver remains unreacted with the ceramic-glass composites, which is one of the requirements for LTCC.

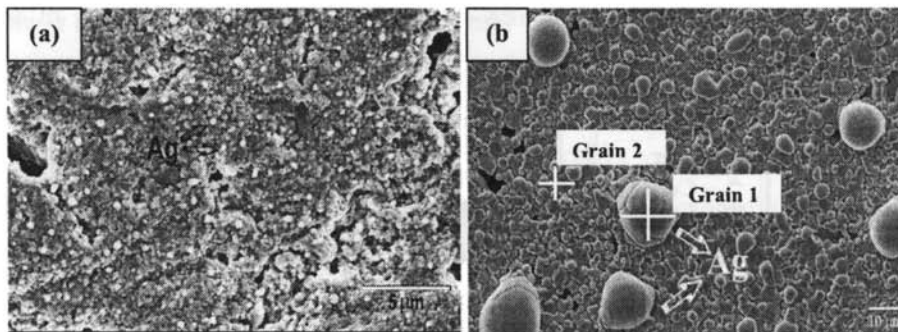
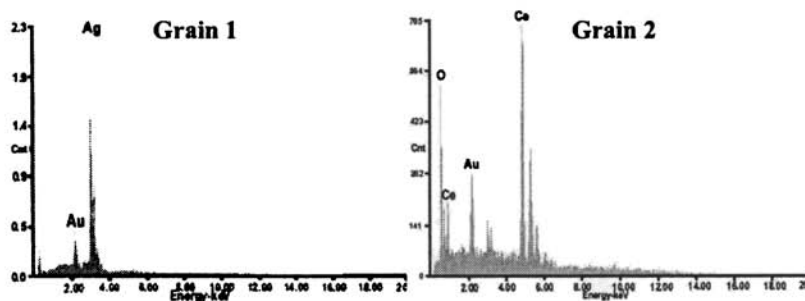


Fig. 7.14 SEM Micrographs of 20 wt% silver added (a) CeO_2 fluxed with 10 wt% BBSZ (sintered at $950^\circ\text{C}/4\text{h}$) and (b) CeO_2 fluxed with 20 wt% B_2O_3 (sintered at $900^\circ\text{C}/4\text{h}$)



Grain 1		Grain 2	
Elements	Atomic%	Elements	Atomic%
AgL	93.31	OK	54.71
AuM	6.39	AuM	2.04
		CeL	43.25

Fig. 7.15 EDXA Spectrum of 20 wt% silver added CeO_2 fluxed with 20 wt% B_2O_3 (sintered at $900^\circ\text{C}/4\text{h}$)

Addition of BS, AS, BBS, MBS, LBS, MAS and LMZBS glass frits although lowered the sintering temperature of CeO_2 ceramics, the dielectric properties are very much degraded. From the above analysis made on the glass added CeO_2 ceramics, it is concluded that 10 wt% BZBS and 20 wt% B_2O_3 added CeO_2 are good candidates for low temperature cofired ceramic applications.

7.2 POLYMER-CERIA COMPOSITES FOR MICROWAVE SUBSTRATE APPLICATIONS

7.2.1 Introduction

High density large scale integrated packaging technologies have been developed for high performance and high functionality of communication electronic devices such as cellular phones and wireless personal digital assistants (PDAs). The microelectronics industry is driven by advances in integrated circuit (IC) technology and hence electronic packaging has advanced in all aspects to meet the interconnection needs of ICs. Materials used in microelectronic packaging have to simultaneously fulfill diverse requirements, like low dielectric loss, low relative permittivity, moderate moisture absorption resistance, a low coefficient of thermal expansion, high dimensional stability and mechanical stiffness.⁵³ Electrical characteristics of the microelectronic devices such as signal attenuation, propagation velocity and cross talk, are influenced by the dielectric properties of the package substrate and encapsulation material.⁵⁴ A low dielectric constant minimizes capacitive coupling as well as signal delay and low dielectric loss reduces signal attenuation along with better device performance.^{55,56}

Thermal considerations in the electronic package have become increasingly important because integration of transistors has resulted in the escalation of power dissipation as well as an increase in heat flux at the devices. Hence the desire for improving thermal properties of materials for electronic component parts is getting stronger and the material performance has become a critical design consideration for packages.⁵⁷ Historically, metal components in integrated circuit packages have provided thermal paths for the removal of heat; however, this mechanism has reached its maximum

potential. As a result, the polymeric materials in the components are increasingly important as thermal paths for the removal of excess heat that builds up. Unfortunately, polymeric materials are inherently poor thermal conductors, and they must be modified to assist in heat removal from electronics^{58, 59, 60}.

Ceramic powder reinforced polymer materials have been extensively used as packaging substrates.^{61,62} These are generally comprised of micron-scale inorganic particulate fillers mixed with a polymer matrix. Polymers and ceramics represent the extremes in electrical and thermal performance of packaging materials. Button *et al.*⁶³ proposed composite strategies combining ceramic and polymer matrices to achieve a superior property balance. Fillers can improve the mechanical,^{64,65} thermal,^{66,67,68} optical and electrical properties^{69,70,71} of a polymeric material. Ceramic-polymer composites form a potential material group suitable for producing demanding and functional packages that combine the electrical properties of ceramic and the mechanical flexibility, chemical stability and low temperature processing possibilities of polymers.^{72,73,74} Moreover, the relative permittivities of filled composites can be varied over a wide range by the choice of the shape, size and connectivity of the constituents in the polymeric matrix.^{75,76}

Fluoropolymeric materials are the most desirable polymer matrix for flexible substrate fabrication due to their superior high frequency electrical properties and excellent temperature and solvent resistance. Among fluropolymers polytetrafluoroethylene (PTFE) is the most preferred host matrix for packaging and substrate applications because of its very low relative permittivity ($\epsilon_r \sim 2.3$), extremely low loss ($\tan \delta \sim 10^{-4}$ at 1 MHz), excellent chemical resistance, easy machinability and good dimensional stability.⁷⁷ PTFE has a high virgin crystalline melting point (342°C), and extremely high shear viscosity (10^{11} Poise at 380°C) in the melt.⁷⁸ However, disadvantages of PTFE substrate include a high linear coefficient of thermal expansion (> 100 ppm/°C) and low surface energy.⁷⁹ The other disadvantages are the difficulty in processing PTFE-based laminates and the relatively high filler loading required for preparing dimensionally stable PTFE composites.^{80,81} A substantial amount of work has

been reported to modify the dielectric and thermal properties of various polymer/ceramic composites for packaging applications.^{82,83,84} Recently, Chen *et al.*⁸⁵ reported the microwave dielectric properties of PTFE-SiO₂ composite and due to its low dielectric constant ($\epsilon_r = 4$) it cannot be used for the miniaturization of microwave devices. Price *et al.*⁷⁸ reported the thermal conductivity of PTFE and PTFE composites. PTFE based composites involving high dielectric constant (~ 100) low loss ceramics are reported earlier.⁸⁶

The use of high density polyethylene (HDPE) by the communications industry as the dielectric in submarine cables encouraged us to investigate the effect of CeO₂ filler loading on the microwave dielectric properties of HDPE-CeO₂ composites. Polyethylene is a non-polar polymer which has a melting temperature of approximately 160°C.⁷⁷ Due to its excellent characteristics such as very low dielectric constant ($\epsilon_r \sim 2.6$), low dielectric loss ($\tan \delta \sim 10^{-4}$ at 1 MHz) better chemical resistance and insulating properties, HDPE has significant applications as an engineering material. Krupa *et al.*⁸⁷ studied the thermal and mechanical properties of polyethylene-graphite composites. The effects of boron nitride content, particle size of HDPE and temperature on the thermal conductivity of HDPE-boron nitride composites have been investigated.⁸⁸ There are reports on the processing and mechanical properties of multiwalled nanotube (MWNT)-HDPE composites.⁸⁹ The effect of material parameters and processing conditions on the foam morphologies and mechanical properties of HDPE-clay nanocomposites have been studied by Jo *et al.*⁹⁰ Even though the mechanical properties of HDPE composites are well studied, less attention has been paid to its electrical and thermal properties.

For electronic packaging and substrate applications, low ϵ_r (< 25) ceramics having low dielectric loss are preferred. TeO₂ has a relative permittivity of 19 but it is very expensive and hence not cost-effective.⁹¹ The Sr₂Ce₂Ti₅O₁₆ composite based on PTFE has a high dielectric loss of 0.01-0.15 (for 0.1-0.6 V) at 7 GHz and is not suitable for substrate applications.⁹² Ceria possess good dielectric and thermal properties. It has a relative permittivity of 23, dielectric loss of $\sim 10^{-4}$ at 7 GHz, thermal conductivity of 12 W/m°C and thermal expansion coefficient of 109 ppm/°C.^{24,93} The present work

investigates the dielectric and thermo-physical properties of PTFE-CeO₂ and HDPE-CeO₂ composites at room temperature for the first time to understand the electrical performance, thermal stability and heat transport performance. The study also discusses the comparison of experimental results with theoretical predictions from well-known models in literature.

7.2.2 Experimental

CeO₂ (99.9%, Indian Rare Earth Ltd., Udyogamandal, India)-PTFE (Hindustan Fluorocarbons, Hyderabad, India) composites were prepared by powder processing technology as explained in section 2.2.1 of Chapter 2. In order to create an active surface for binding with polymer, the fine powder of CeO₂ was mixed with acrylic acid solution for 1 hour and then dried. The dried powder was again treated with 2 wt% tetra butyl titanate. The volume fraction of the filler for a given weight fraction is calculated using the equation

$$V_f = \frac{V_f}{V_f + V_m} = \frac{W_f}{W_f + (\rho_f / \rho_m)(1 - W_f)} \quad (7.1)$$

where V_f and V_m are the volume of filler and matrix respectively. W_f , ρ_f and ρ_m are the weight fraction of filler, density of filler and density of matrix respectively.

Different volume fractions (0 to 0.6) of treated ceramics (CeO₂) and PTFE powders were dispersed in ethyl alcohol using ultrasonic mixer for about 30 minutes. A dry powder mixture was obtained by removing the solvent at 70°C under stirring. This led to the formation of thoroughly mixed PTFE-CeO₂ powders. These homogeneously mixed composite powders were then compacted using a tungsten carbide die under a uniaxial pressure of 50 MPa for 1 minute. The cylindrical (dimensions: 11x1 mm²) and rectangular pellets (dimensions: 25x3x1 mm³) thus obtained were kept at 310°C for 2h.

The HDPE-CeO₂ composites were prepared by sigma-blend technique as explained in section 2.2.2 of Chapter 2. The HDPE is first melted in kneading machine

having sigma blades at 150°C/15 min. Different volume fractions (0 to 0.5) of CeO₂ ceramics were added to the melted polyethylene and blended at 150°C for 30 minutes. Thus obtained composites were thermo laminated using suitable die under a pressure of 200 MPa and 150°C for 15 min using a die. After thermolamination, the composites with desired shapes were polished for characterization.

The density of the composites (ρ) was determined using Archimedes method. The water absorption measurements were conducted following ASTM D570 using disk-shaped specimens having diameter 11 mm and thickness 3 mm. The samples were weighed and submerged in distilled water at 25°C for 24 h. The samples were removed, wiped dry and the amount of water absorbed was calculated based on the weight gain of the samples.

The composites were characterized by X-ray diffraction technique using CuK α radiation and the surface morphology of the composites was studied by Scanning Electron Microscope. The low frequency dielectric properties were measured using an LCR meter. In order to investigate the temperature variation of relative permittivity, these samples were heated in a uniform temperature enclosure from 25–70°C and the corresponding relative permittivities were measured at 1 MHz. The microwave dielectric properties of the sample at the frequency 7 GHz were measured using the cavity perturbation technique using HP 8510 C Network Analyzer^{94,95} as described in section 2.4 of Chapter 2.

The DSC analysis was done by Perkin Elmer DSC 7, Massachusetts, USA. The instrument was computer controlled and calculations were done using Pyris software. 5–10 mg of samples were sealed in aluminum pans and heated from 25°C to 600°C at rate of 5°C/min. and cooled to 25°C at the same rate. Heat treated cylindrical samples of dimensions (diameter = 8 mm and height = 10 mm) were used to measure the coefficient of thermal expansion (CTE) of the PTFE-CeO₂ composites using a thermo-mechanical analyzer in the temperature range 25°C to 270°C. A photopyroelectric (PPE) technique^{96,97} as discussed in section 2.5.4 of Chapter 2 was used to determine the thermal conductivity of the PTFE-CeO₂ composites. Thermal diffusivity (α) and thermal

effusivity (e) were also measured from PPE signal phase and amplitude.⁹⁸ From the values of α and e the thermal conductivity and specific heat capacity of the samples were obtained.

The micromechanical properties of PTFE-CeO₂ composites were measured using micro hardness tester (Clemex Model 4, Germany). Both the surfaces of the samples were polished to have optically flat surface for indentation. The specimen was subjected to a load of 50 g and dwell time of 10 s. For pure ceramic sample the load was increased to 400 g. A total of 8 readings were taken to get the average hardness.

7.2.3 Theoretical Modeling

(a) Relative permittivity

Precise prediction of effective relative permittivity of polymer-ceramic composites is very important for the engineering applications. Composite dielectric is chaotic or is a statistical mixture of several components.⁹⁹ The simple volumetric law of mixing for two component system is given by

$$\varepsilon_{eff} = V_f \varepsilon_f + V_m \varepsilon_m \quad (7.2)$$

where V_f and V_m are the volume fractions and ε_f and ε_m are the permittivities of ceramic filler and polymer matrix respectively and ε_{eff} is the effective permittivity of the composite.

Several quantitative rules^{100,101,102,103} and simulation techniques^{104,105} predict the dielectric behaviour of a composite system based on experimental results and theoretical derivation. In the present study, following equations were used to calculate the effective relative permittivity of low filler content composites:

1. Lichtenecker equation:¹⁰²

$$\ln \varepsilon_{eff} = V_m \ln \varepsilon_m + (1 - V_f) \ln \varepsilon_f \quad (7.3)$$

2. Serial mixing rule:¹⁰⁶

$$\frac{1}{\varepsilon_{eff}} = \frac{V_f}{\varepsilon_f} + \frac{V_m}{\varepsilon_m} \quad (7.4)$$

3. Effective Medium Theory:¹⁰⁶

$$\varepsilon_{eff} = \varepsilon_m \left[1 + \frac{V_f (\varepsilon_f - \varepsilon_m)}{\varepsilon_m + n(1 - V_f)(\varepsilon_f - \varepsilon_m)} \right] \quad (7.5)$$

4. Jayasundare-Smith Equation:¹⁰¹

$$\varepsilon_{eff} = \frac{\varepsilon_m(1 - V_f) + \varepsilon_f V_f \left[\frac{3\varepsilon_m}{\varepsilon_f + 2\varepsilon_m} \left(1 + \frac{3V_f(\varepsilon_f - \varepsilon_m)}{\varepsilon_f + 2\varepsilon_m} \right) \right]}{(1 - V_f) + V_f \left[\frac{3\varepsilon_m}{\varepsilon_f + 2\varepsilon_m} \left(1 + \frac{3V_f(\varepsilon_f - \varepsilon_m)}{\varepsilon_f + 2\varepsilon_m} \right) \right]} \quad (7.6)$$

5. Maxwell-Garnett Equation:¹⁰⁷

$$\frac{\varepsilon_{eff} - \varepsilon_m}{\varepsilon_{eff} + 2\varepsilon_m} = V_f \frac{\varepsilon_f - \varepsilon_m}{\varepsilon_f + 2\varepsilon_m} \quad (7.7)$$

where ε_{eff} , ε_f , ε_m are the relative permittivities of composite, filler and matrix respectively and V_f is the volume fraction of the filler.

In the Effective Medium Theory (EMT) proposed by Rao *et al.*,¹⁰⁶ composites can be treated as an effective medium whose relative permittivity is obtained by averaging over the relative permittivity of the constituents. In EMT model equation (7.5) is used to calculate the effective relative permittivity of the composites. The value of n is determined empirically which is found to be 0.38 for the PTFE-CeO₂ composites. Earlier reports⁸⁹ showed an n value of 0.35 for well-dispersed polymer ceramic composites.

(b) Thermal Conductivity

Determining the thermal conductivity of composite materials is crucial in a number of industrial processes. The effective thermal conductivity of a heterogeneous material is strongly affected by its composition, crystal structure, distribution within the medium and contact between the particles. Numerous theoretical and experimental approaches have been developed to determine the precise value of thermal conductivity.

Comprehensive review articles have discussed the applicability of several models that appear to be more promising.^{108,109,110}

For a two component composite, the simplest model would be with the materials arranged in either parallel or series with respect to heat flow, which gives the upper or lower bounds (also referred to as Weiner bounds) of effective thermal conductivity.¹¹¹ In the present study, following models were used to calculate the effective thermal conductivity of polymer-ceramic composites:

1. Geometric Mean Model:

$$k_c = k_f^{V_f} k_m^{1-V_f} \quad (7.8)$$

where k_c , k_f and k_m are the thermal conductivities of composite, filler and matrix respectively and V_f is the volume fraction of the filler in the composite.

2. Effective-Medium Theory (EMT) Model

The Effective-medium theory (EMT) assumes that the composite system is a homogeneous medium and the EMT equation for thermal conductivity can be derived through the Laplace equation for thermal transfer, which can be expressed as^{112,113}

$$V_m \frac{k_m - k_c}{k_m + 2k_c} + V_f \frac{k_f - k_c}{k_f + 2k_c} = 0 \quad (7.9)$$

where V_m is the volume fraction of polymer in the composite and k_c , k_f , k_m , V_f same as in eqn (7.5).

3. Maxwell - Eucken Model

Maxwell, using potential theory¹¹⁴, obtained an exact solution for the conductivity of randomly distributed and non interacting homogeneous spheres in a homogeneous medium and is given by

$$k_c = k_m \left[\frac{k_f + 2k_m + 2V_f(k_f - k_m)}{k_f + 2k_m - V_f(k_f - k_m)} \right] \quad (7.10)$$

4. Cheng - Vachon Model

Based on Tsao's model which gives the thermal conductivity of two phase solid mixture¹¹⁵, Cheng and Vachon assumed a parabolic distribution of the discontinuous phase in the continuous phase. The constants of this parabolic distribution were determined by analysis and presented as a function of the discontinuous phase volume fraction. Thus, the equivalent thermal conductivity of the two phase solid mixture was derived in terms of the distribution function, and the thermal conductivity of the constituents. For $k_f > k_m$,

$$\frac{1}{k_c} = \frac{1}{\sqrt{C(k_f - k_m)[k_m + B(k_f - k_m)]}} \ln \frac{\sqrt{[k_m + B(k_f - k_m)]} + \frac{B}{2}\sqrt{C(k_f - k_m)}}{\sqrt{[k_m + B(k_f - k_m)]} - \frac{B}{2}\sqrt{C(k_f - k_m)}} + \frac{1-B}{k_m} \quad (7.11)$$

where

$$B = \sqrt{\frac{3V_f}{2}} \quad C = -4\sqrt{\frac{2}{3V_f}}$$

(c) Coefficient of Thermal Expansion (CTE)

Thermal expansion coefficients of composites are very important in relation to the dimensional stability and the mechanical compatibility when used with other materials. A considerable amount of work has been done to predict the thermal expansion coefficients of composites.^{116,117,118} The rule of mixtures serves as the first-order approximation to the overall calculation of the co-efficient of thermal expansion of the composite.¹¹⁹ This can be expressed as

$$\alpha_c = V_f \alpha_f + (1 - V_f) \alpha_m \quad (7.12)$$

where α_c , α_m and α_f are coefficient of thermal expansion of the composite, matrix and filler respectively. Turner developed a model that takes into account the mechanical interaction between different materials in the composite.¹²⁰ Based on the assumption that all phases in the composite have the same dimension change with temperature, he derived a relationship which is expressed as

$$\alpha_c = \frac{(1-V_f)B_m\alpha_m + V_f B_f \alpha_f}{(1-V_f)B_m + V_f B_f} \quad (7.13)$$

where B_f , B_m are Bulk Modulus of filler and matrix respectively. Schapery developed a model to predict the upper and lower bounds of the CTE of a composite.¹²¹ The two bounds are given by

$$\alpha_c^l = \alpha_m + \frac{B_f}{B_c^u} \frac{(B_m - B_c^u)(\alpha_f - \alpha_m)}{(B_m - B_f)} \quad (7.14)$$

$$\alpha_c^u = \alpha_m + \frac{B_f}{B_c^l} \frac{(B_m - B_c^l)(\alpha_f - \alpha_m)}{(B_m - B_f)} \quad (7.15)$$

where superscript “u” and “l” refer to the upper and lower bounds, respectively. It can be seen that the upper and lower bounds as calculated from the Hashin-Shtrikman model are used to calculate the lower and upper bounds in the Schapery model. Hashin and Shtrikman model¹²² assumes a homogeneous and isotropic reference material in which the constituents are dispersed. Depending on whether the stiffness of the reference material is more or less than that of the reinforcement, the lower and upper bounds are calculated as:

$$B_c^u = B_f + \frac{1-V_f}{\frac{1}{B_m - B_f} + \frac{3V_f}{(3B_f + 4G_f)}} \quad (7.16)$$

$$B_c^l = B_m + \frac{V_f}{\frac{1}{B_f - B_m} + \frac{3(1-V_f)}{(3B_m + 4G_m)}} \quad (7.17)$$

where G_f and G_m represents the Shear Modulus of filler and polymer respectively.

7.2.4 Results and Discussion

7.2.4.1 Densification and Microstructural Analysis

The density of a two-component mixture should depend on the densities of the ingredients and also on their volume percentage. Fig. 7.16 (a) and (b) depicts the

measured and theoretical densities of PTFE-CeO₂ and HDPE-CeO₂ composites respectively as a function of volume fraction. The density is measured using Archimedes method and compared with the mixing rule¹²³

$$\rho_{eff} = V_f \rho_f + V_m \rho_m \quad (7.18)$$

where ρ_{eff} , ρ_f , ρ_m are the densities of composite, filler and matrix respectively. The experimental values for lower volume fractions agree well with the theoretical values for PTFE-CeO₂ composites.

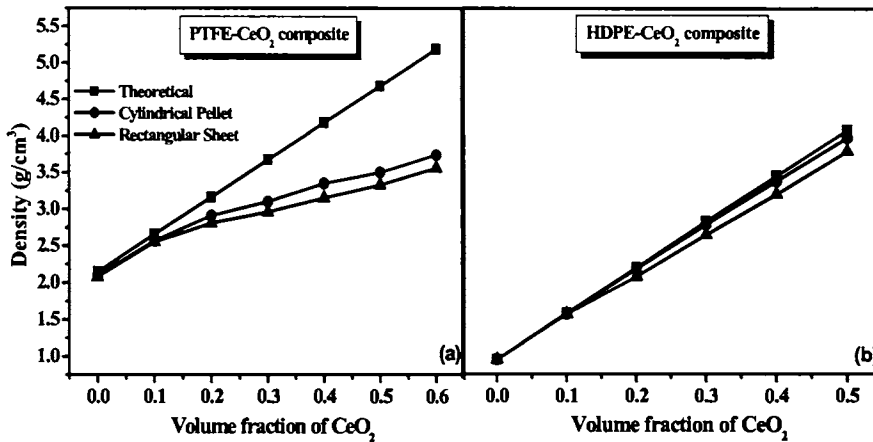


Fig. 7.16 Variation of density with volume fraction in (a) PTFE-CeO₂ composites (b) HDPE-CeO₂ composites

In the case of HDPE-CeO₂ composites, the experimental and theoretical values agree well for all volume fractions. The measured densities of both cylindrical pellet and rectangular sheet increase with filler content due to the higher density of CeO₂. The deviation of measured densities from theoretical values increases with the filler content for both PTFE and HDPE composites. For cylindrical pellets of PTFE-CeO₂ composites, the deviation of 0.29% for 0.1 V_f suddenly increases from 0.2 V_f onwards and reaches a maximum value of 19% for 0.6 V_f . This may be due to the increase in void formation inside the composite for higher filler content. In HDPE-CeO₂ composites, the deviation increases from 0.44% for 0.1 V_f to 2.4% for 0.5 V_f . The densification of PTFE-CeO₂ composites is found to be 96.6% for 0.1 V_f filler loading which decreases with filler

content and reaches a value of 71% with 0.6 V_f filler. The percentage deviation of relative density is less for HDPE composites compared to PTFE composites. This may be due to the difference in the method of preparation of composites. The relative density varies from 99.4 to 97.5% as the volume fraction of HDPE-CeO₂ increases from 0.1 to 0.5 V_f CeO₂ loading. For cylindrical samples, a maximum deviation of 2.5% is obtained for 0.5 V_f of HDPE based composites.

Table 7.2 The theoretical, experimental density and volume of air in PTFE-CeO₂ and HDPE-CeO₂ composites

V_f of CeO ₂	PTFE					HDPE				
	ρ_{eff} (g/cm ³)	ρ_{exp} (g/cm ³)	V_{CeO_2} (vol%)	V_{PTFE} (vol%)	Porosity (%)	ρ_{eff} (g/cm ³)	ρ_{exp} (g/cm ³)	V_{CeO_2} (vol%)	V_{PTFE} (vol%)	Porosity (%)
0.0	2.15	2.10	0.0	97.70	2.4	0.95	0.948	0.0	99.80	0.2
0.1	2.66	2.57	9.68	87.12	3.4	1.58	1.57	9.94	89.42	0.6
0.2	3.16	2.91	18.4	73.60	8.0	2.2	2.18	19.82	79.27	0.9
0.3	3.67	3.04	24.8	58.00	17.2	2.83	2.79	29.58	69.01	1.4
0.4	4.18	3.25	31.2	46.70	22.1	3.45	3.38	39.08	58.89	2.03
0.5	4.68	3.45	36.9	36.90	26.3	4.08	3.98	48.75	48.75	2.50
0.6	5.19	3.69	42.6	28.40	29.0					

Assuming that there are three phases in the composite- matrix, filler and air, volume fraction of air in the composite can be calculated by equation¹²⁴

$$\rho_{eff}(1-V) + \rho_{air}V = \rho_{exp} \quad (7.19)$$

where V is the volume fraction of air in the composites, ρ_{eff} , ρ_{air} , ρ_{exp} are the theoretical densities of composite, density of air and experimental densities of composites respectively. Table 7.2 shows the theoretical density, experimental density and porosity, of the composites with varying filler content for PTFE and HDPE based composites. It can be seen that the porosity of the composites increases with the volume fraction of CeO₂ in both types of composites. A similar variation of porosity is reported by Xiang *et al.*¹²⁵ for SrTiO₃-POE composites.

Table 7.3 and 7.4 gives the water absorption values of PTFE and HDPE composites respectively. The water absorption values of PTFE based composites are higher than that of HDPE based composites. A maximum value of 1.55% is obtained for 0.6 V_f PTFE-CeO₂ and 0.52% for HDPE-CeO₂ composites respectively.

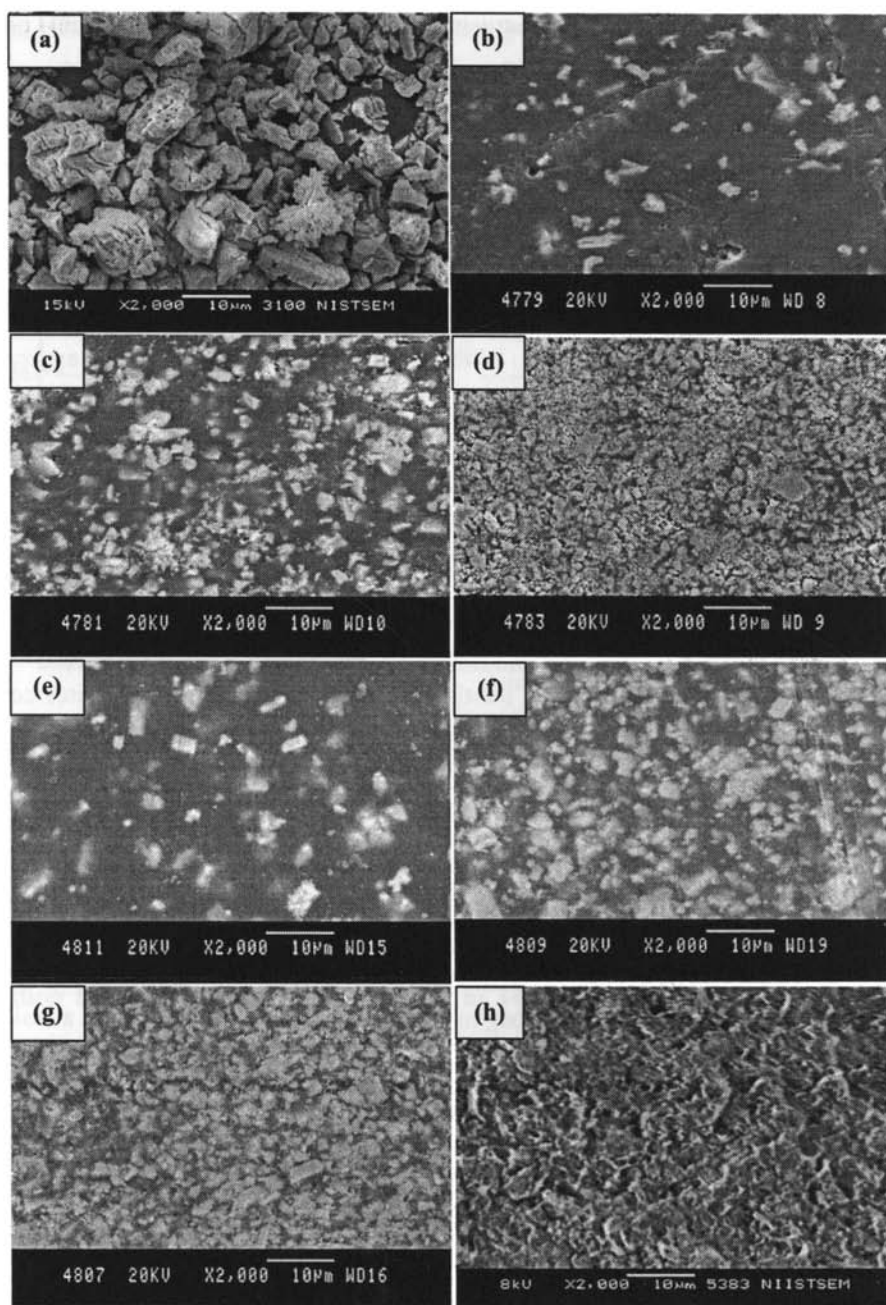


Fig. 7.17 SEM micrographs of (a) CeO₂ powder (b) 0.1 V_f (c) 0.3 V_f (d) 0.6 V_f PTFE-CeO₂ composites and (e) 0.1 V_f (f) 0.3 V_f (g) 0.5 V_f (h) fractured surface of 0.3 V_f HDPE-CeO₂ composites

Fig. 7.17 (a) shows the microstructure of heat treated and ground CeO_2 powder used in the present study. The size of the CeO_2 powder is approximately 2-5 μm . The surface morphology and filler distribution are studied using Scanning Electron Microscope and the results of PTFE composites ($V_f = 0.1, 0.3, 0.6$) are shown in Figs. 7.17(b)-(d) and of HDPE composites ($V_f = 0.1, 0.3, 0.5$) are shown in Figs. 7.17(e)-(g). The micrographs reveal that the CeO_2 particles are uniformly distributed throughout the PTFE and HDPE matrix. For higher volume fractions ($V_f = 0.3, 0.5$) of the composites, there is aggregation of CeO_2 particles. With the increase of filler content, the aggregation of ceramic particles increases (Fig. 7.17(d)) in both PTFE and HDPE composites. The increase in porosity of the composite with the volume fraction of CeO_2 is due to the aggregation of ceramic particles in the continuous PTFE matrix. For higher mixing ratios the connectivity among the ceramic particles increases, which in turn improves the properties. The connectivity of the individual components is important since it controls the electric flux pattern as well as mechanical and thermal properties.¹²⁵ Comparison of SEM micrographs of similar volume fractions of PTFE and HDPE composites confirm that the porosity is higher for PTFE based composites. Fig. 7.17(h) shows the fractured surface of 0.3 V_f HDPE- CeO_2 composite. The higher densification of HDPE- CeO_2 composite is confirmed from the microstructure of 0.3 V_f HDPE- CeO_2 composite.

7.2.4.2 Thermal Analysis

The TGA measurements of PTFE- CeO_2 composites show that the heat resistance of PTFE is very good. The polymer begins to decompose around 530°C and a residue is observed at 600°C which corresponds to the CeO_2 content as shown in Fig. 7.18(a). Table 7.3 lists the decomposition temperature (T_d) of PTFE- CeO_2 composites for different filler contents of CeO_2 . It shows that the total mass loss values are in good agreement with the amount of CeO_2 originally mixed into the different volume fractions of PTFE- CeO_2 samples and the decomposition temperature was not affected by the CeO_2 content. This is due to the unreactive nature of PTFE matrix with CeO_2 . Fig. 7.18 (b) shows the TGA measurements of HDPE- CeO_2 composites. The TGA measurement of

virgin HDPE shows that it starts decomposing around 280°C and decomposition is complete around 500°C. The decomposition temperature of pure HDPE is around 347°C, which increases with CeO₂ loading and reaches 453°C for 0.5 V_f i.e., the thermal stability is improved with filler concentration. The total mass loss values obtained from TGA are in agreement with the amount of CeO₂ originally mixed into HDPE-CeO₂ samples and are given in Table 7.4.

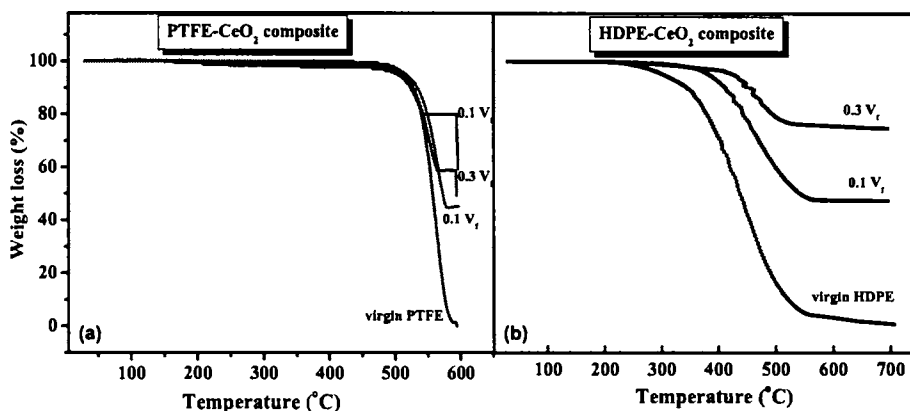


Fig. 7.18 TGA curves of (a) PTFE-CeO₂ composites (b) HDPE-CeO₂ composites

A typical DSC thermogram of 0.3 V_f CeO₂ - reinforced PTFE is shown in Fig. 7.19 (a) in which two peaks appear at 19.9°C and 327.3°C, respectively, in the heating mode. The melting point of PTFE is around 325–335°C and it has several first or second order transition temperatures ranging from –110 to 140°C.¹²⁶ PTFE shows low-temperature phase transitions at about 19 and 30°C at atmospheric pressure.¹²⁷ The crystal structure of PTFE is triclinic at temperatures below 19°C and above that temperature the unit cell changes to hexagonal. The three-dimensional register of chain segments gets lost in the temperature range of 19–30°C and the preferred crystallographic orientation disappears.¹²⁸ Therefore, the result suggests that the CeO₂ filled PTFE composites absorb heat to change the crystal formation at 19.9°C and melt at 327.3°C.¹²⁶ The sample also get re-crystallized by cooling from the molten state so as to observe the crystallization temperature T_c . The crystallization behavior of materials is characterized using

crystallization temperature, T_c and the onset crystallization temperature, T_o . Filler induced changes in T_i , T_m , T_o and T_c of virgin PTFE and PTFE-CeO₂ composites are determined using DSC in the temperature range 0-350°C (see Table 7.3). Both endothermic and exothermic curves of PTFE-CeO₂ composites are similar to those of pure PTFE. T_i , T_m , T_o and T_c of the PTFE-CeO₂ composites are very similar to those of pure PTFE, which implies that the existence of the CeO₂ filler has no effect on the melting and crystallization behavior of PTFE. This is due to the chemical inertness of the PTFE matrix with CeO₂ and the resultant very weak interface between the matrix and the filler.

Table 7.3 Summary of data obtained via TGA and DSC measurements for virgin PTFE and PTFE-CeO₂ composites

Composition of PTFE-CeO ₂	CeO ₂ content ^a W_f^a	CeO ₂ content ^b W_f^b	T_d (°C)	T_i (°C)	T_m (°C)	T_o (°C)	T_c (°C)	Water absorption (%)
100-0	0.0	0.0	529	20.1	328.5	316.2	312.5	0.53
90-10	27.0	25.0	528	19.2	326.4	317.4	313.7	0.72
80-20	45.6	44.8	530	19.8	327.2	316.8	312.8	0.87
70-30	59.0	59.0	529	19.9	327.3	316.7	312.5	0.95
60-40	69.0	68.5	528	19.6	327.5	317.1	313.3	1.05
50-50	77.0	76.0	530	19.5	326.5	316.7	312.6	1.36
40-60	83.0	80.0	527	19.0	326.2	316.9	312.1	1.55

{ T_d is the temperature at which 10 wt% of the sample is lost after heating in nitrogen atmosphere by TGA, T_i is the first order transition temperature, T_m is the melting temperature, T_c is the temperature of crystallization, T_o is the onset crystallization temperature. W_f^a is the weight fraction of CeO₂ content in the PTFE-CeO₂ composite, W_f^b is the weight fraction of CeO₂ content in the PTFE-CeO₂ composite by TGA.}

Table 7.4 Summary of data obtained via TGA and DSC measurements for virgin HDPE and HDPE-CeO₂ composites

Composition of HDPE-CeO ₂	CeO ₂ content ^a W_f^a	CeO ₂ content ^b W_f^b	T_d (°C)	T_m (°C)	T_o (°C)	T_c (°C)	Water absorption (%)
100-0	0	0	347	130.1	119.2	115.6	0.20
90-10	45.7	47.9	427	130.8	119.2	115.6	0.21
80-20	65.5	44.8	438	130.2	118.9	115.4	0.25
70-30	79.4	76.6	450	130.1	118.6	115.5	0.33
60-40	83.5	68.5	452	129.8	118.9	115.3	0.47
50-50	88.4	88.7	453	129.7	118.6	115.2	0.52

Fig. 7.19 (b) shows the DSC curves of different filler loaded HDPE composites in the temperature range 0-300°C. The melting temperature of pure HDPE is 130.1°C and the addition of CeO₂ to virgin HDPE showed no significant effect on the melting point of polymer (Table 7.4). There is no significant change in the T_o and T_c of HDPE composites with filler loading and are given in Table 7.4.

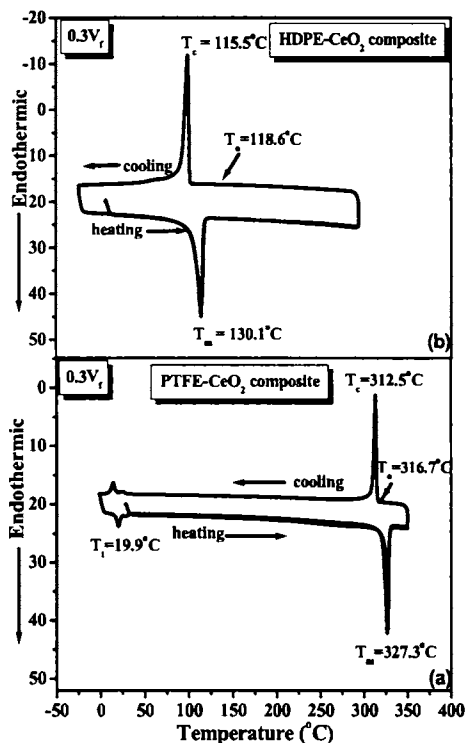


Fig. 7.19 Heating and cooling DSC curves of (a) PTFE-CeO₂ composites (b) HDPE-CeO₂ composites

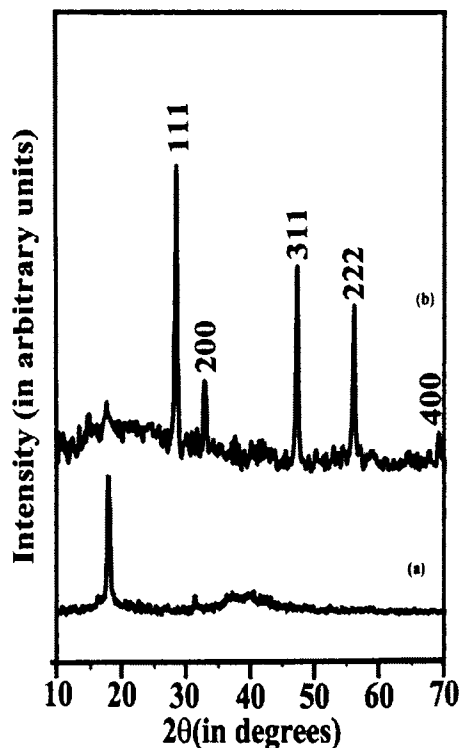


Fig. 7.20 XRD patterns of (a) virgin PTFE (b) 0.3 V_f of PTFE-CeO₂ composite

Figure 7.20 shows the X-ray diffraction of PTFE and 0.3 volume fraction (V_f) PTFE-CeO₂ composite. PTFE is a semi crystalline polymer. The XRD pattern of PTFE shows a strong crystalline peak superimposed over an amorphous halo as reported.¹²⁹ The strong crystalline peak of PTFE is observed at $2\theta = 18^\circ$. The composite (0.3 V_f) was examined with XRD to study any possible interactions with CeO₂ (Fig. 7.20(b)). The

XRD peaks corresponding to CeO_2 are indexed based on JCPDS file no. 34-0394. No unidentified or undesired secondary phases were observed in CeO_2 filler added PTFE.

7.2.4.3 Dielectric Properties

The frequency dependence of relative permittivity of the PTFE and HDPE composites with the different volume fraction of CeO_2 filler is shown in Fig. 7.21 (a) and (b) respectively. CeO_2 and PTFE have relative permittivities of 23 and 2.3 respectively at 1 MHz. In the PTFE- CeO_2 composites of all volume fractions, permittivity remained almost constant in the frequency range 0.5 KHz to 3 MHz. It reveals the good frequency stability of CeO_2 -PTFE composites over a wide frequency range. Devaraju *et al.*¹³⁰ reported a similar observation in BaTiO_3 -polyimide nanocomposite films. In HDPE- CeO_2 composites, at the lower frequency range the relative permittivity decreases with frequency for all volume fractions. It is believed that a decrease in the dipolar polarization of the matrix and the accumulation of charges at the interface between ceramic particles and polymers results in a large scale field distortion.¹³¹ After about 100 kHz, the changes become smaller. Cheng *et al.*¹³² reported similar variation of relative permittivity with frequency for BaTiO_3 -epoxy-resin. The plots of both PTFE and HDPE composites further exhibit that the relative permittivity increases with CeO_2 content.

Fig. 7.22(a) and (b) shows the variation of dielectric loss with frequency for different compositions of PTFE and HDPE composites in the range 0.5 KHz to 3 MHz. For both PTFE and HDPE based composites, at each frequency dielectric loss increases as the concentration of CeO_2 is increased. The increase in dielectric loss for higher volume fraction of the filler is due to the increase in porosity.¹³³ For each volume fraction, the dielectric loss shows a sharp decrease with frequency up to 1 MHz and thereafter the decrease is small and gradual. This means the extent of interfacial polarization is substantially augmented as the frequency is gradually reduced and the CeO_2 is increased, yielding quite a high value of loss at each composition. In polymer composite materials, interfacial polarization is always present because of additives, fillers or even impurities having masses larger than low molecular weight dipoles that make

these systems heterogeneous.¹³⁴ It is known that both relative permittivity and dielectric loss depend on electronic, ionic, dipole-orientation and space charge polarizations. The

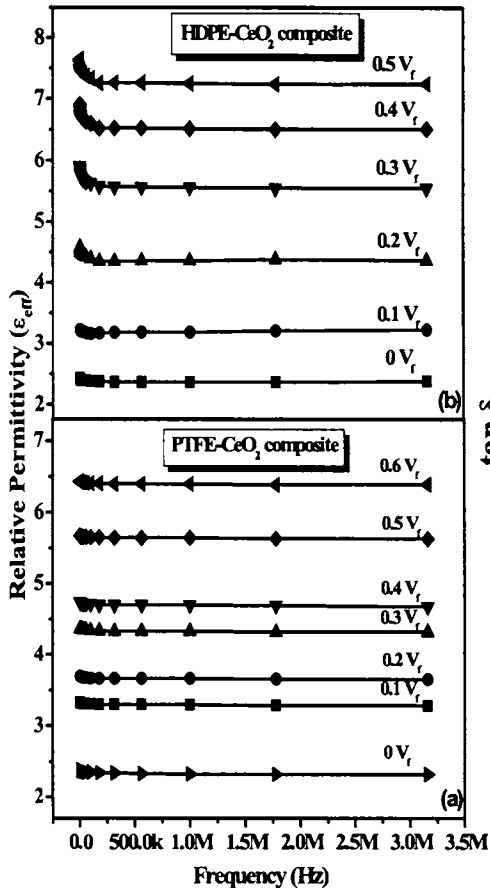


Fig. 7.21 The variation of relative permittivity ϵ_{eff} of different volume fractions of (a) PTFE-CeO₂ composites (b) HDPE-CeO₂ composites with frequency

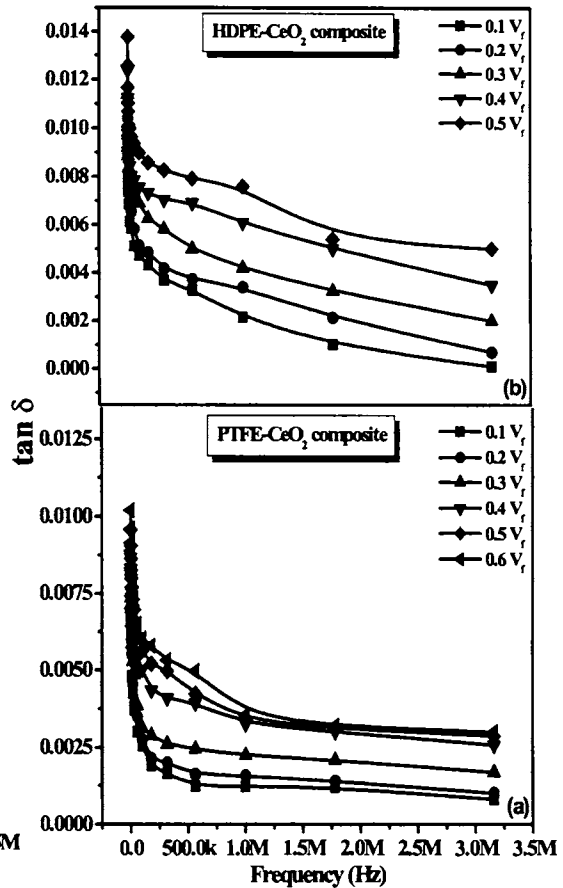


Fig. 7.22 The variation of dielectric loss of different volume fractions of (a) PTFE-CeO₂ composites (b) HDPE-CeO₂ composites with frequency

present system of compact is a biphas mixture of two dielectrically different materials, where ceria is ionic and polycrystalline and PTFE is semi crystalline and non-polar. Such a mixture with a distinct interphase should be appreciably lossy at low frequencies; it has displayed a large space-charge effect owing to Maxwell-Wagner polarization. The dispersion regions become somewhat broader as the amount of CeO₂ is increased for both

PTFE and HDPE composites. Khastgir *et al.*¹³⁵ reported a similar broadening of dispersion curve with titania addition for polystyrene-titania composite.

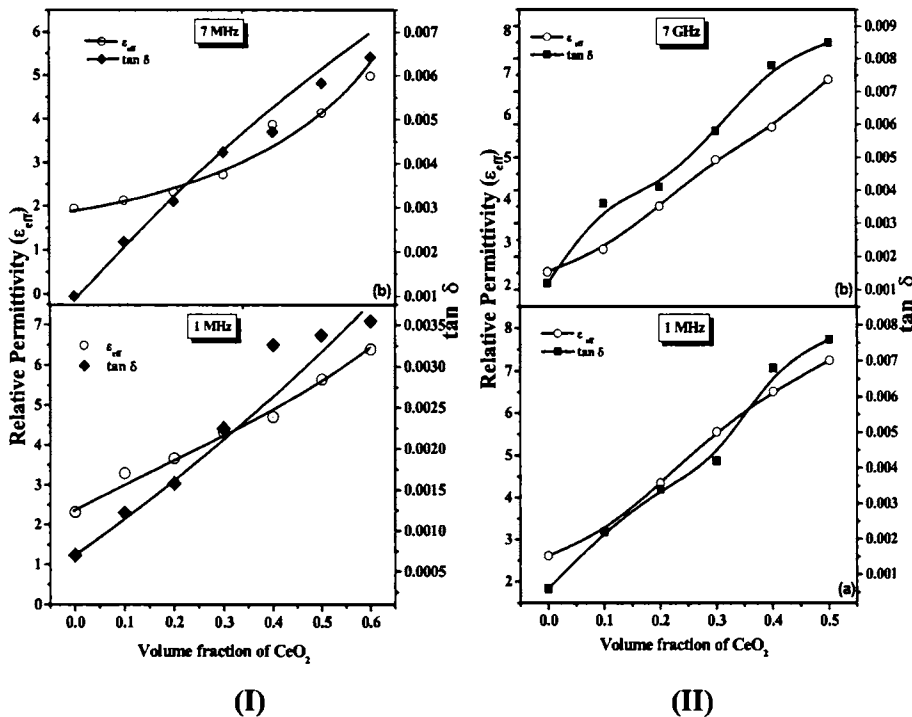


Fig. 7.23 Variation of relative permittivity (ϵ_{eff}) and dielectric loss with volume fraction at 1 MHz and 7 GHz of (I) PTFE-CeO₂ composites (II) HDPE-CeO₂ composites

Fig. 7.23 (I) and (II) show the variation of relative permittivity and dielectric loss at 1 MHz and 7 GHz for both PTFE and HDPE composites. The relative permittivity and dielectric loss increase with the increasing amount of CeO₂ addition both at 1 MHz and 7 GHz. The increase in relative permittivity is expected as the CeO₂ ceramic has higher relative permittivity compared to that of polymer matrix. The dipole-dipole interaction increases and contributes to higher relative permittivities as CeO₂ fillers come closer at higher filler loading (see Fig. 7.17 (c), (d) of PTFE composites and (f), (g) of HDPE composites). The relative permittivity and dielectric loss of HDPE composites are higher than that of PTFE composites. When the CeO₂ is minor and forms a dispersed phase in a

CeO₂-PTFE composite, the relative permittivities of composites are determined mainly by the continuous matrix (ϵ_r of PTFE and HDPE are 2.3 and 2.6 respectively) instead of the minor filler.¹³⁶ The relative permittivity of CeO₂-PTFE composites at 7 GHz (2.1 - 5) is less than that at 1 MHz (3.3 - 6.4) (± 0.2). The dielectric loss of the CeO₂-PTFE composites (0.1 - 0.6 V_f) at 7 GHz (0.0022-0.0064) is higher than that at 1 MHz (0.0012 - 0.0036) ($\pm 1 \times 10^{-4}$). Similarly, the ϵ_{eff} of CeO₂-HDPE (0.1 - 0.5 V_f) composites at 7 GHz and 1 MHz are in the range 2.8-6.9 and 3.2-7.3 respectively. The dielectric loss of these composites is 0.0036-0.0085 (at 7 GHz) and 0.0022-0.0076 (at 1 MHz). The pellets used for low frequency measurements (dimensions: 11x1 mm²) have relatively higher density than the rectangular sheet (dimensions: 25x3x1 mm³) used for microwave measurements. Hence the relative permittivity of samples at microwave frequency is smaller in addition to the difference in the polarization mechanisms. The dielectric loss which is the main factor affecting the frequency selectivity of a material is influenced by many factors such as porosity, microstructure and defects.¹³³ There are defects such as porosity and the interface phase between CeO₂ and PTFE in the composite materials, which can influence the relative permittivity and dielectric loss of composites.¹³⁷ In addition, the increase of CeO₂ amount causes the increase of interphase between CeO₂ and PTFE and hence the influence of interface polarization on the dielectric loss becomes more significant.¹³⁸ Yutao *et al.*¹³⁹ reported that interphase introduced in a polymer matrix by inorganic filler is clear compared to that by polymer blends and interfacial relaxation occurs under field around 50 Hz and cause increased $\tan \delta$. The interphase region is comprised of polymer molecules that are bonded or otherwise oriented at the filler particle interface resulting in unique physical and electrical properties.^{140,141,142} Vo and Shi¹⁴³ model predicts that the effective relative permittivity of a polymer-filled composite material is dependent not only on the relative permittivity of the polymer and filler phases and the concentration of the filler, but also on the relative permittivity of the interphase region and the volume of the interphase region. The interface characteristics that change the relative permittivity of the composite are affected by a change in the filler particle size and/ or surface area or by a change in the chemical structure of the interphase region. Since the chemical

structure of the interphase region is a function of the polymer and its interaction with the surface of the filler particles, a change of the bonding between these two phases will alter the molecular polarizability and hence a change in the effective relative permittivity of the composite.¹⁴⁴ The relative permittivity values of the interphase regions are less than the relative permittivity of either the filler or matrix phases themselves. Polymer orientation or bonding at the surface of the filler eliminates one or more degrees of freedom for movement and alignment of the polymer chains under an applied electric field, which restricts the dipole polarization of the polymer molecules within the interphase region and hence a reduction in the relative permittivity.¹⁴⁵ Todd *et al.*¹⁴⁴ reported that if the relative permittivity of the polymer is less than the relative permittivity of the filler, the effective relative permittivity decreases with decreasing interphase relative permittivity. The volume fraction of the interphase region is dependent upon the volume fraction of the filler which increases as the particle size of the filler decreases due to the increase in surface area of the smaller filler. The chemical structure of the interphase region may be the predominant factor, which affects the relative permittivity of PTFE-CeO₂ system.

The variation in relative permittivity with temperature of the PTFE and HDPE based composites is shown in Fig. 7.24(a) and (b) respectively. It should be noted that the variation in relative permittivity of both PTFE and HDPE based composites are very small. As the temperature increases the relative permittivity decreases. A negative deviation of 0.6 % from the room temperature is observed for 0.1 V_f of PTFE-CeO₂ system. However, as the volume fraction of CeO₂ increases the change in relative permittivity with temperature increases and reaches a maximum value of 1.5 % for 0.6 V_f . In HDPE-CeO₂ system, a percentage deviation of 0.8-2.6 is observed as the volume fraction increases from 0.1-0.5. This slow decrease in relative permittivity with temperature for both the composite systems is due to the large difference in thermal expansion coefficient of polymer (CTE of PTFE is 109 ppm/°C and that of HDPE is 230 ppm/°C)⁸⁵ and CeO₂ filler (12.7 ppm/°C)¹⁴⁶, which would disturb the aggregation of polar components causing a decrease in relative permittivity.^{147,148}

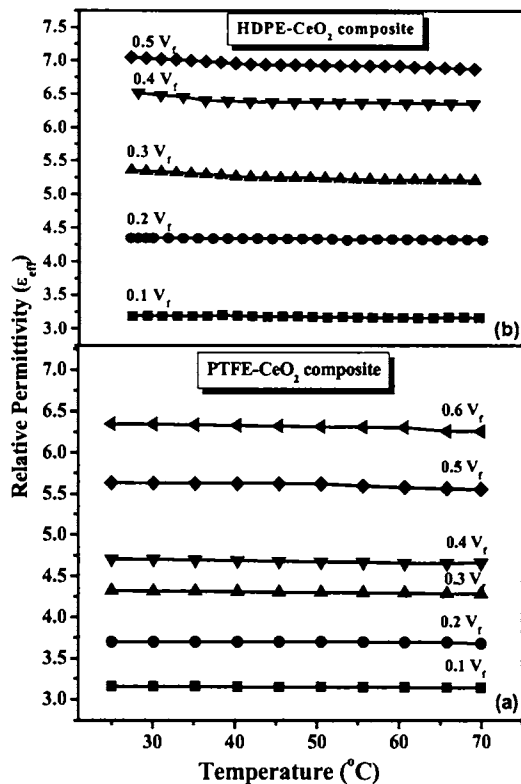


Fig. 7.24 Variation of relative permittivity with temperature for different volume fractions of (a) PTFE-CeO₂ composites (b) HDPE-CeO₂ composite

The predicted values of relative permittivities using equations (7.3)-(7.7) are compared with the experimental results at 7 GHz for PTFE and HDPE based composites and is shown in Fig. 7.25 (a) and (b). In PTFE-CeO₂ composites, it is seen that for lower volume fractions (up to 0.3 V_f), Serial Mixing Model and Maxwell-Garnett Equation holds good and thereafter it deviates from the experimental values. Predicted permittivity using EMT model deviates from the experimental values for PTFE-CeO₂ composites. In HDPE-CeO₂ composites, Litchnecker and Jayasundare-Smith equations are valid up to 0.4 V_f . Maxwell-Garnett and EMT model equations agree with the experimental values for lower volume fractions only. Generally all theoretical predictions are valid for low

filler contents.^{149,150,151,152} This is due to the imperfect dispersion of ceramic particles at higher filler contents and also to the air enclosed by the composites. The complex effective permittivity will depend on the permittivity of each phase in the mixture, their volume fraction, shape and size of the ceramic particle, porosity and interface between components and eventually on the spatial arrangement in the mixture.¹⁵³ Inclusion of all these parameters makes the calculations tedious.

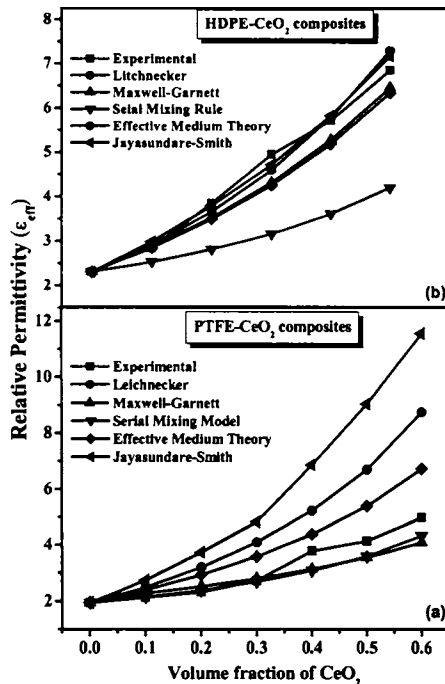


Fig. 7.25 Experimental and predicted ϵ_{eff} of (a) PTFE- CeO_2 composites (b) HDPE- CeO_2 composites at 7 GHz

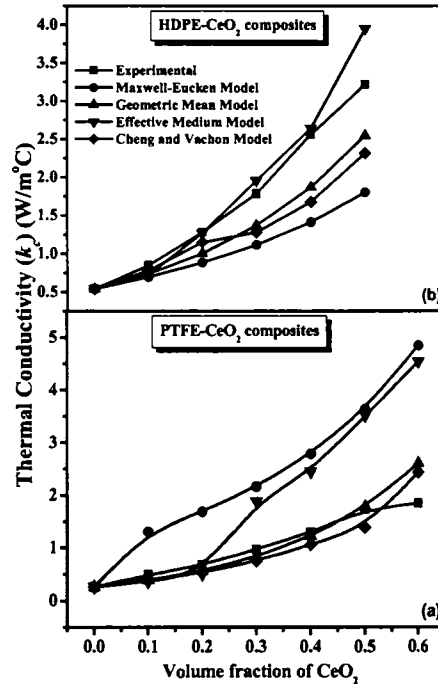


Fig. 7.26 Experimental and predicted k_c of (a) PTFE- CeO_2 composites (b) HDPE- CeO_2 composites

Fig. 7.26(a) and (b) shows comparison of experimental and predicted values of thermal conductivities using equations (7.8)-(7.11) of PTFE- CeO_2 and HDPE- CeO_2 composites with varying filler contents. For both PTFE and HDPE based composites, thermal conductivity increases gradually with CeO_2 filler loading due to the higher

thermal conductivity of CeO_2 (12 $\text{W/m}^\circ\text{C}$). Thermal conductivity is improved to 1.85 $\text{W/m}^\circ\text{C}$ (standard deviation ± 0.01 $\text{W/m}^\circ\text{C}$) for 0.6 V_f from 0.265 $\text{W/m}^\circ\text{C}$ for pure PTFE. In HDPE composites, thermal conductivity increases from 0.54 to 3.22 $\text{W/m}^\circ\text{C}$ as CeO_2 loading increases from $V_f = 0$ to 0.5. This is due to the presence of more connecting path between filler without disturbing the matrix. A similar observation of variation of thermal conductivity was reported by Kim *et al.*¹⁵⁴ in AlN-epoxy composites. Experimental results of PTFE- CeO_2 composites are close to the predictions of Geometric Mean Model and Chen-Vachon Model while for HDPE- CeO_2 composites, EMT model holds good with the experimental values. Predicted thermal conductivity using EMT model holds good for lower volume fractions (up to 0.2 V_f) of PTFE- CeO_2 composites and thereafter it deviates from the experimental values. The EMT model considers the composite system to be homogeneous with an ideal interface. As the volume fraction of the filler increases, the mismatch between the matrix and the filler in the form of interfacial gap becomes serious which is bad for heat conduction.¹⁵⁵ Generally, all theoretical predictions are valid for low filler contents.^{154,156} Agari *et al.*¹⁵⁷ reported that in thermal conduction systems containing a high volume of fillers, particles interact with each other and affect the position of particles in a composite. Hence it is considered that the powder properties of particles (the ease of forming an aggregate of particles, limit of packing etc.) greatly affect the thermal conductivity of the composite. Maxwell-Eucken model predicts values significantly higher than the experimental data in PTFE- CeO_2 composites while in HDPE- CeO_2 composites the values are below experimental data. This difference in values with experimental data is due to the fact that it does not account for differences in morphology or the effects of chain formation. Theoretical models account for variations in the size, shape, intrinsic thermal conductivity and state of dispersion of the filler. The wide variation in filler geometry, orientation and dispersion makes it difficult to compare composites filled with different compounds. Moreover, the interfacial boundary thermal resistance between the filler particles and the matrix referred to as Kapitza resistance¹⁵⁸ is not taken into account while calculating the thermal conductivity of PTFE and HDPE based CeO_2 composites. It is not possible to measure it on the molecular level where it

takes place.¹⁵⁹ Moreover in the theoretical models explained above porosity of the composites is not accounted. As a result, experimental and theoretical thermal conductivity data are often not in agreement.¹⁶⁰

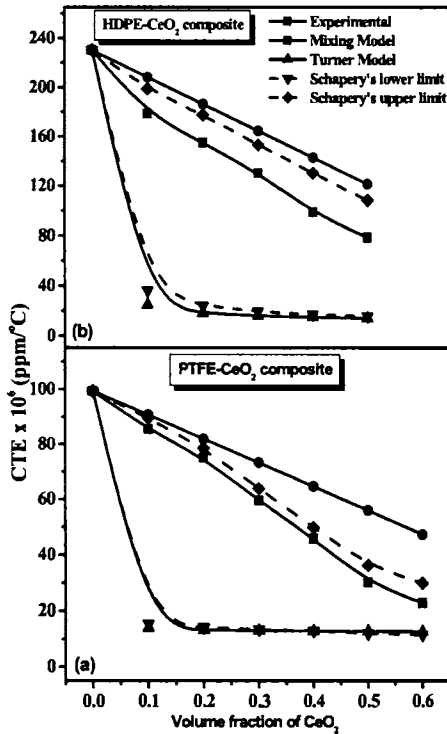


Fig. 7.27 Experimental and predicted thermal expansion coefficients (CTE) of in (a) PTFE- CeO_2 composites (b) HDPE- CeO_2 composite

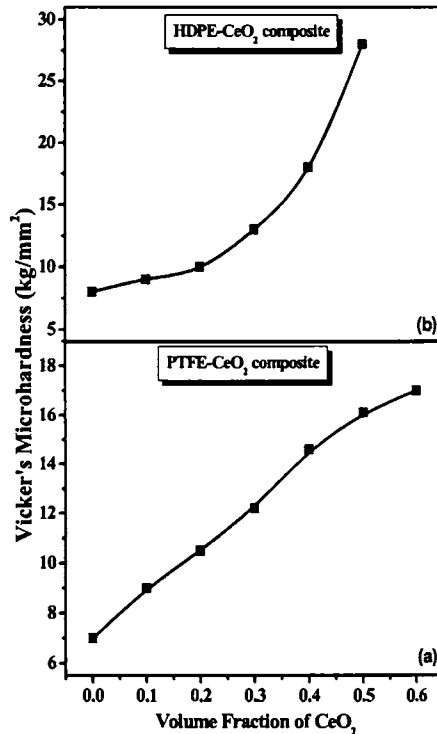


Fig. 7.28 Variation of Vickers microhardness with volume fraction in (a) PTFE- CeO_2 and (b) HDPE- CeO_2 composites

Fig. 7.27(a) and (b) shows the comparison between the experimental data and theoretical models (equations (7.12)-(7.17)) for coefficient of thermal expansion (CTE) of PTFE- CeO_2 and HDPE- CeO_2 composites with varying filler fractions. The CTE decreases with the increasing amount of CeO_2 content for both PTFE and HDPE composites. CeO_2 has CTE of $12.5 \text{ ppm/}^\circ\text{C}$ (Standard deviation, $0.04 \text{ ppm/}^\circ\text{C}$) in the temperature range 25 to 270°C . If a composite is heated, the polymer matrix will expand more than the ceramic fillers. However, if the inter-phases are capable of transmitting

stresses the expansion of the matrix will get reduced.¹⁶¹ CTE is improved to 22.9 ppm/°C from 99.3 ppm/°C (for PTFE) for a filler loading of 0.6 V_f . As V_f increases from 0 to 0.5, CTE varies from 230 to 78.5 ppm/°C. The parameters used for the prediction of CTE are α_m ($\alpha_{PTFE} = 99.3$ ppm/°C and $\alpha_{HDPE} = 230$ ppm/°C), $\alpha_f = 12.58$ ppm/°C, $B_f = 220$ GPa, B_m ($B_{PTFE} = 0.4$ GPa and $B_{HDPE} = 1.46$ GPa), $K_f = 149$ GPa and K_m ($K_{PTFE} = 0.55$ GPa and $K_{HDPE} = 0.30$ GPa). The CTE values calculated using rule of mixtures (equation (7.11)) are slightly higher than the corresponding experimental values for both PTFE and HDPE based composites. This may be due to difference in microstructure, bulk modulus and thermal softening of the components in the composites, which are not accounted in this relation.¹⁶² The values of CTE calculated using Turner equation (7.12) also shows a large deviation from the experimental values for both PTFE and HDPE based composites. It can be seen that in both the composites and for all volume fractions, the CTE obtained lies in between Schapery's upper and lower bounds (equations (7.14) & (7.15)). The deviation from experimental data is smaller for Schapery's upper bound than the lower bounds. Similar variation of CTE is reported by Wong *et al.*¹²⁰ while calculating the CTE values for epoxy resins filled with silica, alumina and aluminum nitride.

Micro indentation with a point indenter involving a deformation on a very small scale is one of the simplest ways to measure the mechanical properties of a polymer composite. Fig. 7.28(a) and (b) shows the variation of micro hardness with CeO₂ filler loading in PTFE and HDPE based composites. Vickers microhardness tests are performed for a range of indentation diagonals. Micro hardness of 700 kg/mm² is obtained for the sintered and dense CeO₂ for a load of 400g. An average Vickers's hardness of 7 and 9 kg/mm² are obtained for virgin PTFE and HDPE respectively. As the volume fraction of CeO₂ loading increases, the hardness also increases in PTFE and HDPE based composites. An increase in hardness to 17 kg/mm² is obtained for 0.6 V_f in PTFE-CeO₂ composite. In HDPE-CeO₂ composite the microhardness obtained is 28 kg/mm² for 0.5 V_f . Optical microscopic images of PTFE and HDPE based composites after indentation are shown in Fig. 7.29(a)-(f).

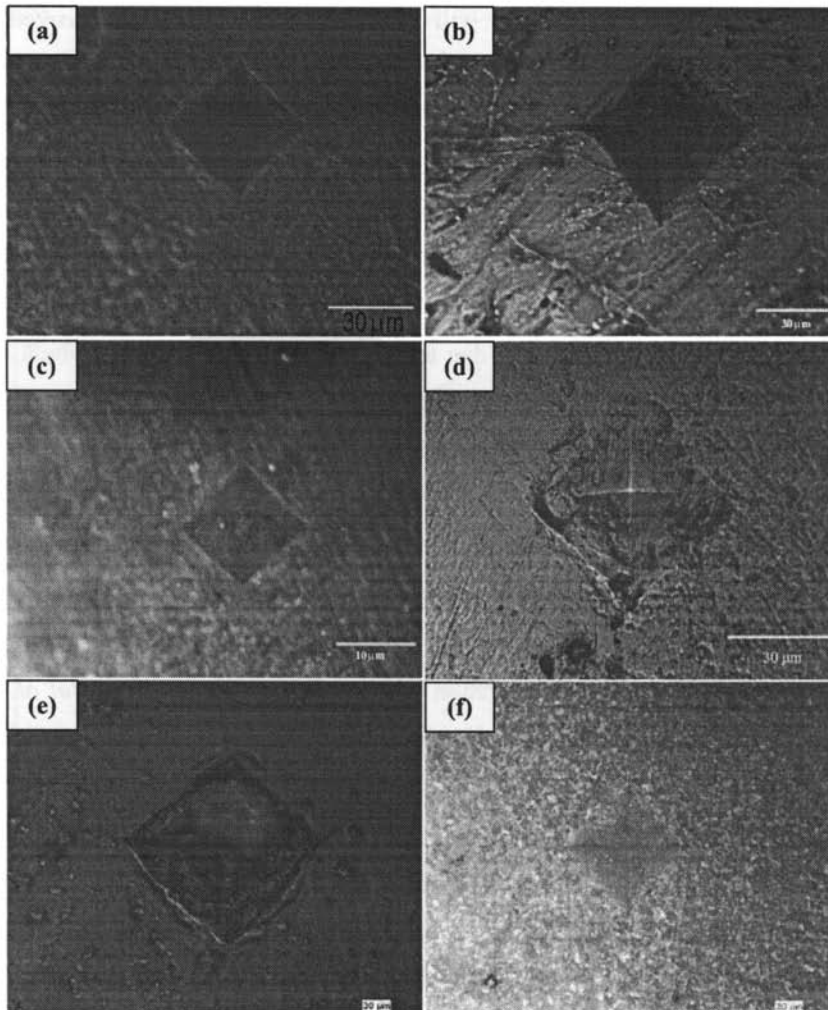


Fig. 7.29 Optical microscopic images of (a) virgin PTFE (b) 0.1 V_f and (c) 0.3 V_f of PTFE-CeO₂ composites (d) virgin HDPE (e) 0.1 V_f (f) 0.3 V_f of HDPE-CeO₂ composites after indentation

Micro hardness determination using the imaging method is a promising technique for the morphology–mechanical property correlations in heterophase systems of known composition.¹⁶³ It is worth to note from the optical micrographs of the composites that CeO₂ particles are well dispersed in the PTFE and HDPE matrix.

Though the dielectric loss and CTE is slightly high for HDPE-CeO₂ composite, it has reasonably good relative permittivity, thermal conductivity and mechanical properties compared to PTFE based composites.

7.3 CERIA-La_{0.5}Sr_{0.5}CoO_{3-δ} COMPOSITES FOR GIANT PERMITTIVITY APPLICATIONS

7.3.1 Introduction

The electronic packaging industry is continuously seeking ways to increase the integration density of printed circuit boards (PCBs) as part of an effort to miniaturize electronic equipments. Towards this goal recent years have witnessed an increasing demand on high relative permittivity materials for its potential application in electrostrictive and embedded passive devices.^{164,165} It is widely known that several high permittivity materials such as Pb(ZrTi)O₃ (PZT),¹⁶⁶ Pb(Mg_{1/3}Nb_{2/3})O₃-PbTiO₃ (PMNT),¹⁶⁷ 50Pb(Ni_{1/3}Nb_{2/3})O₃-35PbTiO₃-15PbZrO₃ (PNN-PT-PZ),¹⁶⁸ are indispensable to modern electronic devices. Lead based ceramics are not environmental friendly and have high dielectric loss compared to low loss ceramics. Moreover, these materials are ferroelectric and have strong temperature dependent properties. A very high relative permittivity with weak temperature and frequency dependency is observed in polycrystalline CuO, which is comparable to those of recently, discovered non-ferroelectric CaCu₃Ti₄O₁₂ and Li and Ti doped NiO ceramics.^{169,170,171,172} Almost all the investigated materials for passive embedded technology are composites.

Electrically percolative composites have attracted much attention because they can possess a high relative permittivity at a critical concentration of fillers and thus can have potential applications as dielectrics for energy storage capacitors and electrostrictive devices. The conductor-insulator composites of several kinds were extensively studied to understand the insulator-conductor transition in percolative networks.^{173,174} There are reports that a certain kind of two-phase composite could improve the dielectric properties.¹⁷⁵ Composites with conducting phases dispersed in an insulating matrix exhibit high permittivity near the percolation limit of the conducting phase. In the

context of high ϵ_r composites several polymer-ceramic,¹⁷⁶ polymer-metal^{167,177} and ceramic-metal composites^{178,179} have been extensively studied. Polymer based composites are flexible and have low processing temperature. However, its permittivity is low compared to ceramic metal composites. Commonly used metallic powders in ceramic metal composites are Al, Ni, Cu, Ag, Pt, Pd. Among these Al, Ni, Cu have oxidation problem and need inert atmosphere at higher sintering temperature. Pt and Pd are too expensive and silver is one of the few metals that can be fired in air at higher temperature without oxidation. But it melts above 960°C and cannot be used at sintering temperatures above 950°C. Generally, ceramic metal composites (cermets) are sintered at the sintering temperature of ceramic. Reports^{180,181} show that silver can diffuse along the open pores and escapes at higher sintering temperature. It is reported that in ceramic silver composite, the sintering temperature has a crucial role in determining the percolation threshold. Hence the sintering temperature of the ceramics should be reduced below the melting point of silver. Another difficulty with cermet composite is that it shows a narrow smearing region and hence difficult to obtain a filler loading close to percolation threshold.

Reports shows that the cubic crystalline $\text{La}_{0.5}\text{Sr}_{0.5}\text{CoO}_{3-\delta}$ (LSCO) ceramic has conductivity (200 S/cm) comparable to that of metals^{182,183,184,185} and avoids the oxidation problems of metal. This motivated us to study the effect of conducting phase $\text{La}_{0.5}\text{Sr}_{0.5}\text{CoO}_{3-\delta}$ (LSCO) on the insulating matrix CeO_2 . As the strontium content of $\text{La}_{1-x}\text{Sr}_x\text{CoO}_{3-\delta}$ perovskite increases, its crystal structure shifts from rhombohedral to cubic (for $x > 0.4$). Cerium oxide has been chosen as the insulating phase due to its good dielectric properties.²⁴ In the present work the electrical properties of CeO_2 -LSCO composites are investigated. The present study reports for the first time the giant permittivity of ceramic-ceramic two phase composite in which one phase is insulating and the other conducting.

7.3.2 Experimental

The samples of CeO_2 -LSCO composites were prepared by the conventional solid-state ceramic route. High purity CeO_2 powder (IRE, 99.9 %) used in the present

investigation was initially heated at 1000°C to remove any volatile impurities. $\text{La}_{1-x}\text{Sr}_x\text{CoO}_{3-\delta}$, $x=0.5$ (LSCO) ceramics were prepared by the conventional solid-state ceramic route as described in section 2.1.2 of Chapter 2. High purity chemicals La_2O_3 (Aldrich, 99.9%), SrCO_3 (Aldrich, 99+%) and Co_3O_4 (Aldrich, 99%) were used as starting powders. Stoichiometric proportions of the chemicals were weighed and ball milled for 24 hours using zirconia balls in distilled water media. The slurry was dried and then calcined for 5 hours at 1100°C. The calcined powder was then ball milled for 24 hours. Different volume fraction of fine LSCO powder were added to the CeO_2 powder and mixed again in distilled water medium. 4 wt % Poly vinyl alcohol solution was then added to the powder, mixed, dried and ground well. The powder was uniaxially pressed into disc shaped pucks of 11 mm diameter and about 1 mm thickness at a pressure of about 100 MPa using a tungsten carbide die. The green compacts were fired at a rate of 5°C/min up to 600°C and soaked at 600°C for 30 minutes to expel the binder. The pellets were sintered in air at temperatures in the range 1050 -1250°C and the dwell time was 2 hours. After sintering, the samples were allowed to cool down to room temperature at the rate of 3°C/min. The samples were then polished to remove surface irregularities.

The densities of the samples were measured by the Archimedes method. The powdered samples were used for analyzing the X-ray diffraction patterns using $\text{CuK}\alpha$ radiation and the surface morphology of sintered samples were studied using a scanning electron microscope. The polished thin pellets were electroded by coating silver on both sides in the form of ceramic capacitors and were used for dielectric measurements using LCR meter (HIOKI 3532-50 LCR Hi TESTER, Japan).

7.3.3 Results and Discussion

7.3.3.1 Densification of CeO_2 -LSCO composites

The synthesizing conditions such as sintering temperature and their durations were optimized for LSCO added CeO_2 ceramics to obtain the best density and dielectric properties. The samples are having good thermal and chemical stability as explained in section 3.3.4 of Chapter 3. The theoretical density of CeO_2 -LSCO composites is

calculated using equation (7.18), section 7.2.4.1. Fig. 7.30 shows the variation of bulk density with sintering temperature for all volume fractions of LSCO added CeO_2 ceramic. The density increases with increase in sintering temperature. The variation in percentage densification with different volume fraction of LSCO added CeO_2 ceramic sintered at 1150 and 1250°C respectively is shown in Fig. 7.31. The percentage densification increases with volume fraction and reaches a maximum value at $V_f = 0.4$ and then decreases. The percentage densification of samples sintered at 1250°C is higher than that sintered at 1150°C. This is due to the increase in grain size and simultaneous reduction in porosity with increase in sintering temperature. The densification of CeO_2 -LSCO composite increases and reaches a maximum at 0.4 V_f and then decreases for samples sintered at 1150 and 1250°C.

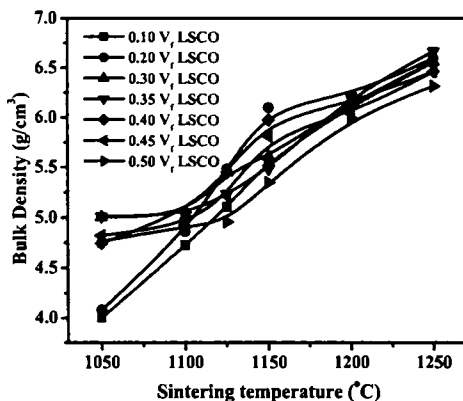


Fig. 7.30 Variation of bulk density with sintering temperature for different volume fraction of LSCO added CeO_2 ceramics

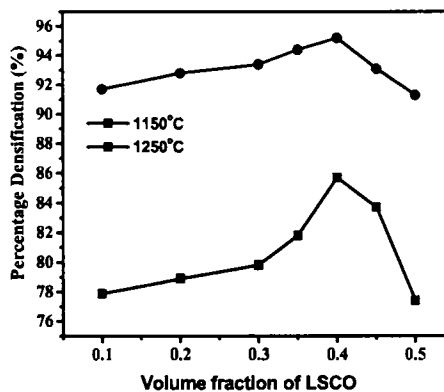


Fig. 7.31 Variation of percentage densification with volume fraction of CeO_2 -LSCO ceramics

7.3.3.2 Phase and Microstructural Analysis

The XRD patterns of LSCO added CeO_2 is shown in Fig. 7.32. The XRD patterns of 0.40 volume fraction (V_f) LSCO added CeO_2 samples sintered at 1150 and 1250°C show that it is a mixture of CeO_2 and LSCO. The XRD patterns of CeO_2 and LSCO are indexed according to ICDD File Nos. 34-0394 and 36-1394 respectively. It is clearly

evident from the XRD pattern of CeO_2 -LSCO samples sintered at 1150 and 1250°C that no additional phases are present.

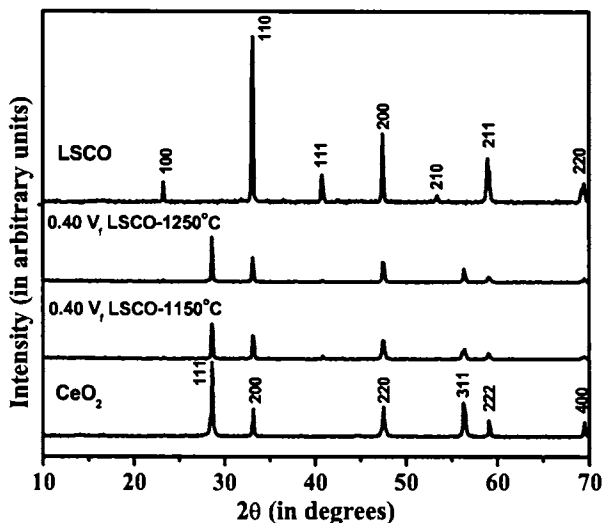


Fig. 7.32 XRD patterns of (a) pure CeO_2 (b) 0.40 V_f CeO_2 -LSCO composite sintered at 1150°C (c) 0.40 V_f CeO_2 -LSCO composite sintered at 1250°C (d) pure LSCO

SEM micrographs of 0.40 volume fraction LSCO added CeO_2 samples sintered at 1150 and 1250°C are shown in Figs. 7.33(a) and (b) respectively. Both the microstructures show two types of grains - brighter contrast is of CeO_2 and darker contrast is of LSCO. The 0.40 V_f LSCO added CeO_2 ceramic sintered at 1150°C shows that the ceramic has a porous microstructure. This is due to the low densification of ceramic at 1150°C (see Fig. 7.31). The grain growth of the sample is observed with increase in the sintering temperature, resulting in the decrease of porosity (Fig. 7.33(b)). The LSCO grain starts melting for the sample sintered at 1250°C. The grain size of pure CeO_2 ceramic sintered at 1650°C/2h is approximately 40 μm (see Fig. 7.5 (a), section 7.1.3.3). For the sample sintered at 1150°C, both CeO_2 and LSCO grains have approximately 0.4-1 μm size and that sintered at 1250°C grain size is approximately 1-3 and 5-10 μm respectively. The reduction in size of CeO_2 grain from 40 to 5-10 μm for sample sintered at 1650 and 1250°C respectively is due to the lower sintering

temperature. The LSCO aids liquid phase sintering and lowers the sintering temperature of CeO_2 -LSCO composite.

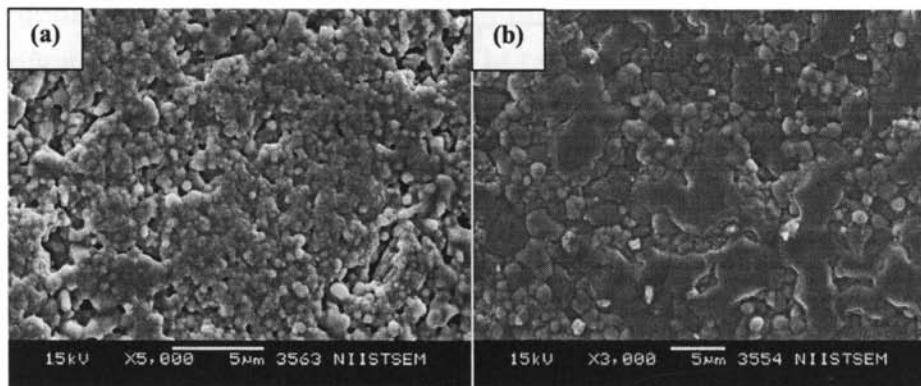


Fig. 7.33 SEM Micrographs of 0.40 volume fraction of CeO_2 -LSCO composite sintered at (a) 1150°C (b) 1250°C

7.3.3.3 Dielectric Properties

The variation of relative permittivity with sintering temperature for different volume fractions of LSCO added CeO_2 samples is shown in Fig. 7.34. For all volume fractions except 0.1 and 0.2, the relative permittivity increases with sintering temperature, reaches a maximum at 1150°C and then on further the increase in permittivity is small. The variation in the relative permittivity with sintering temperature is more prominent for those composites with LSCO content greater than 0.2 volume fraction. For composites containing LSCO less than 0.3 V_f , the variation is much more gradual. At sintering temperatures below 1250°C, the LSCO particles are distributed in the CeO_2 matrix. The size of LSCO grains below 1250°C is small compared to that at higher temperature (see Fig. 7.33). Hence the surface area increases, the number of particles at a particular volume fraction of composite increases, and the interparticle distance decreases.¹⁷⁶ When the LSCO particles come closer, at a particular interparticle distance, an overlapping of diffused double layer charged clouds around the conducting particles can occur.¹⁸⁶ The resulting electromagnetic coupling between the neighboring particles increases the local field, and thereby enhances the dipole moment of individual particles in the composite.

This, in turn, can lead to multipolar interaction between the particles.^{187,144} The net effect of this multipolar interaction between all the particles can account for the rapid increase in relative permittivity and conductivity of the composites at the percolation threshold. As the sintering temperature increases, agglomeration of LSCO particles occurs. Hence, the size of the LSCO particles increases with the sintering temperature and results in an increase in interparticle distance and decrease in number of LSCO particles. This can lead to a decrease in the relative permittivity with an increase in sintering temperature.¹⁸⁸ Another reason for the decrease of relative permittivity at higher sintering temperature may be due to the reduction of Ce^{4+} to Ce^{3+} at temperatures greater than 1200°C . The high electrical conductivity of LSCO depends on the strontium content (x), oxygen deficiency (δ) and temperature.^{182,189,190} According to Jonker,¹⁹¹ in $\text{La}_{1-x}\text{Sr}_x\text{CoO}_{3-\delta}$, when a Sr^{2+} ion occupies La^{3+} site and if $x > 0.4$, the charge compensation is accomplished by the formation of O^{2-} vacancy. The ionic radius of Ce^{3+} and Ce^{4+} are 1.34 and 1.14 Å respectively. The ionic radius of Ce^{3+} is comparable to that of La^{3+} (1.36 Å) and Sr^{2+} (1.44 Å) and hence Ce^{3+} will be substituted in the La/Sr site of LSCO.¹⁹² The value of δ (oxygen vacancy) decreases only when Ce^{3+} is substituted in the Sr^{2+} site. The reduction of Ce^{4+} to Ce^{3+} occurs at temperatures greater than 1200°C .¹⁹³ XPS analysis is required to confirm the valence state of Ce in CeO_2 -LSCO composite at 1150 and 1250°C . Thus the optimum sintering temperature of the composite is found to be 1150°C as far as the relative permittivity is concerned.

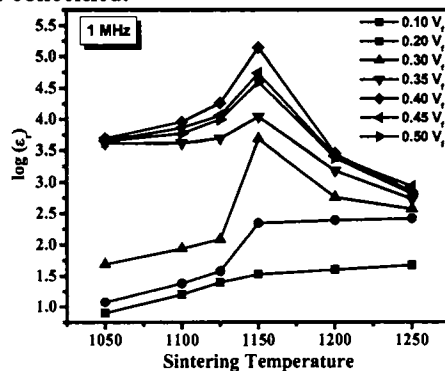


Fig. 7.34 Variation of relative permittivity (ϵ_r) with sintering temperature for different volume fraction of LSCO added CeO_2 ceramic

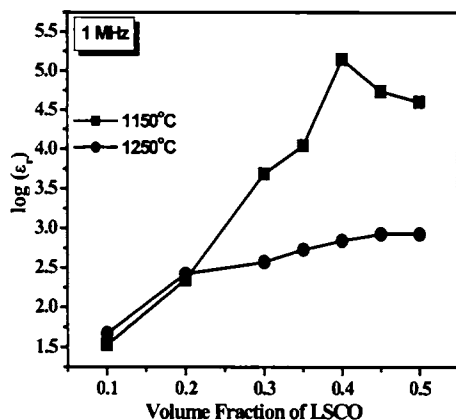


Fig. 7.35 Variation of relative permittivity (ϵ_r) with volume fraction of CeO_2 -LSCO composites

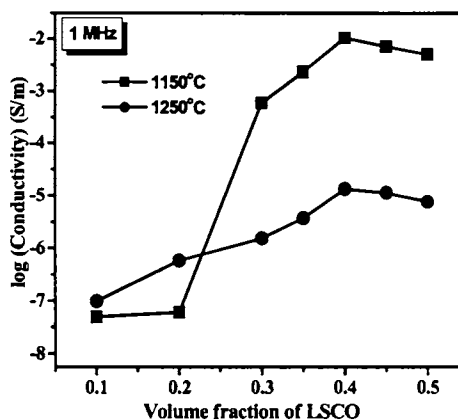


Fig. 7.36 Variation of conductivity with volume fraction of CeO_2 -LSCO composites

The variation in relative permittivity and conductivity with different volume fractions of LSCO sintered at 1150 and 1250°C are as shown in Figs. 7.35 and 7.36. An abrupt increase in the relative permittivity ($\epsilon_r \approx 10^5$) is obtained at 0.40 V_f of LSCO, and this is taken as the percolation threshold. The sharp increase of relative permittivity can be explained by two mechanisms: the generation of a dielectric field around conducting particles and the formation of microcapacitors through isolation of LSCO with thin dielectric layers. It is reported that a dielectric field develops around the conducting particles dispersed in insulating materials.^{194,195} The sharp increase in relative permittivity is a result of an interfacial polarization phenomenon that occurs at the interface of the dissimilar materials.¹⁹⁶ The charge carriers in the different phases of the composite are trapped at the interfaces within the dielectrics. These charges are unable to discharge freely and give rise to an overall field distortion, which results in an increase in capacitance and relative permittivity. In CeO_2 -LSCO composite, the dielectric field developed around the LSCO particle can result in an increase in the effective relative permittivity. The LSCO conducting particles in the composites act as internal electrodes

of a unit micro-capacitor. Such regions contribute to an extremely large capacitance, which adds up macroscopically and results in a large relative permittivity. The variation of conductivity with volume fraction follows the same trend as that of relative permittivity and volume fraction of LSCO and it is shown in Fig. 7.36. As the volume fraction of LSCO increases, the LSCO particles merge and at the percolation limit, there is a continuous path of adjacent allowed sites across the system and this leads to the sudden increase in conductivity. In composites, the conduction occurs either by the transfer of electrons between the particles in intimate contact or by the tunneling of electrons between the grains whose distance is less than 100 \AA .¹⁹⁷ At 1150°C , due to large number of LSCO particles in a particular region, the increased carrier concentration increases the probability of electron hopping and hence higher conductivity than at 1250°C .

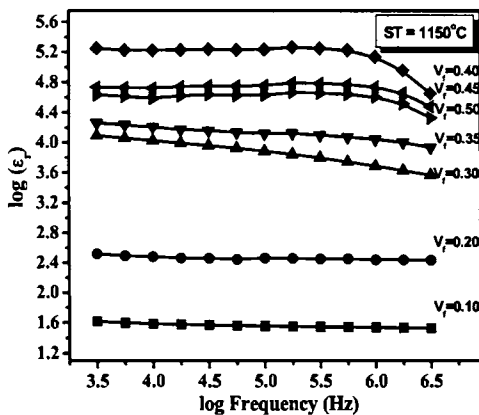


Fig. 7.37 Variation of relative permittivity (ϵ_r) with frequency for different volume fraction of CeO_2 -LSCO composites sintered at 1150°C

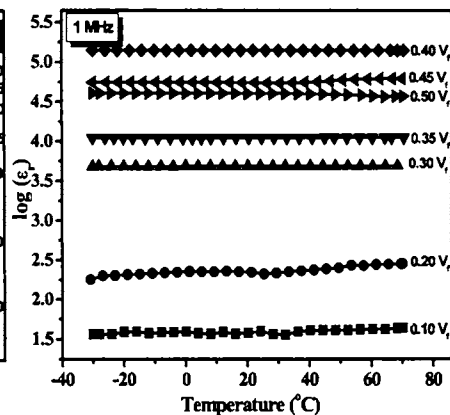


Fig. 7.38 Variation of relative permittivity (ϵ_r) with temperature for different volume fraction of CeO_2 -LSCO composites

The variation of relative permittivity with frequency for different volume fractions of CeO_2 -LSCO composites sintered at 1150°C are shown in Fig. 7.37. The relative permittivity increases gradually with the LSCO content up to $V_f = 0.2$ and beyond that the relative permittivity increases by several orders of magnitude. The decrease in relative permittivity with frequency is slightly higher than that below $V_f = 0.3$. Due to the direct

relation with polarization, relative permittivity has a strong frequency variation as different polarization mechanisms become active. Fig. 7.38 shows the temperature dependence of relative permittivity of CeO₂-LSCO composites with different volume fraction of LSCO measured at 1 MHz. It is clear that for all the volume fractions of LSCO, the relative permittivity is almost independent of temperature in the range -30 to 70°C.

Enhanced electrostriction is related to an enhanced relative permittivity. This suggests that the electrostriction can be enhanced by increasing the relative permittivity of the composite so that the same electric field can induce a higher polarization and thus a higher electrostriction. The present ceramic-ceramic composite overcomes the disadvantages of cermets such as oxidation problem and evaporation of metals at high sintering temperatures. CeO₂-LSCO composites can replace the present cermets used in electromechanical and embedded passive devices.

7.4 CONCLUSIONS

❖ Ceria-Glass Composites

- Effect of B₂O₃, B₂O₃-SiO₂, Al₂O₃-SiO₂, ZnO-B₂O₃, BaO-B₂O₃-SiO₂, MgO-B₂O₃-SiO₂, PbO-B₂O₃-SiO₂, ZnO-B₂O₃-SiO₂, 2MgO-Al₂O₃-5SiO₂, Li₂O-B₂O₃-SiO₂, Bi₂O₃-ZnO-B₂O₃-SiO₂ and Li₂O-MgO-ZnO-B₂O₃-SiO₂ glass addition on the structure, density and microwave dielectric properties of CeO₂ ceramics have been investigated.
- The X-ray Diffraction studies indicate the presence of Ce(BO₂)₃, CeZnB₂O₅, CeZnB₂O₅, PbB₂O₄ and CeBO₃ phases with the addition of higher weight percentage of B₂O₃, ZnO-B₂O₃, ZnO-B₂O₃-SiO₂, PbO-B₂O₃-SiO₂ and Bi₂O₃-ZnO-B₂O₃-SiO₂ respectively.
- Maximum quality factor of 69500 GHz (at 5.92 GHz) is obtained for 0.5 wt% Bi₂O₃-ZnO-B₂O₃-SiO₂ added CeO₂ ceramic at a sintering temperature of 1550°C which also showed the best densification

- Addition of BS, AS, BBS, MBS, LBS, MAS and LMSZB glass frits although lowered the sintering temperature of CeO₂ ceramics, the dielectric properties are very much degraded.
- The microwave dielectric properties of CeO₂ added with 20 wt% B₂O₃ (sintered at 900°C) are $Q_{ur}xf = 24200$ GHz, $\epsilon_r = 13.2$, $\tau_f = -46$ ppm/°C and that of CeO₂ added with 10 wt% BBSZ (sintered at 950°C) are $Q_{ur}xf = 12000$ GHz, $\epsilon_r = 22.4$, $\tau_f = -57$ ppm/°C.
- XRD, SEM and EDX analysis revealed that there is no reaction of 20 wt% B₂O₃ and 10 wt% BBSZ added CeO₂ ceramic with silver.
- From the analysis of above results it is obvious that CeO₂ + 20 wt% B₂O₃ and CeO₂ + 10 wt% Bi₂O₃-ZnO-B₂O₃-SiO₂ are promising materials for low temperature cofired ceramic applications.

❖ Ceria-Polymer Composites

- PTFE-CeO₂ composites are prepared by powder processing method and HDPE-CeO₂ composites by sigma-blend technique.
- SEM micrographs show that with the increase of filler content, the packing of particles grew denser and indicated the excellent compatibility between polymer and CeO₂ particles.
- The dielectric, thermal and mechanical properties of both PTFE and HDPE composites are studied in relation to filler concentration. The relative permittivity (ϵ_{eff}), dielectric loss ($\tan \delta$) and microhardness increased with increase in CeO₂ content. The thermal conductivity (k_c) increased and coefficient of thermal expansion (α_c) decreased with increase in CeO₂ content for both PTFE and HDPE composites.
- For 0.6 volume fraction loading of the ceramic, the PTFE composite has $\epsilon_{eff} = 5$ and $\tan \delta = 0.0064$ (at 7 GHz), $k_c = 1.85$ W/m°C, $\alpha_c = 22.9$ ppm/°C and Vickers' microhardness of 17 kg/mm². The 0.5 volume fraction of

HDPE-CeO₂ composite has $\epsilon_{eff} = 6.9$ and $\tan \delta = 0.0085$ (at 7 GHz), $k_c = 3.22 \text{ W/m}^\circ\text{C}$, $\alpha_c = 78.5 \text{ ppm}^\circ\text{C}$ and Vickers' microhardness of 28 kg/mm^2 .

- Different theoretical approaches have been employed to predict the effective permittivity, thermal conductivity and coefficient of thermal expansion of composite systems and the results are compared with that of experimental data.
- Due to the reasonably good dielectric, thermal and mechanical properties of HDPE composite ($0.5 V_f$) compared to PTFE composites, $0.5 V_f$ HDPE-CeO₂ can be considered as a possible candidate for microwave substrate applications.

❖ Ceria-La_{0.5}Sr_{0.5}CoO_{3-δ} composites

- The samples of CeO₂-LSCO (insulator-conductor) composites are prepared by the conventional solid-state ceramic route. XRD and SEM results show that the composite is a mixture of CeO₂ and LSCO.
- The variation of relative permittivity with sintering temperature shows that the permittivity is maximum at 1150°C for $V_f = 0.4$. Further increase in sintering temperature decreases the permittivity in CeO₂-LSCO composites.
- For all volume fractions of LSCO, the relative permittivity of CeO₂-LSCO composites is almost independent of temperature.
- CeO₂-LSCO composites can replace the present cermets used in electromechanical and embedded passive devices due to its high relative permittivity.

7.5 REFERENCES

- ¹ M. T. Sebastian and H. Jantunen, *Int. Mater. Rev.*, **53**, 57 (2008).
- ² S. T. Ishizaki, M. Fujita, H. Kataga, T. Uwano and H. Miyako, *IEEE Trans. Microwave Theory and Technol.* **42**, 2017 (1994).
- ³ Y. Imanaka, *Multilayers Low Temperature Cofired Ceramics (LTCC) Technology*, Springer (2005).
- ⁴ R. R. Tummala Rao, *J. Am. Ceram. Soc.*, **74**, 895 (1991).
- ⁵ K. W. Long and K. M. Luk, *IEEE Antenna Propagation*, **43**, 517 (1995).
- ⁶ K. H. Yoon, S. J. Yoo, W. S. Kim, J. B. Kim and E. S. Kim, *Jpn. J. Appl. Phys.*, **38**, 5616 (1999).
- ⁷ T. Takada, S. F. Wang, S. Yoshikawa, S. T. Tang and R. E. Newnham, *J. Am. Ceram. Soc.*, **77**, 2485 (1994).
- ⁸ H. Kagata, T. Inoue, J. Kato and I. Kameyama, *Jpn. J. Appl. Phys.*, **31**, 3152 (1992).
- ⁹ H. T. Kim, S. H. Kim, S. Nahm, J. D. Byun and Y. Kim, *J. Am. Ceram. Soc.*, **82**, 3043 (1999).
- ¹⁰ V. Tolmer and G. Desgardin, *J. Am. Ceram. Soc.*, **80**, 1981 (1997).
- ¹¹ T. Takanaka, K. Maruyama and K. Sakata, *Jpn. J. Appl. Phys.*, **30**, 2236 (1991).
- ¹² K. P. Surendran, P. Mohanan and M. T. Sebastian, *J. Solid State Chem.*, **177**, 4031 (2004).
- ¹³ H. Jantunen, R. Rautioaho, A. Uusimaki and S. Leppavuori, *J. Eur. Ceram. Soc.*, **20**, 2331 (2000).
- ¹⁴ J-A. Lee, J-H. Lee and J-J. Kim, *J. Eur. Ceram. Soc.*, **26**, 2135 (2006).
- ¹⁵ Y-W. Liu and P. Lin, *Mater. Chem. and Phys.*, **92**, 98 (2005).
- ¹⁶ H. Jantunen, *A novel Low Temperature Co-firing Ceramic (LTCC) material for telecommunication devices*, PhD. Thesis, University of Oulu, Finland, (2001).

-
- ¹⁷ J-M. Wu and H-L. Huang, *J. Non-Crystal. Sol.*, **260**, 116 (1999).
- ¹⁸ L. Navias and R. L. Green, *J. Am. Ceram. Soc.*, **29**, 267 (1946).
- ¹⁹ S. N. Salama, S.M. Salman and H. Darwish, *Ceram. Int.*, **21**, 159 (1995).
- ²⁰ N. Mori, Y. Sugimoto, J. Harada and Y. Higuchi, *J. Eur. Ceram. Soc.*, **26**, 1925 (2006).
- ²¹ Y.-J. Choi, J.-H. wan Park, J.-H. Park and J.-G. Park, *Mater. Lett.*, **58**, 3102 (2004).
- ²² O. Dernovsek, A. Naeni, G. Preu, W. Wersing, M. Eberstein and W. A. Schiller, *J. Eur. Ceram. Soc.*, **21**, 1693 (2001).
- ²³ S. Thomas and M. T. Sebastian, *Mater. Res. Bull.*, **43**, 843 (2008).
- ²⁴ N. Santha, M. T. Sebastian, P. Mohanan, Mc N. Alford, K. Sarma, R. C. Pullar, S. Kamba, A. Pashkin, P. Samukhina and J. Petzelt, *J. Am. Ceram. Soc.*, **87**, 1233 (2004).
- ²⁵ M. T. Sebastian, N. Santha, P. V. Bijumon, A-K Axelsson and Mc N. Alford, *J. Eur. Ceram. Soc.*, **24**, 2583 (2004).
- ²⁶ E. Matijevic and W. P. Hsu, *J. Colloid and Interface. Sci.*, **118**, 506 (1987).
- ²⁷ X. Chu, W. Chung and L. D. Schmidt, *J. Am. Ceram. Soc.*, **76**, 2115 (1993).
- ²⁸ E. Verdon, M. Devalette and G. Damazeau, *Mater. Lett.*, **25**, 127 (1995).
- ²⁹ Y. C. Zhou, R. J. Philips and J. A. Switzer, *J. Am. Ceram. Soc.*, **78**, 981 (1995).
- ³⁰ M. Hirano and E. Kato, *J. Mater. Sci. Lett.*, **15**, 1249 (1996).
- ³¹ C-H. Hsu, *Ceram. Int.*, **34**, 243 (2008).
- ³² B. W. Hakki and P. D. Coleman, *IRE Trans. on Microwave Theory Tech.*, **MTT-8**, 402 (1960).
- ³³ W. E. Courtney, *IEEE Trans. on Microwave Theory Tech.*, **MTT-18**, 476 (1970).
- ³⁴ J. Krupka, K. Derzakowski, B. Riddle and J. B.-Jarvis, *Meas. Sci. Technol.*, **9**, 1751 (1998)
- ³⁵ M-H Kim, S. N. Nahm, W-S Lee, M-J Yoo, N-K Kang, H-T Kim and H-J Lee, *Jpn. J. Appl. Phy.*, **44**, 3091 (2005).
- ³⁶ J. H. Jean and S. C. Lin, *J. Am. Ceram. Soc.*, **83**, 1417 (2000).

-
- ³⁷ Q. L. Zhang, H. Yang, J. L. Zou and H. P. Wang, *Mat. Lett.*, **59**, 880 (1995).
- ³⁸ D. L. Corker, R. W. Whatmore, E. Ringgaard and W. W. Wolny, *J. Eur. Ceram. Soc.*, **20**, 2039 (2000).
- ³⁹ Q. Zeng, W. Li, J-L. Shi, J-K. Guo, M-W. Zuo and W-J. Wu, *J. Am. Ceram. Soc.*, **89**, 1733 (2006).
- ⁴⁰ M. T. Sebastian, *Dielectric Materials for Wireless Communication*, Elsevier Science Publishers, Oxford, (2008).
- ⁴¹ T. Takada, S. F. Wang, S. Yoshikawa, S-J Jang and R. E. Newnham, *J. Am. Ceram. Soc.*, **77**, 1909 (1994).
- ⁴² M. N. Rahaman, *Ceramic Processing and Sintering*, Int. Ed., Marcel Dekker Inc., New York, (1999).
- ⁴³ J. H. Jean and T. K. Gupta, *J. Mater. Res.*, **10**, 1312 (1995).
- ⁴⁴ ICDD Card Nos. **23-0877, 86-1884, 21-0177, 15-078**.
- ⁴⁵ J. B. Lim, J. O. Son, S. Nahm, W. S. Lee, M. J. Yoo, N. G. Gang, H. J. Lee and Y. S. Kim, *Jpn. J. Appl. Phys.*, **43**, 5388 (2004).
- ⁴⁶ S-Y Chen and Y-J Lin, *Jpn. J. Appl. Phys.*, **40**, 3305 (2001).
- ⁴⁷ P. Liu, E. S. Kim and K. H. Yoon, *Jpn. J. Appl. Phys.*, **40**, 5769 (2001).
- ⁴⁸ P. V. Bijumon and M. T. Sebastian, *Mater. Sci. and Eng. B*, **123**, 31 (2005).
- ⁴⁹ D-W. Kim, K. S. Hong, C. S. Yoon and C. K. Kim, *J. Eur. Ceram. Soc.*, **23**, 2597 (2003).
- ⁵⁰ W. Wersing, *Current Opinion in Solid State and Mater. Sci.*, **1**, 715 (1996).
- ⁵¹ N. Mc N. Alford, J. Breeze, X. Wang, S. J. Penn, S. Dalla, S. J. Webb, N. Ljepojevic and X. Aupi, *J. Eur. Ceram. Soc.*, **21**, 2605 (2001).
- ⁵² R. D. Shannon, A. N. Mariano and G. R. Rossman, *J. Am. Ceram. Soc.*, **75**, 2395 (1992).
- ⁵³ D. L. Chung, *Materials for Electronic Packaging*, Butterworth, Heinemann, Washington, (1995).
- ⁵⁴ P. Garrou and I. Turlik, *Multichip Module Technology Handbook*, Mc. Graw-Hill, New York, (1998).

-
- ⁵⁵ M. B. Tian, *Substrates for High Density Package Engineering*, Tsinghua University Press, Beijing, (2003).
- ⁵⁶ J. F. Chailan, J. M. Robert, J. C. Milano and J. L. Vernet, *Macromol. Chem. Phys.*, **200**, 2387 (1999).
- ⁵⁷ R. R. Tummala and E. J. Rymaszewski, *Microelectronics Packaging Handbook*, van NostrandReinhold, New York: (1989).
- ⁵⁸ P. Procter and J. Sole, *Proc. of 41st Electronic and Components Tech. Conference* (Atlanta, GA), Institute of Electrical and Electronic Engineers, New York, 835 (1991).
- ⁵⁹ P. Bujard, G. Kuhnlein, S. Ine and T. Sclobara, *IEEE Trans. Comp., Packaging and Manufacturing Technology-Part A*, **17**, 527 (1994).
- ⁶⁰ R. Hill, *Proc. of the Tech. Program Surface Mount Technology Association National Symposium* (Research Triangle Park, NC), 125, Surface Mount Technology Association, Edina, MN, 1996.
- ⁶¹ E. Rerchmanis, *Microelectronics Technology: Polymers for Advanced Imaging and Packaging*, ACS Symposium series (American Chemical Society), Washington, DC, (1995).
- ⁶² D. S. Soane and Z. Martynenko, *Polymers in Microelectronics: Fundamentals and Applications*, Elsevier, New York, (1989).
- ⁶³ D. P. Button, B. A. Yost, R. H. French, W. Y. Hsu, J. D. Belt, M. A. Subrahmanian, H-M Zhang, R. E. Geidd, A. J. Whittacker and D. G. Onn, *Advances in Ceramics*, published by the American Ceramic Society, Westerville OH, **26**, 353 (1989).
- ⁶⁴ W. Bare, C. Albano, J. Reyes and N. Dominguez, *Surf. and Coatings Technol.*, **158-159**, 404 (2002).
- ⁶⁵ L. Fan, Z. Dang, C-W Nan and M. Li, *Electrochim. Acta*, **48**, 205 (2002).
- ⁶⁶ J. Korab, P. Stefanik, S. Kavecky, P. Sebo and G. Korb, *Comp. Part A: Appl. Sci. and Manuf.*, **33**, 577 (2002).
- ⁶⁷ D. B. Bigg, *Adv. Poly. Sci.*, **119**, 1 (1995).
- ⁶⁸ Y. D. Kim, N. L. Oh, S-T. Oh and I-H Moon, *Mater. Lett.*, **51**, 420 (2001).
- ⁶⁹ L. Yang and D. L. Schruben, *Poly. Engg. and Sci.* **34**, 1109 (1994).
- ⁷⁰ Y. P. Mamunya, H. Zois, L. Apekis and E. V. Lebedev, *Powd. Technol.*, **140**, 49 (2004).

-
- ⁷¹ F. J. Balta Calleja, T. A. Ezquerro, D. R. Rueda and J. Alonso-Lopez, *J. Mater. Sci. Lett.*, **3**, 165 (1984).
- ⁷² A. A. Okhlopko and F. Y. Shits, *Mech. Comp. Mater.*, **40**, 145 (2004).
- ⁷³ Y. M. Wang, D. C. Jia and Y. Zhou, *Piezoelectrics and Acoustooptics*, **24**, 225 (2002).
- ⁷⁴ Y-C. Chen, H-C. Lin and Y-D. Lee, *J. Poly. Res.*, **11**, 1 (2004).
- ⁷⁵ S. L. Thomas, *Microwave Materials and Fabrication Techniques*, Artech House, Inc., U.S.A., (1984).
- ⁷⁶ F. H. Allen, R. R. Traskos and D. A. Allen, US patent No. 5922453 (1999).
- ⁷⁷ J. A. Bur, *Polymer*, **26**, 963 (1985).
- ⁷⁸ D. M. Price and M. Jarralt, *Thermochimica Acta*, **392-393**, 231 (2002).
- ⁷⁹ D. J. Arthur and G. S. Swei, US patent, 5, 149, 590 (1992).
- ⁸⁰ J. A. Pelesko and G. A. Kreigsmann, *J. Eng. Math.*, **32**, 1 (1997).
- ⁸¹ D. J. Arthur, G. S. Swei, A. F. Horn III and B. Kilhenny, U. S. Patent No. 384 181, (1995).
- ⁸² Y. M. Wang, D. C. Jia and Y. Zhou, *J. Poly. Res.*, **10**, 247 (2003).
- ⁸³ X. Lu and G. Xu, *J. Appl. Poly. Sci.*, **65**, 2733 (1997).
- ⁸⁴ G. Subodh, M. V. Manjusha, J. Philip and M. T. Sebastian, *J. Appl. Poly. Sci.*, **108**, 1716 (2008).
- ⁸⁵ Y-C. Chen, H-C. Lin and Y-D. Lee, *J. Poly. Res.*, **10**, 247 (2003).
- ⁸⁶ Y. M. Wang, D. C. Jia and Y. Zhou, *Piezoelectr. Acoustoopt.*, **24**, 225 (2002).
- ⁸⁷ I. Krupa, I. Novak and I. Chodak, *Synthetic Metals*, **145**, 245 (2004).
- ⁸⁸ W. Zhou, S. Qi, H. Zhao and N. Liu, *Mat. Res. Bull.*, **42**, 1863 (2007).
- ⁸⁹ Y. Zou, Y. Feng, L. Wang and X. Liu, *Carbon*, **42**, 271 (2004).
- ⁹⁰ C. Jo and H. E. Naguib, *Poly.*, **48**, 3349 (2007).
- ⁹¹ G. Subodh, M. Joseph, P. Mohanan and M. T. Sebastian, *J. Am. Ceram. Soc.*, **90**, 3507 (2007)

-
- ⁹² G. Subodh, C. Pavitran, P. Mohanan and M. T. Sebastian, *J. Eur. Ceram. Soc.*, **27**, 3039 (2007).
- ⁹³ M. Osaka, S. Miwa and Y. Tachi, *Ceram. Int.*, **32**, 659 (2006).
- ⁹⁴ L. F. Chen, C. K. Ong, C. P. NeO, V. V. Varadan and V. K. Varadan, *Microwave Electronics: Measurement and Materials Characterization*, John Wiley & Sons, England, (2004).
- ⁹⁵ A. Prakash, J. K. Vaid and A. Mansingh, *IEEE Trans. Microwave Theory. Tech.*, **MTT 27**, 791 (1979).
- ⁹⁶ C. P. Menon and J. Philip, *Meas. Sci. Tech.*, **11**, 1744 (2000).
- ⁹⁷ M. Marinelli, F. Murtas, M. G. Mecozzi and S. Martellucci. *Appl. Phys. A: Mater. Sci. Process.*, **51**, 387 (1990).
- ⁹⁸ M. T. Sebastian, C. P. Menon, J. Philip and R. W. Schwartz, *J. Appl. Phys.*, **94**, 3206 (2003).
- ⁹⁹ V. S. Nisa, S. Rajesh, K. P. Murali, V. Priyadarsini, S. N. Potty and R. Ratheesh, *Comp. Sci. and Tech.*, **68**, 106 (2007).
- ¹⁰⁰ A. H. Sihvola, *IEEE Trans. Geosci. Remote Sens.*, **26**, 420 (1988).
- ¹⁰¹ N. Jayasundere and B. V. Smith, *J. Appl. Phys.*, **73**, 2462 (1993).
- ¹⁰² K. Wakino, *J. Am. Ceram. Soc.*, **76**, 2588 (1993).
- ¹⁰³ Y. M. Poon and F. G. Shin, *J. Mater. Sci.*, **39**, 1277 (2004).
- ¹⁰⁴ L. Jylhai, J. Honkamo, H. Jantunen and A. H. Sihvola, *J. Appl. Phys.*, **97**, 104 (2005).
- ¹⁰⁵ B. Sareni, L. Krahenubuh, A. Beroul and C. Brosseau, *J. Appl. Phys.*, **81**, 2375 (1997).
- ¹⁰⁶ Y. Rao, J. Qu, T. Marinis and C. P. Wong, *IEEE Trans. Comp. Packag. Tech.*, **23**, 80 (2000).
- ¹⁰⁷ L. M. Walpita, M. R. Ahern, P. Chen, H. Goldberg, S. Hanely and W. M. Pleban, *IEEE Trans. Microwave Theory and Tech.*, **47**, 1577 (1999).
- ¹⁰⁸ R. C. Progelhof, J. L. Throne and R. R. Reutsch, *Poly. Eng. Sci.*, **16**, 615 (1976).
- ¹⁰⁹ J. K. Carson, S. J. Lovatt, D. J. Tanner and A. C. Cleland, *J. Food Eng.*, **75**, 297 (2006).
- ¹¹⁰ H. J. Ott, *Plastic and Rubber Proces. and Appl.*, **1**, 9 (1981).

-
- ¹¹¹ J. Wang, J. K. Carson, M. F. North and D. J. Cleland, *Int. J. Heat and Mass Transf.*, **49**, 3075 (2006).
- ¹¹² B. Hakansson and R. G. Ross, *J. Appl. Phys.*, **68**, 3285 (1990).
- ¹¹³ R. Landauer, In: J. C. Garland, D. B. Tanner (Editors), *Am. Inst. Phys. Conf. Proc.:Electrical transport and optical properties of inhomogeneous media*, Am. Inst. Phys., New York, (1978).
- ¹¹⁴ J. C. Maxwell, *A Treatise on Electricity and Magnetism*, Dover, New York, (1954).
- ¹¹⁵ T. N. G. Tsao, *Ind. and Eng. Chem.*, **53**, 395 (1961).
- ¹¹⁶ E. H. Kerner, *Proc. Phys. Soc.*, **69B**, 808 (1956).
- ¹¹⁷ A. Wakashima, M. Otsuka and S. Umekawa, *J. Comp. Mater.*, **8**, 391 (1974).
- ¹¹⁸ T. Ishikawa, K. Koyama and S. Kobayashi, *J. Comp. Mater.*, **12**, 153 (1978).
- ¹¹⁹ M. Orrhede, R. Tolani and K. Salama, *Res. Nondestr. Eval.*, **8**, 23 (1996).
- ¹²⁰ C. P. Wong and R. S. Bollampally, *J. Appl. Poly. Sci.*, **74**, 3396 (1999).
- ¹²¹ R. A. Schapery, *J. Comp. Mat.*, **2**, 380 (1968).
- ¹²² Z. Hashin and S. Shtrikman, *J. Mech. Phys. Solids*, **11**, 127 (1963).
- ¹²³ M. G. Grewe, T. R. Gururaja, T. R. ShROUT and R. E. Newnham, *IEEE Trans. Ultrasonics, Ferroelectrics and Frequency control*, **7**, 506 (1990).
- ¹²⁴ F. Xiang, H. Wang and X. Yao, *J. Eur. Ceram. Soc.*, **27**, 3093 (2006).
- ¹²⁵ S. D. Malachlan, M. Blaskiewicz and R. E. Newham, *J. Am. Ceram. Soc.*, **73**, 2187 (1990).
- ¹²⁶ Y-C. Chen, H-C. Lin and Y-D. Lee, *J. Poly. Res.*, **10**, 247 (2003).
- ¹²⁷ A. Androsch, B. Wunderlich and H. J. Radusch, *J. Therm. Anal. and Calor.*, **79**, 615 (2005).
- ¹²⁸ M. Endo, K. Yamada, K. Tadano, Y. Nishino and S. Yano, *Macromol., Rapid Comm.*, **21**, 396 (2000).
- ¹²⁹ P. J. Rae and B. M. Datebaum, *Polymer*, **45**, 7615 (2004).
- ¹³⁰ N. G. Devaraju, E. S. Kim and B. I. Lee, *Microelectron. Eng.*, **82**, 71 (2005).

-
- ¹³¹ L. Ramajo, M. Reboledo and M. Castro, *Comp. Part A Appl. Sci. Manuf.*, **36**, 1267 (2005).
- ¹³² K-C Cheng, C-M Lin, S-F Wang, S-T Lin and C-F Yang, *Mat. Lett.*, **61**, 757 (2007).
- ¹³³ D-H. Kuo, C-C. Chang, T-Y. Su, W-K. Wang and B-Y. Lin, *J. Eur. Ceram. Soc.*, **21**, 71 (2001).
- ¹³⁴ S. Yu, P. Hing and X. Hu, *J. Appl. Phys.*, **88**, 398 (2000).
- ¹³⁵ D. Khastgir, H. S. Maiti and P. C. Bandhopadhyaya, *Mater. Sci. and Eng.*, **100**, 245 (1998).
- ¹³⁶ J. Zhang, H. Fan, S. Ke, Y. Shi, X. Zeng, M. Bi and H. Huang, *Key Eng. Mater.*, **334-335**, 1053 (2007).
- ¹³⁷ L. Y. Zhang and X. Yao, *Dielectric Physics*, Xi'an Jiaotong University Press, Xi'an, (1991).
- ¹³⁸ X. H. Zhao, Y. G. Wu and Z. G. Fan, *J. Appl. Phys.*, **95**, 8110 (2004).
- ¹³⁹ Z. Yutao, C. Cheng, J. Weifang, X. Hengkun and L. Yaonan, *Int. Symp. on Electrical Insul. Mater.*, **77** (1995).
- ¹⁴⁰ M. S. Ozmusul and R. C. Picu, *Poly. Comp.*, **23**, 110 (2002).
- ¹⁴¹ J. Qu and C. P. Wong, *IEEE Trans. Comp. Packag. Tech.*, **25**, 53 (2002).
- ¹⁴² M. G. Todd and F. G. Shi, *Microelectron. J.*, **33**, 627 (2002).
- ¹⁴³ H. Vo and F. G. Shi, *Microelectron. J.*, **33**, 409 (2002).
- ¹⁴⁴ M. G. Todd and F. G. Shi, *J. Appl. Phys.*, **94**, 4551 (2003).
- ¹⁴⁵ M. G. Todd and F. G. Shi, *IEEE Transactions on Comp. and Packag. Tech.*, **26**, 667 (2003).
- ¹⁴⁶ V. Grover and A. K. Tyagi, *Ceram. Int.*, **31**, 769 (2005).
- ¹⁴⁷ G. M. Tsangaris and G. C. Psarras, *J Mater. Sci.*, **34**, 2151 (1999).
- ¹⁴⁸ M. A. Berger and R. L. McCullough, *Comp. Sci. Tech.*, **22**, 81 (1985).
- ¹⁴⁹ A. H. Sihvola, *IEEE Trans. Geosci. Remote Sens.*, **26**, 420 (1988).
- ¹⁵⁰ N. Jayasundere and B. V. Smith, *J. Appl. Phys.*, **73**, 2462 (1993).
- ¹⁵¹ K. Wakino, *J. Am. Ceram. Soc.*, **76**, 2588 (1993).

-
- ¹⁵² Y. M. Poon and F. G. Shin, *J. Mater. Sci.*, **39**, 1277 (2004).
- ¹⁵³ C. Brosseau, P. Queffelec and P. Talbot, *J. Appl. Phys.*, **89**, 4532 (2000).
- ¹⁵⁴ W. Kim, J. W. Bae, D. Choi and S. K. Yong, *Poly. Eng. Sci.*, **39**, 756 (1999).
- ¹⁵⁵ H. He, R. Fu, Y. Han, Y. Shen and X. Song, *J. Mat. Sci.*, **42**, 6749 (2007).
- ¹⁵⁶ D. Kumlutas, I. H. Tavman and M. T. Coban, *Comp. Sci. and Tech.*, **63**, 113 (2003).
- ¹⁵⁷ Y. Agari, A. Ueda, M. Tanaka and S. Nagai, *J. Appl. Poly. Sci.*, **40**, 929 (1990).
- ¹⁵⁸ Y. Beneviste and T. Miloh, *Int. J. Eng. Sci.*, **24**, 1537 (1986).
- ¹⁵⁹ R. Hill and P.H. Supancic, *J. Am. Ceram. Soc.*, **87**, 1831 (2004).
- ¹⁶⁰ R. Hill and P.H. Supancic, *J. Am. Ceram. Soc.*, **85**, 851 (2002).
- ¹⁶¹ L. Holliday and L. Robinson, *J. Mat. Sci.*, **8**, 301 (1973).
- ¹⁶² G. Subodh, M. V. Manjusha, J. Philip and M. T. Sebastian, *J. Appl. Poly. Sci.*, **108**, 1716 (2008)
- ¹⁶³ F. J. Balta' Calleja, *Trends Poly. Sci.*, **2**, 419 (1994).
- ¹⁶⁴ Y. Rao, S. Ogitani, P. Kohl and C. P. Wong, *J. Appl. Poly. Sci.*, **83**, 1084 (2002).
- ¹⁶⁵ C. Huang, Q. M. Zhang and J. Su., *Appl. Phys. Lett.*, **82**, 3502 (2003).
- ¹⁶⁶ P-H. Xiang, X.-L. Dong, C.-D. Feng, R.-H. Liang and Y.-L. Wang., *Mater. Chem. Phys.*, **97**, 410 (2006).
- ¹⁶⁷ Y. Bai, Z.-Y. Cheng, V. Bharti, H. S Xu and Q. M. Zhang. *Appl. Phys. Lett.*, **76**, 3804 (2000).
- ¹⁶⁸ D. J. Lewis, D. Gupta, M. R. Notis and Y. Imanaka, *J. Am. Ceram. Soc.*, **79**, 261 (1996).
- ¹⁶⁹ M. A. Subramanian, D. Li, N. Duan, B. A. Reisner and A. W. Sleight, *J. Solid State Chem.*, **151**, 323 (2000).
- ¹⁷⁰ C. C. Homes, T. Vogt, S. M. Shapiro, S. Wakimoto and A. P. Ramirez, *Science*, **293**, 673 (2001).
- ¹⁷¹ J. Wu, C.-W. Nan, Y. H. Lin and Y. Deng, *Phys. Rev. Lett.*, **89**, 217601 (2002).
- ¹⁷² S. Sarkar, P. K. Jana and B. K. Chaudhuri, *Appl. Phys. Lett.*, **89**, 212905 (2006).

-
- ¹⁷³ D. J. Bergman and D. Stroud, *Solid State Phys.*, **46**, 147 (1992).
- ¹⁷⁴ J. P. Clere, G. Giraud, J. M. Laugier and J. M. Luck, *Adv. Phys.*, **39**, 191 (1990).
- ¹⁷⁵ B. Bochu, M. N. Deschizeaux and J. C. Joubert, *J. Solid State Chem.*, **29**, 291 (1979).
- ¹⁷⁶ K. S. Deepa, M. T. Sebastian and J. James, *Appl. Phys. Lett.*, **91**, 202904 (2007)
- ¹⁷⁷ D. M. Grannan, J. C. Garland and D.B. Tanner, *Phys. Rev. Lett.*, **46**, 375 (1981).
- ¹⁷⁸ S. Y. Cho, H. J. Youn, D. W. Kim, T.G. Kim and D. S. Hong. *J. Am. Ceram. Soc.*, **81**, 3038 (1998).
- ¹⁷⁹ H. J. Hawang, M. Yasunoka, M. Sando, M. Toriyama and K. Niihara, *J. Am. Ceram. Soc.*, **80**, 791 (1997).
- ¹⁸⁰ C. Y. Chen and W. H. Tuan, *J. Am. Ceram. Soc.*, **83**, 1693 (2000).
- ¹⁸¹ H. C. Ling, *J. Am. Ceram. Soc.*, **72**, 770 (1989).
- ¹⁸² A. N. Petrov, O. R. Kononchuk, A. V. Andreev, V. A. Cherepanov and P. Kofstad, *Solid State Ionics*, **80**, 189 (1995).
- ¹⁸³ L. M. VanderHaar, M. W. D. Otter, M. Morskate, H. J. M. Bouwmeester and H. Verweij, *J. Electrochem. Soc.*, **149**, 141 (2002).
- ¹⁸⁴ H. Ohbayashi, T. Kudo and T. Gejo, *Jpn. J. Appl. Phys.*, **13**, 1 (1974).
- ¹⁸⁵ A. Chainani, M. Mathew and D. D. Sarma, *Phys. Rev. B*, **46**, 9976 (1992).
- ¹⁸⁶ F. Claro, *Phys. Rev. B*, **25**, 7875 (1982).
- ¹⁸⁷ Y. Song, T. W. Noh, S. I. Lee and J. R. Gaines, *Phys. Rev. B*, **33**, 904, 1986.
- ¹⁸⁸ S. George, J. James and M. T. Sebastian, *J. Am. Ceram. Soc.*, **90**, 3522 (2007).
- ¹⁸⁹ J. Mizusaki, Y. Mima, S. Yamauchi, K. Fueki and H. Tagawa, *J. Solid State Chem.*, **80**, 69 (1990).
- ¹⁹⁰ T. Ishigaki, S. Yamauchi, J. Mizusaki, K. Feuki and H. Tamura, *J. Solid State Chem.*, **54**, 100 (1984).
- ¹⁹¹ G. H. Jonker, *Philips Res. Rep.*, **24**, 1 (1969).
- ¹⁹² R. D. Shannon, *Acta Crystallogr.*, **A32**, 751 (1976).

-
- ¹⁹³ H. Sreemoolanadhan, M. T. Sebastian, R. Ratheesh, R. Blachnik, M. Woehlecke, B. Schneider, M. Neumann and P. Mohanan, *J. Solid State Chem.*, **177**, 3995 (2004).
- ¹⁹⁴ P. Chylek and V. Srivastava, *Phys. Rev. B.*, **30**, 1008 (1984).
- ¹⁹⁵ W. J. Kaiser, E. M. Logothetis and L. E. Wenger, *J. Phys. C: Solid State Phys.*, **18**, L 837 (1985).
- ¹⁹⁶ S. H. Foulger, *J. Poly. Sci. Part B: Poly. Phys.*, **37**, 1899 (1999).
- ¹⁹⁷ J. I. Hong, L. S. Schadler and R. W. Siegel, *Appl. Phys. Lett.*, **82**, 1956 (2003).

Chapter 8

CONCLUSIONS AND FUTURE CHALLENGES

This chapter features summary of the research work described in this thesis. The significant highlights of the results presented in each chapter are outlined in chronological order. The prospects for extending the work in future directions such as in the area of dielectric resonators, low temperature cofired ceramics and polymer composites are also discussed.

The thesis presents microwave dielectric properties of ceria based ceramics useful as dielectric resonators (DR) and low temperature cofired ceramics (LTCC) in the microwave integrated circuits. Ceria based polymer composites useful for electronic packaging applications and $\text{CeO}_2\text{-La}_{0.5}\text{Sr}_{0.5}\text{CoO}_{3-\delta}$ composites for electromechanical applications are also discussed in the thesis. The microwave dielectric properties of the ceramics are tailored by several methods such as doping, glass addition and solid solution formation in the Ce-site of CeO_2 with suitable substituents.

The first chapter of the thesis explains the fundamental concepts related to dielectric resonators, low temperature cofired ceramics and polymer/ceramic composites. The second chapter describes the synthesis and characterization techniques of the dielectric ceramics and polymer composites in the radio and microwave frequency region.

Chapter 3 outlines the general introduction about fluorite structure and a brief history and literature survey related to the dielectric study of cerium oxide ceramics. This chapter details the synthesis, characterization and microwave dielectric properties of $\text{CeO}_2\text{-0.5AO-0.5TiO}_2$ (A = Mg, Zn, Ca, Mn, Co, Ni, W) ceramics. These ceramic systems are a composite consisting of fluorite CeO_2 and ATiO_3 with good densification and interesting dielectric properties depending on the coexisting ATiO_3 being formed. The ceramics have relative permittivities (ϵ_r) in the range 17.0 to 65.5 and quality factor $Q_{\nu} \times f$ up to 50000 GHz. The τ_f ranges from 399 ppm/ $^{\circ}\text{C}$ to -62 ppm/ $^{\circ}\text{C}$. The quality factor increased considerably on cooling the $\text{CeO}_2\text{-0.5AO-0.5TiO}_2$ (A = Mg, Zn, Ca, Mn, Co, Ni, W) ceramics in a manner, similar to pure CeO_2 . Highest $Q_{\nu} \times f$ is found for the $\text{CeO}_2\text{-0.5MgO-0.5TiO}_2$ system and at 20 K it reaches as high as 539000 GHz. The effect of dopants on the microwave dielectric properties of $\text{CeO}_2\text{-0.5AO-0.5TiO}_2$ (A = Mg, Zn, Ca, Mn, Co, Ni, W) ceramics are investigated. Addition of Cr_2O_3 to $\text{CeO}_2\text{-0.5CaO-0.5TiO}_2$ system improved the τ_f to zero ppm/ $^{\circ}\text{C}$ from the originally 399 ppm/ $^{\circ}\text{C}$ respectively. A quality factor of 90000 and 87700 GHz is found by the addition of 2 wt% WO_3 and 2 wt% $\text{WO}_3 + 0.5$ wt% TiO_2 respectively to the $\text{CeO}_2\text{-0.5MgO-0.5TiO}_2$ composite with $\epsilon_r \sim 21$ and $\tau_f \sim -50$ ppm/ $^{\circ}\text{C}$. By combining 0.5 wt% WO_3 and 20 wt%

TiO₂ to CeO₂-0.5CoO-0.5TiO₂ ceramic, a $Q_{ur}xf$ of 58200 GHz, $\epsilon_r = 21.2$ and $\tau_f = +5$ ppm/°C is obtained. ATiO₃ (A = Co, Mn, Ni) dielectric ceramics synthesized by the conventional solid state ceramic route have hexagonal symmetry with $R\bar{3}(148)$ space group. The microwave dielectric properties of ATiO₃ (A = Co, Mn, Ni) ceramics are reported for the first time with ϵ_r in the range 19 to 25, $Q_{ur}xf$ from 13900 to 62500 GHz and τ_f of about -50 ppm/°C.

The fourth chapter gives the preparation, characterization and microwave dielectric properties of BaO-2CeO₂- n TiO₂ ($n = 6...15$) and BaO- p CeO₂-4TiO₂ ($p = 3...13$) ceramics. BaO-2CeO₂- n TiO₂ ($n = 6...15$) ceramics are multiphase compounds containing CeO₂, Ba₂Ti₉O₂₀ and TiO₂ while BaO- p CeO₂-4TiO₂ ($p = 3...13$) ceramics consists of CeO₂ and BaTi₄O₉ phases. The ϵ_r increases from 41.5 to 69.9, $Q_{ur}xf$ decreases from 27400 to 23200 GHz and τ_f increases from 40 to 272 ppm/°C with the value of n in BaO-2CeO₂- n TiO₂ ($n = 6...15$) ceramics due to the increasing amount of rutile. The ϵ_r decreases from 32.6 to 26.1, $Q_{ur}xf$ increases from 25400 to 36800 GHz and τ_f increases to the negative side from -11 to -41 ppm/°C with the value of p in BaO- p CeO₂-4TiO₂ ($p = 3...13$) ceramics due to the increasing amount of ceria. The effect of different dopants on the microwave dielectric properties of BaO-3CeO₂-4TiO₂ ceramics is studied and BaO-3CeO₂-4TiO₂ doped with 1.5 wt% CuO sintered at 1050°C/2h has $\epsilon_r = 30$, $Q_{ur}xf = 32200$ GHz and $\tau_f = -12$ ppm/°C. This can be used as an ideal candidate for LTCC applications with copper electrode. The 0.5CeO₂-0.5BaTi₄O₉ sample sintered at 1260°C/2h exhibits excellent microwave dielectric properties: $\epsilon_r = 34.5$, $Q_{ur}xf = 20750$ GHz and $\tau_f = 2$ ppm/°C. The 12 wt% B₂O₃ and 1 wt% CuO added 0.5CeO₂-0.5BaTi₄O₉ ceramic sintered at 950°C for 4 hours shows $\epsilon_r = 20.6$, $Q_{ur}xf = 17000$ GHz and $\tau_f = 48$ ppm/°C. Silver remains unreacted with the 0.5CeO₂-0.5BaTi₄O₉+12 wt% B₂O₃+1 wt% CuO composite, which is one of the requirements of LTCC.

Chapter 5 reports for the first time the microwave dielectric properties of two new ceramics based on cerium - Ce₂(WO₄)₃ and Ba₂CeV₃O₁₁ for microwave substrate applications. The Ce₂(WO₄)₃ and Ba₂CeV₃O₁₁ ceramics sintered at 1000 and 1025°C/4h have a relative permittivity of 10.8 and 14.9 with quality factors of 10500 and 12700

GHz and temperature coefficient of resonant frequency, -39 and -14 ppm/°C respectively. The Ba₃V₄O₁₃ which formed as a secondary phase along with Ba₂CeV₃O₁₁ ceramic has been prepared separately and has relative permittivity 12, quality factor 22500 GHz and $\tau_f = -67$ ppm/°C at a sintering temperature of 700°C/4h. Glasses such as B₂O₃, ZnO-B₂O₃, BaO-B₂O₃-SiO₂, ZnO-B₂O₃-SiO₂ and PbO-B₂O₃-SiO₂ are added to Ce₂(WO₄)₃ and Ba₂CeV₃O₁₁ ceramic to lower the sintering temperature for LTCC applications. The microwave dielectric properties of 0.2 wt% ZBS added Ce₂(WO₄)₃ ceramic sintered at 900°C and 1 wt% ZBS glass added Ba₂CeV₃O₁₁ ceramic sintered at 825°C are $\epsilon_r = 11.3$ and 15.1, $Q_{\mu}xf = 20200$ and 20300 GHz and $\tau_f = -39$ and -21 ppm/°C respectively. The 0.2 wt% ZBS added Ce₂(WO₄)₃ and 1 wt% ZBS glass added Ba₂CeV₃O₁₁ ceramic are possible candidates for LTCC applications.

The influence of rare earth substitution in Ce site of CeO₂ ceramics are outlined in Chapter 6. Ceramic compositions in Ce_{1-x}RE_xO_{2-δ} (RE = La, Nd, Sm, Eu, Gd, Dy, Er, Tm, Yb and Y), $0 \leq x \leq 1$ have been prepared and the solubility of different rare earth and yttrium ions in ceria is found out. The microwave dielectric properties of Ce_{1-x}RE_xO_{2-δ} (RE = La, Nd, Sm, Eu, Gd, Dy, Er, Tm, Yb and Y) for different compositions from for $0 \leq x \leq 1$ are measured and found that these properties depend on the solid solution formation at different levels of substitution ion. The best properties are obtained for Ce_{0.9}Eu_{0.1}O_{1.95} ($\epsilon_r = 25.4$, $Q_{\mu}xf = 70300$ GHz, $\tau_f = -64$ ppm/°C); Ce_{0.8}Dy_{0.2}O_{1.9} ($\epsilon_r = 26.2$, $Q_{\mu}xf = 70150$ GHz, $\tau_f = -57$ ppm/°C) and Ce_{0.3}Sm_{0.7}O_{1.65} ($\epsilon_r = 19.7$, $Q_{\mu}xf = 79450$ GHz, $\tau_f = -51$ ppm/°C).

Ceria based composites for microwave substrate and electronic packaging applications are described in Chapter 7. The first section of this chapter discusses the glass-ceria composites for LTCC applications. Different weight percentage of glasses such as B₂O₃, B₂O₃-SiO₂, Al₂O₃-SiO₂, ZnO-B₂O₃, BaO-B₂O₃-SiO₂, MgO-B₂O₃-SiO₂, PbO-B₂O₃-SiO₂, ZnO-B₂O₃-SiO₂, 2MgO-Al₂O₃-5SiO₂, Li₂O-B₂O₃-SiO₂, Bi₂O₃-ZnO-B₂O₃-SiO₂ and Li₂O-MgO-ZnO-B₂O₃-SiO₂ are added to CeO₂ powder. The 0.5 wt% of glass fluxed CeO₂ gives the maximum density and best microwave dielectric properties.

CeO₂ added with 20 wt% B₂O₃ (sintered at 900°C) shows $\epsilon_r = 13.2$, $Q_{ur}xf = 24200$ GHz, $\tau_f = -46$ ppm/°C and that of CeO₂ added with 10 wt% Bi₂O₃-ZnO-B₂O₃-SiO₂ (sintered at 950°C) has $\epsilon_r = 22.4$, $Q_{ur}xf = 12000$ GHz, $\tau_f = -57.2$ ppm/°C. No reaction with silver is observed for 20 wt% B₂O₃ and 10 wt% Bi₂O₃-ZnO-B₂O₃-SiO₂ added CeO₂ ceramic.

The second section of Chapter 7 deals with the polymer/ceria composites for electronic packaging applications. PTFE based composites are prepared by powder processing technique and HDPE composites by sigma-blend method. In both PTFE and HDPE based composites, with the increase of filler content, the packing of particles grew denser and indicated the excellent compatibility between polymer and CeO₂ particles. The relative permittivity (ϵ_{eff}), dielectric loss ($\tan \delta$) and microhardness increased with increase in CeO₂ content. The thermal conductivity (k_c) increased and coefficient of thermal expansion (α_c) decreased with increase in CeO₂ content for both PTFE and HDPE composites. For 0.6 volume fraction loading of the ceramic, the PTFE composite has $\epsilon_{eff} = 5$ and $\tan \delta = 0.0064$ (at 7 GHz), $k_c = 1.85$ W/m°C, $\alpha_c = 22.9$ ppm/°C and Vickers' microhardness of 17 kg/mm². The 0.5 volume fraction of HDPE/CeO₂ composite has $\epsilon_{eff} = 6.9$ and $\tan \delta = 0.0085$ (at 7 GHz), $k_c = 3.22$ W/m°C, $\alpha_c = 78.5$ ppm/°C and Vickers' microhardness of 28 kg/mm². Different theoretical approaches have been employed to predict the effective permittivity, thermal conductivity and coefficient of thermal expansion of composite systems and the results are compared with that of experimental data. Due to the reasonably good dielectric, thermal and mechanical properties of HDPE composite (0.5 V_f) compared to PTFE composites, 0.5 V_f HDPE-CeO₂ can be considered as a possible candidate for microwave substrate applications.

The last section of Chapter 7 explains the giant permittivity of CeO₂-La_{0.5}Sr_{0.5}CoO_{3-δ} (LSCO) composites. The variation of relative permittivity with sintering temperature shows that the permittivity is maximum at 1150°C for all volume fractions. The permittivity decreases with further increase in sintering temperature. The relative permittivity is maximum ($\epsilon_r > 10^5$) at 0.4 V_f of LSCO at a sintering temperature of 1150°C. For all volume fractions of LSCO, the relative permittivity of CeO₂-LSCO

composites is almost independent of temperature. CeO₂-LSCO composites can replace the present cermets used in electromechanical and embedded passive devices due to its high permittivity.

The following table gives the important and selective ceria based microwave dielectric resonator and LTCC materials, their sintering temperatures and microwave dielectric properties developed during the course of this Ph. D. work.

Sl. No	Material	ST (°C)	ρ (g/cm ³)	ϵ_r	$Q_{\mu} \times f$ (GHz)	τ_f (ppm/°C)
1	CeO ₂	1650	6.82	23.0	60200	-53
2	CeO ₂ -0.5CaO-.5TiO ₂	1550	5.81	65.5	9500	399
3	CeO ₂ -0.5MgO-0.5TiO ₂	1400	5.73	22.4	17500 539000 [#]	-62
4	CeO ₂ -0.5ZnO-0.5TiO ₂	1250	6.19	26.1	24100	-43
5	CeO ₂ -0.5MnO-0.5TiO ₂	1200	6.07	26.3	17100	-30
6	CeO ₂ -0.5CoO-0.5TiO ₂	1200	6.20	22.0	50000*	-47
7	CeO ₂ -0.5NiO-0.5TiO ₂	1200	5.39	18.0	25300	-58
8	CeO ₂ -0.5WO ₃ -0.5TiO ₂	1130	5.45	17.0	45550*	7
9	CeO ₂ -0.5CaO-.5TiO ₂ +8 wt% Cr ₂ O ₃	1550	5.77	35.0	4350	0
10	CeO ₂ -0.5MgO-0.5TiO ₂ +2 wt% WO ₃	1400	5.64	21.4	90000	-50
11	CeO ₂ -0.5MgO-0.5TiO ₂ +2 wt% WO ₃ +0.5 wt% TiO ₂	1400	5.64	21.3	87700	-48
12	CeO ₂ -0.5CoO-0.5TiO ₂ + 1 wt% WO ₃	1200	6.05	21.0	70000*	-30
13	CeO ₂ -0.5CoO-0.5TiO ₂ +0.5wt%WO ₃ +20 wt% TiO ₂	1200	4.90	21.2	58200*	5
14	CeO ₂ -0.5CoO-0.5TiO ₂ +10 wt% CeO ₂	1130	5.82	16.0	53000*	5
15	CoTiO ₃	1375	4.91	19.8	62500	-49
16	MnTiO ₃	1350	4.09	24.3	15200	-56
17	NiTiO ₃	1475	4.69	19.7	13900	-51
18	BaO-2CeO ₂ -7TiO ₂	1240	5.04	41.5	26900	37
19	BaO-3CeO ₂ -4TiO ₂	1260	5.51	32.6	25400	-11
20	0.5CeO ₂ -0.5BaTi ₄ O ₉	1260	5.3	34.5	20750	2
21	Ba ₂ CeV ₃ O ₁₁	1025	4.4	14.9	12700	-14
22	Ce ₂ (WO ₄) ₃	1000	5.9	10.8	10500	-39
23	Ba ₃ V ₄ O ₁₃	700	3.86	12.0	22500	-67
24	Ce _{0.3} Nd _{0.7} O _{1.65}	1600	6.92	18.3	44700	-63
25	Ce _{0.9} Eu _{0.1} O _{1.95}	1625	6.78	25.4	70300	-64
26	Ce _{0.8} Dy _{0.2} O _{1.9}	1650	6.60	26.2	70150	-57
27	Ce _{0.3} Sm _{0.7} O _{1.65}	1650	5.82	19.7	79450	-51
28	0.5CeO ₂ -0.5BaTi ₄ O ₉ + 12 wt% B ₂ O ₃ +1 wt% CuO	950	6.82	20.6	17000	48
29	Ce ₂ (WO ₄) ₃ +0.2 wt% ZBS	900	5.89	11.3	20200	-39
30	Ba ₂ CeV ₃ O ₁₁ +1 wt% ZnO-B ₂ O ₃ -SiO ₂	825	4.46	15.1	20300	-21
31	CeO ₂ + 20 wt% B ₂ O ₃	900	4.55	13.2	24200	-46
32	CeO ₂ + 20 wt% BZBS	950	6.88	22.4	12000	-57

*measured in vacuum, [#] measured at 20K, ZBS-ZnO-B₂O₃-SiO₂, BZBS- Bi₂O₃-ZnO-B₂O₃-SiO₂

As is evident from the table, dielectric resonators with $10 \leq \epsilon_r \leq 70$, $4000 \leq Q_{ur}xf \leq 539000$ GHz and $+399 \leq \tau_f - 65$ ppm/ $^{\circ}$ C have been developed during this investigation. In the present work several temperature stable polymer-ceria composites having relative permittivity in the range 2.10-6.9 and dielectric loss in the range 0.0012-0.0085 have been developed. Giant permittivity ($\epsilon_r > 10^5$) CeO₂-LSCO composites suitable for electrostrictive applications have also been developed in the present study.

The possible error in the measurement of permittivity is of the order of 0.3%. Such an error is possible when dimensional uncertainties of the sample are in the order of 0.15%. The uncertainty in the quality factor using TE₀₁₈ mode cavity method with optimized enclosure is of the order of $\pm 2 \times 10^{-6}$. In the cavity perturbation method, the experimental error is found to be less than 2% in the case of permittivity and 1.3% in the case of dielectric loss. The uncertainty in loss tangent measurements is of the order of $\pm 2 \times 10^{-5}$ or $\pm 0.3 \tan \delta$. Within a batch and from batch to batch deviation of about 10-20% in $Q_{ur}xf$ (± 1000 GHz), 3% in relative permittivity (± 1) and 10% in τ_f (± 5 ppm/ $^{\circ}$ C) is observed. These deviations are essentially due to the slight variations in porosity, microstructure and crystal defects.

The scope for the extension of the work described in this thesis lies mainly in three areas. One of the newest and most prolific of the advances in wireless communication has been the development and implementation of tape casting as a manufacturing process for the production of thin sheets of ceramic materials for LTCC technology. The primary one is to prepare LTCC tapes using the LTCC materials developed in the present study. The sintering behaviour, shrinkage, dielectric properties, mechanical properties and chemical compatibility with electrode materials of the LTCC tapes should also be investigated. Although the sintering temperature of the materials in the present investigation is reduced by the addition of low melting oxides and glasses, it negatively affected the microwave dielectric properties. Hence chemical synthesizing techniques like hydrothermal, co-precipitation, citrate-gel, sol-gel etc. would be of great interest.

It is established that the dielectric properties of single crystals are superior to their polycrystalline counterparts. Hence another future directing in dielectric resonator research is to grow single crystals of $ATiO_3$ ($A = Co, Mn, Ni$) ceramics for microwave applications. However, growing large single crystals of these materials is challenging.

The polymer composites developed in the present investigation must be utilized to fabricate substrates for antenna and printed circuit board applications. Broadband DRAs of different geometries and DRA array using temperature stable DRs should also be fabricated using the developed DR materials.

LIST OF PATENTS AND PUBLICATIONS

International Patent

1. M. T. Sebastian, S. George and **P. S. Anjana**, Low loss Low Temperature Cofired Ceramics for millimeter wave applications (Applied: Ref. No. 0104NF2008 - filed for US, Europe, Japan, France and India).

Publications in SCI Journals

1. **P. S. Anjana** and M. T. Sebastian, Synthesis, Characterization and Microwave Dielectric Properties of $ATiO_3$ (A = Co, Mn, Ni) ceramics, *J. Am. Ceram. Soc.*, **89** [7], 2114–2117 (2006)
2. **P. S. Anjana**, M. T. Sebastian, A-K. Axelsson and N. McN. Alford, Microwave Dielectric Properties of $CeO_2-0.5AO-0.5TiO_2$ (A = Ca, Mg, Zn, Mn, Co, Ni, W) ceramics, *J. Eur. Ceram. Soc.*, **27**, 2445-2452 (2007).
3. **P. S. Anjana**, M. N. Suma, P. Mohanan and M. T. Sebastian, Microwave dielectric properties and low temperature sintering of $(1-x)CeO_2-xBaTi_4O_9$ ceramics, *Int. J. Appl. Ceram. Technol.*, **5** [1], 84-93 (2008).
4. **P. S. Anjana** and M. T. Sebastian, Preparation, characterization and dielectric properties of PTFE/ CeO_2 composite for microwave substrate applications, *Int. J. Appl. Ceram. Technol.*, **5** [4], 325-333 (2008).
5. **P. S. Anjana**, I. N. Jawahar and M. T. Sebastian, Low Loss, Temperature Stable Dielectric Ceramics in $ZnNb_2O_6-Zn_3Nb_2O_8$ System for LTCC Applications, *Mater. Sci. and Mater. Electron*, (in press).
6. **P. S. Anjana** and M. T. Sebastian, Microwave dielectric properties and low temperature sintering of cerium oxide for LTCC applications, *J. Am. Ceram. Soc.* (in press).

7. **P. S. Anjana**, C. Viji, J. Philip and M. T. Sebastian, Thermal properties of Low Loss PTFE/CeO₂ Dielectric Ceramic Composites for Microwave Substrate Applications, (communicated to *Comp. Sci. and Tech.*).
8. **P. S. Anjana**, L. A. Khalam and M. T. Sebastian, Low temperature sintering and microwave dielectric properties of Ba₂CeV₃O₁₁ ceramics (communicated to *J. Am. Ceram. Soc.*).
9. Sumesh George, **P. S. Anjana**, V. Deepu, P. Mohanan and M. T. Sebastian, Low temperature sintering and microwave dielectric properties Li₂MgSiO₄ ceramic for LTCC based devices (communicated to *J. Am. Ceram. Soc.*).
10. Tony Joseph, **P. S. Anjana**, M. T. Sebastian, S. Letourneau, R. Uvic and Sander van Smaalen, Structure and Microwave Dielectric Properties of Ca₅A₄TiO₁₇ (A = Nb, Ta) Ceramics (communicated to *J. Solid State Chem.*).

Papers to be communicated

11. **P.S. Anjana**, Tony Joseph and M. T. Sebastian, Low temperature sintering and microwave dielectric properties of Ce₂(WO₄)₃ ceramics.
12. **P.S. Anjana**, Tony Joseph and M. T. Sebastian, Microwave Dielectric Properties of Ce_xRE_{1-x}O_{2-δ} (RE = La, Nd, Sm, Eu, Gd, Dy, Er, Tm, Yb and Y), 0 ≤ x ≤ 1 ceramics.
13. **P. S. Anjana**, V. Deepu, P. Mohanan and M. T. Sebastian, Microwave dielectric and thermal properties of CeO₂ filled HDPE composites for microwave substrate applications.
14. **P. S. Anjana**, S. George and M. T. Sebastian, Giant permittivity of CeO₂-La_{0.5}Sr_{0.5}CoO_{3-δ} composites.
15. **P. S. Anjana** and M. T. Sebastian, Microwave dielectric properties of ZnNb₂O₆-Zn₃Nb₂O₈- ZnTa₂O₆ system for LTCC Applications.

16. Sumesh George, **P. S. Anjana**, J. Krupka and M. T. Sebastian, Low permittivity, loss polymer-ceramic composites for electronic packaging applications.

Publication in National Journal

17. **P. S. Anjana**, S. Thomas, M. T. Sebastian and J. James, Synthetic Minerals for Electronic Applications, *Earth Science India*, **1** [1], 36-52 (2008).

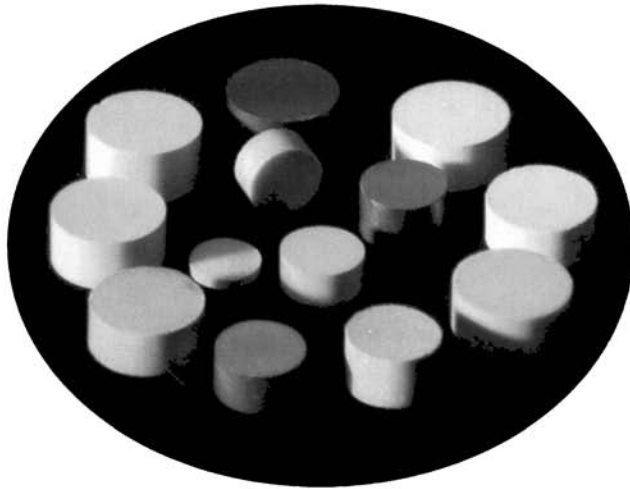
International Conference Proceedings

18. **BEST POSTER AWARD - P. S. Anjana**, M. T. Sebastian, A-K. Axelsson, N. McN. Alford, Effect of dopants on the microwave dielectric properties of $Ce_{1/2}A_{1/4}Ti_{1/4}O_{2-\delta}$ (A = Ca, Mg, Mn, Zn, Co, Ni, W) ceramics, *Microwave Materials Applications Conference* held at Japan from 24-28th October, 2004.
19. **P. S. Anjana**, M. T. Sebastian, A-K. Axelsson and N. McN. Alford, Effect of dopants on the microwave dielectric properties of $Ce_{1/2}Ca_{1/4}Ti_{1/4}O_{2-\delta}$ ceramics, *Asia Pacific Microwave Conference* held at New Delhi from 15-18th December, 2004.
20. **P. S. Anjana**, I. N. Jawahar and M. T. Sebastian, Low loss, Temperature stable dielectric ceramics in $ZnNb_2O_6$ - $Zn_2Nb_3O_8$ - $ZnTa_2O_6$ system, *Ceratech-2007* held at Visakhapatnam on 11-15th January, 2007.
21. **P. S. Anjana**, Sumesh George, Sherin Thomas, G. Subodh, P. Mohanan and M. T. Sebastian, Effect of filler on the microwave dielectric properties of PTFE/ceramic composites, *International Conference on Advanced Materials and Composites*, 24-26th October, 2007.
22. Sumesh George, Sherin Thomas, S. Renjini, T. S. Sasikals, **P. S. Anjana** and M. T. Sebastian, Effect of lithium borosilicate glass addition on the microwave dielectric properties of low loss ceramics, *International Conference on Advanced Materials and Composites*, 24-26th October, 2007.

23. **P.S. Anjana**, Tony Joseph and M. T. Sebastian, Microwave dielectric properties of $\text{Ca}_{5-x}\text{Mg}_x\text{Nb}_4\text{TiO}_{17}$ ($x = 0-3$) ceramics, *Applied Electromagnetics Conference, AEMC-2007 IEEE*, pp 1-4.
24. **P. S. Anjana**, Tony Joseph and M. T. Sebastian, Synthesis, characterization, low temperature sintering and microwave dielectric properties of $\text{Ce}_2(\text{WO}_4)_3$ ceramics, *Microwave Materials Applications Conference* to be held in China from 1-4th November, 2008.
25. S. George, **P. S Anjana**, J. Krupka and M. T. Sebastian, Microwave dielectric properties of Polystyrene/ $\text{Li}_2\text{MgSiO}_4$ composites for microelectronic applications, *Microwave Materials Applications Conference* to be held in China from 1-4th November, 2008.

Papers in National Conference Proceedings - 3

CERIA BASED DR AND LTCC MATERIALS



CERIA BASED POLYMER COMPOSITES

